910469/D
VOL. 2

GA–4
LEGAL WEIGHT TRUCK
SPENT FUEL SHIPPING CASK

SAFETY ANALYSIS REPORT FOR PACKAGING (SARP)

Prepared by
General Atomics

JANUARY 1997

GENERAL ATOMICS

910469/D
VOL. 2

GA–4
LEGAL WEIGHT TRUCK
SPENT FUEL SHIPPING CASK

SAFETY ANALYSIS REPORT FOR PACKAGING (SARP)

Prepared by
General Atomics
San Diego, California 92186-5608

GENERAL ATOMICS PROJECT 4439
JANUARY 1997

GENERAL ATOMICS

CHAPTER 3
TABLE OF CONTENTS

FIGURES

TABLES

THIS PAGE LEFT BLANK INTENTIONALLY

3. THERMAL EVALUATION

3.1 Discussion

The thermal evaluation of the GA-4 cask design considers normal and hypothetical accident conditions of transport as specified in 10 CFR Part 71. We have carried out extensive analytical modeling and testing to perform this evaluation. This section addresses the thermal design features of the cask, discusses thermal criteria, and summarizes the results of the thermal evaluation.

3.1.1 Design Features

Several aspects of the cask design and operation provide significant thermal advantages. The first of these is the mass of steel and depleted uranium (DU) used in the cask body, closure end, and gamma shielding. These materials provide a large heat sink for hypothetical accident conditions and help minimize peak temperatures, particularly for the containment seals. For normal conditions, the use of helium within the primary containment boundary and within the DU cavity enhances heat transfer out of the cask since helium provides a conductivity five times greater than nitrogen or air. Although the fuel support structure (FSS) primarily performs a mechanical function, it also serves as a set of internal fins to help dissipate heat. The neutron shield, [**Proprietary Information**], provides convection heat transfer between the cask body and the outer shell (skin).

3.1.2 Thermal Criteria

Under normal conditions of transport, the maximum fuel cladding temperature must remain below 380°C (716°F), and the accessible package surface temperature with no solar radiation must not exceed 85°C (185°F), as specified in 10 CFR Part 71.43. The temperature history of the seals must indicate that the seals will continue to function and maintain containment integrity.

For other components the only criteria are that the temperatures must not exceed values which would compromise any required structural integrity.

3.1.3 Summary of Evaluation

We utilize ANSYS (Version 5.2), PATRAN Plus 2.4, and TAC2D (Version 0002) for the thermal evaluation. ANSYS is a general-purpose finite-element computer program that solves engineering problems in statics, dynamics, heat transfer, and fluid flow. PATRAN Plus (PATRAN) is a software package that provides solid geometry construction, finite-element modeling, and enhanced graphics. Our analysis uses PATRAN to construct the finite-element meshes for the thermal models and ANSYS to perform the actual heat transfer calculations. We employ the translator program PATANS 2.2 to interface between PATRAN and ANSYS. TAC2D is a general-purpose, finite-difference, two-dimensional heat transfer computer program. Models may be quickly set up, and output results are easily interpreted. The geometry of the model must conform to a rectangular, cylindrical, or circular coordinate system.

We use three main models in the thermal evaluation. For normal conditions of transport, we consider a TAC2D model of the whole cask, using cylindrical geometry (also used for the post-accident analysis). For the hypothetical accident thermal condition we use two models:

- A TAC2D model of the closure end, with a damaged end impact limiter, and a punch directly above the closure seal.
- A 3-D ANSYS model of the closure end, with the end impact limiter damaged and punched through the center.

We use all three models to predict temperatures for the thermal evaluation. In addition, we use the ANSYS model to provide a temperature distribution for the thermal stress analysis of the structural evaluation (see Section 2.7.3). The thermal stress analysis also provides an evaluation of the seal interface distortion for the containment analysis.

The evaluation also uses two local TAC2D models: a cross-section of the cask, and a spent fuel assembly for determining its effective thermal properties. Descriptions of these models are also included.

Results for the GA-4 cask design indicate that it meets all criteria for normal conditions of transport. Approximately 86% of the heat is dissipated through the neutron shield while 14% flows out the cask ends through the impact limiters. The maximum fuel cladding temperature is 313°F, while the allowable is 716°F. We determined a maximum external surface temperature of 170°F with no solar radiation and this is within the criterion of 185°F set by 10 CFR Part 71.43 for accessible package surfaces in the shade. The maximum temperature of the seals is 135°F in the closure and 143°F for the drain. The selected seal material, ethylene propylene, can function at 300°F for 1000 hr, according to manufacturer's data. GA tested the seal and found it to be leaktight at –42°F, ambient (~75°F), and 250°F. The maximum temperature of the impact limiters is 135°F, while the aluminum honeycomb material has been qualified at 200°F.

For hypothetical accident conditions the analysis shows that the maximum primary seal temperature is 300°F. This includes the closure seal and the seal for the gas sample and drain ports. Manufacturer's data indicate the seal material can withstand a temperature of 350°F for 50 hr and 400°F for several hours. Using conditions more severe than those predicted by the analysis, we have tested the seal at 380°F, after heating for 1.5 hr above 350°F, and determined it to be leaktight. Therefore, the seal will function during the hypothetical accident thermal event. For the post-accident steady-state condition the maximum temperature of any seal is 175°F.

For the accident analysis the impact limiters are in place, since they are designed to remain attached following the drop and puncture events. Conservatively, the end of the impact limiter is damaged and punched directly above the seal. The test results, summarized in Section 2.10.13, demonstrate that the impact limiters remain in place and that the damage caused by the puncture event is less severe than modeled in the analysis. The neutron shield is assumed absent and replaced with air, but the neutron shield outer shell (skin) is intact.

For the post-accident analysis the impact limiters and neutron shield outer shell (skin) are intact while the neutron shield is absent and replaced with air. This configuration maximizes steady-state temperatures.

The reference decay heat used in the analysis is 617 W per assembly, and we apply an axial power profile that results in a peaking factor of 1.24.

Table 3.1-1 gives maximum temperatures and pressures for cask components during normal and hypothetical accident conditions.

TABLE 3.1-1
SUMMARY OF GA-4 THERMAL RESULTS

	Normal	Fire Accident Transient	Post-accident Steady State
	Maximum Temperatures (°F)		
Outer Skin	188[a]	1244	176
Neutron Shield	191	926[b]	245[b]
Cask Body	198	612	332
DU	202	453	336
Cavity Liner	222	437	345
FSS	294	426	412
Cavity Gas (avg.)	233	360	324
Fuel Clad	313	442	428
Closure Plug	136	780	162
Closure Seals	134	300	158
Gas Sample Port Seals	135	300	159
Drain Seals	143	300	175
Impact Limiters	135	1472[c]	156
	Pressures (psig)		
Cavity Pressure	74	90	86

[a]170°F with no solar radiation.
[b]Neutron shield replaced with air.
[c]Maximum impact limiter bolt temperature = 1010°F.

3.2 Summary of Thermal Properties of Materials

Tables 3.2-1 and 3.2-2 provide a compilation of the thermal conductivity, density, and specific heat of the cask materials, while Table 3.2-3 gives the thermal radiation properties (emissivity and absorptivity). The emissivity of any material is a strong function of its surface characteristics and may be subject to considerable uncertainty. For the spent fuel assemblies (SFAs) a rod emissivity of 0.7 was used, and the emissivity of the cavity liner interior (shroud) was assumed to be 0.2. A review of other analytical as well as experimental work in SFA heat transfer (Refs. 3.2-11 through 3.2-15) shows that these are conservatively low values. Fuel rod emissivity values cited varied from 0.42 to 0.93, with the majority ranging from 0.7 to 0.9. Shroud emissivities were between 0.2 and 0.8, with the majority varying from 0.2 to 0.4.

For those cases in which a value of emissivity could not be readily determined or justified, the analysis assumed a conservatively low value of 0.2 for normal conditions of transport, in which heat flows out of the cask, and 0.8 for hypothetical accident conditions, in which heat flows into the cask.

Frequently the thermal properties were not used directly as input to the thermal models but were used to calculate effective or composite thermal properties, which were then input. Section 3.6.1 gives these effective properties.

TABLE 3.2-1
MATERIAL PROPERTIES

Material	k (Btu/hr-ft –°R)	ρ (lb_m/ft^3)	c_p (Btu/lb_m–°R)	Reference (3.2- ...)
Uranium oxide (UO_2)	5.0	--	0.065	1
Zircaloy-4	9.0	--	0.071	2(k); 1(c_p)
304 stainless steel	10.0	490	0.11	3
XM-19 stainless steel	7.6[a]	492	0.11 – 0.15[b]	4(k,c_p); 5(ρ)
Depleted uranium (DU)	14.8	1185	0.0315	6; Sec. 2.3 (ρ)
Neutron shielding	See Table 3.2-2			
Boron carbide (B_4C)	15.0	151	0.29	8; Sec. 2.3 (ρ)
Aluminum alloy 5052	80.0	168	0.22	4, 9
Air	(c)	~0	0.24	3
Helium	(d)	~0	--	10

[a]At 300°F. For those areas where a wide range of temperatures was possible, the equation $k = 3.6 + 5.32 \times 10^{-3}$ T was used, based on a linear fit to the data of Ref. 3.2-4. T is °R.
[b]Determined from thermal diffusivity data of Ref. 3.2-4.
[c]$k = 5.438 \times 10^{-3} + 1.812 \times 10^{-5}$ T, based on a fit to the data of Ref. 3.2-3. T is °R.
[d]$k = 1.062 \times 10^{-3}\ T^{.701}$. The linear equation $k = 0.03295 + 1.003 \times 10^{-4}$ T represents this with a maximum of 2% error in the range of 420 < T < 1460 (i.e., –40 to 1000°F). T is °R.

[ ]

Proprietary Information

TABLE 3.2-3
THERMAL RADIATION PROPERTIES

Surface	ε	α (Solar)	Reference (3.2- ...)
Fuel rod	0.7	--	See text of Section 3.2
Interior of cavity liner (Fuel assembly shroud)	0.2	--	See text of Section 3.2
B_4C	0.8	--	7
Depleted uranium	0.5	--	6
Outer skin (electropolished) (normal conditions only)	0.15	0.4	3(ε); 18(α)
Impact limiter skin (steel) (normal conditions only)	0.85	0.6	3(ε); 18(α)
All other surfaces			
Normal conditions	0.2	--	Conservatively low value
Accident conditions	0.8	--	Conservatively high value
Surfaces exposed to thermal accident environment	0.8 or 0.85	--	10 CFR Part 71.73

3.3 Technical Specifications of Components

The package components which are of concern from a thermal standpoint are the spent fuel assembly, the primary seals (which form part of the containment boundary), the neutron shielding material, and the impact limiters. Three seals constitute part of the containment boundary: the inner closure seal and gas sample port seal in the closure lid, and the drain seal at the bottom end.

During normal conditions of transport the fuel cladding temperature must not exceed 380°C (716°F). Temperature criteria for the seals are taken from Ref. 3.3-1. All seals are Parker E740-75 O-rings and use an ethylene propylene compound. This material has a lower temperature limit of –65°F. For elevated temperatures, Fig. 3.3-1 gives the life-at-temperature curve (Ref. 3.3-1). Section 4.5.1 discusses full-scale testing of the closure seals.

Proprietary Information

The honeycomb impact limiters are made from aluminum alloy 5052 and use adhesives which have been tested under normal condition structural loads at –20°F and 200°F (Section 2.10.3.5). The adhesive bond is not required to survive a hypothetical thermal accident.

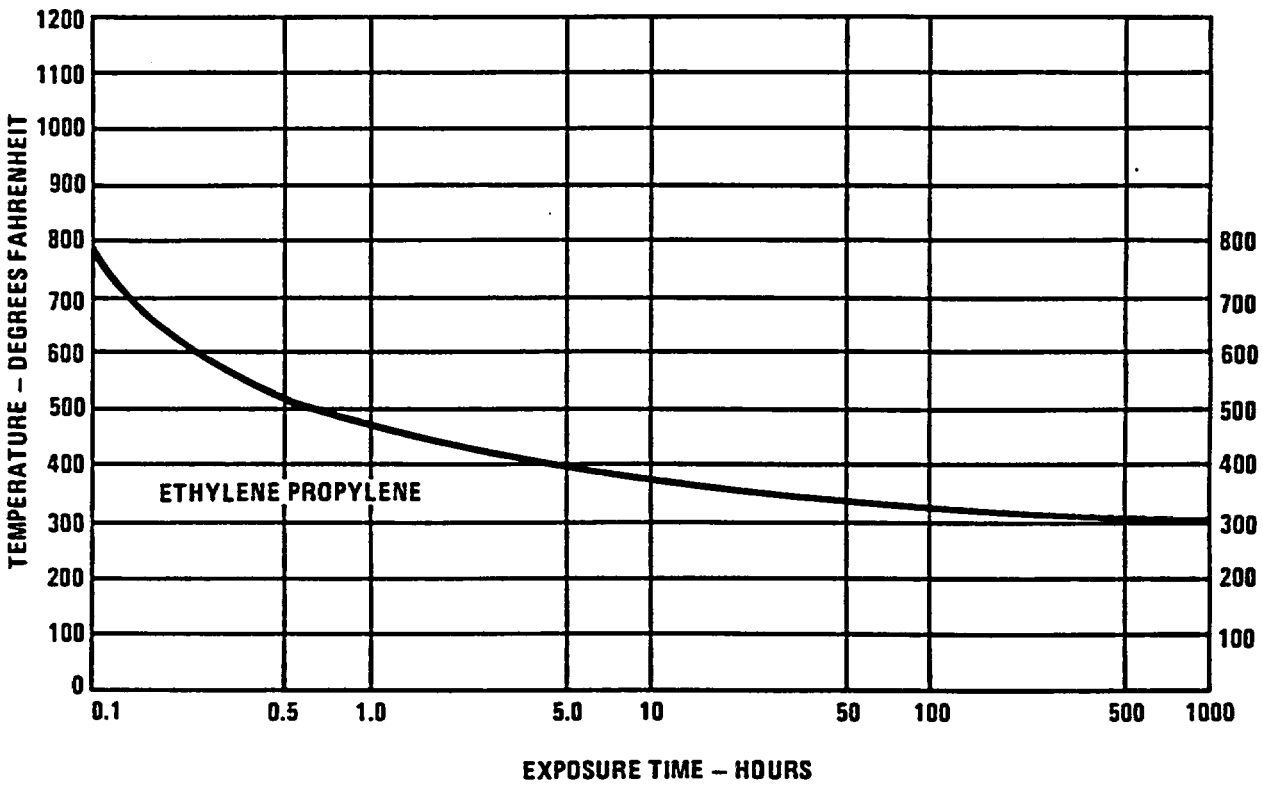

K-215(38)
6-16-93

Fig. 3.3-1. Seal life at various temperatures for ethylene propylene

3.4 Thermal Evaluation for Normal Conditions of Transport

Regulations in 10 CFR Part 71 specify that the package shall be evaluated for normal conditions of transport under both hot and cold ambient temperatures. The hot ambient temperature is 100°F, and for this case solar radiation and maximum decay heat must also be considered. The solar radiation is specified by 10 CFR Part 71.71 to be the following for a 12-hr period:

800 cal/cm^2 (2950 Btu/ft^2) for horizontal surfaces.
200 cal/cm^2 (737 Btu/ft^2) for flat surfaces not horizontal.
400 cal/cm^2 (1475 Btu/ft^2) for curved surfaces.

The cold ambient temperature is –40°F with no solar radiation. Both maximum decay heat and zero decay heat must be considered. (Note that for zero decay heat, all temperatures will attain steady-state values of –40°F.)

3.4.1 Thermal Model

The thermal evaluation uses the TAC2D computer program, Version 0002 (Ref. 3.4-1). TAC2D is a finite-difference, two-dimensional heat transfer computer program. It solves steady-state and transient problems in rectangular, cylindrical, or circular coordinates.

The TAC2D model of the GA-4 cask is shown in Fig. 3.4-1. A cylindrical (r-z) coordinate system is assumed for the model. Where the actual boundaries are "square/round," the equivalent radial gridline location for the model is computed on the basis of equal perimeters. (See Section 3.6.6.)

The following sections discuss other general aspects of the thermal model:

1. Effective Thermal Properties. A detailed, explicit representation of all cask components is not feasible. Therefore it is necessary to use composite or effective thermal properties in the models. The calculation of effective thermal properties follows two general procedures. One is to combine two modes of heat transfer (typically conduction and thermal radiation) into a single effective thermal conductivity. Another procedure is to treat two or more materials as a single composite material. The prime example utilizing these two procedures is the combination of the spent fuel assemblies (SFAs), fuel support structure (FSS) and boron carbide pellets. Section 3.6.1 lists effective thermal properties for normal and hypothetical accident conditions. Detailed derivations are provided in Section 3.6.5.

2. Gaps. The gaps between the liner and DU and between the DU and cask body shown in Fig. 3.4-1 are filled with helium. Since TAC2D does not permit circumferential variation, model gap thicknesses are computed based on averaging the true gaps around the circumference. Section 3.6.7 presents these calculations.

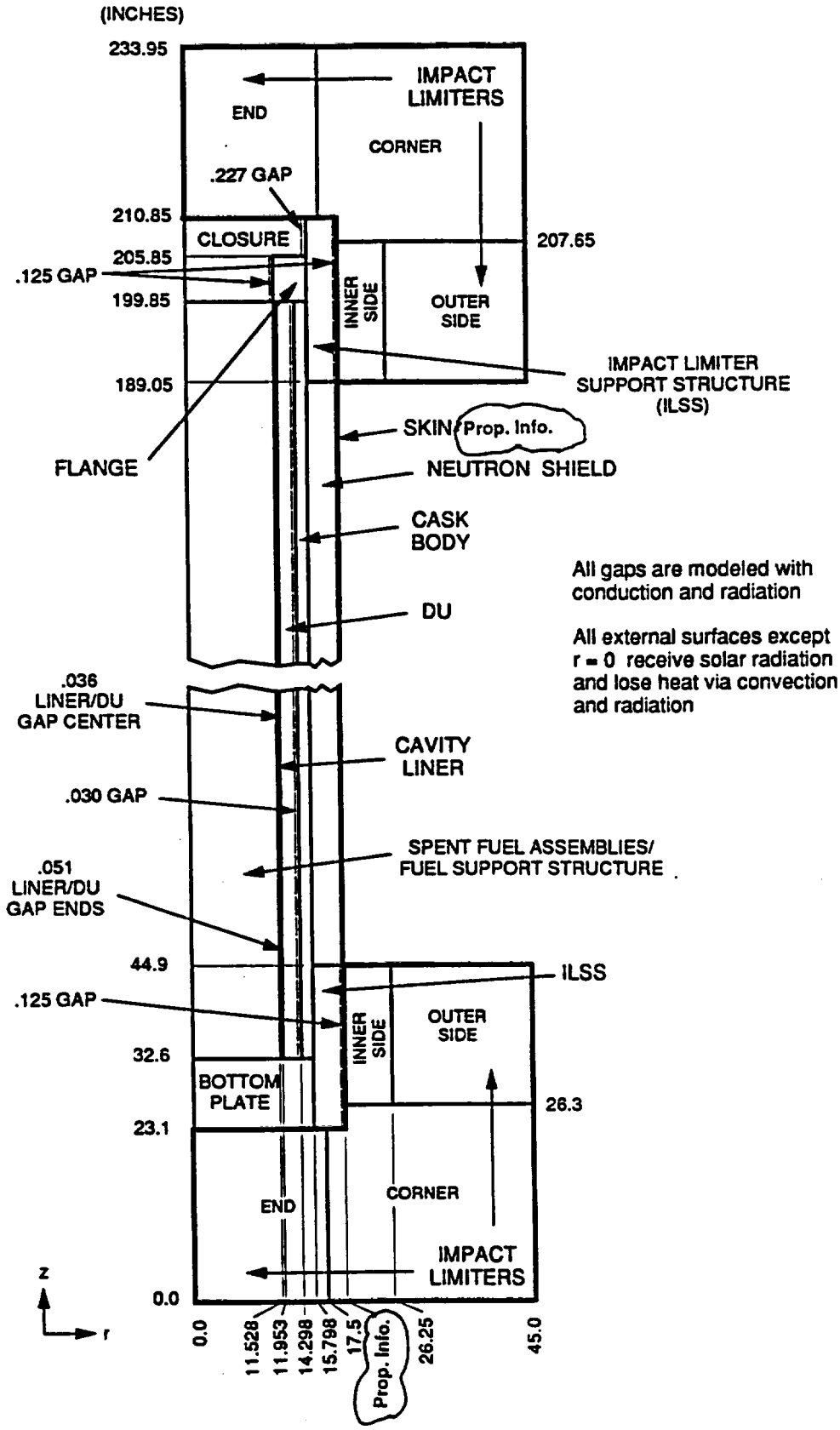

Fig. 3.4-1. TAC2D model for normal conditions

3. Decay Heat. The GA-4 cask design basis decay heat is 617 W per assembly and is distributed according to the axial power profile of Fig. 3.4-2. The axial power profile gives a peaking factor of 1.24. The decay heat and profile are based on use of the ORIGEN-S computer code, as discussed in Section 5.2, and assume 35 GWd/MTU burnup, 10-yr cooling, and a conservative enrichment of 3 percent. Section 3.6.8 provides the adaptation of the axial power profile to the TAC2D input.

   Ref. 3.4-2 shows that the peaking factor decreases with increasing burnup. That is, the axial power profile becomes flatter. Therefore, the curve used is conservative for burnups higher than 35 GWd/MTU.

4. Boundary Conditions. During transport, heat transfer from the external surface to ambient assumes combined natural convection and thermal radiation. For an ambient temperature of 100°F and a skin temperature of 175°F, a typical combined coefficient is 1.1 Btu/hr-ft^2-°F. Correlations for natural convection and thermal radiation are given in Section 3.6.2.

5. Solar Radiation. Using the data of 10 CFR Part 71.71 and the solar absorptivity from Table 3.2-3, we compute the rate of absorbed solar radiation on external surfaces required for the TAC2D model. For the flat ends of the impact limiters, the rate of absorbed solar radiation is calculated as the total 12-hour vertical surface value (from 10 CFR Part 71.71) multiplied by the absorptivity and averaged over 24 hours.

$$q_{\text{flat, impact limiter}} = \frac{(737)(0.6)}{24} = 18.4 \frac{\text{Btu}}{\text{hr-ft}^2}.$$

   A similar procedure is used for the curved surfaces of the impact limiter and for the outer skin

$$q_{\text{curved, impact limiter}} = \frac{(1475)(0.6)}{24} = 36.9 \frac{\text{Btu}}{\text{hr-ft}^2}, \text{ and}$$

$$q_{\text{outer skin}} = \frac{(1475)(0.4)}{24} = 24.6 \frac{\text{Btu}}{\text{hr-ft}^2}.$$

6. Neutron Shield. Heat transfer through the [Prop. Info.] neutron shield is modeled on the basis of [**Proprietary Information**] Section 3.6.2 gives the correlation.

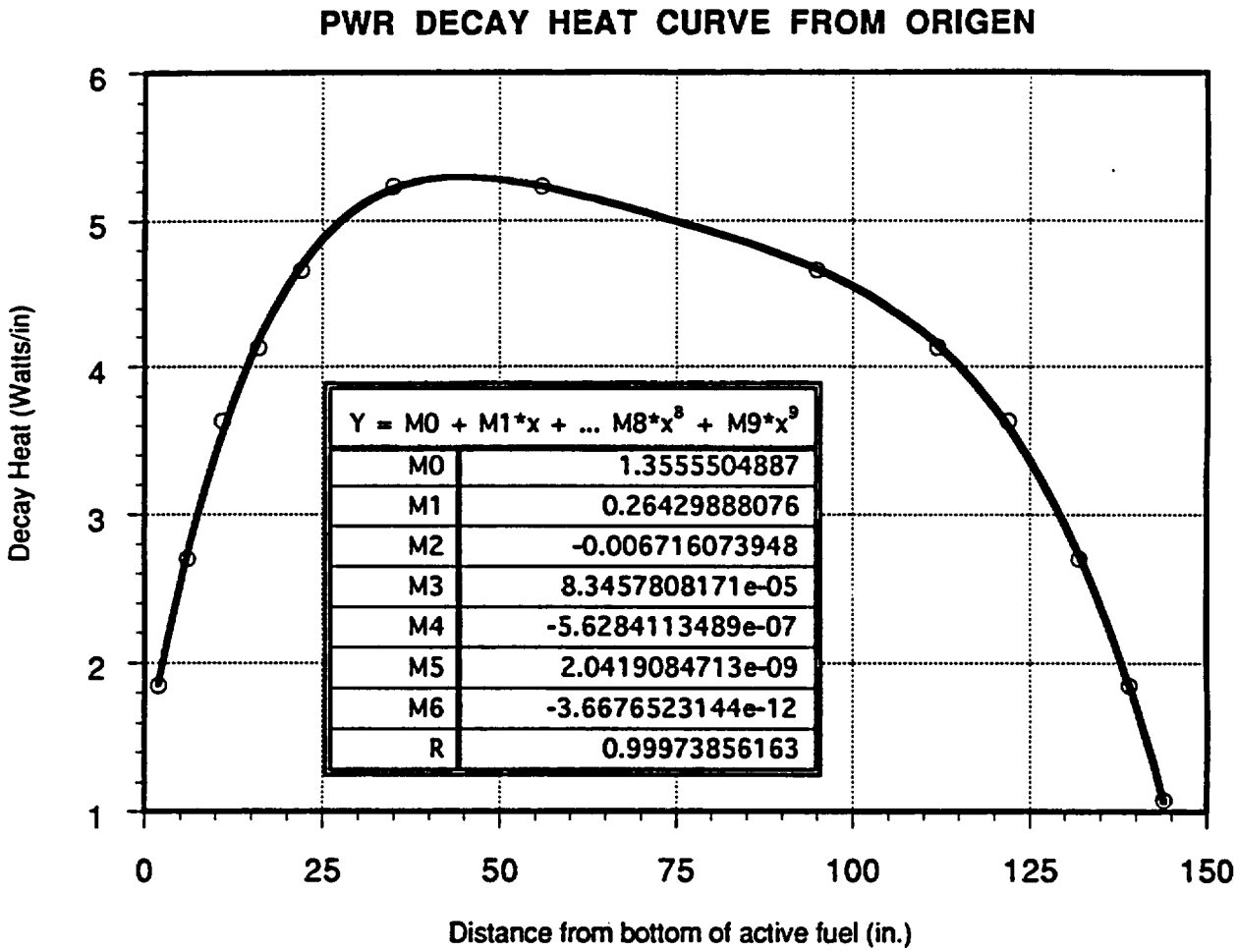

Fig. 3.4-2. PWR decay heat axial profile

3.4.2 Maximum Temperatures

Figure 3.4-3 provides a steady-state temperature map of the cask under conditions of 100°F ambient, decay heat with axial power profile, and solar radiation. Fig. 3.4-4 plots axial temperature profiles along the length of the fuel cavity. In this plot, the curves bear the following relationship to the temperature map of Fig. 3.4-3:

T(FSS Center)	=	0.696*T(3,J) + 0.304*T(4,J),
T(FSS Average)	=	0.771*T(4,J) + 0.229*T(5,J),
T(FSS End)	=	Interface temperature between T(5,J) & T(6,J) calculated by the program,
T(Liner Flat)	=	0.579*T(FSS End) + 0.421*T(6,J),
T(Liner Corner)	=	0.167*T(6,J) + 0.833*T(7,J),
T(Liner Avg)	=	T(6,J),
T(DU)	=	T(7,J),
T(Cask Body)	=	T(8,J),
T(Neutron Shield)	=	Volume-average of T(9,J)...T(11,J), and
T(Skin)	=	T(12,J).

where J is the axial index (9–36 in Fig. 3.4-3). The first five equations are derived in Section 3.6.9. The others are self-explanatory and are taken directly from Fig. 3.4-3.[

Proprietary Information

]

Figure. 3.4-5 gives a temperature history of the cask components for a transient situation in which the cask goes from a uniform loading temperature of 100°F to hot normal transport conditions. Note that the cask achieves steady-state conditions in about 100 hours. We produce these results with the same TAC2D model as used for steady-state.

Table 3.4-1 summarizes maximum and average component temperatures. These temperatures are used to compare with allowables and to calculate thermal growth and stresses in Section 2.6.1.

3.4.3 Minimum Temperatures

Figure 3.4-6 gives a temperature history of the cask components for a transient situation in which the cask goes from a uniform loading temperature of 100°F to transport conditions at –40°F ambient with maximum decay heat. However, the minimum cask temperatures occur with no decay heat and will eventually all attain –40°F.

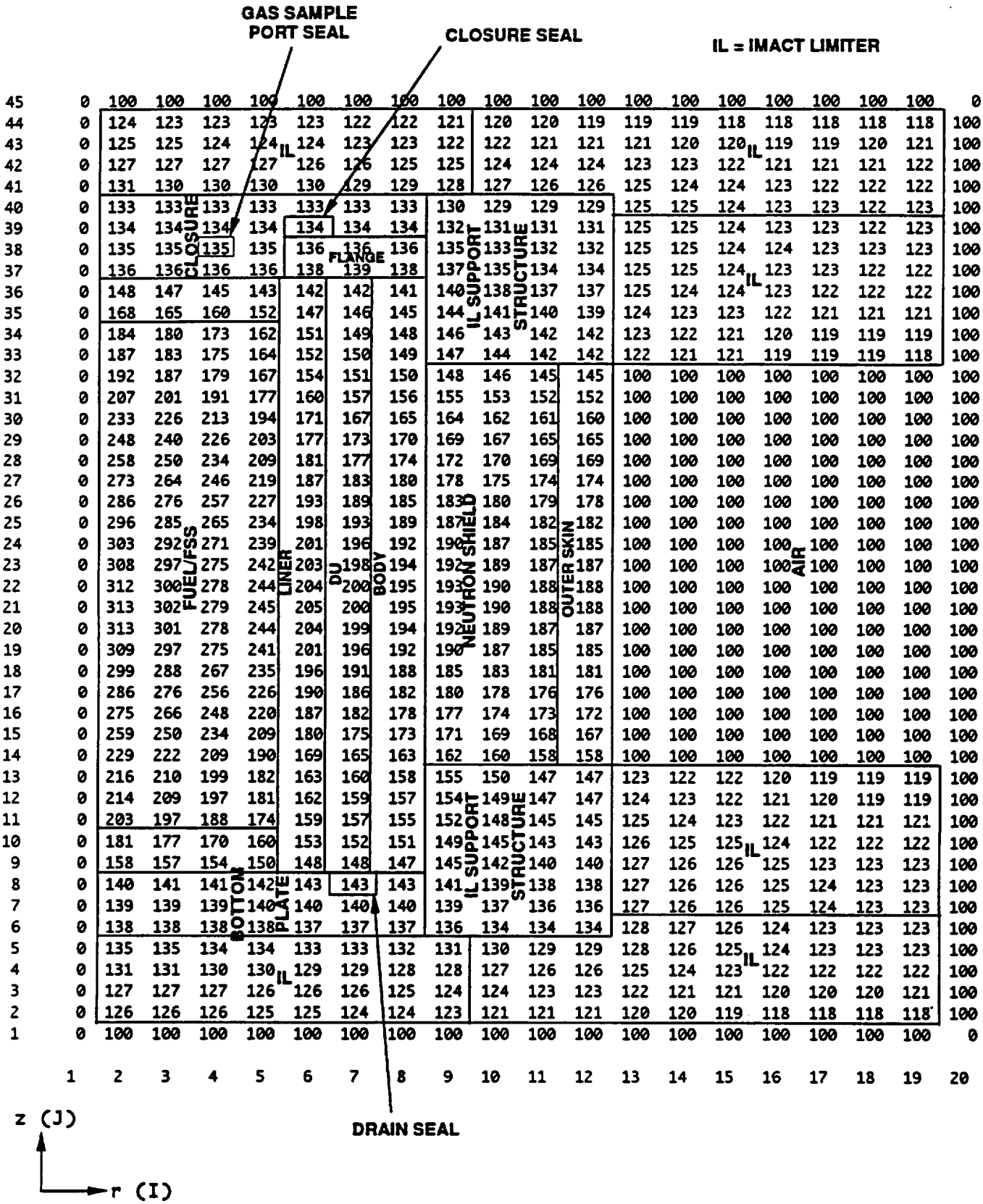

Fig. 3.4-3. Temperatures (°F) for TAC2D model (hot normal conditions)

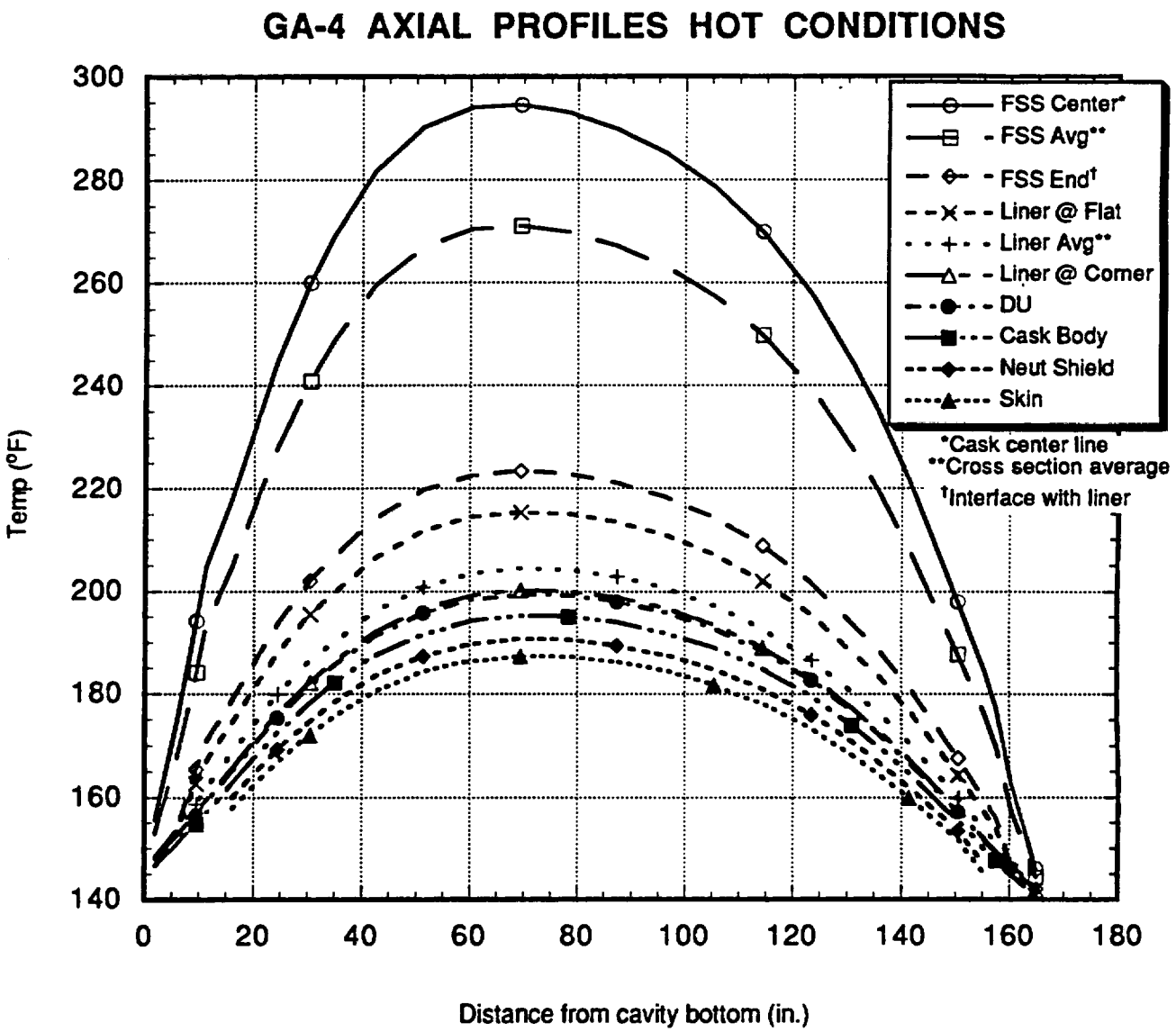

Fig. 3.4-4. Axial temperature profiles (hot normal conditions)

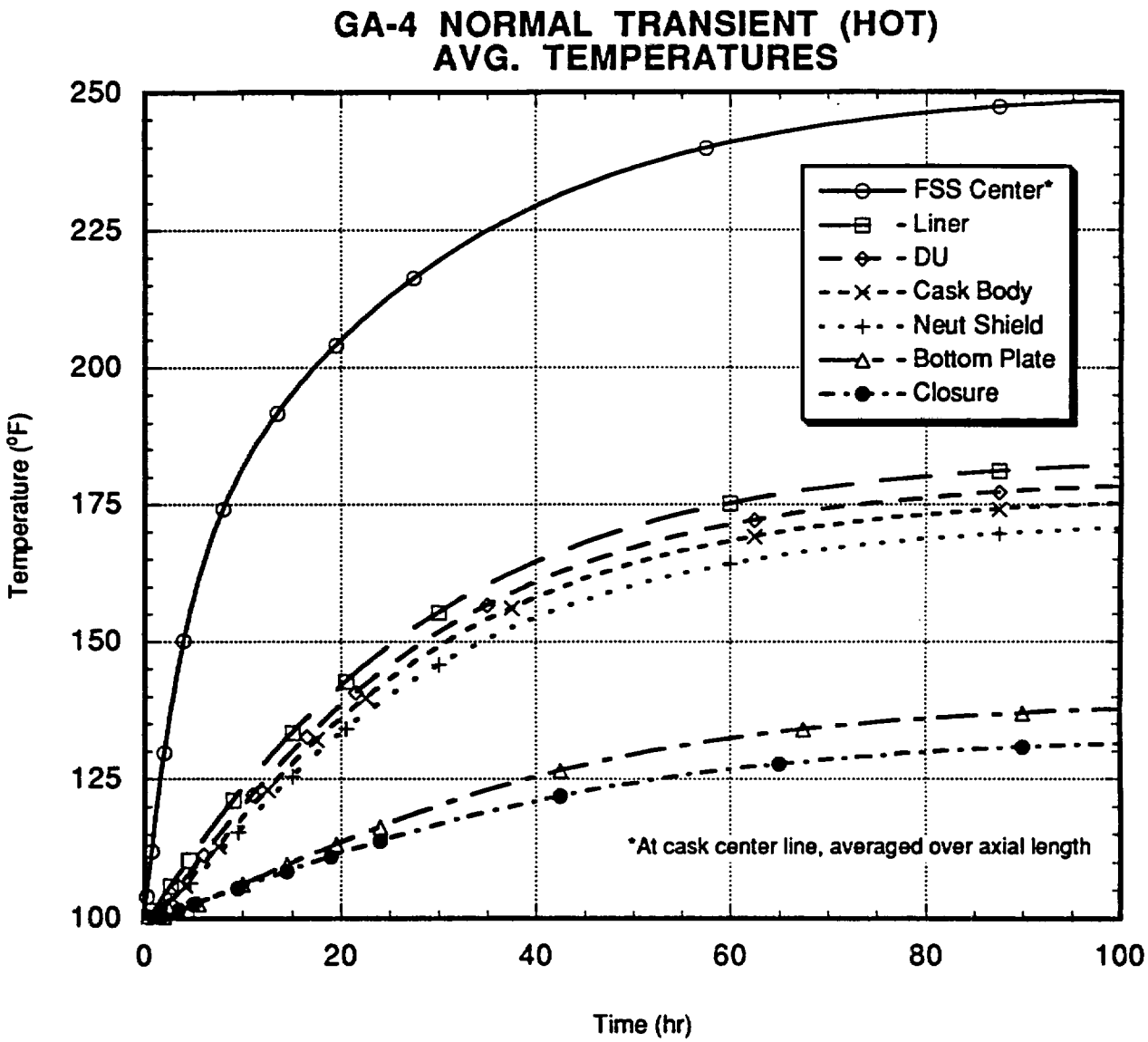

Fig. 3.4-5. Temperatures for normal transient (hot conditions)

TABLE 3.4-1
SUMMARY OF TEMPERATURES FOR NORMAL CONDITIONS, STEADY STATE (°F)

Component	Maximum			Cross-section Average		Axial Average
	Top End[a]	Midlength	Bottom End[b]	Midlength	Bottom End[b]	
FSS	194	294	215	271	202	251[c]
Cavity liner	162	222[d]	173	205	167	184
Gamma shield (DU)	156[e]	202[e]	166[e]	200	164	180
Cask body	155[f]	198[f]	163[f]	195	162	177
Neutron shield	151	191	160	191	160	172
Outer skin	150	188[g]	158	188	158	175

Fuel cladding	313 max.
Cavity gas	233 avg.
Closure and gas sample port seals	135
Drain seal	143
Closure (plug)	136
Impact limiters	135 max.
Trunnions	178[h]

[a] 15 in. from cavity top.
[b] 15 in. from cavity bottom.
[c] At center.
[d] 7°F added to account for non-concentric gaps.
[e] Calculated from Fig. 3.4-4 as 0.5 *T (liner avg.) + 0.5 *T (DU). See Section 3.6.9.
[f] Calculated from Fig. 3.4-4 as 0.5 *T (DU) + 0.5 *T (cask body). See Section 3.6.9.
[g] 170°F with no solar radiation.
[h] Cask body temperature 30 in. from cavity bottom.

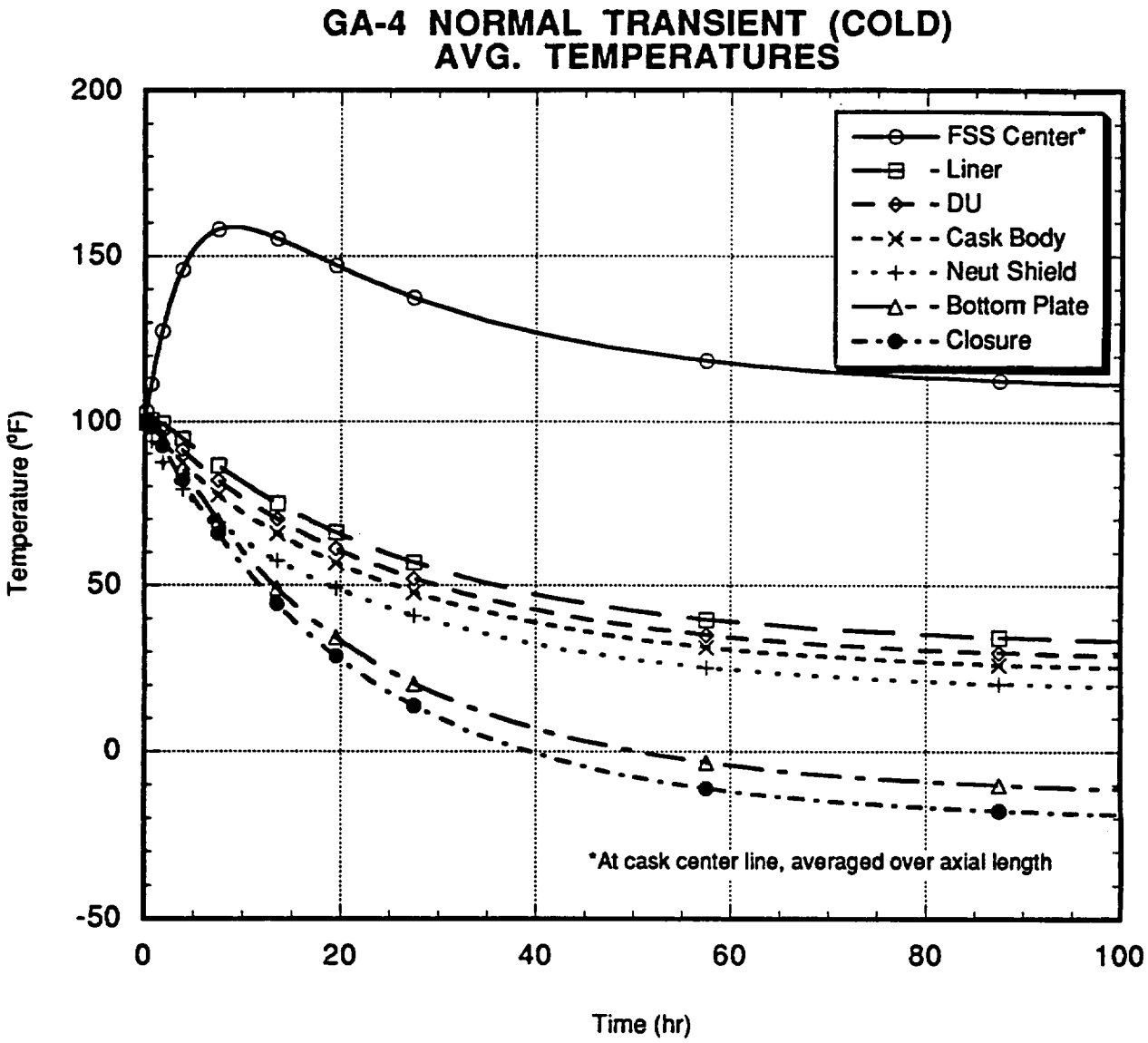

Fig. 3.4-6. Temperatures for normal transient (cold conditions)

3.4.4 Maximum Internal Pressures

The maximum normal operating pressure (MNOP) for the GA-4 cask results from three sources: (1) cavity temperature increase, and under the assumed condition of 100% rod cladding failure, (2) release of initial fill pressure, and (3) release of gas fission products.

We analyze all the spent fuel element types identified in Section 1.2.3, Contents of Packaging. The B&W 15 x 15 Mark B fuel element gives the highest MNOP of 74 psig (89 psia) for the GA-4 cask. At –20°F, the maximum internal pressure is 42 psig (57 psia). Calculations are given in Section 3.6.3.

3.4.5 Maximum Thermal Stresses

The calculation of thermal stresses is given in Section 2.6.1 and uses the information of Table 3.4-1. Temperature gradients through the cavity liner and cask body wall are very small (≤ 2°F).

3.4.6 Evaluation of Package Performance for Normal Conditions of Transport

Table 3.4-1 shows that all component temperatures for the case of 100°F ambient are within design limits. The maximum cladding temperature of 313°F is well below the allowable of 716°F. The maximum outer skin temperature is 170°F with no solar radiation, so the criterion of 185°F maximum in the shade set by 10 CFR 71.43 is satisfied. The maximum temperature of the closure and gas sample port seals, 135°F, is well within the limit of 300°F at which the ethylene propylene can function for 1000 hr. The same is true for the drain seal at 143°F. At the opposite end the minimum seal temperature of –40°F is above the low-temperature limit of –65°F. Performance of the seals at normal-condition temperatures is verified by testing at temperatures of –42°F, ambient (~75°F), and 250°F (Section 4.5.1). For the impact limiters, the maximum temperature of 135°F is below the 200°F at which the impact limiters were tested.

Figure 3.4-7 shows the temperature difference between the FSS/liner and DU during hot and cold normal transients. (Since the FSS and liner are welded together, these two components will behave structurally as a unit.) Maximum decay heat is used for hot conditions, and zero decay heat for cold conditions. The figure shows that for hot conditions the maximum temperature difference occurs at steady-state conditions. Therefore, calculating the gap size at steady-state conditions, as done in Table 2.6-2, gives the minimum gap. For cold conditions, the temperature difference peaks within 20 hr, but is less than 10°F. At steady-state, the temperature difference is 0.

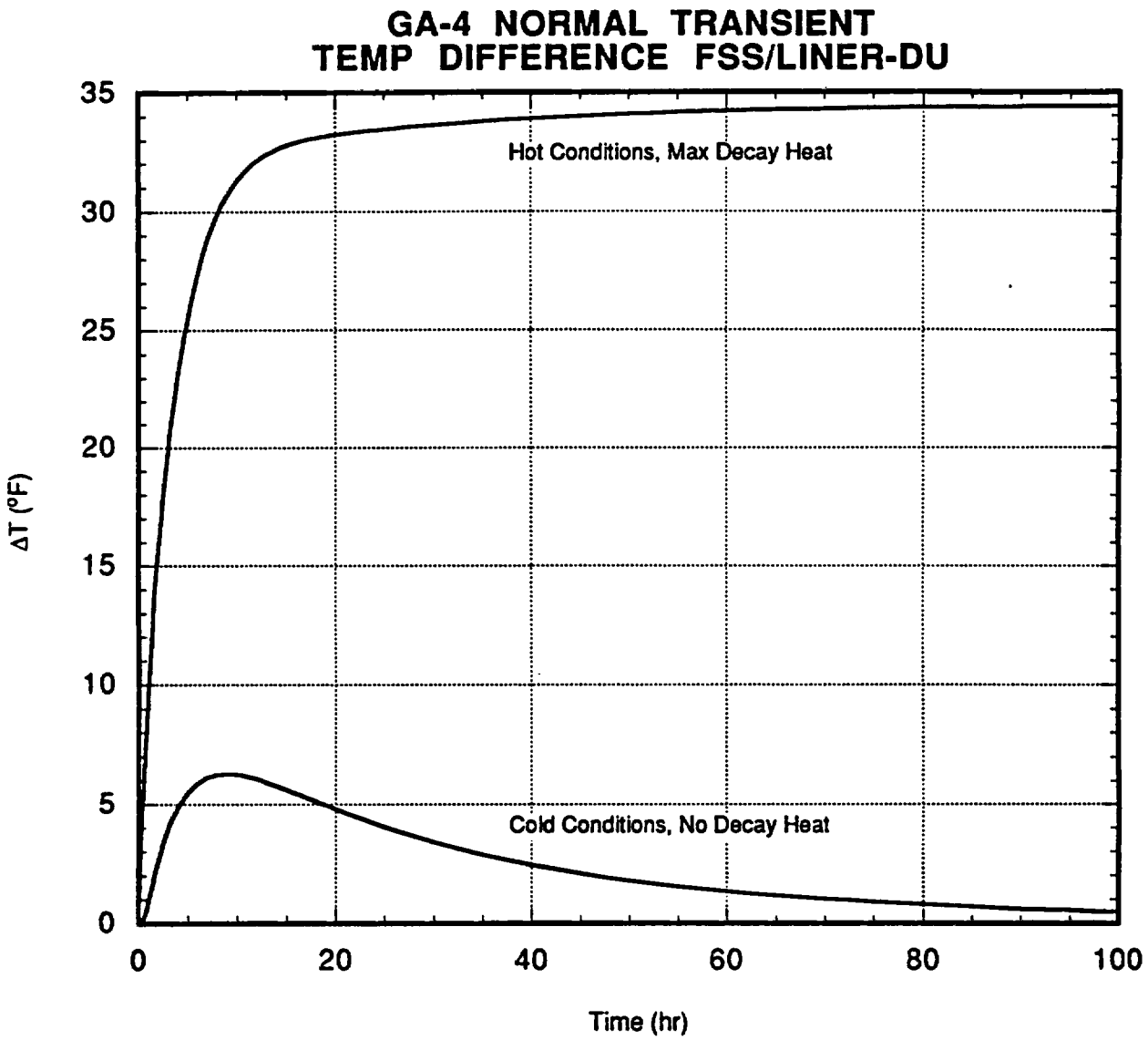

Fig. 3.4-7. Temperature difference between FSS/liner and DU

3.5 Hypothetical Accident Thermal Evaluation

For hypothetical accident conditions, 10 CFR Part 71.73 states that the package must be exposed for at least 30 min to an environment whose temperature is 800°C (1475°F). The environment emissivity must be 0.9 and the surface absorptivity of the package must be 0.8, or larger if expected. Convection must be accounted for on the basis of exposing the package to a fire of the given temperature. No artificial cooling is to be applied to the package after the 30 min of exposure. Initial conditions must be based on 100°F ambient with maximum decay heat or –20°F ambient with no decay heat, whichever is worse.

3.5.1 Thermal Models

In addition to TAC2D, we use the ANSYS (Version 5.2, Ref. 3.5-1) and PATRAN Plus (Ref. 3.5-2) codes. ANSYS is a general-purpose finite-element program for structural and thermal problems. PATRAN Plus (PATRAN) provides solid geometry construction, finite element modeling, and enhanced graphics. We use PATRAN to prepare the meshes for ANSYS (the preprocessing phase). To interface between the two programs, the analysis employs the PATANS translator program, Version 2.2 (Ref. 3.5-3). We develop three analytical models to analyze the cask under accident and post-accident conditions. Section 3.6.1 gives effective thermal properties for these models.

3.5.1.1 TAC2D Models.

3.5.1.1.1 Accident Transient. Figure 3.5-1 shows the TAC2D model for calculating the cask temperatures during the accident. For this situation we consider only the portion of the cask from the axial midpoint to the closure. Restricting the scope of the model allows a much finer grid spacing to adequately handle the expected thermal gradients without using an excessive number of gridlines.

The model assumes the neutron shield is absent and replaced with air. The neutron shield outer shell (skin) is intact and natural convection and radiation occur across the air space. We assume the cask to be vertically oriented to maximize the natural convection. We take credit for the structural integrity of the impact limiters because they are designed to remain attached. (Test results in Section 2.10.13 confirm this.) However, as a result of the drop and puncture events, the thickness of the impact limiter at the closure end is reduced from 23 to 7.5 in. (see Section 3.5.2), and we allow for a 6-in.-diameter hole completely through this impact limiter directly over the closure seals. We assume the corner impact limiter thickness to be reduced by the same amount (23 – 7.5 = 15.5 in.) in the same direction. We simulate damage from an end (rather than a corner or side) drop because this would provide the most direct thermal path from the accident environment (1475°F) to the closure seals.

An inherent and significant conservatism in this approach lies in the fact that, because of the axisymmetric model, the 6-in.-diameter hole is actually a 6-in.-wide "ring." (See inset, Fig. 3.5-1.) As a result, the closure surface area exposed to the accident (426 in.^{2}) is about 15 times greater than a 6-in.-diameter hole, and more than twice the largest exposed area that

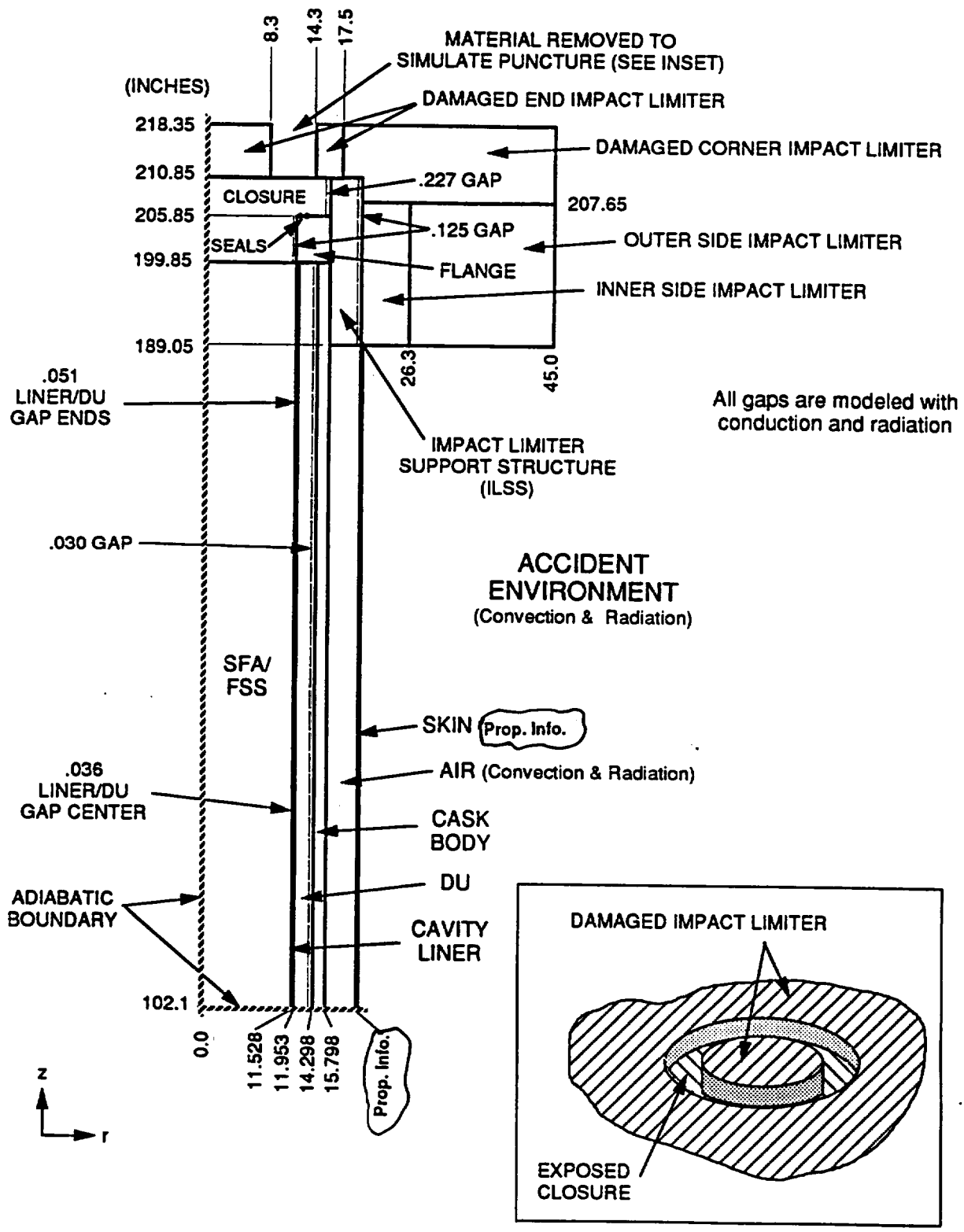

Fig. 3.5-1. TAC2D model for hypothetical accident conditions

could be created by the punch, as shown in Section 3.5.1.2. The hole size as modeled is also considerably larger than that obtained by the puncture test (Section 2.10.13), an area approximately 3 in. x 7.5 in. (22.5 in.^{2}).

We use initial conditions for a hot (100°F) ambient with maximum decay heat and no solar radiation. To generate an initial temperature distribution, we obtain a steady-state case using a slight modification of the accident model. (Temperatures determined by the normal-condition TAC2D model cannot be imposed as initial temperatures on the accident model because the nodes for the two models are not in the same locations.) Prior to the accident there is no damage to the cask, and for the initial-condition case we thus replace the "hole" with impact limiter material. We maintain the impact limiter thickness at 7.5 in. but alter its thermal conductivity so that the conductance reflects an initial undamaged state. By using the correct conductance, we produce initial temperatures that match those that would be obtained from a model with an undamaged impact limiter.

We determine the external heat transfer coefficient during the accident and cooldown on the basis of convection and radiation. During the 30-min exposure we use a forced convection coefficient of 2.0 Btu/hr-ft^2-°F, which is based on an external velocity of 20 ft/s. We calculate the radiation portion to be between 13 and 36 Btu/hr-ft^2-°F, depending on the surface temperature. Correlations are given in Section 3.6.2.

3.5.1.1.2 Post-Accident Steady-State. To calculate post-accident maximum temperatures, we use the model for normal conditions of transport (Fig. 3.4-1) but replace the neutron shield with air. The outer skin is intact. Heat transfer across the air space occurs by natural convection and radiation. No other damage is assumed.

As with normal conditions of transport, the analysis uses the decay heat of 4 PWR spent fuel assemblies with 617 W per assembly, solar radiation, and an ambient temperature of 100°F.

3.5.1.2 ANSYS Model. Figure 3.5-2 shows the ANSYS model geometry, materials, and dimensions, while Fig. 3.5-3 shows the finite-element mesh. This model is constructed specifically to provide temperatures for the corresponding thermal stress analysis in Section 2.7.3. The model is a 1/8 section of the cask and extends axially from a point 18 in. below the impact limiter support structure to the closure end. The distance of 18 in. is sufficiently long to adequately model any thermal effects the cask body might exert on the closure end. Components included in the model are the cask body, gamma shield, cavity liner, flange, closure, impact limiters, and impact limiter support structure. We do not consider the spent fuel assemblies and fuel support structure. The cavity's inner surface is therefore an adiabatic boundary during the thermal accident.

As with the TAC2D model, we assume the end impact limiter to be reduced to 7.5 in. For the puncture damage, thermal stresses in the closure will increase with the size of the hole in the impact limiter. The largest possible area that can be created by a 6-in. bar is a diagonal gash across the cask closure. Since only a 1/8 section of the cask is modeled, the total closure area exposed by the gash is calculated and converted to an equivalent-area square hole centered on the closure. See Fig. 3.5-4.

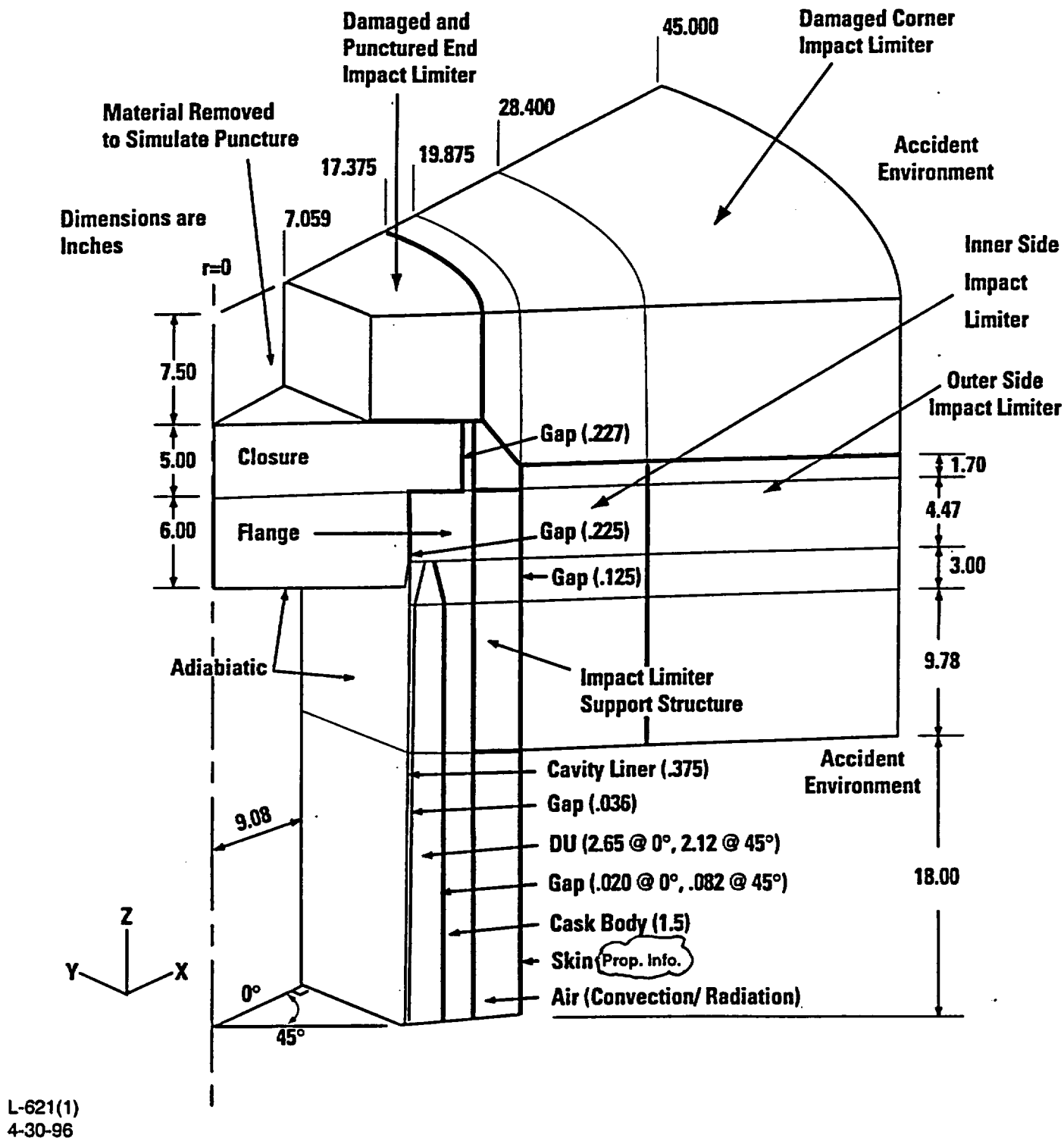

Fig. 3.5-2. Geometry of ANSYS model for hypothetical accident conditions

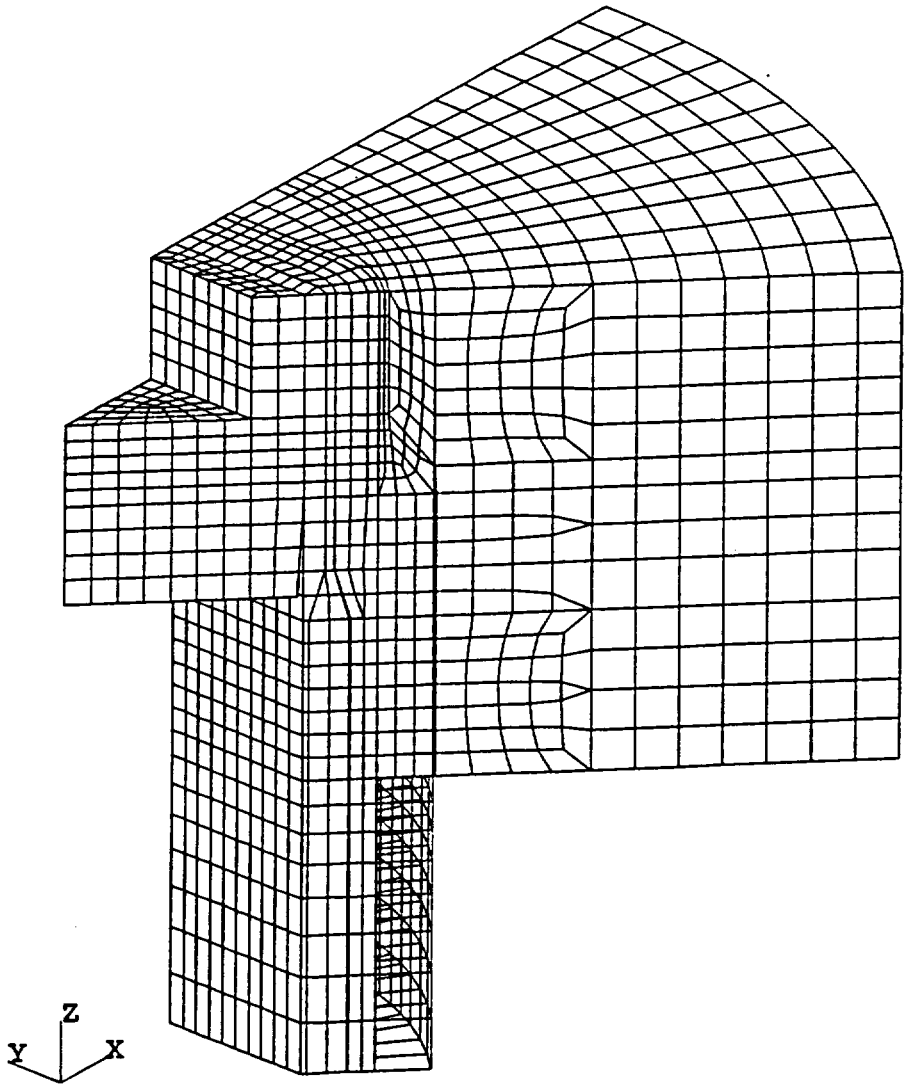

Fig. 3.5-3. Finite-element mesh for ANSYS model

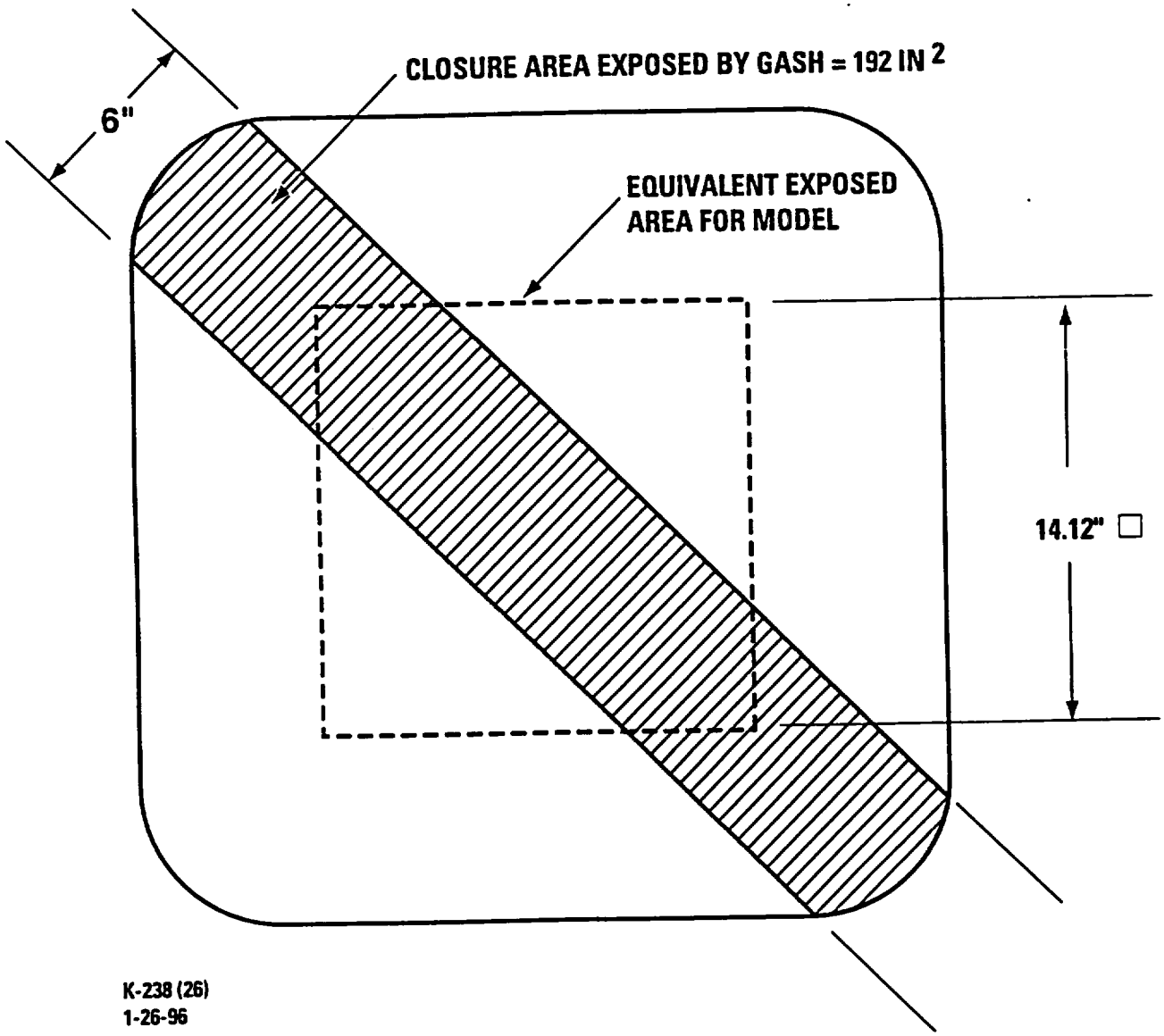

Fig. 3.5-4. Modeling of closure area exposed by puncture

We use the ANSYS model with both hot and cold (–20°F) initial conditions to find the worst case for the thermal stresses. Initial temperatures for the hot condition assume a uniform temperature of 120°F, based on the results at the TAC2D model for normal conditions with maximum decay heat but neglecting solar radiation. This is essentially the closure temperature under these conditions. For a cold initial condition there is no decay heat, and the initial temperature distribution is therefore –20°F.

Heat transfer coefficients during the hypothetical accident are calculated with the same correlations used for the TAC2D model.

3.5.2 Package Conditions and Environment

In order to maximize the effect of the damage on the primary closure seals, the transient analysis assumes an end drop precedes the thermal event. GACAP analysis has shown that the distance of travel for the end impact limiter with an end drop is 11.5 in. (Table 2.10.4-10). From the results of the quarter-scale impact limiter tests, if sufficient load is applied to cause the end impact limiter to "bottom out," the travel is 17 in. (same table), and the remaining 23 – 17 = 6 in. is crushed material. Thus, if the travel is 11.5 in., the amount d_c of crushed material remaining is given by:

$$\frac{d_c}{11.5} = \frac{6}{17}.$$

or

$$d_c = 4 \text{ in.}$$

This leaves 23 – 11.5 – 4 = 7.5 in. of uncrushed material. This thickness is therefore used for the end impact limiter, and we conservatively neglect the thermal resistance and capacitance of the crushed material. The axial thickness of the corner impact limiter is reduced by the same amount, i.e., 23 – 7.5 = 15.5 in.

Other damage to the package has been discussed in the previous section.

3.5.3 Package Temperatures

Figure 3.5-5 presents transient temperature plots as produced with the TAC2D model. Since the model considers the impact limiter puncture directly over the seal and begins with hot initial conditions, the peak seal temperature represents the maximum encountered in the thermal accident. The gas sample port seal is located at a depth further into the closure, in both the radial and axial directions, than the primary closure seal. It will therefore see a maximum temperature lower than will the primary closure seal. The primary drain seal is located in the bottom plate. Although the bottom end is not included in the TAC2D model, this seal is situated in approximately the same radial position as the primary closure seal and at an axial depth about 1 in. further into the bottom plate than the primary closure seal is into the closure. Thus the primary drain seal will also see a peak temperature lower than will the closure seal. Table 3.5-1 gives maximum temperatures for the seals, average cavity gas, and containment boundary. Additional results are given in Table 3.1-1.

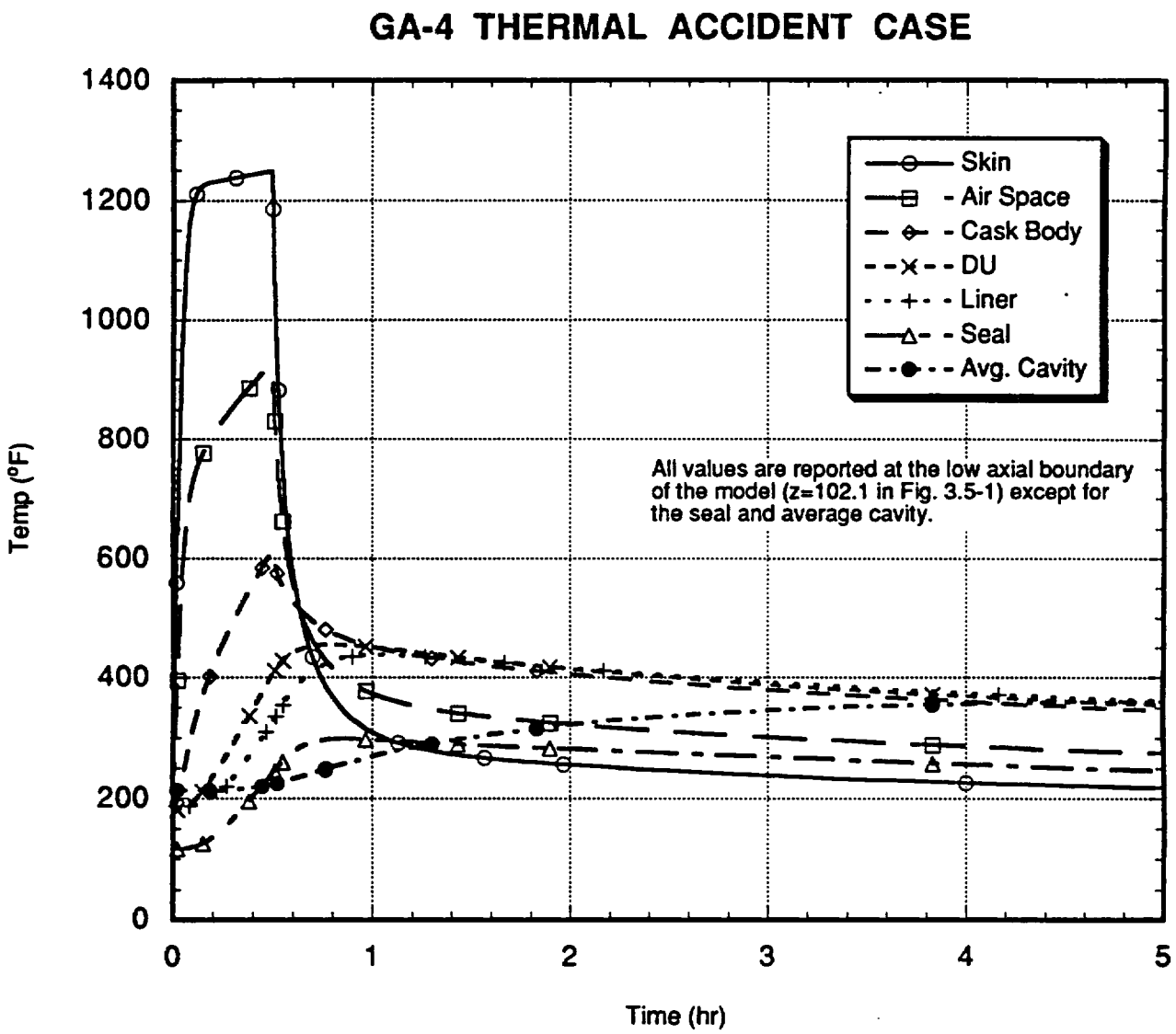

Fig. 3.5-5. TAC2D model temperatures for hypothetical accident conditions

Melting of the aluminum honeycomb impact limiters is not considered in these results. Although the thermal models predict that temperatures of these components may exceed their melting point (~1100°F), the assumption that the impact limiters remain intact and solid has been shown to be acceptable. (See Section 3.6.4.1.)

The post-accident steady state analysis shows that the maximum seal temperature, considering the damaged state described in Section 3.5.1.1.2, is 175°F (primary drain seal) and the maximum cavity gas temperature is 324°F. These are less than the peak temperatures for the transient. Figure 3.5-6 provides a temperature map for the post-accident steady state.

3.5.4 Maximum Internal Pressures

The maximum internal pressure during hypothetical accident conditions results from an increase in cavity temperature. Using the maximum average cavity temperature of 360°F, we calculate a maximum internal pressure of 90 psig (105 psia) in Section 3.6.3.

3.5.5 Maximum Thermal Stresses

The analysis to predict thermal stresses and thermal-induced distortion of the closure and flange seal interface used the ANSYS model described in Section 3.5.1. We impose the temperature distributions from this model as loads on a separate structural model and use the ANSYS capability to interpolate between finite-element meshes. The structural model uses a mesh more appropriate for stress calculations and eliminates those components that are of no interest structurally.

Sections 2.7.3 and 2.10.12 give results of the thermal stress analysis and a description of the structural model.

3.5.6 Evaluation of Package Performance for Hypothetical Accident Thermal Conditions

Referring to Table 3.5-1, the maximum primary closure seal temperature during the hypothetical accident is 300°F. This temperature may conservatively be used for all containment seals. The sealing ability of an elastomeric gasket is typically a function of its time-at-temperature history. The manufacturer's data for the seal material (Section 3.3) indicate that it can function for 1000 hr at 300°F and for 50 hr at 350°F. In addition, we have tested the seal at 380°F, after heating for 1.5 hr above 350°F, and have shown that it will function under these conditions (Section 4.5.1), which are more severe than those predicted by the analysis.

For the post-accident steady-state, the maximum seal and average cavity gas temperatures are well within the values of Table 3.5-1.

The thermal analysis and testing thus demonstrates that the package will perform satisfactorily during hypothetical thermal accident conditions and will maintain containment integrity.

GAS SAMPLE PORT SEAL

CLOSURE SEAL

IL = IMACT LIMITER

45	0	100	100	100	100	100	100	100	100	100	100	100	100	100	100	100	100	100	100	100	0
44	0	133	133	132	132	131	130	129	128	125	124	124	123	122	121	120	119	119	118	100	
43	0	136	135	135	134	133	132	131	130	129	128	128	127	125	124	122	121	121	121	100	
42	0	141	141	140	139	138	138	136	135	134	133	132	131	129	128	126	124	123	123	100	
41	0	148	148	147	146	146	145	143	141	139	137	136	135	132	130	128	125	124	124	100	
40	0	152	153	153	153	153	153	152	145	144	144	144	134	132	131	129	126	125	124	100	
39	0	154	154	155	155	156	156	156	149	148	147	147	133	132	131	129	127	125	125	100	
38	0	156	156	157	157	159	160	159	156	153	151	151	133	132	131	129	127	126	125	100	
37	0	158	158	159	160	165	166	164	162	157	155	155	133	132	131	129	127	126	125	100	
36	0	179	178	176	174	174	174	171	168	163	160	160	133	132	131	129	126	125	125	100	
35	0	210	206	200	191	185	184	181	176	169	165	165	132	130	129	126	124	123	123	100	
34	0	233	228	220	208	194	192	189	181	170	165	165	129	128	126	124	122	121	121	100	
33	0	237	233	224	211	197	194	191	182	170	165	164	128	127	125	123	121	120	120	100	
32	0	243	238	229	216	200	197	195	175	175	175	160	100	100	100	100	100	100	100	100	
31	0	263	258	247	232	216	213	211	177	177	177	150	100	100	100	100	100	100	100	100	
30	0	299	292	280	262	241	238	236	190	190	190	154	100	100	100	100	100	100	100	100	
29	0	320	313	300	280	256	252	250	199	199	199	158	100	100	100	100	100	100	100	100	
28	0	335	328	313	291	266	263	261	205	205	205	161	100	100	100	100	100	100	100	100	
27	0	358	350	334	310	282	278	276	214	214	214	165	100	100	100	100	100	100	100	100	
26	0	379	370	353	327	298	294	291	223	223	223	169	100	100	100	100	100	100	100	100	
25	0	395	386	368	341	310	306	303	230	230	230	173	100	100	100	100	100	100	100	100	
24	0	406	397	378	351	318	314	311	235	235	235	175	100	100	100	100	100	100	100	100	
23	0	414	404	385	357	324	320	316	239	239	239	177	100	100	100	100	100	100	100	100	
22	0	418	408	389	360	326	322	318	240	240	240	177	100	100	100	100	100	100	100	100	
21	0	418	408	389	359	325	321	317	239	239	239	177	100	100	100	100	100	100	100	100	
20	0	414	404	384	355	320	316	312	236	236	236	175	100	100	100	100	100	100	100	100	
19	0	405	394	375	346	311	307	304	231	231	231	173	100	100	100	100	100	100	100	100	
18	0	388	378	359	331	297	293	290	223	223	223	169	100	100	100	100	100	100	100	100	
17	0	367	357	340	313	282	278	275	214	214	214	165	100	100	100	100	100	100	100	100	
16	0	351	342	326	301	271	267	264	207	207	207	162	100	100	100	100	100	100	100	100	
15	0	327	319	304	282	255	251	249	198	198	198	158	100	100	100	100	100	100	100	100	
14	0	288	282	269	250	228	225	223	186	186	186	156	100	100	100	100	100	100	100	100	
13	0	272	266	254	237	215	211	207	196	180	172	172	130	128	127	124	122	121	121	100	
12	0	270	264	252	235	212	209	205	195	180	173	172	131	129	128	125	123	122	121	100	
11	0	255	249	239	223	206	203	199	191	179	173	173	133	132	130	127	124	123	123	100	
10	0	225	221	214	202	194	192	189	184	175	170	170	136	134	132	130	127	125	125	100	
9	0	193	192	189	185	183	183	180	176	169	165	165	136	135	134	131	128	126	126	100	
8	0	166	166	167	169	171	173	172	168	163	160	160	136	135	134	131	129	127	126	100	
7	0	163	164	164	165	165	165	165	162	158	156	156	136	135	134	131	128	127	126	100	
6	0	161	161	161	160	160	160	159	156	154	153	152	138	136	134	131	128	126	125	100	
5	0	155	154	154	153	152	151	149	146	144	142	141	139	136	133	130	127	125	124	100	
4	0	147	146	146	144	143	143	141	140	138	136	136	134	132	130	127	125	123	123	100	
3	0	140	140	139	138	137	136	135	134	132	130	130	129	127	126	124	122	121	122	100	
2	0	137	137	136	135	134	134	132	131	128	126	126	125	124	123	121	120	119	119	100	
1	0	100	100	100	100	100	100	100	100	100	100	100	100	100	100	100	100	100	100	0	
	1	2	3	4	5	6	7	8	9	10	11	12	13	14	15	16	17	18	19	20	

CLOSURE
FLANGE
IL SUPPORT STRUCTURE
FUEL/FSS
LINER
DU
BODY
AIR
OUTER SKIN
BOTTOM PLATE
IL

DRAIN SEAL

z (J)

r (I)

Fig. 3.5-6. Temperatures (°F) for post-accident steady state

TABLE 3.5-1
MAXIMUM TEMPERATURES FOR THERMAL ACCIDENT CONDITIONS

Location	Temperature (°F)
Primary closure seal	300
Average cavity gas	360
Closure	780
Flange/taper	
outer	279
midwall	279
inner	279
Cask midlength	
outer	612
midwall	549
inner	514

THIS PAGE LEFT BLANK INTENTIONALLY

3.6 Appendix

3.6.1 Effective Thermal Properties

This section lists the effective thermal properties used in the analytical models. Unless stated otherwise, detailed derivations are given in Section 3.6.5.1. The following definitions are used in this section:

k_{He} = helium conductivity (Table 3.2-1),

k_{Air} = air conductivity (Table 3.2-1),

k_{Steel} = XM-19 steel conductivity (Table 3.2-1),

k_{NS} = neutron shield conductivity (Table 3.2-2),

$f(T_1,T_2) = (T_1^2 + T_2^2)(T_1 + T_2)$ where T_1 and T_2 are boundary temperatures (absolute).

Pr = Prandtl number,

Gr = Grashof number,

h_{rad} = $4\sigma\,(0.667)\,T^3$ (T is local absolute temperature), and

σ = 1.714×10^{-9} Btu/hr-ft^2-°R^4.

All thermal conductivities (k) are expressed in Btu/hr-ft-°F and volumetric specific heats (ρc_p) in Btu/ft^3-°F unless stated otherwise. The subscripts x, y, z, and r refer to coordinate directions, with r being radial. Wherever k is expressed as a function of temperature T, the temperature is assumed to be in degrees Rankine (°R), unless otherwise indicated.

3.6.1.1 TAC2D Model, Section 3.4 (Normal Conditions).

1. Spent fuel assembly

   $k_r = 2.5\,k_{He} + 2.106 \times 10^{-10}\,T^3$, and

   $k_z = 2.4$.

2. Gap between fuel assembly and enclosure (FSS or liner)

   $k = k_{He} + 2.461 \times 10^{-11} T^3$.

3. Fuel support structure/B_4C

   k = 5.50 (parallel to axis of holes and B_4C pellets), and

   = 2.71 (normal to axis of holes).

4. Spent fuel assembly/fuel support structure/B_4C (combining materials 1 and 3)

$k_r = 1.46\ [0.966(2.5\ k_{He} + 2.106 \times 10^{-10}\ T^3) + 0.033\ (5.50)]$,

$k_z = 1.97$ active fuel zone
0.868 cladding only, and

$\rho c_p = 12.7$.

5. Void space at cavity ends (helium/steel)

$k_r = 0.966\ k_{He} + 0.033\ k_{steel}$,

$k_z = 0.761\ k_{He} + 0.054\ k_{steel}$, and

$\rho c_p = 12.7$.

6. Cavity liner
Use steel properties.

7. DU
Increase k_z and ρ by factor of 1.13 from the values in Table 3.2-1.

8. Cask body
Use steel properties.

9. Neutron shield

$$k_r = 0.0957\ k_{NS}\left(\frac{Pr^2 Gr}{1.36+Pr}\right)^{0.278}$$ (See Section 3.6.2.1)

k_z and ρc_p use basic properties from Table 3.2-2.

10. Outer skin
Use steel properties.

11. Closure, flange, and bottom plate

$k_r = k_{steel}$,

$k_z = f\ k_{steel}$, and

$\rho c_p = f\ (\rho c_p)_{steel}$;

where

$f = 0.799$ bottom 6" closure,
1.057 flange,
0.913 top 5" closure, and

0.915 bottom plate.

12. Impact limiter support structures (See Section 3.6.5.2 for derivation.)

Top: $k_r = 0.220\ k_{steel}$,

$k_z = 0.0943\ k_{steel}$, and

$\rho c_p = 13.5 + 0.706\ (\rho c_p)_{NS}$ hot conditions,
13.5 cold conditions.

Bottom: $k_r = 0.165\ k_{steel}$,

$k_z = 0.0742\ k_{steel}$, and

$\rho c_p = 11.0 + 0.782(\rho c_p)_{NS}$.

13. Impact limiters (See Section 3.6.5.2 for derivation. Top and bottom impact limiters are identical.)

Inner side: $k_r = 5.0$,

$k_z = 1.5$, and

$\rho c_p = 2.31$.

Outer side: $k_r = 3.77$,

$k_z = 1.13$, and

$\rho c_p = 1.74$.

Corner: $k_r = 0.952$,

$k_z = 1.65$, and

$\rho c_p = 0.717$.

End: $k_r = 1.5$,

$k_z = 5.0$, and

$\rho c_p = 2.31$.

3.6.1.2 TAC2D Model, Section 3.5 (Accident Conditions).

Properties are identical to those in 3.6.1.1 except as noted below:

1. Spent fuel assembly/FSS/B_4C

   A radiation term $2.90 \times 10^{-10}\ T^3$ is added to k_z.

2. Neutron shield

   The neutron shield is replaced with air using a natural convection correlation for a vertical annulus (transient) or a horizontal annulus (post-accident steady-state). See Section 3.6.2.

3. Impact limiter support structure (top)

   $k_r = F_1 k_{steel} + F_2 k_{air} + F_3 h_{rad}$,

   $k_z = G\ k_{steel}$,

   Table 3.6.1-1 gives the values of F_i, G, and ρc_p.

4. Impact limiters

   Inner side: A radiation term $0.0395\ \sigma\ f(T_1, T_2)$ is added to k_r;

   Outer side: A radiation term $0.0687\ \sigma\ f(T_1, T_2)$ is added to k_r;

Corner:	k_r	$= 0.952 + 0.05\ \sigma\ f(T_1, T_2)$	accident,
		2.29	initial conditions,
	k_z	$= 1.65 + 0.05\ \sigma\ f(T_1, T_2)$	accident,
		0.688	initial conditions, and
	ρc_p	$= 1.73$;	
End:	k_r	$= 1.50$	accident,
		4.60	initial conditions,
	k_z	$= 5.0 + 0.042\ \sigma\ f(T_1, T_2)$	accident,
		1.63	initial conditions, and
	ρc_p	$= 7.08$.	

TABLE 3.6.1-1
CONSTANTS FOR IMPACT LIMITER SUPPORT STRUCTURE (ILSS) THERMAL PROPERTIES, TAC2D MODEL

Rib Hole Dia. (in.)	F_1	F_2	F_3 (in.)	G	ρc_p Btu/in.^{3}-°F
0.624	0.111	6.07	2.59	.072	.00562
0.250[a]	.195	6.07	2.59	.216	.0100
0.250[b]	.261	8.45	2.59	.167	.00772

[a]Below shear plate
[b]Above shear plate

TABLE 3.6.1-2
THERMAL PROPERTIES FOR ILSS, ANSYS MODEL

ILSS Section	k_r Btu/hr-in-°F								k_z	ρc_p Btu/in.^{3}-°F
	Temperature (°F)									
Rib Hole Dia. (in.)	40	240	440	640	840	1040	1240	1440		
0.624	.0754	.105	.148	.210	.292	.401	.539	.711	.072 k_{steel}	.00396
0.250	.119	.156	.207	.276	.366	.482	.628	.807	.216 k_{steel}	.00612

3.6.1.3 ANSYS Model, Section 3.5 (Accident Conditions).

1. Impact limiter support structure.

   Properties are given in Table 3.6.1-2. Conductivities are identical to those for the TAC2D model. Differences in heat capacity reflect differences in model volumes. See Section 3.5.1.2.

2. Impact limiters.

   These properties are identical to those given in Section 3.6.1.2 for the TAC2D model, except that the radiation term $\sigma f(T_1, T_2) = \sigma (T_1^2 + T_2^2)(T_1 + T_2)$ in the thermal conductivity is replaced by the alternate expression $4\sigma T^3$ in terms of the local temperature.

3.6.2 Convection and Radiation Heat Transfer Correlations

3.6.2.1 Normal Conditions, TAC2D Model.

1. Natural convection - exterior surfaces

$$h = C\left(\frac{k}{d}\right)(Gr\ Pr)^n, \qquad \text{(Eq. 3.6.2-1)}$$

where

h = heat transfer coefficient,
k = thermal conductivity of air,
d = characteristic length,
Gr = Grashof number, and
Pr = Prandtl number.

C, n, and d are determined according to the following table (Ref. 3.6.2-1). The maximum value of h, as determined by either the laminar or turbulent correlation, is used.

Surface	d (in.)	C		n	
		Laminar	Turbulent	Laminar	Turbulent
Outer skin	40	0.53	0.13	0.25	0.333
Impact limiters					
Cylindrical surface	90	0.53	0.13	0.25	0.333
Flat surface (vertical)	0.9 x 90	0.59	0.021	0.25	0.40

Proprietary Information

3. Thermal radiation

$$q'' = \sigma \mathcal{F}_{1\text{-}2}(T_1^{\,4} - T_2^{\,4}), \text{ and}$$

$$h = \frac{q''}{T_1 - T_2} = \sigma \mathcal{F}_{1\text{-}2}\,(T_1^{\,2} + T_2^{\,2})(T_1 + T_2);$$

where

q'' = heat flux,

σ = Stefan-Boltzmann constant,

$\mathcal{F}_{1\text{-}2}$ = interchange factor,

T_1 = temperature of surface 1, and

T_2 = temperature of surface 2.

The interchange factor is computed as:

$$\mathcal{F}_{1\text{-}2} = \frac{1}{\frac{1}{\varepsilon_1} + \frac{A_1}{A_2}\left(\frac{1-\varepsilon_2}{\varepsilon_2}\right)} \approx \frac{1}{\frac{1}{\varepsilon_1} + \frac{1}{\varepsilon_2} - 1} \quad \text{for small gaps } (A_1 \approx A_2).$$

If surface 1 is external and surface 2 is the environment, $A_1/A_2 << 1$, and

$$\mathcal{F}_{1\text{-}2} = \varepsilon_1.$$

3.6.2.2 Accident Conditions, TAC2D and ANSYS Models.

1. Forced convection - exterior surfaces (0 to 30 min, heating phase)

$$h = C\left(\frac{k}{d}\right)Re^n; \qquad \text{(Ref. 3.6.2-4)}$$

where

Re = Reynolds number,
d = 40 in.,
C = 0.0239, and
n = 0.805.

The Reynolds number is calculated on the basis of an assumed velocity of 20 ft/sec for the gas in the fire. Using the above correlation, h ranges between 1.6 and 2.1 Btu/hr-ft^2-°F. We use an average value of 2.0.

[**Proprietary Information**]

Proprietary Information

[

Proprietary Information

]

3. Thermal radiation (heating and cooldown).

We use the same correlation as for normal conditions. For external surfaces during the heating phase, $\varepsilon_1 = 0.8$ or 0.85 (see Table 3.2-3) surface and $\varepsilon_2 = 0.9$ (fire environment). Thus,

$$\mathcal{F}_{1\text{-}2} = \frac{1}{\frac{1}{.8} + \frac{1}{.9} - 1} = 0.735 \quad \text{or} \quad \frac{1}{\frac{1}{.85} + \frac{1}{.9} - 1} = 0.777.$$

During the cooldown portion, $\varepsilon_2 = 1.0$. Thus $\mathcal{F}_{1\text{-}2} = \varepsilon_1$.

4. Natural convection (external surfaces, cooldown phase)

$$h = \frac{k}{d}\left[C_1 + 0.387\left(\frac{Gr\ Pr}{\left[1 + (C_2/Pr)^{9/16}\right]^{16/9}}\right)^{1/6}\right]^2; \qquad \text{(Ref. 3.6.2-1)}$$

where

C_1 = 0.825 vertical surfaces,
0.600 horizontal surfaces,

C_2 = 0.492 vertical surfaces, and
0.559 horizontal surfaces.

5. Combined coefficient (external surfaces, cooldown phase).

A single coefficient is used that combines the effects of natural convection and radiation. The natural convection coefficient given in the preceding section is relatively insensitive to surface orientation (horizontal or vertical) and characteristic dimension d. The combined coefficient is then a function only of surface and environment temperatures (T_s and T_∞). It is given in the following table:

T_∞ = 100°F	
T_s (°F)	h (Btu/hr-ft^2-F)
110	1.40
140	1.70
200	2.08
500	3.66
800	5.88
1000	7.92
1200	10.5
1500	15.6

T_∞ = −20°F	
T_s (°F)	h (Btu/hr-ft^2-F)
−10	0.979
20	1.29
50	1.47
100	1.72
200	2.10
500	3.43
800	5.43
1000	7.34
1200	9.76
1500	14.6

3.6.3 Maximum Internal Pressure Calculation

The calculations were based on the following assumptions:

1. Fuel data from Ref. 3.6.3-1 and 3.6.3-2.

2. Maximum burnup = 60,000 MWd/MTU.

3. Fission gas inventory determined from Ref. 3.6.3-1 database using 20-yr cooled fuel.

Isotope	Grams/Mtu	Moles/Mtu
He 4	1.149E+01	2.87
Br 81	3.592E+01	0.22
Kr 83	5.738E+01	0.69
Kr 84	2.045E+02	2.43
Kr 85	1.005E+01	0.12
Kr 86	3.164E+02	3.68
I 127	1.013E+02	0.40
I 129	3.228E+02	1.25
Xe 128	1.240E+01	0.10
Xe 130	3.942E+01	0.30
Xe 131	5.509E+02	4.21
Xe 132	2.210E+03	16.74
Xe 134	2.638E+03	19.69
Xe 136	4.074E+03	29.96
	Total	82.66

4. 30% fission gas release for normal and accident conditions.

5. 100% failure of fuel rod cladding for normal and accident conditions.

6. Cask backfilled with helium to 14.7 psia.

7. Temperature when cask closed = 70°F.

Tables 3.6.3-1 through 3.6.3-4 show internal pressures as calculated for all fuel assemblies that fit the description of the contents of packaging in Section 1.2.3. (The calculations also include some 16x16 and 17x17 assemblies, which are not currently part of the authorized contents.) The items in boldface are input to the spreadsheet, while those in regular type are calculated. For conservatism, non-fuel assembly hardware in the form of control rod and spider assemblies is included, reducing the available void volume. The only exception to this is the CE 15x15 Palisades assembly, which uses a cruciform control assembly that cannot be carried by the GA-4 cask. The tables show that the B&W 15x15 assembly gives the largest maximum normal operating pressure (MNOP) at 74 psig as well as the largest internal pressure for accident conditions at 90 psig.

The formulas used to perform the calculations in the spreadsheet are shown in Table 3.6.3-5 using the example of the B&W 15x15. In rows 39 and 40 the following constants are used:

8.775 in.	= cavity size for one assembly,
167.25 in.	= cavity length,
$40.84 \frac{\text{psia-in}^3}{\text{gm mole-°R}}$	= universal gas constant,
530°R	= temperature when cask is closed, and
	= temperature when rods pressurized.

TABLE 3.6.3-1
INTERNAL PRESSURE FOR B&W ASSEMBLIES

Assembly by Mfr.	B&W 15X15	B&W15X15 SS	B&W 17X17
Assembly Class & Data	B&W 15X15	Haddam Neck	B&W 17x17
No. Fuel rods	208	204	264
Rod diam (in.)	0.43	0.422	0.379
Rod length (in.)	153.68	126.68	151.635
Active length (in.)	141.8	120.5	143
Fuel pellet diam (in.)	0.3686	0.3825	0.3232
Clad thickness (in.)	0.0265	0.0165	0.024
Plenum length (in.)	11.72	4.81	9.52
Total free volume V1 (in3)	2.01	1.05	1.39
Initial fill pressure (psig)	415	40	435
Loading (MTU)	0.46363	0.40946	0.45619
Burnup (GWD/MTU)	60	60	60
Fission gas (g-moles/MTU)	82.7	82.7	82.7
Gas release fraction	0.3	0.3	0.3
Assembly hardware wts. (lb)			
Zircaloy	20.46	0.00	25.93
Inconel	19.93	10.52	23.06
SS	38.08	52.04	44.34
CE Ni Alloy	0.00	0.00	0.00
Assembly Hardware Volume (in3)	285.75	217.48	341.01
Control Rods			
No.	16	20	24
Diameter (in.)	0.44	0.422	0.379
Length (in.)	160	158.5	162
Volume (in3)	389.26	443.38	438.63
Spider			
Weight (lb)	7.80	7.86	9.25
Volume (in3)	27.27	27.48	32.34
Total NFAH Volume (in3)	416.53	470.86	470.97
Shielding insert volume (in3)	5028	5028	5028
Number of assemblies	4	4	4
Total cavity void volume (in3)	30136	34302	30201
Moles gas from 1 failed rod (g-moles	0.0951	0.0524	0.0718
Moles backfill gas (g-moles)	20.47	23.30	20.51
Rod failure fraction	1	1	1
Total gas moles after failure (g-mole	99.61	66.09	96.33
Max normal temp. (°F)	233	233	233
Min normal temp. (°F)	-20	-20	-20
Accident temp (°F)	360	360	360
Press. @ max normal temp. (psig)	73.94	38.50	71.38
Press. @ min normal temp. (psig)	41.58	19.08	39.96
Press. @ accident temp (psig)	90.18	48.25	87.16

TABLE 3.6.3-2
INTERNAL PRESSURE FOR CE ASSEMBLIES

Assembly by Mfr.	CE14x14 Std	CE14 x 14 Ft. C.	CE15X15	CE16X16 Lucie
Assembly Class & Data	CE14x14	Ft. Calhoun	Palisades	St. Lucie 2
No. Fuel rods	164	168	204	224
Rod diam (in.)	0.440	0.44	0.418	0.382
Rod length (in.)	147	137	140	146.5
Active length (in.)	137	128	132	136.7
Fuel pellet diam (in.)	0.3765	0.3765	0.358	0.325
Clad thickness (in.)	0.028	0.028	0.026	0.025
Plenum length (in.)	8.375	7.01	9.5	8.158
Total free volume V1 (in3)	1.58	1.39	1.60	1.20
Initial fill pressure (psig)	450	450	450	450
Loading (MTU)	0.386	0.376	0.413	0.39
Burnup (GWD/MTU)	60	60	60	60
Fission gas (g-moles/MTU)	82.7	82.7	82.7	82.7
Gas release fraction	0.3	0.3	0.3	0.3
Assembly hardware wts. (lb)				
Zircaloy	38.01	36.91	63.97	36.96
Inconel	3.00	3.00	1.81	3.00
SS	22.23	19.96	21.83	32.85
CE Ni Alloy	2.43	0.99	0.00	3.97
Assembly Hardware Volume (in3)	254.72	237.17	348.96	292.87
Control Rods				
No.	5	5	0	5
Diameter (in.)	0.948	0.948	0	0.816
Length (in.)	161	152	0	162.8
Volume (in3)	568.20	536.44	0.00	425.69
Spider				
Weight (lb)	7.50	7.50	0.00	7.50
Volume (in3)	26.22	26.22	0.00	26.22
Total NFAH Volume (in3)	594.43	562.66	0.00	451.91
Shielding insert volume (in3)	5028	5028	5028	5028
Number of assemblies	4	4	4	4
Total cavity void volume (in3)	33454	34315	34441	33490
Moles gas from 1 failed rod (g-mole	0.0924	0.0853	0.0846	0.0690
Moles backfill gas (g-moles)	22.72	23.30	23.39	22.74
Rod failure fraction	1	1	1	1
Total gas moles after failure (g-mole	83.33	80.60	92.41	84.53
Max normal temp. (°F)	233	233	233	233
Min normal temp. (°F)	-20	-20	-20	-20
Accident temp (°F)	360	360	360	360
Press. @ max normal temp. (psig)	53.67	50.02	58.46	54.51
Press. @ min normal temp. (psig)	28.71	26.39	31.75	29.25
Press. @ accident temp (psig)	66.20	61.88	71.87	67.20

TABLE 3.6.3-3
INTERNAL PRESSURE FOR EXXON ASSEMBLIES

Assembly by Mfr.	Exxon14X14 CE	Exxon14X14 WE	Exxon15x15 WE	Exxon 17x17 WE
Assembly Class & Data	CE 14x14	WE 14x14	WE 15x15	WE 17x17
No. Fuel rods	176	179	204	264
Rod diam (in.)	0.44	0.424	0.424	0.36
Rod length (in.)	146.5	149.1	152.065	152
Active length (in.)	134.06	142	144	144
Fuel pellet diam (in.)	0.37	0.3505	0.3565	0.303
Clad thickness (in.)	0.031	0.03	0.03	0.025
Plenum length (in.)	8.375	5.9	6.8	7.26
Total free volume V1 (in3)	1.57	1.69	1.32	1.03
Initial fill pressure (psig)	375	290	290	290
Loading (MTU)	0.381	0.379	0.43197	0.401
Burnup (GWD/MTU)	60	60	60	60
Fission gas (g-moles/MTU)	82.7	82.7	82.7	82.7
Gas release fraction	0.3	0.3	0.3	0.3
Assembly hardware wts. (lb)				
Zircaloy	33.15	30.42	31.83	44.75
Inconel	10.75	2.73	2.28	5.28
SS	29.52	29.39	26.00	26.31
CE Ni Alloy	0.00	0.00	0.00	0.00
Assembly Hardware Volume (in3)	277.68	238.71	231.23	296.28
Control Rods				
No.	5	16	20	24
Diameter (in.)	0.948	0.435	0.443	0.385
Length (in.)	161	158.5	158.5	160.9
Volume (in3)	568.20	376.89	488.60	449.55
Spider				
Weight (lb)	7.50	7.86	7.86	9.25
Volume (in3)	26.22	27.48	27.48	32.34
Total NFAH Volume (in3)	594.43	404.38	516.09	481.89
Shielding insert volume (in3)	5028	5028	5028	5028
Number of assemblies	4	4	4	4
Total cavity void volume (in3)	32343	33868	31004	32063
Moles gas from 1 failed rod (g-mole:	0.0820	0.0763	0.0711	0.0522
Moles backfill gas (g-moles)	21.97	23.00	21.06	21.77
Rod failure fraction	1	1	1	1
Total gas moles after failure (g-mole	79.67	77.64	79.07	76.93
Max normal temp. (°F)	233	233	233	233
Min normal temp. (°F)	-20	-20	-20	-20
Accident temp (°F)	360	360	360	360
Press. @ max normal temp. (psig)	52.72	47.95	55.06	50.97
Press. @ min normal temp. (psig)	28.10	25.08	29.59	27.00
Press. @ accident temp (psig)	65.07	59.43	67.85	63.01

TABLE 3.6.3-4
INTERNAL PRESSURE FOR WE ASSEMBLIES

Assembly by Mfr.	WE 14X14	WE14X14 OFA	WE14x14 Mod C	WE 15X15	WE 15x15 OFA	WE 17X17	WE 17X17 OFA	WE 17x17 Vant 5
Assembly Class & Data	WE 14x14	WE 14x14	CE 14x14	WE 15x15	WE 15x15	WE 17x17	WE 17x17	WE 17x17
No. Fuel rods	179	179	176	204	204	264	264	264
Rod diam (in.)	0.422	0.4	0.44	0.422	0.422	0.374	0.36	0.36
Rod length (in.)	152.4	151.85	146.44	151.88	151.85	151.6	151.635	152.3
Active length (in.)	145.2	144	136.7	144	144	144	144	144
Fuel pellet diam (in.)	0.364	0.3444	0.3805	0.3659	0.3659	0.3225	0.3088	0.3088
Clad thickness (in.)	0.0225	0.0243	0.026	0.0242	0.0242	0.0225	0.0225	0.0225
Plenum length (in.)	6.99	7.158	8.375	8.2	8.2	6.3	6.9	7.405
Total free volume V1 (in3)	1.88	1.25	1.61	1.54	1.54	1.01	0.98	1.01
Initial fill pressure (psig)	460	350	400	475	350	500	350	500
Loading (MTU)	0.407	0.358	0.397	0.469	0.4627	0.4636	0.426	0.42302
Burnup (GWD/MTU)	60	60	60	60	60	60	60	60
Fission gas (g-moles/MTU)	82.7	82.7	82.7	82.7	82.7	82.7	82.7	82.7
Gas release fraction	0.3	0.3	0.3	0.3	0.3	0.3	0.3	0.3
Assembly hardware wts. (lb)								
Zircaloy	0.00	39.18	24.14	20.70	38.26	21.00	36.49	Data lacking -
Inconel	14.46	5.64	19.25	19.31	6.39	14.67	6.11	assume same as
SS	55.99	25.85	31.85	38.90	27.19	29.59	28.60	WE 17x17 OFA
CE Ni Alloy	0.00	0.00	0.00	0.00	0.00	0.00	0.00	
Assembly Hardware Volume (in3)	244.63	272.68	276.99	287.50	276.05	240.55	272.68	273
Control Rods								
No.	16	16	5	20	20	24	24	24
Diameter (in.)	0.435	0.435	0.948	0.443	0.443	0.385	0.385	0.385
Length (in.)	158.5	158.5	161	158.5	158.5	160.9	160.9	160.9
Volume (in3)	376.89	376.89	568.20	488.60	488.60	449.55	449.55	449.55
Spider								
Weight (lb)	7.86	7.86	7.50	7.86	7.86	9.25	9.25	9.25
Volume (in3)	27.48	27.48	26.22	27.48	27.48	32.34	32.34	32.34
Total NFAH Volume (in3)	404.38	404.38	594.43	516.09	516.09	481.89	481.89	481.89
Shielding insert volume (in3)	5028	5028	5028	5028	5028	5028	5028	5028
Number of assemblies	4	4	4	4	4	4	4	4
Total cavity void volume (in3)	33655	35142	32352	30965	31014	31036	32196	32123
Moles gas from 1 failed rod (g-moles	0.0976	0.0706	0.0868	0.0919	0.0823	0.0677	0.0565	0.0639
Moles backfill gas (g-moles)	22.86	23.87	21.97	21.03	21.06	21.08	21.87	21.82
Rod failure fraction	1	1	1	1	1	1	1	1
Total gas moles after failure (g-mole	92.75	74.41	83.07	96.06	88.19	92.56	81.49	89.27
Max normal temp. (°F)	233	233	233	233	233	233	233	233
Min normal temp. (°F)	-20	-20	-20	-20	-20	-20	-20	-20
Accident temp (°F)	360	360	360	360	360	360	360	360
Press. @ max normal temp. (psig)	60.30	43.75	55.51	69.67	62.64	66.89	54.72	61.41
Press. @ min normal temp. (psig)	32.92	22.41	29.88	38.87	34.41	37.10	29.37	33.63
Press. @ accident temp (psig)	74.04	54.46	68.38	85.13	76.82	81.84	67.44	75.36

TABLE 3.6.3-5
FORMULAS USED FOR INTERNAL PRESSURE CALCULATION

	A	F
1	Assembly by Mfr.	B&W 15X15
2	Assembly Class & Data	B&W 15X15
3	No. Fuel rods	208
4	Rod diam (in.)	0.43
5	Rod length (in.)	153.68
6	Active length (in.)	141.8
7	Fuel pellet diam (in.)	0.3686
8	Clad thickness (in.)	0.0265
9	Plenum length (in.)	11.72
10	Total free volume V1 (in3)	=(PI/4)*((F4-2*F8)^2-F7^2)*F6+(PI/4)*(F4-2*F8)^2*F9
11	Initial fill pressure (psig)	415
12	Loading (MTU)	0.46363
13	Burnup (GWD/MTU)	60
14	Fission gas (g-moles/MTU)	82.7
15	Gas release fraction	0.3
16		
17	Assembly hardware wts. (lb)	
18	Zircaloy	=(8+0.64+0.64)*2.205
19	Inconel	=(1.04+1.3+4.9+1.8)*2.205
20	SS	=(7.48+8.16+0.91+0.06+0.51+0.15)*2.205
21	CE Ni Alloy	0
22		
23	Assembly Hardware Volume (in3)	=F18/0.24+F19/0.296+F20/0.286+F21/0.286
24		
25	Control Rods	
26	No.	16
27	Diameter (in.)	0.44
28	Length (in.)	160
29	Volume (in3)	=F26*(PI/4)*F27^2*F28
30		
31	Spider	
32	Weight (lb)	7.8
33	Volume (in3)	=F32/0.286
34		
35	Total NFAH Volume (in3)	=F29+F33
36		
37	Shielding insert volume (in3)	5028
38	Number of assemblies	4
39	Total cavity void volume (in3)	=4*(8.775^2*167.25)-F38*(F3*(PI/4)*F4^2*F5+F23+F35)-(4-F38)*F37
40	Moles gas from 1 failed rod (g-moles)	=(F11+14.7)*F10/40.84/530+F14*F12*F15/F3
41	Moles backfill gas (g-moles)	=14.7*F39/40.84/530
42	Rod failure fraction	1
43	Total gas moles after failure (g-moles)	=F3*F38*F42*F40+F41
44	Max normal temp. (°F)	233
45	Min normal temp. (°F)	-20
46	Accident temp (°F)	360
47	Press. @ max normal temp. (psig)	=F43*40.84*(F44+460)/(F39+F38*F42*F3*F10)-14.7
48	Press. @ min normal temp. (psig)	=(F47+14.7)*(F45+460)/(F44+460)-14.7
49	Press. @ accident temp (psig)	=(F47+14.7)*(F46+460)/(F44+460)-14.7

THIS PAGE LEFT BLANK INTENTIONALLY

3.6.4 Other Thermal Considerations

3.6.4.1 Melting of Impact Limiters. We consider a modification of the TAC2D model of Section 3.5.1.1 to check the effect of melting of the aluminum honeycomb impact limiters. See Fig. 3.6.4-1. The melting model assumes that the 0.04-in. steel skin surrounding the impact limiters remains intact except in the vicinity of the puncture where it would be torn off. Therefore, we assume the skin to be absent from the entire end impact limiter. Impact limiter material retaining a skin is replaced with air after it melts, and the heat transfer across the void occurs by convection and thermal radiation. Impact limiter material without a skin is simply replaced by the fire environment upon melting (as in ablation).

The melting point of the aluminum 5052 alloy is 1100°F (Ref. 3.2-9) and the latent heat of fusion is taken to be 171 Btu/lb (Ref. 3.6.4-1). The specific heat during melting is theoretically infinite as the material absorbs the latent heat of fusion at a constant temperature. For numerical purposes a finite temperature interval of ±10°F about the melting point is taken within which the material was considered to be melting. The effective Al specific heat during melting is thus:

$$c_p = \frac{\Delta h}{\Delta T} = \frac{171}{20} = 8.55 \text{ Btu/lb-°F.}$$

Results for the hypothetical accident with melting impact limiters show that the peak seal and average cavity temperatures are virtually the same as if melting is not considered (i.e., ~1°F difference). See Fig. 3.6.4-2. This occurs because the impact limiter absorbs heat during melting and the void regions present a thermal resistance. The assumption of no melting is therefore acceptable.

3.6.4.2 Verification of Fuel Assembly Temperature Method. The method used to calculate fuel assembly temperatures compares favorably to test data and also to the Wooten-Epstein correlation as shown below.

3.6.4.2.1 Test Data Comparison. Reference 3.6.4-2 presents experimental measurements of temperatures of standard Westinghouse 15x15 spent fuel assemblies in a 21-assembly PWR storage cask. Test run 4 utilized helium as the backfill with the cask in a horizontal configuration. Using the HYDRA (thermal analysis computer code) post-test predictions to fill in the temperatures between the data points (Fig. 5-21 of Ref. 3.6.4-2), the peak clad temperature was found to be 375°C (707°F) (assembly A1) and the corresponding enclosure temperature was 353°C (667°F). The decay heat for the assembly with these temperatures was 1 kW (3413 Btu/hr) over a 12-ft active length, or 284.4 Btu/hr-ft.

Using the GA method, the maximum rod temperature for this configuration would be calculated as follows.

Temperature rise across the gap from enclosure to edge of assembly (ΔT_2):

$$\Delta T_2 = \frac{Q'\Delta x}{k_g P},$$

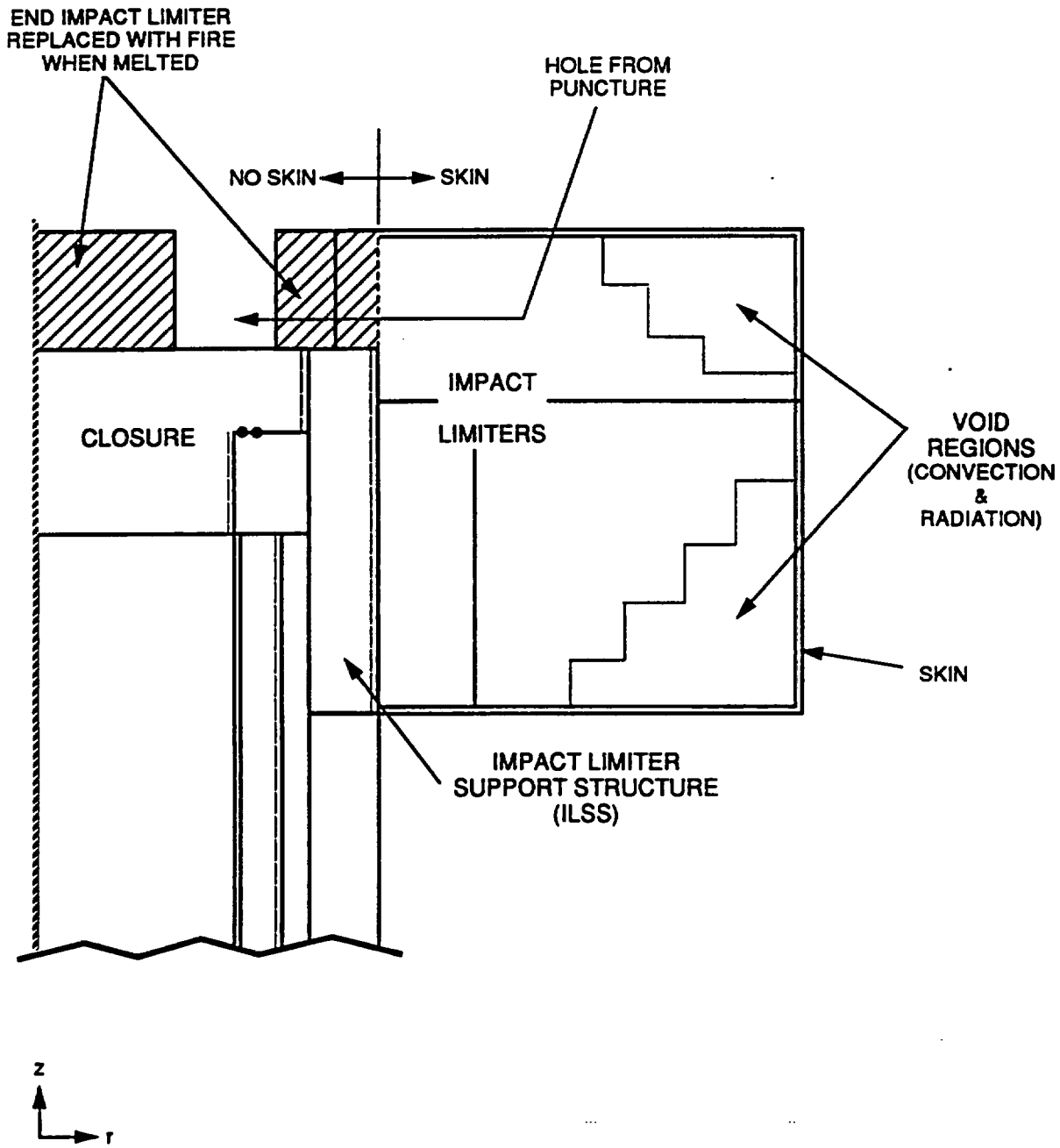

Fig. 3.6.4-1. TAC2D model with melting impact limiters

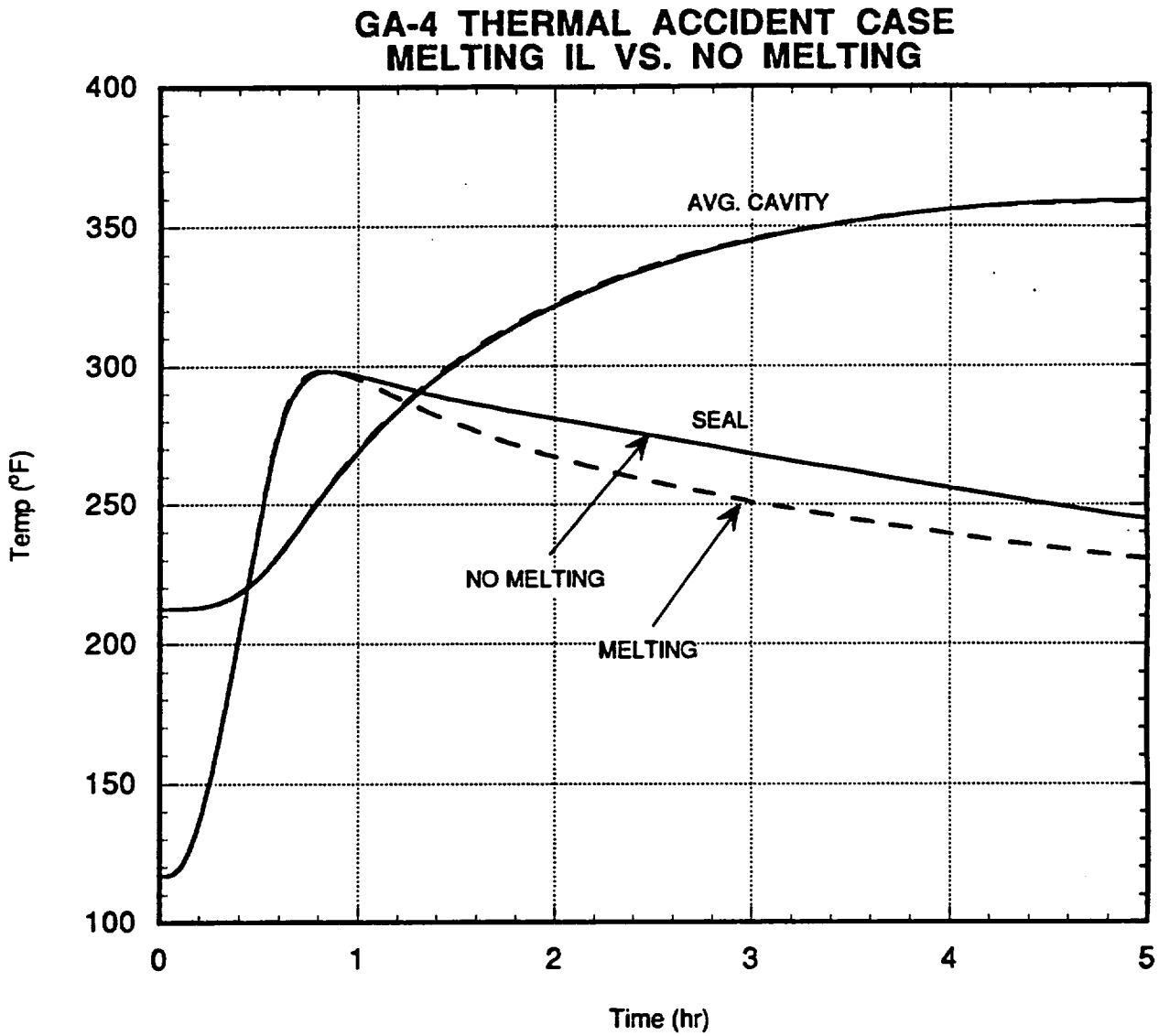

Fig. 3.6.4-2. Comparison of results for melting impact limiters

where

Q' = heat rate per unit length = 284.4 Btu/hr-ft,

Δx = gap from wall to assembly edge = 0.1745 in.,

k_g = gap (helium and radiation) conductivity, and

P = average wall perimeter = 4 x 8.6 = 34.4 in.

From Section 3.6.1.1, the gap conductivity evaluated at 667°F = 1127°R is 0.181 Btu/hr-ft-°F. Thus:

$$\Delta T_2 = 8°F.$$

For heat generation in a square assembly, the temperature rise ΔT_1 from the edge to the center is (Ref. 3.6.4-3):

$$\Delta T_1 = \frac{0.294 q''' L^2}{k_{fa}},$$

where q''' is the heat generation per unit volume, L is the half-side length, and k_{fa} is the fuel assembly effective conductivity. Since $Q' = (2L)^2 q'''$,

$$\Delta T_1 = \frac{0.0735 Q'}{k_{fa}}.$$

Using the spent fuel assembly k_r from Sec. 3.6.1.1 and evaluating at the mean assembly temperature 0.5*(707 + 667 + 8) = 691°F = 1151°R, we obtain $k_r = k_{fa} = 0.692$ Btu/hr-ft-°F. Thus:

$$\Delta T_1 = 30.2°F.$$

The center temperature is predicted to be 667 + 8 + 30 = 705°F, in good agreement with the measured value.

3.6.4.2.2 Wooten-Epstein Comparison. The Wooten-Epstein (WE) correlation was developed for spent fuel assemblies in air, whereas the GA method presumes helium. In order to facilitate a meaningful comparison, the GA method will be converted to an air medium. We will assume a 15 x 15 assembly with a rod pitch of 0.563 in. The decay heat will be taken as 617 W over an active length of 12 ft. A typical enclosure temperature of 250°F is used.

1. WE Method

$$q'' = \sigma \left[\frac{C_1}{\frac{1}{\varepsilon_1} + \frac{1}{\varepsilon_2} - 1} \right] \left(T_1^4 - T_2^4 \right) + C_2 (T_1 - T_2)^{\frac{4}{3}};$$

where

q'' = heat flux based on assembly envelope area (Btu/hr-ft^2),
σ = 0.1714×10^{-8} Btu/hr-ft^2–°R^4,
$\varepsilon_1, \varepsilon_2$ = cladding and enclosure emissivities = 0.7, 0.2 (Table 3.2-3),
C_1 = regression constant,
$= \dfrac{4N}{(N+1)^2}$ for odd values of N,
$= \dfrac{4}{N+2}$ for even values of N,
N = number of rows in assembly,
C_2 = regression constant = 0.118, and
T_1, T_2 = cladding and enclosure temperatures (°R).

The length of the assembly edge is 15 x pitch = 15 x 0.563 = 8.445 in., and the length is 12 ft. The heat flux is then

$$q'' = \frac{(617)(3.413)}{(12)(4)\left(\dfrac{8.445}{12}\right)} = 62.3.$$

With a 15 x 15 assembly, $C_1 = 0.234$. The enclosure temperature T_2 is 250°F = 710°R. Inserting all the values, the WE correlation gives:

$$62.3 = 7.39 \times 10^{-11}\left(T_1^4 - 710^4\right) + 0.118(T_1 - 710)^{\frac{4}{3}}.$$

Solving by iteration gives T_1 = 804°R = <u>344°F</u>.

2. GA Method

Temperature rise across the gap from enclosure to edge of assembly:

$$\Delta T_2 = \frac{Q'\Delta x}{k_g P},$$

where

Q' = (617)(3.413)/12 = 175.5 Btu/hr-ft,

Δx = 0.1745 in., k_g = gap (air and radiation) conductivity, and

P = average wall perimeter = 4 x 8.6 = 34.4 in.

From Section 3.6.1.1 and substituting air for helium, the gap conductivity evaluated at 250°F = 710°R is 0.0271 Btu/hr-ft-°F. Thus:

$$\Delta T_2 = 32.8°F.$$

Temperature rise from the assembly edge to center:

$$\Delta T_1 = \frac{0.0735Q'}{k_{fa}}.$$

If the expression for the fuel assembly effective conductivity from Sec. 3.6.1.1 is modified for air (substitute k_{Air} for k_{He}) and evaluated at the estimated mean temperature 300°F = 760°R, we obtain k_{fa} = 0.140 Btu/hr-ft-°F. Thus:

$$\Delta T_1 = 92.1°F.$$

The center temperature is predicted to be 250 + 32.8 + 92.1 = <u>375°F</u>. Thus, the GA method is conservative when compared to the WE correlation.

3.6.4.3 <u>Effect of a Personnel Barrier</u>. All analysis has been performed without a personnel barrier. However, use of a personnel barrier with at least 50% open area for air flow will not affect the thermal performance of the cask. This can be demonstrated by estimating the pressure drop across the personnel barrier and comparing to the buoyancy developed from natural convection, which is the main cooling mechanism. Taking a typical natural convection velocity of 1 ft/sec (see Ref. 3.6.4-4) and using the normal temperature of 100°F (density = 0.071 lb/ft^3), the velocity head $\rho V^2/2g_c$ is:

$$\frac{0.071*(1)^2}{2*32.2} = 1.1 \times 10^{-3} \text{ psf.}$$

To estimate the loss coefficient, assume the personnel barrier is a perforated grid with 50% free area and circular holes. Taking a hole diameter of 0.5 in., the Reynolds number based on the hole is:

$$Re = \frac{VD}{\nu} = \frac{2*0.5/12}{0.180 \times 10^{-3}} = 463,$$

where the velocity V is 2 ft/sec through the hole if the free area is 50%. From Ref. 3.6.4-5 the loss coefficient for this configuration may be calculated as:

$$K = \left[0.12 + 0.46(1.5 - 5)^2 \right] \frac{1}{0.5^2} = 2.3.$$

(The Ref. 3.6.4-5 parameters are $\bar{f} = 0.5$, $\zeta_\phi = 0.12$, $\bar{\varepsilon}_0^{Re} = 0.46$, and $\zeta_0 = 1.5$, evaluated at Re = 400.)

The pressure drop through the grid is then $K(\rho V^2/2g_c)$, or

$$2.3*1.1 \times 10^{-3} = 2.5 \times 10^{-3} \text{ psf.}$$

(Ref. 3.6.4-5 bases the loss coefficient on the free stream velocity head.)

The buoyancy is $(\rho_{cold} - \rho_{hot})*h$, where

ρ_{cold} = 0.071 lb/ft^3 (@ 100°F ambient),
ρ_{hot} = 0.0626 lb/ft^3 (@ 175°F, avg. skin temperature),
h = 40 in. (cask diameter),

and

$$(0.071 - 0.0626)*40/12 = 2.8 \times 10^{-2} \text{ psf.}$$

Since the pressure loss through the grid is less than 10% of the buoyancy, the natural convection cooling is essentially unaffected. Note that the partial shading effect of a grid would provide a reduction in the solar load.

It should be noted further that the velocity of 1 ft/sec used in the calculation is the typical velocity in the boundary layer adjacent the cask. To determine the pressure drop through the grid we need the free stream velocity, which is much less (theoretically zero) than the boundary layer velocity. Use of the boundary layer velocity is therefore very conservative and overestimates the effect of the grid.

3.6.4.4 Temperature Distribution for ANSYS Thermal Stress Model of FSS/Liner. In Section 2.10.9.3.4 an ANSYS analysis of the FSS/liner combination is performed to calculate thermal stresses under normal conditions of transport. The analysis uses the temperature distribution shown in Fig. 3.6.4-3. This temperature distribution is based on an earlier cask design; however, the temperatures and gradients are representative of the present cask design, and at most locations are conservative as shown below.

FSS		
Temperature or Gradient (°F)	Fig. 3.6.4-3	Present Design Fig. 3.4-4
Max. Temp	335	294
ΔT_z at center (x=0, y=9.27) from midlength (z=83.625) to bottom (z=0)	180	144
ΔT_z at radial end (x=0, y=0) from midlength to bottom	120	91
ΔT_y at midlength from center to radial end (x=0, y=0)	65	69
Liner		
Temperature or Gradient (°F)	Fig. 3.6.4-3	Present Design Fig. 3.4-4
Max. Temp	273	222
ΔT_z at corner (x=9.27, y=0) from midlength to bottom	90	60
ΔT_y at midlength from interface with FSS (x=0, y=0) to corner	25	15

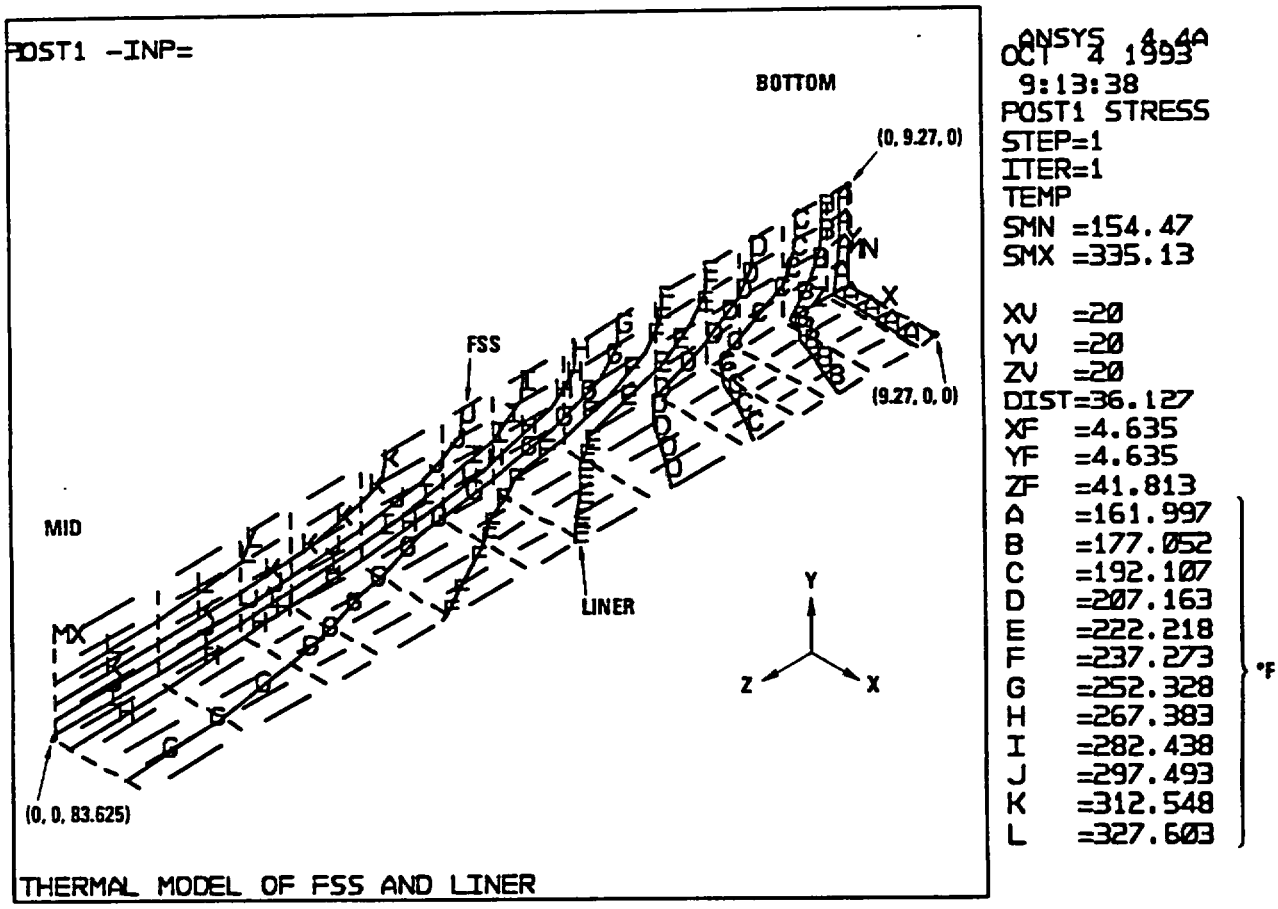

L-047(2)
10-19-93

Fig. 3.6.4-3. Temperature distribution in FSS and liner for ANSYS model of Section 2

3.6.5 Derivation of Effective Thermal Properties

This section presents detailed derivations of all effective thermal properties listed in Section 3.6.1.

3.6.5.1 TAC2D Model, Section 3.4 (Normal Conditions)

3.6.5.1.1 Spent Fuel Assembly. The spent fuel assembly (SFA) is modeled as a homogeneous, heat-generating mass. The thermal conductivities in the x and y directions (k_x, k_y) combine the effects of thermal radiation and conduction through the intermediate gas, helium. In the z direction, the thermal conductivity (k_z) accounts for conduction through the fuel and cladding. As a conservative assumption, natural convection is neglected. Owing to the horizontal position of the cask during transport, natural convection would tend to be inhibited.

Radial Conductivity k_x and k_y

As an aid to determining the radiation portion of k_x (= k_y), a computer program developed by Oak Ridge National Laboratory (ORNL) is employed (Ref. 3.6.5-1, 3.6.5-2). The program (designated TUBERAD by GA) predicts the dimensionless temperature distribution in a square array of rods as a function of the rod heating, rod diameter, pitch-to-diameter ratio (PDR) and emissivity (ε). A shroud is assumed to enclose the array, and the shroud has a dimensionless reference temperature of 0. See Fig. 3.6.5-1. The dimensionless temperature is defined as

$$Y_i = \frac{\sigma\left(T_i^{\,4} - T_s^{\,4}\right)}{q''};$$

where

Y_i = dimensionless rod temperature,

σ = Stefan-Boltzmann radiation constant,

T_i = rod temperature, deg. absolute,

T_s = shroud temperature, deg. absolute, and

q'' = reference heat flux based on total rod surface area.

All spent fuel assembly (SFA) configurations that will be shipped (see Section 1.2.3) are analyzed with this program in order to select the one with the highest predicted center rod temperature for a given assembly heat generation and shroud temperature. Although not part of the authorized contents, 16x16 and 17x17 assemblies are also included.

The program requires the pitch-diameter ratio (PDR), the fuel rod emissivity, the shroud emissivity, and the shroud dimensions. The PDR is obtained from Table 1.2-2. From Section 3.2, the fuel rod emissivity is 0.7 and the shroud emissivity is 0.2. The shroud is the fuel cavity and is 8.78 in. square.

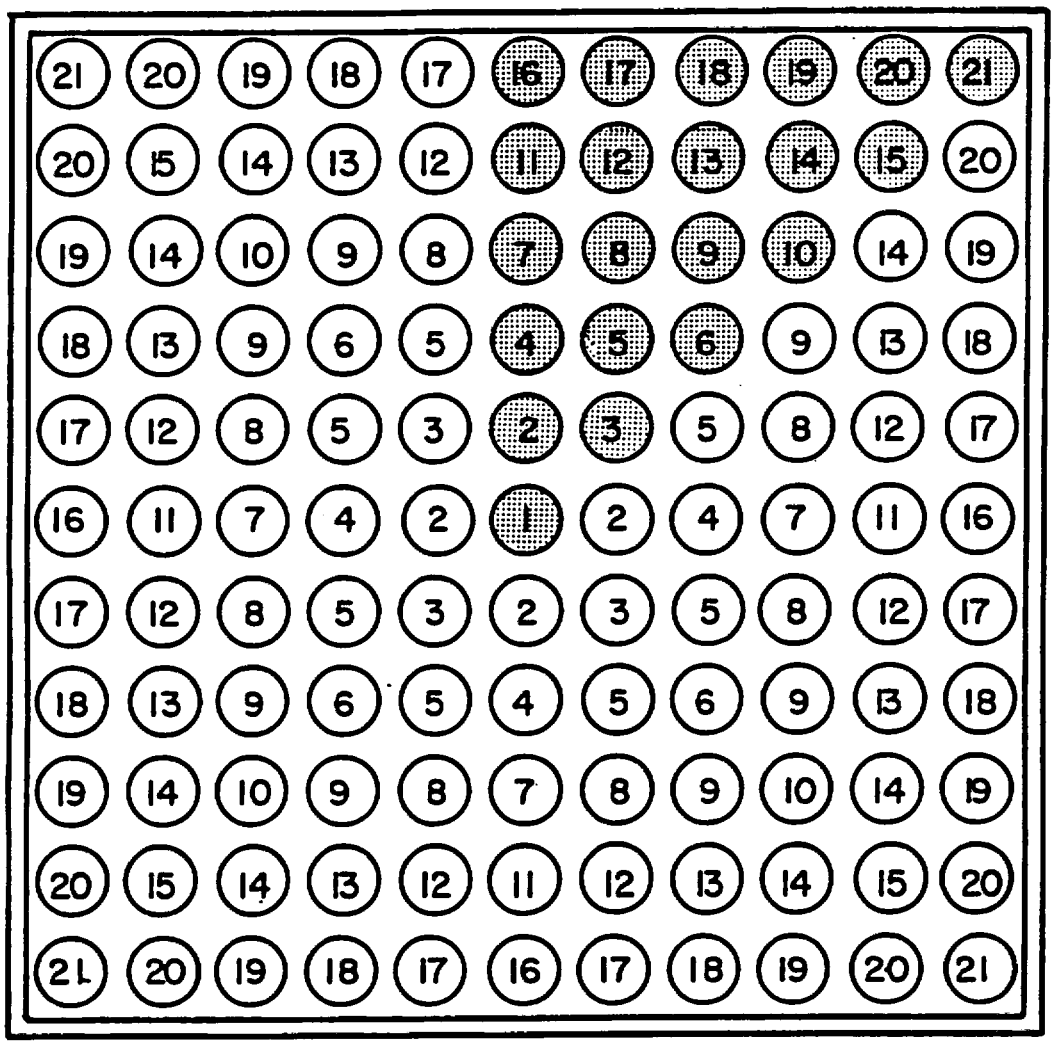

Fig. 3.6.5-1. Rod array for TUBERAD analysis

Either uniform or nonuniform radiosity may be assumed around the periphery of a rod when using the TUBERAD program. (Radiosity is the sum of emitted plus reflected radiation.) Uniform radiosity simplifies the analysis but can be significantly nonconservative in that temperatures are under-predicted, as Ref. 3.6.5-1 demonstrates by comparison to test data. However, a program restriction on using the nonuniform radiosity option is that all emissivities, including that of the shroud, must be equal. In order to approximate the effects of non-uniform radiosity but use unequal emissivities (i.e., rods different from the shroud) the following procedure recommended in Ref. 3.6.5-2 is followed for each assembly:

1. TUBERAD is run with nonuniform radiosity, taking all emissivities = 0.7. The dimensionless temperatures for each rod in the assembly are labeled as column Y1 in Figs. 3.6.5-2 to 3.6.5-13.

2. TUBERAD is then run with uniform radiosity, again with all emissivities = 0.7. These results are labeled as column Y2 in the same figures.

3. TUBERAD is then run with uniform radiosity, a rod emissivity of 0.7, and a shroud emissivity of 0.2. These results are labeled as column Y3.

4. The results of step 3 are then multiplied by the ratio of step 1 results to step 2 results. In addition, since TUBERAD assumes a unit heat flux q″, a factor is applied to put results for all assemblies on an equal <u>total</u> heat generation basis. The Westinghouse 15x15 is arbitrarily taken as the reference case with a factor of unity. The final dimensionless temperature is labeled as column Y, which is calculated as:

$$Y = \left(\frac{Y1}{Y2}\right) * Y3 * HTFAC,$$

$$\text{where } HTFAC = \frac{\text{Total rod surface area of Westinghouse 15x15}}{\text{Total rod surface area of SFA}}.$$

Figure 3.6.5-14 lists the VAX commands used to run TUBERAD for all the assemblies. The command procedure PWRTUBE.COM, which executes the above 4 steps for each assembly, is shown in Fig. 3.6.5-15. The FORTRAN program YCALC to carry out the final step is given in Fig. 3.6.5-16.

Since the values of Y are based on all assemblies generating the same total heat, the assembly with the highest Y for the center rod has the lowest effective conductivity (worst case). It is seen from the results (Figs. 3.6.5-2 to 3.6.5-13) that either the B&W 17x17 or the Westinghouse 17x17 Std element gives the highest center rod temperature (maximum Y value for surface 1) and the values of Y for the other rods are virtually identical. (Use of a 17x17 assembly for determining thermal conductivity is therefore conservative since this assembly size is not part of the authorized contents.)

CE_14X14_STD

SURFACE	Y	Y1	Y2	Y3	HTFAC
1	9.124E+01	4.774E+01	3.727E+01	6.485E+01	1.098E+00
2	8.960E+01	4.635E+01	3.629E+01	6.387E+01	1.098E+00
3	8.804E+01	4.501E+01	3.533E+01	6.291E+01	1.098E+00
4	8.628E+01	4.352E+01	3.427E+01	6.185E+01	1.098E+00
5	8.481E+01	4.229E+01	3.340E+01	6.098E+01	1.098E+00
6	8.180E+01	3.977E+01	3.161E+01	5.919E+01	1.098E+00
7	8.107E+01	3.915E+01	3.116E+01	5.874E+01	1.098E+00
8	7.976E+01	3.807E+01	3.040E+01	5.798E+01	1.098E+00
9	7.709E+01	3.587E+01	2.883E+01	5.641E+01	1.098E+00
10	7.285E+01	3.243E+01	2.639E+01	5.397E+01	1.098E+00
11	7.365E+01	3.307E+01	2.684E+01	5.442E+01	1.098E+00
12	7.257E+01	3.220E+01	2.622E+01	5.380E+01	1.098E+00
13	7.033E+01	3.041E+01	2.495E+01	5.253E+01	1.098E+00
14	6.672E+01	2.760E+01	2.297E+01	5.055E+01	1.098E+00
15	6.146E+01	2.362E+01	2.015E+01	4.773E+01	1.098E+00
16	6.367E+01	2.518E+01	2.118E+01	4.876E+01	1.098E+00
17	6.284E+01	2.455E+01	2.073E+01	4.831E+01	1.098E+00
18	6.108E+01	2.326E+01	1.983E+01	4.741E+01	1.098E+00
19	5.827E+01	2.123E+01	1.840E+01	4.598E+01	1.098E+00
20	5.403E+01	1.832E+01	1.637E+01	4.395E+01	1.098E+00
21	4.791E+01	1.439E+01	1.358E+01	4.116E+01	1.098E+00
22	4.899E+01	1.498E+01	1.395E+01	4.153E+01	1.098E+00
23	4.843E+01	1.464E+01	1.371E+01	4.129E+01	1.098E+00
24	4.719E+01	1.392E+01	1.322E+01	4.080E+01	1.098E+00
25	4.523E+01	1.280E+01	1.244E+01	4.002E+01	1.098E+00
26	4.220E+01	1.118E+01	1.132E+01	3.890E+01	1.098E+00
27	3.765E+01	8.972E+00	9.778E+00	3.736E+01	1.098E+00
28	2.955E+01	5.810E+00	7.597E+00	3.518E+01	1.098E+00

Fig. 3.6.5-2. Dimensionless temperatures for CE 14x14 Std assembly

WE_14X14_STDZC

SURFACE	Y	Y1	Y2	Y3	HTFAC
1	9.376E+01	4.774E+01	3.713E+01	6.352E+01	1.148E+00
2	9.206E+01	4.635E+01	3.614E+01	6.253E+01	1.148E+00
3	9.042E+01	4.501E+01	3.519E+01	6.158E+01	1.148E+00
4	8.859E+01	4.352E+01	3.413E+01	6.052E+01	1.148E+00
5	8.708E+01	4.229E+01	3.325E+01	5.964E+01	1.148E+00
6	8.394E+01	3.977E+01	3.147E+01	5.786E+01	1.148E+00
7	8.318E+01	3.915E+01	3.102E+01	5.741E+01	1.148E+00
8	8.183E+01	3.807E+01	3.025E+01	5.664E+01	1.148E+00
9	7.905E+01	3.587E+01	2.869E+01	5.508E+01	1.148E+00
10	7.466E+01	3.243E+01	2.625E+01	5.264E+01	1.148E+00
11	7.550E+01	3.307E+01	2.669E+01	5.308E+01	1.148E+00
12	7.438E+01	3.220E+01	2.607E+01	5.246E+01	1.148E+00
13	7.204E+01	3.041E+01	2.481E+01	5.120E+01	1.148E+00
14	6.832E+01	2.760E+01	2.282E+01	4.921E+01	1.148E+00
15	6.287E+01	2.362E+01	2.001E+01	4.640E+01	1.148E+00
16	6.518E+01	2.518E+01	2.103E+01	4.742E+01	1.148E+00
17	6.430E+01	2.455E+01	2.059E+01	4.698E+01	1.148E+00
18	6.249E+01	2.326E+01	1.969E+01	4.608E+01	1.148E+00
19	5.959E+01	2.123E+01	1.826E+01	4.465E+01	1.148E+00
20	5.525E+01	1.832E+01	1.622E+01	4.261E+01	1.148E+00
21	4.896E+01	1.439E+01	1.344E+01	3.983E+01	1.148E+00
22	5.006E+01	1.498E+01	1.381E+01	4.020E+01	1.148E+00
23	4.949E+01	1.464E+01	1.357E+01	3.996E+01	1.148E+00
24	4.824E+01	1.392E+01	1.307E+01	3.946E+01	1.148E+00
25	4.622E+01	1.280E+01	1.230E+01	3.869E+01	1.148E+00
26	4.313E+01	1.118E+01	1.118E+01	3.757E+01	1.148E+00
27	3.851E+01	8.972E+00	9.636E+00	3.603E+01	1.148E+00
28	3.028E+01	5.810E+00	7.454E+00	3.384E+01	1.148E+00

Fig. 3.6.5-3. Dimensionless temperatures for We 14x14 Std/ZC assembly

WE_14X14_OFA

SURFACE	Y	Y1	Y2	Y3	HTFAC
1	9.229E+01	4.408E+01	3.424E+01	5.930E+01	1.209E+00
2	9.063E+01	4.280E+01	3.334E+01	5.840E+01	1.209E+00
3	8.903E+01	4.157E+01	3.248E+01	5.754E+01	1.209E+00
4	8.725E+01	4.020E+01	3.151E+01	5.657E+01	1.209E+00
5	8.577E+01	3.907E+01	3.071E+01	5.577E+01	1.209E+00
6	8.273E+01	3.676E+01	2.908E+01	5.414E+01	1.209E+00
7	8.199E+01	3.619E+01	2.867E+01	5.373E+01	1.209E+00
8	8.066E+01	3.520E+01	2.798E+01	5.304E+01	1.209E+00
9	7.795E+01	3.317E+01	2.655E+01	5.161E+01	1.209E+00
10	7.366E+01	3.001E+01	2.432E+01	4.938E+01	1.209E+00
11	7.450E+01	3.061E+01	2.473E+01	4.979E+01	1.209E+00
12	7.338E+01	2.980E+01	2.417E+01	4.923E+01	1.209E+00
13	7.109E+01	2.815E+01	2.301E+01	4.807E+01	1.209E+00
14	6.747E+01	2.557E+01	2.119E+01	4.625E+01	1.209E+00
15	6.213E+01	2.191E+01	1.862E+01	4.368E+01	1.209E+00
16	6.441E+01	2.337E+01	1.958E+01	4.464E+01	1.209E+00
17	6.355E+01	2.279E+01	1.918E+01	4.424E+01	1.209E+00
18	6.177E+01	2.160E+01	1.835E+01	4.341E+01	1.209E+00
19	5.890E+01	1.972E+01	1.704E+01	4.210E+01	1.209E+00
20	5.463E+01	1.704E+01	1.517E+01	4.023E+01	1.209E+00
21	4.844E+01	1.342E+01	1.262E+01	3.768E+01	1.209E+00
22	4.976E+01	1.408E+01	1.303E+01	3.809E+01	1.209E+00
23	4.920E+01	1.376E+01	1.280E+01	3.786E+01	1.209E+00
24	4.796E+01	1.309E+01	1.234E+01	3.740E+01	1.209E+00
25	4.594E+01	1.204E+01	1.162E+01	3.668E+01	1.209E+00
26	4.288E+01	1.053E+01	1.058E+01	3.564E+01	1.209E+00
27	3.830E+01	8.475E+00	9.151E+00	3.421E+01	1.209E+00
28	3.029E+01	5.552E+00	7.135E+00	3.220E+01	1.209E+00

Fig. 3.6.5-4. Dimensionless temperatures for We 14x14 OFA assembly

EX_14X14_WE

SURFACE	Y	Y1	Y2	Y3	HTFAC
1	9.412E+01	4.831E+01	3.757E+01	6.410E+01	1.142E+00
2	9.243E+01	4.691E+01	3.657E+01	6.310E+01	1.142E+00
3	9.076E+01	4.555E+01	3.561E+01	6.214E+01	1.142E+00
4	8.893E+01	4.404E+01	3.453E+01	6.106E+01	1.142E+00
5	8.740E+01	4.279E+01	3.364E+01	6.017E+01	1.142E+00
6	8.425E+01	4.024E+01	3.183E+01	5.836E+01	1.142E+00
7	8.348E+01	3.961E+01	3.137E+01	5.790E+01	1.142E+00
8	8.212E+01	3.852E+01	3.060E+01	5.713E+01	1.142E+00
9	7.934E+01	3.629E+01	2.901E+01	5.554E+01	1.142E+00
10	7.492E+01	3.281E+01	2.654E+01	5.307E+01	1.142E+00
11	7.576E+01	3.346E+01	2.699E+01	5.352E+01	1.142E+00
12	7.462E+01	3.257E+01	2.636E+01	5.289E+01	1.142E+00
13	7.228E+01	3.076E+01	2.508E+01	5.161E+01	1.142E+00
14	6.855E+01	2.792E+01	2.307E+01	4.960E+01	1.142E+00
15	6.307E+01	2.389E+01	2.022E+01	4.675E+01	1.142E+00
16	6.537E+01	2.546E+01	2.125E+01	4.778E+01	1.142E+00
17	6.452E+01	2.483E+01	2.080E+01	4.733E+01	1.142E+00
18	6.270E+01	2.352E+01	1.988E+01	4.641E+01	1.142E+00
19	5.976E+01	2.146E+01	1.844E+01	4.497E+01	1.142E+00
20	5.540E+01	1.852E+01	1.638E+01	4.291E+01	1.142E+00
21	4.909E+01	1.454E+01	1.356E+01	4.009E+01	1.142E+00
22	5.017E+01	1.512E+01	1.392E+01	4.045E+01	1.142E+00
23	4.957E+01	1.477E+01	1.368E+01	4.021E+01	1.142E+00
24	4.834E+01	1.405E+01	1.318E+01	3.971E+01	1.142E+00
25	4.634E+01	1.292E+01	1.239E+01	3.892E+01	1.142E+00
26	4.323E+01	1.128E+01	1.126E+01	3.779E+01	1.142E+00
27	3.858E+01	9.048E+00	9.702E+00	3.623E+01	1.142E+00
28	3.032E+01	5.849E+00	7.496E+00	3.403E+01	1.142E+00

Fig. 3.6.5-5. Dimensionless temperatures for Exxon 14x14 We PWR assembly

BW_15X15

SURFACE	Y	Y1	Y2	Y3	HTFAC
1	9.228E+01	5.453E+01	4.248E+01	7.341E+01	9.792E-01
2	9.156E+01	5.383E+01	4.198E+01	7.292E+01	9.792E-01
3	9.085E+01	5.315E+01	4.150E+01	7.244E+01	9.792E-01
4	8.935E+01	5.173E+01	4.049E+01	7.142E+01	9.792E-01
5	8.867E+01	5.108E+01	4.003E+01	7.096E+01	9.792E-01
6	8.659E+01	4.911E+01	3.863E+01	6.956E+01	9.792E-01
7	8.559E+01	4.815E+01	3.794E+01	6.887E+01	9.792E-01
8	8.496E+01	4.756E+01	3.752E+01	6.845E+01	9.792E-01
9	8.307E+01	4.576E+01	3.624E+01	6.718E+01	9.792E-01
10	7.978E+01	4.269E+01	3.406E+01	6.500E+01	9.792E-01
11	8.009E+01	4.297E+01	3.425E+01	6.519E+01	9.792E-01
12	7.954E+01	4.246E+01	3.389E+01	6.483E+01	9.792E-01
13	7.783E+01	4.090E+01	3.279E+01	6.372E+01	9.792E-01
14	7.493E+01	3.823E+01	3.089E+01	6.183E+01	9.792E-01
15	7.061E+01	3.434E+01	2.813E+01	5.907E+01	9.792E-01
16	7.253E+01	3.604E+01	2.932E+01	6.026E+01	9.792E-01
17	7.206E+01	3.563E+01	2.903E+01	5.996E+01	9.792E-01
18	7.066E+01	3.437E+01	2.814E+01	5.908E+01	9.792E-01
19	6.821E+01	3.222E+01	2.662E+01	5.755E+01	9.792E-01
20	6.457E+01	2.906E+01	2.438E+01	5.532E+01	9.792E-01
21	5.933E+01	2.473E+01	2.133E+01	5.226E+01	9.792E-01
22	6.254E+01	2.725E+01	2.302E+01	5.395E+01	9.792E-01
23	6.219E+01	2.695E+01	2.281E+01	5.375E+01	9.792E-01
24	6.109E+01	2.605E+01	2.218E+01	5.312E+01	9.792E-01
25	5.918E+01	2.451E+01	2.110E+01	5.203E+01	9.792E-01
26	5.631E+01	2.223E+01	1.950E+01	5.044E+01	9.792E-01
27	5.212E+01	1.908E+01	1.729E+01	4.823E+01	9.792E-01
28	4.610E+01	1.491E+01	1.434E+01	4.528E+01	9.792E-01
29	4.802E+01	1.610E+01	1.512E+01	4.605E+01	9.792E-01
30	4.780E+01	1.594E+01	1.500E+01	4.594E+01	9.792E-01
31	4.703E+01	1.544E+01	1.466E+01	4.560E+01	9.792E-01
32	4.567E+01	1.459E+01	1.408E+01	4.501E+01	9.792E-01
33	4.362E+01	1.333E+01	1.321E+01	4.414E+01	9.792E-01
34	4.061E+01	1.159E+01	1.200E+01	4.294E+01	9.792E-01
35	3.608E+01	9.250E+00	1.037E+01	4.131E+01	9.792E-01
36	2.812E+01	5.957E+00	8.098E+00	3.904E+01	9.792E-01

Fig. 3.6.5-6. Dimensionless temperatures for B&W 15x15 We assembly

WE_15X15_STDZC

SURFACE	Y	Y1	Y2	Y3	HTFAC
1	9.282E+01	5.388E+01	4.192E+01	7.222E+01	1.000E+00
2	9.209E+01	5.320E+01	4.144E+01	7.173E+01	1.000E+00
3	9.136E+01	5.252E+01	4.096E+01	7.125E+01	1.000E+00
4	8.987E+01	5.112E+01	3.996E+01	7.025E+01	1.000E+00
5	8.920E+01	5.048E+01	3.950E+01	6.980E+01	1.000E+00
6	8.712E+01	4.854E+01	3.812E+01	6.842E+01	1.000E+00
7	8.609E+01	4.758E+01	3.744E+01	6.774E+01	1.000E+00
8	8.545E+01	4.700E+01	3.703E+01	6.732E+01	1.000E+00
9	8.354E+01	4.523E+01	3.577E+01	6.607E+01	1.000E+00
10	8.022E+01	4.220E+01	3.362E+01	6.391E+01	1.000E+00
11	8.052E+01	4.247E+01	3.381E+01	6.410E+01	1.000E+00
12	7.999E+01	4.197E+01	3.345E+01	6.375E+01	1.000E+00
13	7.829E+01	4.043E+01	3.236E+01	6.266E+01	1.000E+00
14	7.532E+01	3.779E+01	3.050E+01	6.079E+01	1.000E+00
15	7.099E+01	3.395E+01	2.777E+01	5.807E+01	1.000E+00
16	7.293E+01	3.563E+01	2.894E+01	5.924E+01	1.000E+00
17	7.247E+01	3.522E+01	2.865E+01	5.895E+01	1.000E+00
18	7.103E+01	3.398E+01	2.778E+01	5.807E+01	1.000E+00
19	6.856E+01	3.185E+01	2.628E+01	5.657E+01	1.000E+00
20	6.490E+01	2.873E+01	2.407E+01	5.437E+01	1.000E+00
21	5.967E+01	2.446E+01	2.105E+01	5.135E+01	1.000E+00
22	6.286E+01	2.695E+01	2.273E+01	5.302E+01	1.000E+00
23	6.253E+01	2.666E+01	2.252E+01	5.282E+01	1.000E+00
24	6.141E+01	2.577E+01	2.190E+01	5.219E+01	1.000E+00
25	5.949E+01	2.424E+01	2.083E+01	5.112E+01	1.000E+00
26	5.660E+01	2.199E+01	1.925E+01	4.955E+01	1.000E+00
27	5.239E+01	1.888E+01	1.707E+01	4.737E+01	1.000E+00
28	4.633E+01	1.476E+01	1.416E+01	4.445E+01	1.000E+00
29	4.829E+01	1.595E+01	1.494E+01	4.523E+01	1.000E+00
30	4.804E+01	1.579E+01	1.483E+01	4.512E+01	1.000E+00
31	4.728E+01	1.530E+01	1.449E+01	4.478E+01	1.000E+00
32	4.595E+01	1.446E+01	1.391E+01	4.420E+01	1.000E+00
33	4.387E+01	1.321E+01	1.305E+01	4.334E+01	1.000E+00
34	4.087E+01	1.149E+01	1.185E+01	4.215E+01	1.000E+00
35	3.631E+01	9.172E+00	1.024E+01	4.054E+01	1.000E+00
36	2.834E+01	5.918E+00	7.997E+00	3.829E+01	1.000E+00

Fig. 3.6.5-7. Dimensionless temperatures for We 15x15 Std/ZC assembly

EX_15X15_WE

SURFACE	Y	Y1	Y2	Y3	HTFAC
1	9.252E+01	5.388E+01	4.194E+01	7.240E+01	9.947E-01
2	9.181E+01	5.320E+01	4.145E+01	7.191E+01	9.947E-01
3	9.106E+01	5.252E+01	4.098E+01	7.143E+01	9.947E-01
4	8.958E+01	5.112E+01	3.998E+01	7.043E+01	9.947E-01
5	8.892E+01	5.048E+01	3.952E+01	6.998E+01	9.947E-01
6	8.685E+01	4.854E+01	3.814E+01	6.860E+01	9.947E-01
7	8.581E+01	4.758E+01	3.746E+01	6.792E+01	9.947E-01
8	8.518E+01	4.700E+01	3.705E+01	6.750E+01	9.947E-01
9	8.328E+01	4.523E+01	3.579E+01	6.625E+01	9.947E-01
10	7.997E+01	4.220E+01	3.364E+01	6.409E+01	9.947E-01
11	8.027E+01	4.247E+01	3.383E+01	6.428E+01	9.947E-01
12	7.974E+01	4.197E+01	3.347E+01	6.393E+01	9.947E-01
13	7.805E+01	4.043E+01	3.238E+01	6.284E+01	9.947E-01
14	7.512E+01	3.779E+01	3.051E+01	6.097E+01	9.947E-01
15	7.079E+01	3.395E+01	2.779E+01	5.825E+01	9.947E-01
16	7.272E+01	3.563E+01	2.896E+01	5.942E+01	9.947E-01
17	7.226E+01	3.522E+01	2.867E+01	5.913E+01	9.947E-01
18	7.082E+01	3.398E+01	2.780E+01	5.825E+01	9.947E-01
19	6.836E+01	3.185E+01	2.630E+01	5.675E+01	9.947E-01
20	6.471E+01	2.873E+01	2.409E+01	5.455E+01	9.947E-01
21	5.951E+01	2.446E+01	2.107E+01	5.153E+01	9.947E-01
22	6.269E+01	2.695E+01	2.275E+01	5.320E+01	9.947E-01
23	6.236E+01	2.666E+01	2.254E+01	5.300E+01	9.947E-01
24	6.124E+01	2.577E+01	2.192E+01	5.237E+01	9.947E-01
25	5.933E+01	2.424E+01	2.085E+01	5.130E+01	9.947E-01
26	5.645E+01	2.199E+01	1.927E+01	4.973E+01	9.947E-01
27	5.225E+01	1.888E+01	1.709E+01	4.755E+01	9.947E-01
28	4.621E+01	1.476E+01	1.418E+01	4.463E+01	9.947E-01
29	4.816E+01	1.595E+01	1.496E+01	4.541E+01	9.947E-01
30	4.791E+01	1.579E+01	1.485E+01	4.530E+01	9.947E-01
31	4.716E+01	1.530E+01	1.451E+01	4.496E+01	9.947E-01
32	4.583E+01	1.446E+01	1.393E+01	4.438E+01	9.947E-01
33	4.375E+01	1.321E+01	1.307E+01	4.352E+01	9.947E-01
34	4.076E+01	1.149E+01	1.187E+01	4.233E+01	9.947E-01
35	3.621E+01	9.172E+00	1.026E+01	4.072E+01	9.947E-01
36	2.825E+01	5.918E+00	8.016E+00	3.847E+01	9.947E-01

Fig. 3.6.5-8. Dimensionless temperatures for Exxon 15x15 We assembly

CE_15X15

SURFACE	Y	Y1	Y2	Y3	HTFAC
1	9.395E+01	5.453E+01	4.237E+01	7.242E+01	1.008E+00
2	9.320E+01	5.383E+01	4.188E+01	7.193E+01	1.008E+00
3	9.249E+01	5.315E+01	4.139E+01	7.145E+01	1.008E+00
4	9.095E+01	5.173E+01	4.038E+01	7.043E+01	1.008E+00
5	9.025E+01	5.108E+01	3.992E+01	6.997E+01	1.008E+00
6	8.812E+01	4.911E+01	3.852E+01	6.857E+01	1.008E+00
7	8.709E+01	4.815E+01	3.783E+01	6.788E+01	1.008E+00
8	8.645E+01	4.756E+01	3.741E+01	6.746E+01	1.008E+00
9	8.450E+01	4.576E+01	3.613E+01	6.619E+01	1.008E+00
10	8.111E+01	4.269E+01	3.396E+01	6.401E+01	1.008E+00
11	8.143E+01	4.297E+01	3.415E+01	6.420E+01	1.008E+00
12	8.089E+01	4.246E+01	3.378E+01	6.384E+01	1.008E+00
13	7.914E+01	4.090E+01	3.268E+01	6.273E+01	1.008E+00
14	7.615E+01	3.823E+01	3.079E+01	6.084E+01	1.008E+00
15	7.173E+01	3.434E+01	2.803E+01	5.808E+01	1.008E+00
16	7.372E+01	3.604E+01	2.921E+01	5.927E+01	1.008E+00
17	7.323E+01	3.563E+01	2.892E+01	5.897E+01	1.008E+00
18	7.180E+01	3.437E+01	2.803E+01	5.809E+01	1.008E+00
19	6.929E+01	3.222E+01	2.651E+01	5.656E+01	1.008E+00
20	6.555E+01	2.906E+01	2.428E+01	5.433E+01	1.008E+00
21	6.023E+01	2.473E+01	2.122E+01	5.127E+01	1.008E+00
22	6.350E+01	2.725E+01	2.291E+01	5.296E+01	1.008E+00
23	6.314E+01	2.695E+01	2.270E+01	5.276E+01	1.008E+00
24	6.202E+01	2.605E+01	2.207E+01	5.213E+01	1.008E+00
25	6.008E+01	2.451E+01	2.099E+01	5.104E+01	1.008E+00
26	5.715E+01	2.223E+01	1.939E+01	4.945E+01	1.008E+00
27	5.285E+01	1.908E+01	1.719E+01	4.724E+01	1.008E+00
28	4.678E+01	1.491E+01	1.423E+01	4.429E+01	1.008E+00
29	4.872E+01	1.610E+01	1.501E+01	4.506E+01	1.008E+00
30	4.847E+01	1.594E+01	1.490E+01	4.495E+01	1.008E+00
31	4.769E+01	1.544E+01	1.456E+01	4.461E+01	1.008E+00
32	4.634E+01	1.459E+01	1.397E+01	4.402E+01	1.008E+00
33	4.426E+01	1.333E+01	1.310E+01	4.315E+01	1.008E+00
34	4.122E+01	1.159E+01	1.189E+01	4.195E+01	1.008E+00
35	3.664E+01	9.250E+00	1.026E+01	4.032E+01	1.008E+00
36	2.859E+01	5.957E+00	7.992E+00	3.805E+01	1.008E+00

Fig. 3.6.5-9. Dimensionless temperatures for CE 15x15 assembly

CE_16X16_LUCIE

SURFACE	Y	Y1	Y2	Y3	HTFAC
1	9.836E+01	6.103E+01	4.712E+01	7.838E+01	9.689E-01
2	9.697E+01	5.965E+01	4.613E+01	7.740E+01	9.689E-01
3	9.559E+01	5.830E+01	4.517E+01	7.644E+01	9.689E-01
4	9.407E+01	5.683E+01	4.413E+01	7.540E+01	9.689E-01
5	9.278E+01	5.557E+01	4.323E+01	7.450E+01	9.689E-01
6	9.012E+01	5.299E+01	4.140E+01	7.267E+01	9.689E-01
7	8.963E+01	5.251E+01	4.105E+01	7.232E+01	9.689E-01
8	8.843E+01	5.136E+01	4.024E+01	7.151E+01	9.689E-01
9	8.600E+01	4.904E+01	3.859E+01	6.985E+01	9.689E-01
10	8.223E+01	4.544E+01	3.603E+01	6.730E+01	9.689E-01
11	8.343E+01	4.656E+01	3.681E+01	6.808E+01	9.689E-01
12	8.236E+01	4.557E+01	3.612E+01	6.738E+01	9.689E-01
13	8.024E+01	4.357E+01	3.470E+01	6.596E+01	9.689E-01
14	7.692E+01	4.046E+01	3.250E+01	6.377E+01	9.689E-01
15	7.222E+01	3.614E+01	2.943E+01	6.070E+01	9.689E-01
16	7.517E+01	3.881E+01	3.130E+01	6.257E+01	9.689E-01
17	7.431E+01	3.802E+01	3.074E+01	6.201E+01	9.689E-01
18	7.253E+01	3.641E+01	2.961E+01	6.088E+01	9.689E-01
19	6.975E+01	3.392E+01	2.785E+01	5.911E+01	9.689E-01
20	6.581E+01	3.043E+01	2.538E+01	5.665E+01	9.689E-01
21	6.031E+01	2.577E+01	2.209E+01	5.336E+01	9.689E-01
22	6.449E+01	2.917E+01	2.439E+01	5.566E+01	9.689E-01
23	6.383E+01	2.861E+01	2.400E+01	5.527E+01	9.689E-01
24	6.245E+01	2.746E+01	2.320E+01	5.446E+01	9.689E-01
25	6.031E+01	2.568E+01	2.195E+01	5.321E+01	9.689E-01
26	5.722E+01	2.317E+01	2.019E+01	5.146E+01	9.689E-01
27	5.282E+01	1.979E+01	1.782E+01	4.909E+01	9.689E-01
28	4.664E+01	1.540E+01	1.471E+01	4.598E+01	9.689E-01
29	4.932E+01	1.713E+01	1.586E+01	4.713E+01	9.689E-01
30	4.889E+01	1.683E+01	1.565E+01	4.692E+01	9.689E-01
31	4.794E+01	1.620E+01	1.522E+01	4.649E+01	9.689E-01
32	4.646E+01	1.522E+01	1.454E+01	4.581E+01	9.689E-01
33	4.426E+01	1.384E+01	1.359E+01	4.486E+01	9.689E-01
34	4.108E+01	1.197E+01	1.230E+01	4.357E+01	9.689E-01
35	3.645E+01	9.511E+00	1.058E+01	4.185E+01	9.689E-01
36	2.834E+01	6.096E+00	8.231E+00	3.950E+01	9.689E-01

Fig. 3.6.5-10. Dimensionless temperatures for CE 16x16 Lucie 2 assembly

BW_17X17

SURFACE	Y	Y1	Y2	Y3	HTFAC
1	9.871E+01	6.864E+01	5.294E+01	8.793E+01	8.658E-01
2	9.807E+01	6.794E+01	5.245E+01	8.744E+01	8.658E-01
3	9.745E+01	6.726E+01	5.196E+01	8.695E+01	8.658E-01
4	9.616E+01	6.585E+01	5.096E+01	8.595E+01	8.658E-01
5	9.556E+01	6.519E+01	5.049E+01	8.548E+01	8.658E-01
6	9.373E+01	6.320E+01	4.908E+01	8.407E+01	8.658E-01
7	9.290E+01	6.229E+01	4.843E+01	8.342E+01	8.658E-01
8	9.234E+01	6.168E+01	4.799E+01	8.298E+01	8.658E-01
9	9.062E+01	5.982E+01	4.667E+01	8.166E+01	8.658E-01
10	8.770E+01	5.667E+01	4.444E+01	7.943E+01	8.658E-01
11	8.818E+01	5.718E+01	4.479E+01	7.978E+01	8.658E-01
12	8.769E+01	5.664E+01	4.440E+01	7.939E+01	8.658E-01
13	8.613E+01	5.497E+01	4.322E+01	7.821E+01	8.658E-01
14	8.347E+01	5.214E+01	4.121E+01	7.620E+01	8.658E-01
15	7.960E+01	4.805E+01	3.831E+01	7.330E+01	8.658E-01
16	8.184E+01	5.040E+01	3.997E+01	7.496E+01	8.658E-01
17	8.140E+01	4.993E+01	3.963E+01	7.462E+01	8.658E-01
18	8.004E+01	4.851E+01	3.863E+01	7.362E+01	8.658E-01
19	7.772E+01	4.608E+01	3.691E+01	7.190E+01	8.658E-01
20	7.433E+01	4.257E+01	3.442E+01	6.941E+01	8.658E-01
21	6.966E+01	3.784E+01	3.107E+01	6.606E+01	8.658E-01
22	7.359E+01	4.178E+01	3.383E+01	6.882E+01	8.658E-01
23	7.322E+01	4.141E+01	3.357E+01	6.856E+01	8.658E-01
24	7.209E+01	4.027E+01	3.277E+01	6.776E+01	8.658E-01
25	7.019E+01	3.834E+01	3.140E+01	6.639E+01	8.658E-01
26	6.734E+01	3.553E+01	2.942E+01	6.440E+01	8.658E-01
27	6.341E+01	3.172E+01	2.673E+01	6.172E+01	8.658E-01
28	5.806E+01	2.675E+01	2.322E+01	5.821E+01	8.658E-01
29	6.305E+01	3.123E+01	2.627E+01	6.126E+01	8.658E-01
30	6.278E+01	3.097E+01	2.609E+01	6.108E+01	8.658E-01
31	6.192E+01	3.016E+01	2.552E+01	6.051E+01	8.658E-01
32	6.044E+01	2.879E+01	2.456E+01	5.955E+01	8.658E-01
33	5.822E+01	2.678E+01	2.316E+01	5.815E+01	8.658E-01
34	5.513E+01	2.406E+01	2.125E+01	5.624E+01	8.658E-01
35	5.083E+01	2.047E+01	1.873E+01	5.372E+01	8.658E-01
36	4.477E+01	1.586E+01	1.548E+01	5.047E+01	8.658E-01
37	4.819E+01	1.825E+01	1.707E+01	5.206E+01	8.658E-01
38	4.798E+01	1.810E+01	1.697E+01	5.196E+01	8.658E-01
39	4.738E+01	1.766E+01	1.667E+01	5.166E+01	8.658E-01
40	4.636E+01	1.691E+01	1.615E+01	5.114E+01	8.658E-01
41	4.481E+01	1.581E+01	1.539E+01	5.038E+01	8.658E-01
42	4.258E+01	1.431E+01	1.436E+01	4.935E+01	8.658E-01
43	3.943E+01	1.233E+01	1.299E+01	4.798E+01	8.658E-01
44	3.484E+01	9.757E+00	1.120E+01	4.619E+01	8.658E-01
45	2.692E+01	6.228E+00	8.764E+00	4.375E+01	8.658E-01

Fig. 3.6.5-11. Dimensionless temperatures for B&W 17x17 assembly

WE_17X17_STD

SURFACE	Y	Y1	Y2	Y3	HTFAC
1	9.871E+01	6.782E+01	5.229E+01	8.686E+01	8.762E-01
2	9.809E+01	6.714E+01	5.180E+01	8.638E+01	8.762E-01
3	9.746E+01	6.646E+01	5.132E+01	8.590E+01	8.762E-01
4	9.617E+01	6.507E+01	5.033E+01	8.490E+01	8.762E-01
5	9.557E+01	6.442E+01	4.987E+01	8.444E+01	8.762E-01
6	9.375E+01	6.245E+01	4.847E+01	8.305E+01	8.762E-01
7	9.292E+01	6.155E+01	4.783E+01	8.241E+01	8.762E-01
8	9.236E+01	6.095E+01	4.740E+01	8.198E+01	8.762E-01
9	9.065E+01	5.912E+01	4.610E+01	8.068E+01	8.762E-01
10	8.774E+01	5.601E+01	4.389E+01	7.847E+01	8.762E-01
11	8.819E+01	5.651E+01	4.425E+01	7.882E+01	8.762E-01
12	8.770E+01	5.597E+01	4.386E+01	7.844E+01	8.762E-01
13	8.614E+01	5.433E+01	4.270E+01	7.727E+01	8.762E-01
14	8.350E+01	5.153E+01	4.071E+01	7.529E+01	8.762E-01
15	7.962E+01	4.749E+01	3.785E+01	7.243E+01	8.762E-01
16	8.188E+01	4.982E+01	3.948E+01	7.406E+01	8.762E-01
17	8.141E+01	4.935E+01	3.916E+01	7.373E+01	8.762E-01
18	8.008E+01	4.795E+01	3.816E+01	7.274E+01	8.762E-01
19	7.774E+01	4.555E+01	3.647E+01	7.104E+01	8.762E-01
20	7.436E+01	4.208E+01	3.401E+01	6.859E+01	8.762E-01
21	6.970E+01	3.741E+01	3.070E+01	6.528E+01	8.762E-01
22	7.362E+01	4.130E+01	3.343E+01	6.801E+01	8.762E-01
23	7.325E+01	4.093E+01	3.317E+01	6.775E+01	8.762E-01
24	7.213E+01	3.981E+01	3.238E+01	6.696E+01	8.762E-01
25	7.021E+01	3.790E+01	3.103E+01	6.561E+01	8.762E-01
26	6.737E+01	3.512E+01	2.907E+01	6.365E+01	8.762E-01
27	6.344E+01	3.136E+01	2.642E+01	6.100E+01	8.762E-01
28	5.809E+01	2.646E+01	2.296E+01	5.753E+01	8.762E-01
29	6.309E+01	3.089E+01	2.598E+01	6.056E+01	8.762E-01
30	6.278E+01	3.062E+01	2.580E+01	6.037E+01	8.762E-01
31	6.194E+01	2.983E+01	2.524E+01	5.982E+01	8.762E-01
32	6.046E+01	2.847E+01	2.429E+01	5.887E+01	8.762E-01
33	5.826E+01	2.649E+01	2.290E+01	5.748E+01	8.762E-01
34	5.515E+01	2.380E+01	2.102E+01	5.559E+01	8.762E-01
35	5.085E+01	2.025E+01	1.853E+01	5.311E+01	8.762E-01
36	4.480E+01	1.570E+01	1.532E+01	4.989E+01	8.762E-01
37	4.823E+01	1.808E+01	1.691E+01	5.148E+01	8.762E-01
38	4.805E+01	1.794E+01	1.681E+01	5.139E+01	8.762E-01
39	4.745E+01	1.750E+01	1.651E+01	5.109E+01	8.762E-01
40	4.641E+01	1.676E+01	1.600E+01	5.057E+01	8.762E-01
41	4.485E+01	1.567E+01	1.525E+01	4.982E+01	8.762E-01
42	4.264E+01	1.418E+01	1.422E+01	4.880E+01	8.762E-01
43	3.947E+01	1.222E+01	1.287E+01	4.744E+01	8.762E-01
44	3.491E+01	9.676E+00	1.109E+01	4.567E+01	8.762E-01
45	2.699E+01	6.186E+00	8.689E+00	4.327E+01	8.762E-01

Fig. 3.6.5-12. Dimensionless temperatures for We 17x17 Std assembly

WE_17X17_OFA

SURFACE	Y	Y1	Y2	Y3	HTFAC
1	9.771E+01	6.402E+01	4.928E+01	8.251E+01	9.115E-01
2	9.709E+01	6.337E+01	4.882E+01	8.206E+01	9.115E-01
3	9.649E+01	6.274E+01	4.837E+01	8.161E+01	9.115E-01
4	9.521E+01	6.142E+01	4.744E+01	8.068E+01	9.115E-01
5	9.462E+01	6.081E+01	4.701E+01	8.025E+01	9.115E-01
6	9.283E+01	5.897E+01	4.571E+01	7.894E+01	9.115E-01
7	9.200E+01	5.812E+01	4.511E+01	7.834E+01	9.115E-01
8	9.145E+01	5.755E+01	4.471E+01	7.794E+01	9.115E-01
9	8.978E+01	5.583E+01	4.349E+01	7.672E+01	9.115E-01
10	8.692E+01	5.290E+01	4.142E+01	7.466E+01	9.115E-01
11	8.740E+01	5.338E+01	4.175E+01	7.499E+01	9.115E-01
12	8.690E+01	5.287E+01	4.139E+01	7.463E+01	9.115E-01
13	8.536E+01	5.132E+01	4.030E+01	7.354E+01	9.115E-01
14	8.276E+01	4.869E+01	3.844E+01	7.168E+01	9.115E-01
15	7.894E+01	4.488E+01	3.576E+01	6.900E+01	9.115E-01
16	8.115E+01	4.708E+01	3.730E+01	7.053E+01	9.115E-01
17	8.072E+01	4.664E+01	3.699E+01	7.023E+01	9.115E-01
18	7.938E+01	4.532E+01	3.606E+01	6.929E+01	9.115E-01
19	7.709E+01	4.306E+01	3.447E+01	6.770E+01	9.115E-01
20	7.373E+01	3.979E+01	3.217E+01	6.540E+01	9.115E-01
21	6.915E+01	3.540E+01	2.907E+01	6.230E+01	9.115E-01
22	7.304E+01	3.907E+01	3.163E+01	6.487E+01	9.115E-01
23	7.266E+01	3.872E+01	3.139E+01	6.462E+01	9.115E-01
24	7.155E+01	3.766E+01	3.065E+01	6.388E+01	9.115E-01
25	6.967E+01	3.586E+01	2.938E+01	6.262E+01	9.115E-01
26	6.687E+01	3.324E+01	2.754E+01	6.078E+01	9.115E-01
27	6.300E+01	2.970E+01	2.505E+01	5.829E+01	9.115E-01
28	5.769E+01	2.507E+01	2.180E+01	5.503E+01	9.115E-01
29	6.264E+01	2.928E+01	2.467E+01	5.790E+01	9.115E-01
30	6.238E+01	2.903E+01	2.449E+01	5.773E+01	9.115E-01
31	6.153E+01	2.828E+01	2.397E+01	5.721E+01	9.115E-01
32	6.002E+01	2.699E+01	2.308E+01	5.631E+01	9.115E-01
33	5.785E+01	2.512E+01	2.177E+01	5.500E+01	9.115E-01
34	5.481E+01	2.258E+01	1.999E+01	5.323E+01	9.115E-01
35	5.054E+01	1.923E+01	1.765E+01	5.089E+01	9.115E-01
36	4.456E+01	1.494E+01	1.463E+01	4.787E+01	9.115E-01
37	4.810E+01	1.729E+01	1.620E+01	4.944E+01	9.115E-01
38	4.788E+01	1.715E+01	1.611E+01	4.934E+01	9.115E-01
39	4.732E+01	1.674E+01	1.582E+01	4.906E+01	9.115E-01
40	4.629E+01	1.603E+01	1.533E+01	4.857E+01	9.115E-01
41	4.473E+01	1.499E+01	1.462E+01	4.786E+01	9.115E-01
42	4.251E+01	1.358E+01	1.365E+01	4.688E+01	9.115E-01
43	3.938E+01	1.171E+01	1.236E+01	4.560E+01	9.115E-01
44	3.481E+01	9.289E+00	1.068E+01	4.391E+01	9.115E-01
45	2.704E+01	5.988E+00	8.405E+00	4.164E+01	9.115E-01

Fig. 3.6.5-13. Dimensionless temperatures for We 17x17 OFA assembly

```
                P1  P2   P3  P4    P5       P6

$ @PWRTUBE 14 1.32 0.7 0.2 0.0394 CE_14X14_STD
$ @PWRTUBE 14 1.32 0.7 0.2 0.0377 WE_14X14_STDZC
$ @PWRTUBE 14 1.39 0.7 0.2 0.0358 WE_14X14_OFA
$ @PWRTUBE 14 1.31 0.7 0.2 0.0379 EX_14X14_WE
$ @PWRTUBE 15 1.32 0.7 0.2 0.0385 BW_15X15
$ @PWRTUBE 15 1.33 0.7 0.2 0.0377 WE_15X15_STDZC
$ @PWRTUBE 15 1.33 0.7 0.2 0.0379 EX_15X15_WE
$ @PWRTUBE 15 1.32 0.7 0.2 0.0374 CE_15X15
$ @PWRTUBE 16 1.32 0.7 0.2 0.0342 CE_16X16_LUCIE
$ @PWRTUBE 17 1.32 0.7 0.2 0.0339 BW_17X17
$ @PWRTUBE 17 1.33 0.7 0.2 0.0335 WE_17X17_STD
$ @PWRTUBE 17 1.38 0.7 0.2 0.0322 WE_17X17_OFA
```

Parameter definitions:

P1	Array size
P2	Pitch-Diameter ratio
P3	Rod emissivity
P4	Shroud emissivity
P5	Single rod area/Shroud area
P6	Assembly name

Fig. 3.6.5-14. VAX/VMS commands to run TUBERAD

```
$ IF P6 .EQS. "" THEN INQUIRE P6 "PROBLEM NAME?"
$ IF P6 .NES. "" THEN GOTO CONT
$ WRITE SYS$OUTPUT "MODEL NAME MISSING, JOB TERMINATED"
$ GOTO END
$ CONT:
$ NRODS = P1*P1
$ OPEN/WRITE INPUT TUBERAD.IN
$ WRITE INPUT P6," NON-UNIFORM RADIOSITY, EMTUBE = EMSHROUD"
$ WRITE INPUT "    2    2    1    2    1    1    1"
$ WRITE INPUT "   ",P1,"  ",NRODS                                  STEP 1
$ WRITE INPUT P2,"     ",P3,"       ",P3,"       ",P5
$ CLOSE INPUT
$ TUBERAD
$ RENAME TUBERAD.OUT 'P6'.OUT1
$ OPEN/WRITE INPUT TUBERAD.IN
$ WRITE INPUT P6," UNIFORM RADIOSITY, EMTUBE = EMSHROUD"
$ WRITE INPUT "    1    2    1    1    1    1    1"
$ WRITE INPUT "   ",P1,"  ",NRODS                                  STEP 2
$ WRITE INPUT P2,"     ",P3,"       ",P3,"       ",P5
$ CLOSE INPUT
$ TUBERAD
$ RENAME TUBERAD.OUT 'P6'.OUT2
$ OPEN/WRITE INPUT TUBERAD.IN
$ WRITE INPUT P6," UNIFORM RADIOSITY, EMTUBE /= EMSHROUD"
$ WRITE INPUT "    1    2    1    1    1    1    1"
$ WRITE INPUT "   ",P1,"  ",NRODS                                  STEP 3
$ WRITE INPUT P2,"     ",P3,"       ",P4,"       ",P5
$ CLOSE INPUT
$ TUBERAD
$ RENAME TUBERAD.OUT 'P6'.OUT3
$ ASSIGN TUBERAD.IN FOR016
$ ASSIGN 'P6'.OUT1 FOR017
$ ASSIGN 'P6'.OUT2 FOR018                                           STEP 4
$ ASSIGN 'P6'.OUT3 FOR019
$ ASSIGN 'P6'.YTEMS FOR020
$ RUN YCALC
$ END:
```

Fig. 3.6.5-15. VAX/VMS command procedure PWRTUBE.COM

```
      CHARACTER*1 CHAR(80)
      READ (16,100) CHAR
      DO I=1,80
      IF (CHAR(I).EQ.' ') THEN
        NC=I-1
        GO TO 4
      ENDIF
      ENDDO
    4 READ (16,101) NROWS,AR
      M=0
      I2=(NROWS+1)/2
      DO 5 I=1,I2
    5 M=M+I
C     SCALE ALL DIMENSIONLESS TEMPERATURES 'Y' SO THAT THEY ARE BASED ON
C     THE SAME TOTAL HEAT.  USE W15 X 15 STD/ZC ASSEMBLY AS A REFERENCE.
C     0.0377 = SINGLE TUBE AREA/SHROUD AREA FOR W15 X 15
C            = PI*0.422/(4*8.78)
      HTFAC = (225./NROWS**2)*(0.0377/AR)
C     SKIP LINES IN OUTPUT FILE TO GET TO 'Y's
      READ (17,102)
      DO 6 I=1,13
      READ (17,102)
      READ (18,102)
    6 READ (19,102)
      WRITE (20,105) (CHAR(I),I=1,NC)
      DO 7 I=1,M
      READ (17,103) Y1  ! NON-UNIF RADIOSITY, EMTUBE = ESHROUD
      READ (18,103) Y2  ! UNIF RADIOSITY, EMTUBE = EMSHROUD
      READ (19,103) Y3  ! UNIF RADIOSITY, EMTUBE /= EMSHROUD
      Y = (Y1/Y2)*Y3*HTFAC
    7 WRITE (20,104) I,Y,Y1,Y2,Y3,HTFAC
      STOP
  100 FORMAT (80A1)
  101 FORMAT (/,I5,/,30X,E10.4)
  102 FORMAT ()
  103 FORMAT (58X,E9.3)
  104 FORMAT (1X,I4,6X,5(1PE12.3))
  105 FORMAT (30X,<NC>A1,/////,1X,'SURFACE',9X,'Y',12X,'Y1',10X,'Y2',
     >10X,'Y3',8X,'HTFAC',/)
      END
```

Fig. 3.6.5-16. Program YCALC

Having thus generated the temperature distribution due to thermal radiation for the worst-case assembly, the next step is to use this information to calculate the effective thermal conductivity. To accomplish this, a small TAC2D model is constructed to represent a 1/4-section of a 17x17 SFA together with the shroud. The model is shown in Fig. 3.6.5-17. Each nodal cell in the model represents a single fuel rod. Since the heat transfer is entirely by thermal radiation, the SFA and gap thermal conductivities are assumed to be of the form $k = CT^3$ where T is degrees absolute and C is a constant to be determined. The total SFA heat generation rates used are 617 W (maximum) and 308 W. Since the Y values are referenced to the Westinghouse 15x15 assembly, the heat flux q″ used to calculate actual rod temperatures is based on this assembly's rod area. The shroud temperature is taken as 200°F and 300°F.

With these boundary conditions, the constant C is varied for the SFA and gap conductivities until the temperature distribution predicted by the TAC2D model agrees as closely as possible with the temperature distribution given by the ORNL code using the particular values of decay heat and shroud temperature. Table 3.6.5-1 shows the TUBERAD results (applied to the We 17x17 assembly) versus TAC2D results for 3 different cases of decay heat and shroud temperature. It is possible to match the temperature distributions within 8°F for both PWR and BWR assemblies. The thermal conductivities required to achieve this agreement are:

$$\left.\begin{aligned} k_{SFA} &= 2.106 \times 10^{-10}\ T^3 \text{ Btu/hr-ft-°F} \\ k_{GAP} &= 2.461 \times 10^{-11}\ T^3 \text{ Btu/hr-ft-°F} \end{aligned}\right\} \text{ radiation only}$$

Having determined the radiation portion of the SFA thermal conductivity k_x (= k_y), the contribution from conduction through the helium is added. If the fuel rods are regarded as conducting wires in an "insulating" medium (the helium), Ref. 3.6.5-3 indicates that the conduction in the SFA is increased by a factor of 2.3 to 2.6 for PDRs of 1.39 to 1.32. Using a factor of 2.5, the final conductivities for the SFA and gap are as follows:

$$k_{SFA} = 2.5\ k_{He} + 2.106 \times 10^{-10}\ T^3 \qquad \text{Btu/hr-ft-°F,}$$

$$k_{GAP} = k_{He} + 2.461 \times 10^{-11}\ T^3 \qquad \text{Btu/hr-ft-°F.}$$

Axial Conductivity k_z

The effective axial conductivity for the SFA is developed in Table 3.6.5-2. The average value of 2.4 Btu/hr-ft-°F is used.

Heat Capacity

The effective heat capacity for the SFA is developed in Table 3.6.5-3. The average value of 97.4 Btu/°F is used.

3.6.5.1.2 Gap between Fuel Assembly and Enclosure (FSS or Liner). The effective conductivity of this gap is calculated in the previous section.

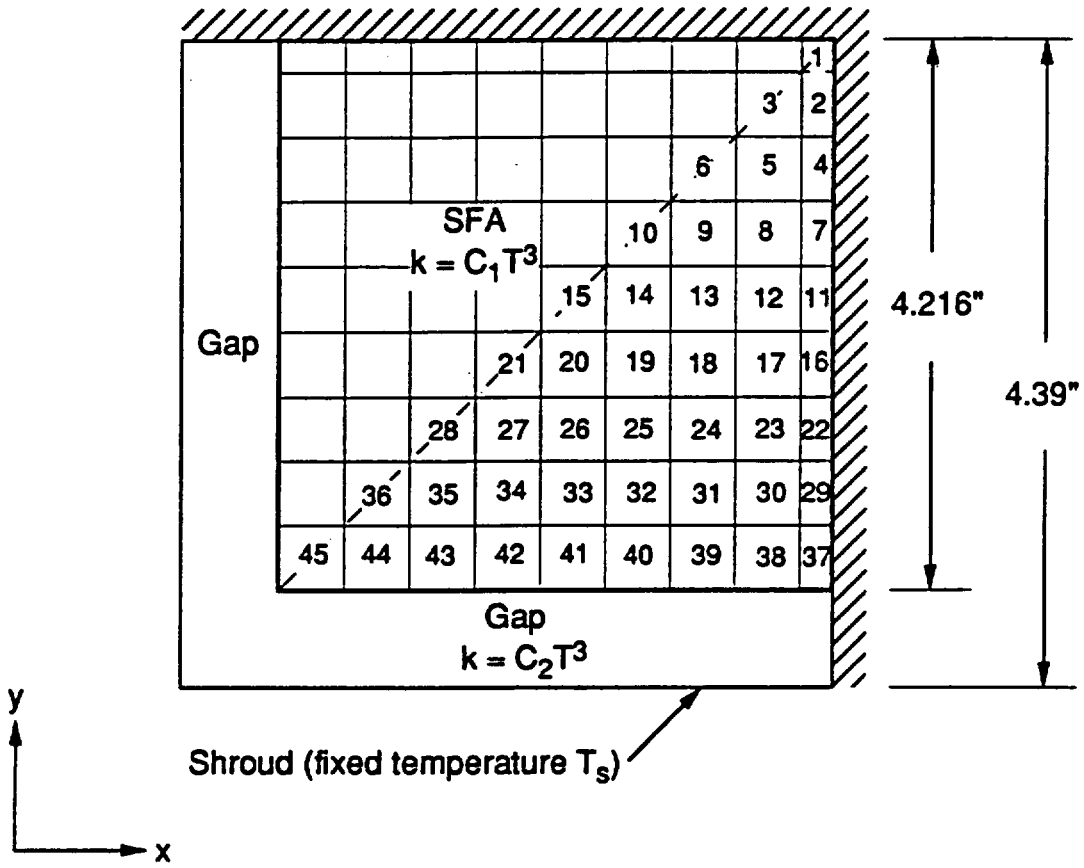

Fig. 3.6.5-17. TAC2D 1/4-scale model of 17x17 SFA

TABLE 3.6.5-1
TUBERAD VS. TAC2D RESULTS FOR SFA

		q"(B/h-ft^2)= 7.06 Q (W)= 617 T_s (F) = 200		q" = 3.53 Q = 308.5 T_s = 200		q" = 7.06 Q = 617 T_s = 300	
		TUBERAD	TAC2D	TUBERAD	TAC2D	TUBERAD	TAC2D
SURFACE	Y_i	T_i (F)		T_i (F)		T_i (F)	
1	98.71	419	419	332	332	468	468
2	98.09	418	418	331	331	467	467
3	97.46	417	417	330	331	466	466
4	96.17	415	415	329	329	464	464
5	95.57	414	414	329	329	463	464
6	93.75	411	411	327	326	461	461
7	92.92	410	409	326	325	460	460
8	92.36	409	409	325	325	459	459
9	90.65	406	406	323	323	457	456
10	87.74	402	400	320	319	453	452
11	88.19	402	401	321	320	454	453
12	87.70	402	401	320	319	453	452
13	86.14	399	398	318	317	451	450
14	83.50	395	393	316	314	447	445
15	79.62	388	385	311	309	442	439
16	81.88	392	391	314	313	445	444
17	81.41	391	390	313	312	444	443
18	80.08	389	387	312	310	443	441
19	77.74	385	382	309	307	439	437
20	74.36	379	375	305	302	434	431
21	69.70	371	366	300	296	428	423
22	73.62	378	376	304	303	433	432
23	73.25	377	376	304	303	433	431
24	72.13	375	373	303	301	431	429
25	70.21	372	368	300	298	428	425
26	67.37	367	362	297	294	424	420
27	63.44	360	353	292	288	418	413
28	58.09	349	341	286	281	410	404
29	63.09	359	358	292	291	418	417
30	62.78	358	357	292	291	417	416
31	61.94	357	355	291	289	416	414
32	60.46	354	351	289	287	414	411
33	58.26	350	345	286	283	410	406
34	55.15	344	337	282	278	405	400
35	50.85	335	326	277	271	398	392
36	44.80	322	313	269	263	388	381
37	48.23	329	334	273	276	394	397
38	48.05	329	333	273	275	394	397
39	47.45	328	331	272	274	393	395
40	46.41	326	328	271	272	391	393
41	44.85	322	323	269	269	389	389
42	42.64	317	316	266	265	385	383
43	39.47	310	307	262	259	379	376
44	34.91	300	295	255	252	371	367
45	26.99	281	280	244	243	357	356

TABLE 3.6.5-2
AXIAL THERMAL CONDUCTIVITY OF SFA

Assembly Type	Array Size	No. Fuel Rods	Pitch (in.)	Fuel Pellet OD (in.)	Clad OD (in.)	Clad Thick. (in.)	A fuel / A tot	A clad / A tot	Rod length (in.)	Act. fuel length (in.)	k_z clad only (B/h-f-F)	k_z clad+ active fuel (B/h-f-F)
CE 14x14 Std.	14	164	0.58	0.3765	0.44	0.028	0.277	0.108	147	137	0.970	2.354
CE 14x14 Ft. Cal.	14	168	0.58	0.3765	0.44	0.028	0.284	0.108	137	128	0.970	2.388
Ex. 14x14 CE	14	176	0.58	0.37	0.44	0.031	0.287	0.118	146.5	134.1	1.066	2.501
We. 14x14 Mod C	14	176	0.58	0.3805	0.44	0.026	0.304	0.101	146.4	136.7	0.905	2.422
We. 14x14	14	179	0.556	0.364	0.422	0.0225	0.307	0.091	150.5	143.2	0.822	2.359
We. 14x14 OFA	14	179	0.556	0.3444	0.4	0.0243	0.275	0.093	150.2	139.6	0.835	2.211
Ex. 14x14 We.	14	179	0.556	0.3505	0.424	0.03	0.285	0.120	152.1	144	1.081	2.506
B&W 15x15	15	208	0.568	0.3686	0.43	0.0265	0.306	0.104	153.7	141.8	0.937	2.466
We. 15x15 ZC & OFA	15	204	0.563	0.366	0.422	0.0242	0.301	0.095	150.2	143	0.859	2.363
Ex. 15x15 We.	15	204	0.563	0.3565	0.424	0.03	0.286	0.117	152.1	144	1.054	2.482
CE 15x15 Palis.	15	204	0.55	0.358	0.418	0.026	0.302	0.106	140	132	0.953	2.461
										AVG =	0.950	2.410

k_{fuel} = 5 Btu/hr-ft-°F (Table 3.2-1)

k_{clad} = 9 " "

TABLE 3.6.5-3
HEAT CAPACITY OF SFA

Assembly Type	Assembly weight (lb)[a]	Typical NFAH weight (lb)[b]	Total weight (lb)	Thermal mass (Btu/°F)[c]
CE 14x14 Std.	1270	82	1352	91.9
CE 14x14 Ft. Cal.	1220	65	1285	87.4
Ex. 14x14 CE	1292	82	1374	93.4
We. 14x14 Mod C	1283	82	1365	92.8
We. 14x14	1272	119	1391	94.6
We. 14x14 OFA	1136	119	1255	85.3
Ex. 14x14 We.	1271	119	1390	94.5
B&W 15x15	1515	130	1645	111.9
We. 15x15 ZC & OFA	1457	165	1622	110.3
Ex. 15x15 We.	1433	165	1598	108.7
CE 15x15 Palis.	1360	0	1360	92.5
			AVG =	96.7

[a]DOE/RW-0184, Vol. 3, App. 2A

[b]DOE/RW-0184-R1, Vol. 1. 0 indicates NFAH not carried with this assembly

[c]Based on c_p = 0.068 Btu/lb-°F (avg. of UO_2 and Zr-4 values from Table. 3.2-1)

3.6.5.1.3 Fuel Support Structure/B_4C

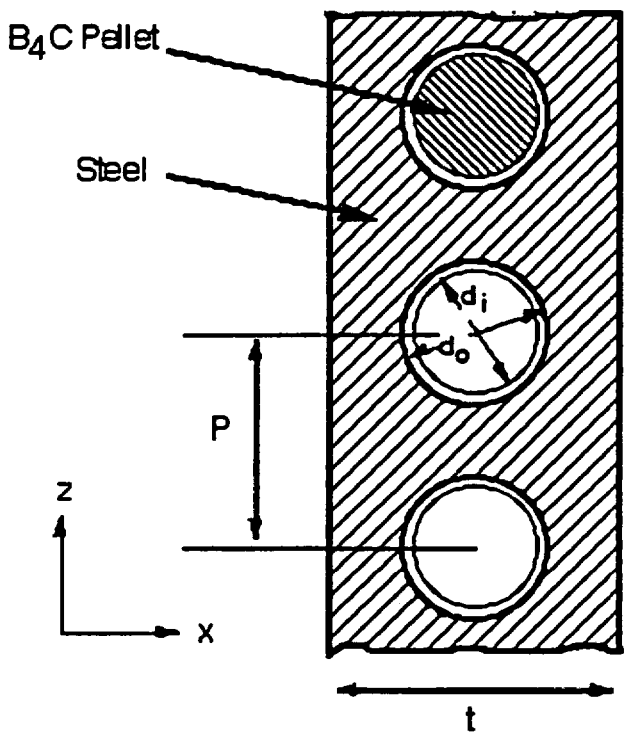

Sec. A-A

$t := 0.610$ in.

$P := 0.5$

$d_o := 0.436$

$d_i := 0.428$

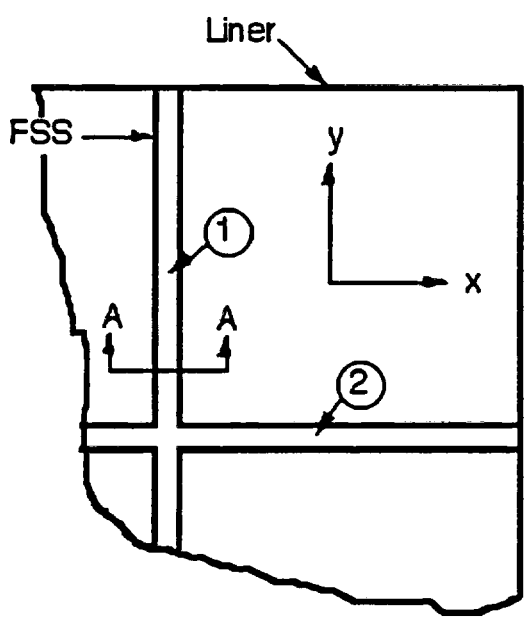

$kx_1 = ky_2$ $ky_1 = kx_2$

Assume $kz = kx_1$ $(=ky_2)$

For kx_1, assume round pellets can be treated as square

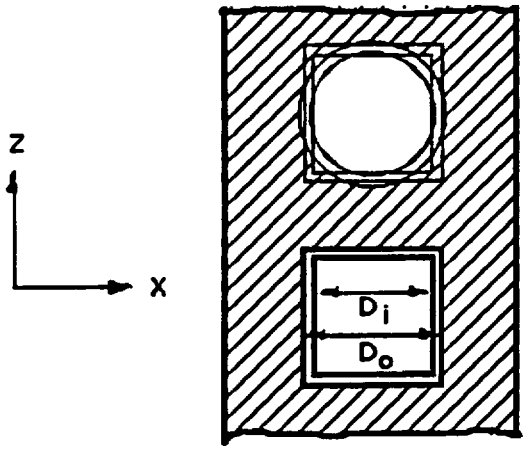

Calculate D_i to give equivalent cross sectional area

$$D_i := \sqrt{\frac{\pi}{4} \cdot d_i} \qquad D_i = 0.37931$$

$$D_o := D_i + (d_o - d_i) \qquad D_o = 0.38731$$

Total x-conductance of basic element

$$C_T = C_1 + \frac{1}{\left(\frac{1}{C_2} + \frac{1}{C_3} + \frac{1}{C_4}\right)}$$

Basic element

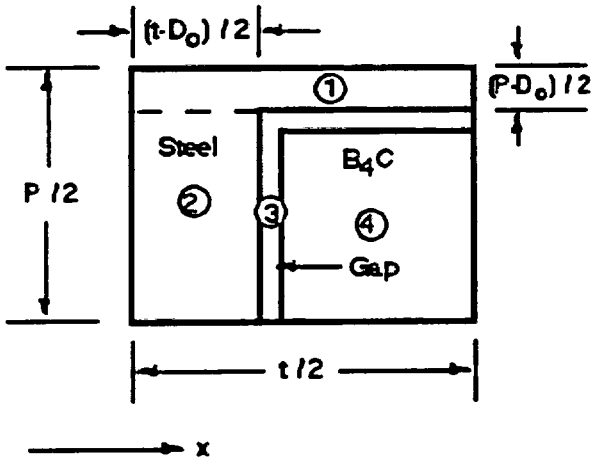

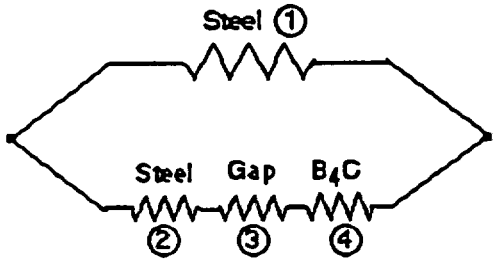

Conductivities (evaluate at 300°F): $T := 300$ °F

Steel $k_s := 3.6 + 5.32 \cdot 10^{-3} \cdot (T + 460)$ $k_s = 7.6432$ Btu/hr-ft-°F

B_4C $k_B := 15$

Air $k_a := 0.005438 + 1.812 \cdot 10^{-5} \cdot (T + 460)$ $k_a = 0.019209$

Emissivities: B_4C $\varepsilon_B := 0.8$

Steel $\varepsilon_s := 0.2$

Conductances:

$$C_i = k \cdot \frac{A}{\Delta x}$$

$$C_1 := k_s \cdot \frac{\left(\frac{P - D_o}{2}\right)}{\left(\frac{t}{2}\right)}$$

$C_1 = 1.41205$ Btu/hr-ft-°F (units of in. cancel out)

$$C_2 := k_s \cdot \frac{\left(\frac{D_o}{2}\right)}{\left(\frac{t - D_o}{2}\right)}$$

$C_2 = 13.29285$

$$C_3 := \left(\frac{k_a}{gap} + h_{rad}\right) \cdot \frac{D_i}{2}$$

$$gap := \frac{D_o - D_i}{2 \cdot 12}$$

$gap = 3.33333 \cdot 10^{-4}$ ft

$$h_{rad} = \sigma \cdot F \cdot \frac{T_1^4 - T_2^4}{T_1 - T_2} \approx 4 \cdot \sigma \cdot F \cdot T_{avg}^3 \qquad \sigma := 0.1714 \cdot 10^{-8} \ \text{Btu/hr-ft}^2\text{-°R}^4$$

$$F := \frac{1}{\frac{1}{\varepsilon_S} + \frac{1}{\varepsilon_B} - 1} \qquad F = 0.19048 \qquad T_{avg} := T$$

$$C_3 := \left[\frac{k_a}{gap} + 4 \cdot \sigma \cdot F \cdot (T_{avg} + 460)^3\right] \cdot \frac{D_i}{2 \cdot 12} \qquad C_3 = 0.91983$$

$$C_4 := k_B \cdot \left(\frac{0.5 \cdot D_i}{0.5 \cdot D_i}\right) \qquad C_4 = 15$$

$$C_T := C_1 + \frac{1}{\frac{1}{C_2} + \frac{1}{C_3} + \frac{1}{C_4}} \qquad C_T = 2.22568$$

$$C_T := kx_1 \cdot \frac{0.5 \cdot P}{0.5 \cdot t} \qquad kx_1 := C_T \cdot \frac{t}{P} \qquad kx_1 = 2.71533 \ \text{Btu/hr-ft-°F}$$

$$= ky_2 = kz$$

For $kx_2 = ky_1$ (parallel to the pellets), the gaps between the pellets must be considered.

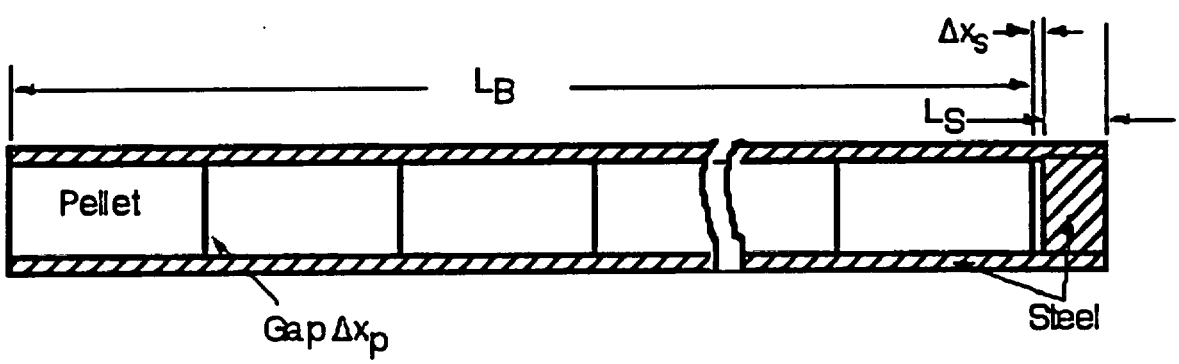

$L_B := 8.01$ in. assembled length of pellets

$\Delta x_p := 0.002$ estimated gap between pellets

$L_s := 0.55$ steel length at end

$\Delta x_s := 0.009$ pellet-steel gap

$N := 11$ max no. pellets

$\Delta x_t := (N - 1) \cdot \Delta x_p + \Delta x_s$ $\Delta x_t = 0.029$ total gap

Total length L (pellets + gaps): $L := L_B + \Delta x_s$ $L = 8.019$

The gap will open at temperature since steel expands more than B4C.
Use $T = 300$ °F

$\alpha_{steel} := 8.6 \cdot 10^{-6}$ in/in-°F $\alpha_{B4C} := 2.7 \cdot 10^{-6}$ (Thermophysical Properties of Matter, Purdue U, Thermal Expansion)

$\Delta L_{steel} := \alpha_{steel} \cdot L \cdot (T - 70)$ $\Delta L_{steel} = 0.01586$

$\Delta L_{B4C} := \alpha_{B4C} \cdot (L - \Delta x_t) \cdot (T - 70)$ $\Delta L_{B4C} = 0.00496$

Operating gap = $\Delta x := \Delta x_t + \Delta L_{steel} - \Delta L_{B4C}$ $\Delta x = 0.0399$ in.

$L := L + \Delta L_{steel}$ $L = 8.03486$

Total Resitance (per unit area) = thru B_4C pellets and gaps

$$\frac{L}{k_{eff}} = \frac{L - \Delta x}{k_B} + \frac{\left(\frac{N-1}{N}\right)\cdot\Delta x}{k_g} + \frac{\frac{\Delta x}{N}}{k'_g}$$

Pellets | Pellet-pellet gaps | Pellet-steel gap

$k_B = 15$

$k_g, k'_g = k_{air} + k_{rad}$

$k_{air} := k_a$ $\quad k_a = 0.01921$ Btu/hr-ft-°F

$$k_{rad} = 4\cdot\sigma\cdot\frac{\Delta x}{N}\cdot F\cdot T^3$$

$$F = F := \frac{1}{\frac{1}{\varepsilon_B} + \frac{1}{\varepsilon_B} - 1}$$ $F = 0.66667$ for pellet-pellet gaps

$$= F' := \frac{1}{\frac{1}{\varepsilon_B} + \frac{1}{\varepsilon_s} - 1}$$ $F' = 0.19048$ for pellet-steel gap

$$k_g := k_{air} + 4\cdot\sigma\cdot\frac{\Delta x}{N\cdot 12}\cdot F\cdot(T + 460)^3$$ $k_g = 0.01982$

These show radiation is small

$$k'_g := k_{air} + 4\cdot\sigma\cdot\frac{\Delta x}{N\cdot 12}\cdot F'\cdot(T + 460)^3$$ $k'_g = 0.01938$

$$k_{eff} := \frac{L}{\frac{L - \Delta x}{k_B} + \frac{\left(\frac{N-1}{N}\right)\cdot\Delta x}{k_g} + \frac{\left(\frac{\Delta x}{N}\right)}{k'_g}}$$

B_4C only

$k_{eff} = 3.15014$ Btu/hr-ft-°F

Now combine with surrounding steel as a parallel / series heat flow path

$$ky_1 = \frac{L + L_s}{\dfrac{L}{\left(\dfrac{A_{B4C}}{A_{tot}} \cdot k_{eff} + \dfrac{A_{steel}}{A_{tot}} \cdot k_{steel}\right)} + \dfrac{L_s}{k_s}}$$

$L_s = 0.55$
(steel length to FSS end)

$t = 0.61$ $P = 0.5$
$d_i = 0.428$ $d_o = 0.436$
$k_s = 7.6432$

$$ky_1 := \frac{L + L_s}{\left[\dfrac{L}{\dfrac{\pi \cdot d_i^2}{4 \cdot t \cdot P} \cdot k_{eff} + \left(1 - \dfrac{\pi}{4} \cdot \dfrac{d_o^2}{t \cdot P}\right) \cdot k_s}\right] + \dfrac{L_s}{k_s}}$$

$ky_1 = 5.49155$ Btu/hr-ft-°F
$= kx_2$

3.6.5.1.4 Fuel Assembly Rods/FSS (1 = fuel, 2 = FSS)

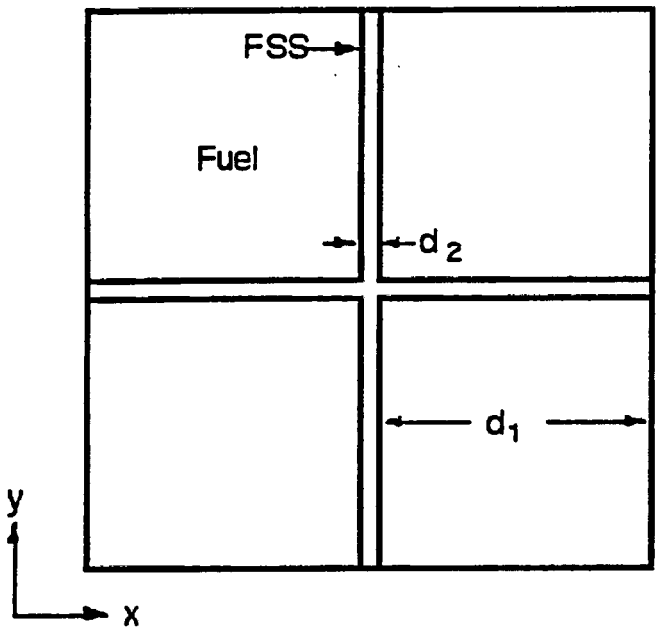

Radial Thermal Conductivity

Assume $k_r = k_x = k_y$

$$k_x := \frac{A_1}{A_{tot}} \cdot k_1 + \frac{A_2}{A_{tot}} \cdot k_2$$

$d_1 := 8.775$ in

$d_2 := 0.61$

$k_1 := 2.5 \cdot k_{He} + 2.106 \cdot 10^{-10} \cdot T^3$ Btu/hr-ft-°F (Sec. 3.6.5.1.1) T = °R

$k_2 := 5.50$ Btu/hr-ft-°F (Sec. 3.6.5.1.3)

$A_1 := 2 \cdot d_1$ $A_{tot} := A_1 + d_2$ $\frac{A_1}{A_{tot}} = 0.966$

$A_2 := d_2$ $\frac{A_2}{A_{tot}} = 0.034$

k_x is adusted so that the volume-averaged temperature predicted by a 1-D radial slice of the r-z model matches that predicted by a 2-D x-y model which explicitly treats the fuel assembly and FSS. It is shown (Sec. 3.6.9) that the conductivity developed above may be multiplied by a factor of 1.46. Thus

$$k_x := 1.46 \cdot \left(\frac{A_1}{A_{tot}} \cdot k_1 + \frac{A_2}{A_{tot}} \cdot k_2 \right)$$

Axial Thermal Conductivity

Fuel Rods FSS

$$k_z := k'_z \cdot \left(\frac{A_{actual}}{A_{model}}\right) \quad \text{where} \quad k'_z := \frac{A_1}{A_{tot}} \cdot k_1 + \frac{A_2}{A_{tot}} \cdot k_2$$

For active fuel zone (144 in.):

$k_1 := 2.4$ Btu/hr-ft-°F (Table 3.6.5-2)

$k_2 := 2.71$ (Sec. 3.6.5.1.3)

$A_{tot} := (2 \cdot d_1 + d_2)^2$ $A_{tot} = 329.786$ in^2

$A_1 := 4 \cdot d_1^2$ $A_1 = 308.002$ $A_2 := A_{tot} - A_1$ $A_2 = 21.783$

$\frac{A_1}{A_{tot}} = 0.934$ $\frac{A_2}{A_{tot}} = 0.066$

$A_{actual} := A_{tot}$ $A_{model} := \pi \cdot (11.528 - 0.174)^2$ $A_{model} = 404.993$

$k'_z := \frac{A_1}{A_{tot}} \cdot k_1 + \frac{A_2}{A_{tot}} \cdot k_2$ $k'_z = 2.42$

$k_z := k'_z \cdot \left(\frac{A_{actual}}{A_{model}}\right)$ $k_z = 1.971$

For cladding only (3 in. top and bottom):

$k_1 := 0.95$ (Table 3.6.5-2) $k'_z := \frac{A_1}{A_{tot}} \cdot k_1 + \frac{A_2}{A_{tot}} \cdot k_2$ $k'_z = 1.066$

$k_z := k'_z \cdot \left(\frac{A_{actual}}{A_{model}}\right)$ $k_z = 0.868$

Thermal radiation contribution (accident case only).

The radiation conductivity axially along a bundle of tubes may be estimated as:

$$k_{rad} := \frac{16}{3} \cdot \sigma \cdot D_h \cdot T^3$$

where D_h is the hydraulic diameter. Estimating $D_h := 0.5$

$$k_{z.rad} = \left(\frac{A_1}{A_{tot}}\right) \cdot \left(\frac{A_{actual}}{A_{model}}\right) \cdot k_{rad} = C \cdot T^3$$

$$\text{where } C = \left(\frac{A_1}{A_{tot}}\right) \cdot \left(\frac{A_{actual}}{A_{model}}\right) \cdot \frac{16}{3} \cdot 0.1714 \cdot 10^{-8} \cdot \frac{D_h}{12} = 2.897 \cdot 10^{-10}$$

<u>Specific Heat</u>

C_t = Total thermal capacitance = $\underbrace{C_f}_{\text{Fuel}} + \underbrace{C_s}_{\text{Steel}} + \underbrace{C_b}_{B_4C}$

$C_f := (4) \cdot 96.7$ Btu/°F, 4 assemblies, Table 3.6.5-3 $C_b := m_b \cdot c_{pb}$

$$m_b := \rho_b \cdot (\underbrace{N_1 \cdot V_1}_{\text{large pellets}} + \underbrace{N_2 \cdot V_2}_{\text{small pellets}})$$

$N_1 := (4) \cdot 283$ $V_1 := \pi \cdot 8.01 \cdot \left(\frac{0.426}{2}\right)^2$ in^3

$N_2 := (4) \cdot 39$ $V_2 := \pi \cdot 8.054 \cdot \left(\frac{0.28}{2}\right)^2$

$\rho_b := 151$ B_4C, lb/ft^3, Table 3.2-1

$m_b := \frac{\rho_b}{1728} \cdot (N_1 \cdot V_1 + N_2 \cdot V_2)$ $m_b = 119.694$ lb B_4C

$c_{pb} := 0.29$ B_4C, Btu/lb-°F, Table 3.2-1

$C_b := m_b \cdot c_{pb}$ $C_b = 34.711$ Btu/°F

$C_s := m_s \cdot c_{ps}$ $m_s := m_{FSS} - m_b$ $m_{FSS} := 751$ lb (Table 2.2-1)

$m_s := m_{FSS} - m_b$ $m_s = 631.306$ $c_{ps} := 0.13$ (Table 3.2-1)

$C_s := m_s \cdot c_{ps}$ $C_s = 82.07$ Btu/°F

For the TAC2D model, $\rho c_{p.eff} := \frac{C_t}{V_{model}}$

$L := 167.25$ in length of fuel cavity

$V_{model} := A_{model} \cdot L$ $\rho c_{p.eff} := \frac{C_f + C_s + C_b}{V_{model}} \cdot 1728$

$\rho c_{p.eff} = 12.847$ Btu/ft^3-°F

(Model uses 12.7 based on a earlier FSS weight of 675 lb. The difference is ~ 1%).

3.6.5.1.5 Space between fuel rods and cavity ends

$d_1 := 8.775$ cavity size

$d_2 := 0.61$ FSS thickness

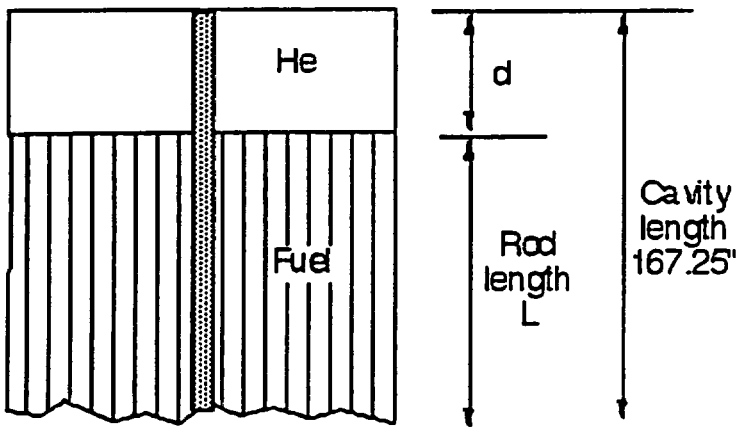

Use a typical rod length of

$L := 150$ in.

Then

$d := 0.5 \cdot (167.25 - L)$

$d = 8.625$

The space beyond the fuel rods is occupied by nozzles, end fittings, the FSS, fuel spacers (at the bottom), and helium gas. For conservatism only the solid area represented by the FSS will be considered, and the conductivity of this area will be taken as steel.

Radial:

$k_r = k_x = k_y$

$$k_x := \frac{A_{He}}{A_{tot}} \cdot k_{He} + \frac{A_{steel}}{A_{tot}} \cdot k_{steel}$$

$$\frac{A_{He}}{A_{tot}} = \frac{2 \cdot d_1}{2 \cdot d_1 + d_2} = 0.966 \qquad \frac{A_{steel}}{A_{tot}} = \frac{d_2}{2 \cdot d_1 + d_2} = 0.034$$

Axial:

$$A_{tot} := (2 \cdot d_1 + d_2)^2 \qquad k_z := \frac{A_{He}}{A_{model}} \cdot k_{He} + \frac{A_{steel}}{A_{model}} \cdot k_{steel}$$

$$A_{model} := \pi \cdot (11.528 - 0.174)^2 \qquad A_{model} = 404.993 \quad in^2$$

$$\frac{A_{He}}{A_{model}} = \frac{4 \cdot d_1^2}{A_{model}} = 0.761 \qquad \frac{A_{steel}}{A_{model}} = \frac{A_{tot} - 4 \cdot d_1^2}{A_{model}} = 0.054$$

Heat Capacity: Use same as for previous material since calculations based on entire fuel assembly and FSS weights.

$\rho c_{p.eff} := 12.9$ Btu/ft^3-°F (12.7 used)

3.6.5.1.6 Cavity Liner

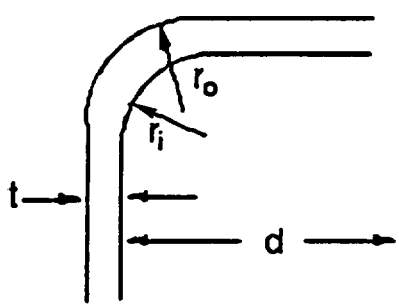

$d := 18.16$ $t := 0.375$

$r_i := 0.12$ $r_o := r_i + t$

Radial $k_r = k_{steel}$

Axial $k_z := \frac{A_{actual}}{A_{model}} \cdot k_{steel}$

Specific heat $\rho c_p := \frac{A_{actual}}{A_{model}} \cdot \rho c_{p.steel}$

$$A_{actual} := (d + 2 \cdot t)^2 - d^2 + (\pi - 4) \cdot \left(r_o^2 - r_i^2\right)$$

$$A_{model} := \pi \cdot \left(11.902^2 - 11.528^2\right) \qquad \frac{A_{actual}}{A_{model}} = 1.003$$

No adjustments to propeties needed.

3.6.5.1.7 DU

$d := d + 2 \cdot t + 2 \cdot 0.036 \qquad d = 18.982 \qquad t := 2.65$

$r_i := 0.48 \qquad r_o := 4.47$

$$A_{actual} := (d + 2 \cdot t)^2 - d^2 + (\pi - 4) \cdot \left(r_o^2 - r_i^2\right)$$

$$A_{model} := \pi \cdot \left(14.237^2 - 11.953^2\right) \qquad \frac{A_{actual}}{A_{model}} = 1.13$$

3.6.5.1.8 Cask Body

$d := d + 2 \cdot t + 2 \cdot 0.02 \qquad d = 24.322 \qquad t := 1.5$

$r_i := 4.34 \qquad r_o := 5.84$

$$A_{actual} := (d + 2 \cdot t)^2 - d^2 + (\pi - 4) \cdot \left(r_o^2 - r_i^2\right)$$

$$A_{model} := \pi \cdot \left(15.798^2 - 14.298^2\right) \qquad \frac{A_{actual}}{A_{model}} = 1$$

No adjustments to properties needed.

3.6.5.1.9 Neutron Shield

Natural convection correlation presented in Sec. 3.6.2.1.

3.6.5.1.10 Outer Skin

No adjustments needed - round skin modeled exactly.

3.6.5.1.11 Steel at Closure and Bottom Ends

$k_r := k_{steel}$

$k_z := k_{steel} \cdot \left(\frac{A_{actual}}{A_{model}}\right)$

Location	$\frac{A_{actual}}{A_{model}}$
Bottom 6" closure (plug)	$\frac{18.16^2}{\pi \cdot 11.528^2} = 0.79$
Flange	$\frac{\left(27.322^2 - 18.16^2\right) + (\pi - 4) \cdot \left(5.84^2 - 0.12^2\right)}{\pi \cdot \left(15.798^2 - 11.528^2\right)} = 1.057$
Top 5" closure, including flange extension	$\frac{(26.57 - 2 \cdot 0.227)^2 + (\pi - 4) \cdot (5.464 - 0.227)^2 \ldots + \left(27.322^2 - 26.57^2\right) + (\pi - 4) \cdot \left(5.84^2 - 5.464^2\right)}{\pi \cdot (15.798 - 0.227)^2} = 0.913$
Bottom plate	$\frac{27.322^2 + (\pi - 4) \cdot 5.84^2}{\pi \cdot 15.798^2} = 0.915$

Heat capacity $\rho c_{p.model} := \frac{A_{actual}}{A_{model}} \cdot \rho c_{p.steel}$

where the $\frac{A_{actual}}{A_{model}}$ are as above

3.6.5.2 TAC2D Model, Section 3.5 (Accident Conditions)

3.6.5.2.1 Impact Limiter Support Structure

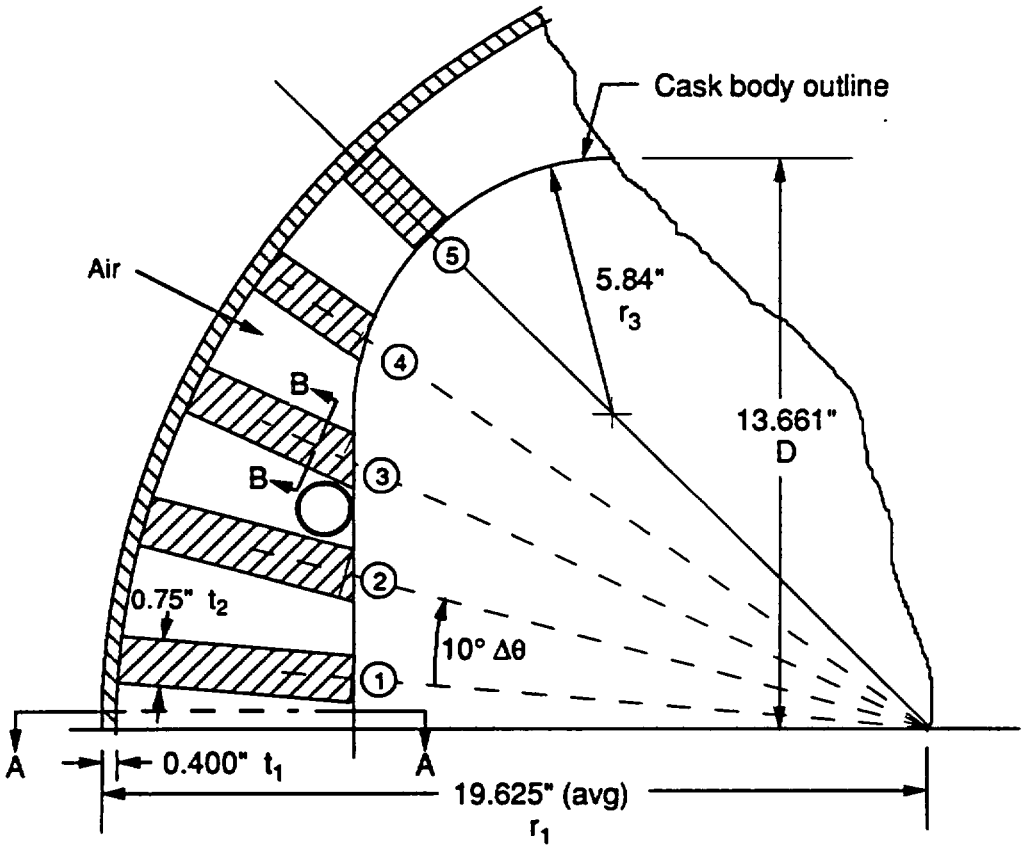

TAC2D MODEL GEOMETRY

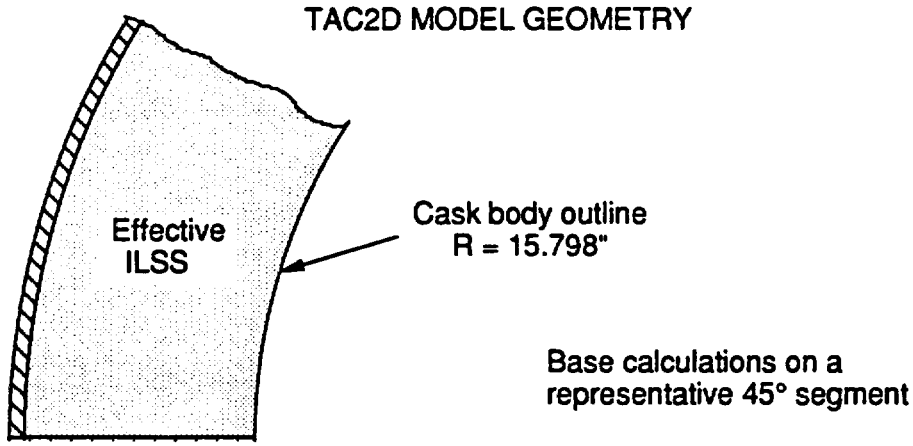

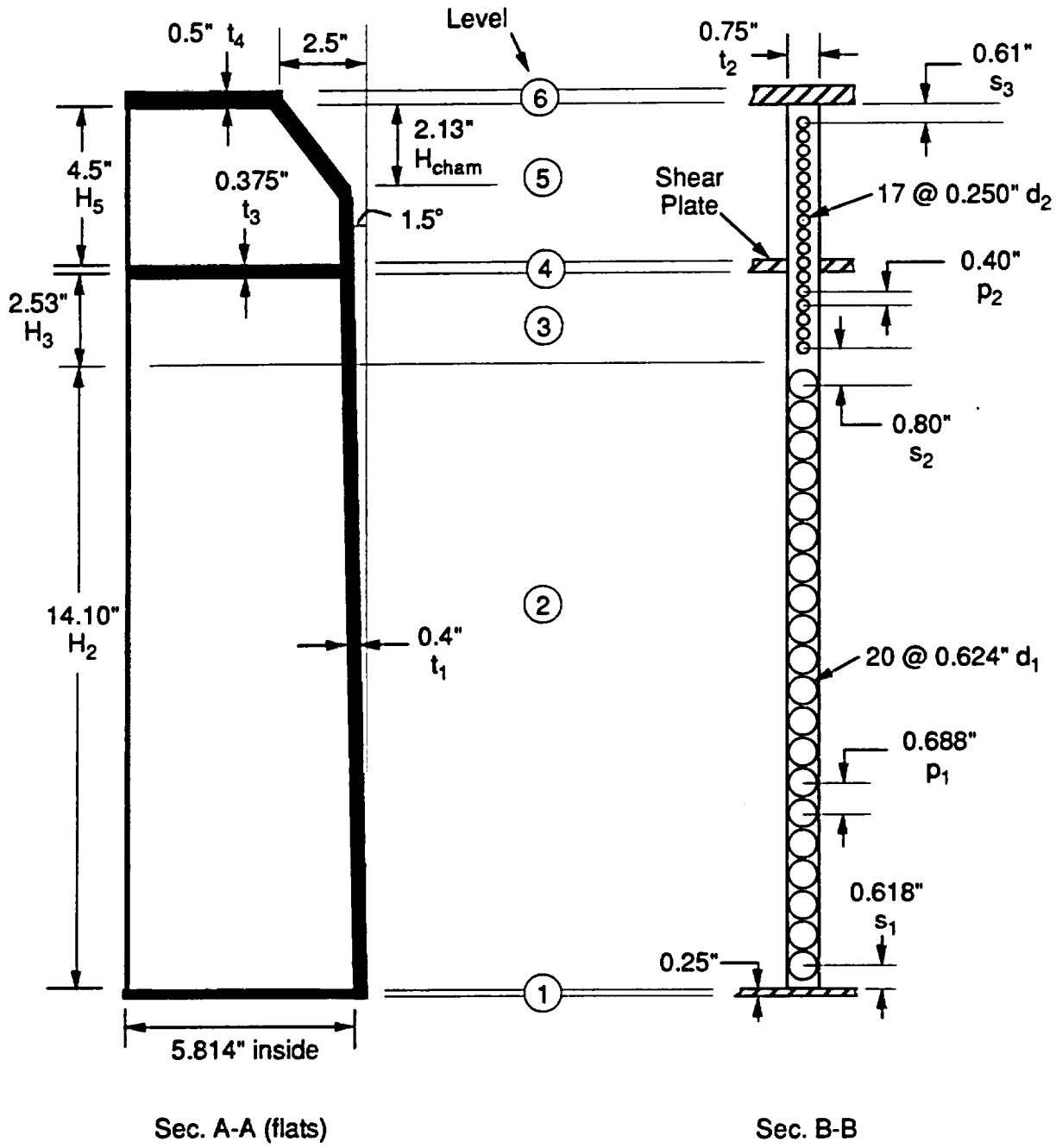

Divide into 6 axial levels in z-direction. Compute effective properties for each level. "Smear" in radial and circumferential directions at each level.

Consider the outer shell (0.4") separately. Include with it the 0.25" of the impact limiter housing. This is all steel.

Definitions (all dimensions in inches)

$r_1 := 19.625$	outside radius	$t_1 := 0.4$	outer shell thickness
$r_2 := r_1 - t_1$	inside radius	$t_2 := 0.75$	rib thickness
$r_3 := 5.84$	cask body corner radius	$t_3 := 0.375$	shear plate
$D := 13.661$	cask body side length (1/2 distance across flats)	$t_4 := 0.5$	top plate

$\Delta\theta := 10 \cdot \frac{\pi}{180}$ angle between supports

$\theta := (0.5) \cdot \Delta\theta$ first angle

Hole diameters and pitches

$d_1 := 0.624$

$p_1 := 0.688$

$d_2 := 0.250$

$p_2 := 0.40$

Heights of levels

$H_2 := 14.10$

$H_3 := 2.53$

$H_5 := 4.5$

Hole spacings

$s_1 := 0.618$

$s_2 := 0.80$

$s_3 := 0.61$

$R := 15.798$ Effective radius of cask body (ILSS inner boundary)

Level 1 – Bottom plate

Level 2 – 0.624" holes in ribs

Level 3 – 0.250" holes in ribs

Level 4 – Shear plate

Level 5 – Above shear plate, 0.250" holes in ribs

Level 6 – Top plate

Level 1 Bottom plate

$k_r = k_{steel} = k_z$

$\rho c_p = (\rho c_p)_{steel}$

Level 2

Radial k

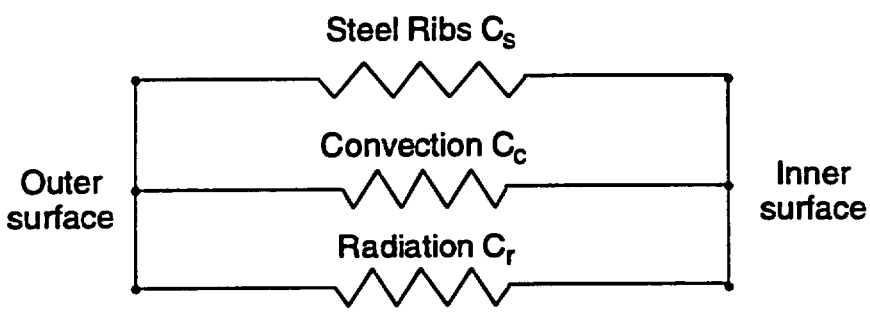

Total Conductance $= C_T = C_s + C_c + C_r$

Steel Conductance $C_s = k_{steel} \sum_{i=1}^{5} \frac{A_i}{\Delta r_i}$

where A_i = area of ith rib, Δr_i = length of ith rib

Calculation of rib lengths

$\Delta r_1 := r_2 - D$

$j := 2..4$

$\Delta r_j := r_2 - \frac{D}{\cos(\theta + (j-1)\cdot\Delta\theta)}$

$\Delta r_5 := r_2 - (D - r_3)\cdot\sqrt{2} - r_3$

$j := 1..5$

Δr_j

5.564
5.08209
4.15175
2.548
2.32444

Calculation of heat transfer areas

n = number of holes contained in Level 2

$n := 20$ for ribs 1 - 3

$n_1 := 13$ for 4/8 ribs 4 $\quad i := 1..3$

$n_2 := 8$ for 2/4 ribs 5

$A_i := H_2\cdot t_2 - n\cdot\pi\cdot\left(\frac{d_1}{2}\right)^2 \quad (i = 1,..3)$

$A_{4a} := A_1$ 4 ribs at position 4

$A_{4b} := H_2\cdot t_2 - n_1\cdot\pi\cdot\left(\frac{d_1}{2}\right)^2$ 4 other ribs at position 4

$A_4 := 0.5\cdot(A_{4a} + A_{4b})$ Avg rib 4 area

$A_{5a} := A_1$ 2 ribs at position 5

$A_{5b} := H_2\cdot t_2 - n_2\cdot\pi\cdot\left(\frac{d_1}{2}\right)^2$ 2 other ribs at position 5

$A_5 := 0.5\cdot 0.5\cdot(A_{5a} + A_{5b})$ Avg. 1/2 area of rib 5 (1/2 rib in a 1/8 segment)

$i := 1..5$

A_i

4.4587
4.4587
4.4587
5.52905
3.14679

$\sum_i \frac{A_i}{\Delta r_i} = 6.27636$ in.

Natural convection

$C_c := h_c \cdot A_c$

$= k_{air} \cdot Nu \cdot \left(\frac{A_c}{\Delta r_c}\right)$

Take $A_c := \left[0.5 \cdot \left[\frac{\pi \cdot r_2}{4} + (D - r_3) + \frac{\pi \cdot r_3}{4}\right] - 4.5 \cdot t_2\right] \cdot H_2$

avg. perimeter ribs

$A_c = 146.33689$ in^2

Use avg. rib length for Δr_c

Take $\Delta r_c := \frac{1}{5} \cdot \sum_j \Delta r_j$ $\Delta r_c = 3.93406$ $\frac{A_c}{\Delta r_c} = 37.19746$ in.

To calculate Nu, assume natural convection in a vertical passage. Use a spacing of

$L := \Delta r_c$ or $L = 3.93406$ and a height of $H := H_2 + H_3$ or $H = 16.63$

$\frac{H}{L} = 4.22719$

Rayleigh Number $Ra := \frac{g \cdot \beta \cdot \Delta T \cdot L^3}{\nu \cdot \alpha}$ $\Delta T = T_{outer\ steel} - T_{inner\ steel}$

Use $\Delta T := 500 - 200$ $\Delta T = 300$ $T_{avg} := 0.5 \cdot (500 + 200)$

$\beta := \frac{1}{(T_{avg} + 460)}$ $\nu := 0.342 \cdot 10^{-3}$ ft^2/sec

(Kreith)

$\alpha := \frac{1.7}{3600}$ ft^2/sec

$Ra := \frac{32.2 \cdot \beta \cdot \Delta T \cdot \left(\frac{L}{12}\right)^3}{\nu \cdot \alpha}$ $Ra = 2.60194 \cdot 10^6$

Use Eq'n 126 - 129 in Chapter 6, *Handbook of Heat Transfer*, 2nd ed.

$$Nu_{ct} := \left[1 + \left[\frac{0.104 \cdot Ra^{0.293}}{1 + \left(\frac{6310}{Ra}\right)^{1.36}}\right]^3\right]^{0.333} \qquad Nu_{ct} = 7.87034$$

$$Nu_{l} := 0.242 \cdot \left(\frac{Ra \cdot L}{H}\right)^{0.273} \qquad Nu_{l} = 9.21042$$

$$Nu_{t} := 0.0605 \cdot Ra^{0.333} \qquad Nu_{t} = 8.28036$$

Use $Nu := Nu_{l}$ (maximum) $\qquad Nu \cdot \frac{A_c}{\Delta r_c} = 342.60423$ in.

Radiation

$C_r := h_r \cdot A_r$ $\qquad h_r := 4 \cdot \sigma \cdot F \cdot T^3$ $\qquad$ Take $\varepsilon_{steel} := 0.8$

$$F := \frac{1}{\frac{1}{\varepsilon_{steel}} + \frac{1}{\varepsilon_{steel}} - 1} \qquad F = 0.66667$$

$$\sigma := 0.1714 \cdot 10^{-8}$$

$A_r := A_c \qquad A_r = 146.33689 \ in^2$

Axial k

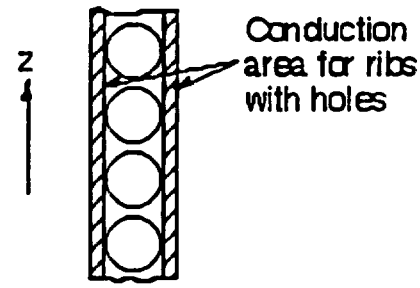

Assume conduction through steel only

$$A_r = \text{rib conduction area} = (t_2 - d_1)\cdot\sum_{i=1..3}\Delta r_i + A_4 + A_5$$

where A_4 = average conduction area through rib 4 (4/8 with 20 holes, 4/8 with 13 holes)
A_5 = " " " " " 5 (2/4 with 20 holes, 2/4 with 8 holes)

$A_{4a} := (t_2 - d_1)\cdot\Delta r_4$ rib 4 with 20 holes

$$A_{4b} = \frac{\Delta z}{\left(\frac{\Delta z}{A}\right)_{holes} + \left(\frac{\Delta z}{A}\right)_{no\ holes}} \quad \text{or} \quad A_{4b} := \frac{20}{\frac{13}{(t_2 - d_1)\cdot\Delta r_4} + \frac{7}{t_2\cdot\Delta r_4}}$$

(approx.) rib with 13 holes

$A_4 := 0.5\cdot(A_{4a} + A_{4b})$ $A_4 = 0.387$ Avg. for rib 4

$A_{5a} := (t_2 - d_1)\cdot\Delta r_5$ rib 5 with 20 holes

$$A_{5b} := \frac{20}{\frac{8}{(t_2 - d_1)\cdot\Delta r_5} + \frac{12}{t_2\cdot\Delta r_5}}$$

(approx.) rib with 8 holes

$A_5 := 0.5\cdot0.5\cdot(A_{5a} + A_{5b})$ $A_5 = 0.21943$ Avg. for rib 5 (1/2 rib per 1/8 segment)

$i := 1..3$

$A_r := (t_2 - d_1)\cdot\sum_i \Delta r_i + A_4 + A_5$ $A_r = 2.47095$

Add area of guide tube and bolt = A_g

$$A_g := \pi\cdot\left[.875^2 - (.875 - .070)^2\right] + \pi\cdot.419^2 \qquad A_g = 0.92099 \quad in^2$$

tube bolt

Total steel area = $A_{steel} := A_r + A_g \qquad A_{steel} = 3.39194$

$$k_{eff}\cdot\left(\frac{A}{\Delta z}\right)_{model} = k_{steel}\cdot\left(\frac{A}{\Delta z}\right)_{steel} \qquad A_{model} := \frac{\pi}{8}\cdot\left(r_2^2 - R^2\right)$$

$$k_{eff} := \frac{A_{steel}}{A_{model}}\cdot k_{steel} \qquad \frac{A_{steel}}{A_{model}} = 0.07196$$

<u>Heat capacity ρc_p</u> Steel

Volume steel = $V_{steel} := V_{ribs} + V_{bolt}$ $\qquad i := 1..4$

$$V_{ribs} := \left[H_2\cdot t_2 - n\cdot\pi\cdot\left(\frac{d_1}{2}\right)^2\right]\cdot\left(\sum_i \Delta r_i + \frac{\Delta r_5}{2}\right) \qquad V_{ribs} = 82.52183 \quad in^3$$

(n is no. holes in level 2 - see C_s calc)

Add volume of non-existent holes in ribs in 4th and 5th positions:

4/8 ribs

$$V_{add.4} := 0.5\cdot 7\cdot\pi\cdot\left(\frac{d_1}{2}\right)^2\cdot\Delta r_4 \qquad V_{add.4} = 2.72726$$

1/2 rib in
1/8 segment 2/4 ribs

$$V_{add.5} := 0.5 \cdot 0.5 \cdot 12 \cdot \pi \cdot \left(\frac{d_1}{2}\right)^2 \cdot \Delta r_5 \qquad V_{add.5} = 2.13254$$

$$V_{ribs} := V_{ribs} + V_{add.4} + V_{add.5}$$

$$V_{bolt} := A_g \cdot H_2 \qquad V_{bolt} = 12.98599 \qquad V_{steel} := V_{ribs} + V_{bolt}$$

$$\rho Vc_{p.steel} := 0.286 \cdot V_{steel} \cdot 0.13$$

$$V_{steel} = 100.36762 \quad in^3$$

$$V_{model} := \frac{\pi}{8} \cdot \left(r_2^2 - R^2\right) \cdot H_2$$

$$\rho c_{p.eff} := \frac{\rho Vc_{p.steel}}{V_{model}} \qquad \rho c_{p.eff} = 0.00562 \quad Btu/in^3\text{-}°F$$

Level 3 Same approach as level 2

Radial k

$$C_s := k_{steel} \cdot \sum_i \frac{A_i}{\Delta r_i}$$

A_i = heat transfer area of i-th rib

n = number of holes contained in Level 3. From Sec. B-B

$H_3 = 0.5s_2 - 0.5p_2 + n(p_2)$

$$n := \frac{H_3 - 0.5 \cdot s_2 + 0.5 \cdot p_2}{p_2} \qquad n = 5.825$$

$i := 1..4$

$A_i := H_3 \cdot t_2 - n \cdot \pi \cdot \left(\frac{d_2}{2}\right)^2$ $(i = 1,..4)$ $A_5 := 0.5 \cdot A_1$

$i := 1..5$

$\sum_i \frac{A_i}{\Delta r_i} = 1.97405$

A_i
1.61157
1.61157
1.61157
1.61157
0.80578

$C_c := Nu \cdot k_{air} \cdot \frac{A_c}{\Delta r_c}$ Same as level 2 only A_c based on H_3

$$Nu \cdot \frac{A_c}{\Delta r_c} = \underbrace{\left(Nu \cdot \frac{A_c}{\Delta r_c}\right)}_{\text{level 2}} \cdot \frac{H_3}{H_2} = 61.47438 \text{ in.}$$

$C_r := h_r \cdot A_r$ $A_r := A_c \cdot \frac{H_3}{H_2}$ $A_r = 26.25761$ in^2

h_r same as level 2

Axial k

Assume conduction through steel only

$$i := 1..4$$

$$A_r = \text{rib onduction area} = (t_2 - d_2)\cdot\sum_i \Delta r_i + \frac{t_2 - d_2}{2}\cdot\Delta r_5$$

$$A_r := (t_2 - d_2)\cdot\sum_i \Delta r_i + \frac{t_2 - d_2}{2}\cdot\Delta r_5 \qquad A_r = 9.25403$$

Total steel area = $A_{steel} := A_r + \overset{\text{guide tube \& bolt}}{A_g}$ $\qquad A_{steel} = 10.17502$

$$k_{eff}\cdot\left(\frac{A}{\Delta z}\right)_{model} = k_{steel}\cdot\left(\frac{A}{\Delta z}\right)_{steel} \qquad A_{model} := \frac{\pi}{8}\cdot\left(r_2^2 - R^2\right)$$

$$k_{eff} := \frac{A_{steel}}{A_{model}}\cdot k_{steel} \qquad \frac{A_{steel}}{A_{model}} = 0.21588$$

Heat capacity ρc_p Steel

Volume steel = $V_{steel} := V_{ribs} + V_{bolt}$ $\qquad i := 1..4$

$$V_{ribs} := \left[H_3\cdot t_2 - n\cdot\pi\cdot\left(\frac{d_2}{2}\right)^2\right]\cdot\left(\sum_i \Delta r_i + \frac{\Delta r_5}{2}\right) \qquad V_{ribs} = 29.82696 \ \text{in}^3$$

(n is no. holes in level 3 - see C_s calc)

$V_{bolt} := A_g\cdot H_3$ $\qquad V_{bolt} = 2.33011$ $\qquad V_{steel} := V_{ribs} + V_{bolt}$

$\rho Vc_{p.steel} := 0.286 \cdot V_{steel} \cdot 0.13$ $V_{steel} = 32.15707$ in^3

$V_{model} := \frac{\pi}{8} \cdot \left(r_2^2 - R^2\right) \cdot H_3$

$\rho c_{p.eff} := \frac{\rho Vc_{p.steel}}{V_{model}}$ $\rho c_{p.eff} = 0.01003$ $Btu/in^3 \cdot °F$

Level 4 Shear Plate

$k_r = k_{steel} = k_z$

$\rho c_p = (\rho c_p)_{steel}$

Level 5 Same approach as level 2. Use 3/4 of Δr_i values from level 2 calculation to account for shortened rib lengths in the corners

Radial k

$C_s := k_{steel} \cdot \sum_i \frac{A_i}{\Delta r_i}$ $i := 1..5$ A_i = heat transfer area of i-th rib

n = number of holes contained in Level 5. From Sec. B-B

$H_5 = s_3 - 0.5p_2 + n(p_2)$

$n := \frac{H_5 - s_3 + 0.5 \cdot p_2}{p_2}$ $n = 10.225$

$i := 1..4$

$A_i := H_5 \cdot t_2 - n \cdot \pi \cdot \left(\frac{d_2}{2}\right)^2$ $(i = 1,..4)$ $A_5 := 0.5 \cdot A_1$

$i := 1..5$

A_i
2.87308
2.87308
2.87308
2.87308
1.43654

$\frac{4}{3} \cdot \left(\sum_i \frac{A_i}{\Delta r_i}\right) = 4.69243$

$C_c := h_c \cdot A_c$

$= k_{air} \cdot Nu \cdot \left(\frac{A_c}{\Delta r_c}\right)$

$A_c := A_{c_{level\ 2}} \cdot \frac{H_5}{H_2}$ $A_c = 46.70326$ in^2

$\Delta r_c := \Delta r_{c_{level\ 2}} \cdot \frac{3}{4}$ (approx.) $\Delta r_c = 2.95054$ in.

To calculate Nu, assume natural convection in a vertical passage. Use a spacing of

$L := \Delta r_c$ or $L = 2.95054$ and a height of $H := H_5$ or $H = 4.5$ in.

$\frac{H}{L} = 1.52514$

Rayleigh Number $Ra := \frac{g \cdot \beta \cdot \Delta T \cdot L^3}{\nu \cdot \alpha}$ $\Delta T = T_{outer\ steel} - T_{inner\ steel}$

Use $\Delta T := 500 - 200$ $\Delta T = 300$ $T_{avg} := 0.5 \cdot (500 + 200)$

$$\beta := \frac{1}{(T_{avg} + 460)}$$ ν, α same as for Level 2

$$Ra := \frac{32.2 \cdot \beta \cdot \Delta T \cdot \left(\frac{L}{12}\right)^3}{\nu \cdot \alpha}$$ $Ra = 1.09769 \cdot 10^6$

Use Eq'n 126 - 129 in Chapter 6, *Handbook of Heat Transfer*, 2nd ed.

$$Nu_{ct} := \left[1 + \left[\frac{0.104 \cdot Ra^{0.293}}{1 + \left(\frac{6310}{Ra}\right)^{1.36}}\right]^3\right]^{0.333}$$ $Nu_{ct} = 6.11433$

$$Nu_l := 0.242 \cdot \left(\frac{Ra \cdot L}{H}\right)^{0.273}$$ $Nu_l = 9.6122$

$$Nu_t := 0.0605 \cdot Ra^{0.333}$$ $Nu_t = 6.21206$

Use $Nu := Nu_l$ (maximum) $Nu \cdot \frac{A_c}{\Delta r_c} = 152.14873$

$C_r := h_r \cdot A_r$ $A_r := A_c$ $A_r = 46.70326$ in^2

h_r same as level 2 & 3

Axial k

Assume conduction through steel

$i := 1..4$

A_r = rib conduction area ≈ $\frac{3}{4}\cdot\left[(t_2 - d_2)\cdot\sum_i \Delta r_i + \frac{t_2 - d_2}{2}\cdot\Delta r_5\right]$

$A_r := \frac{3}{4}\cdot\left[(t_2 - d_2)\cdot\sum_i \Delta r_i + \frac{t_2 - d_2}{2}\cdot\Delta r_5\right]$ $A_r = 6.94052$

Total steel area = $A_{steel} := A_r + A_{g}$ (guide tube & bolt) $A_{steel} = 7.86152$

$k_{eff}\cdot\left(\frac{A}{\Delta z}\right)_{model} = k_{steel}\cdot\left(\frac{A}{\Delta z}\right)_{steel}$ $A_{model} := \frac{\pi}{8}\cdot\left(r_2^2 - R^2\right)$

$k_{eff} := \frac{A_{steel}}{A_{model}}\cdot k_{steel}$ $\frac{A_{steel}}{A_{model}} = 0.16679$

Heat capacity ρc_p Steel

Volume steel = $V_{steel} := V_{ribs} + V_{bolt}$

$i := 1..4$

$V_{ribs} := \left[H_5\cdot t_2 - n\cdot\pi\cdot\left(\frac{d_2}{2}\right)^2\right]\cdot\left(\frac{3}{4}\right)\cdot\left(\sum_i \Delta r_i + \frac{\Delta r_5}{2}\right)$ $V_{ribs} = 39.88138$ in^3

(n is no. holes in level 5 - see C_s calc)

$V_{bolt} := A_g \cdot H_5$ $V_{bolt} = 4.14447$ $V_{steel} := V_{ribs} + V_{bolt}$

$\rho Vc_{p.steel} := 0.286 \cdot V_{steel} \cdot 0.13$ $V_{steel} = 44.02584$ in^3

$V_{model} := \frac{\pi}{8} \cdot \left(r_2^2 - R^2\right) \cdot H_5$

$\rho c_{p.eff} := \frac{\rho Vc_{p.steel}}{V_{model}}$ $\rho c_{p.eff} = 0.00772$ $Btu/in^3\text{-}°F$

Level 6 Top Plate

Radial k

$$\frac{k_{eff}}{\ln\left(\frac{r_o}{r_i}\right)_{model}} = \frac{k_{steel}}{\ln\left(\frac{r_o}{r_i}\right)_{steel}}$$

$r_{o.model} := r_2$

$r_{i.model} := R$

$r_{o.steel} := 19.875 - 2.5$

$r_{i.steel} := r_{i.model}$

$$\frac{k_{eff}}{k_{steel}} = \frac{\ln\left(\frac{r_{o.model}}{r_{i.model}}\right)}{\ln\left(\frac{r_{o.steel}}{r_{i.steel}}\right)} = 2.06338$$

Axial k

$$k_{eff} \cdot A_{model} = k_{steel} \cdot A_{steel}$$

$$A_{model} := \frac{\pi}{8} \cdot \left(r_2^2 - R^2\right) \qquad A_{model} = 47.13324$$

$$S := 2 \cdot (D - r_3)$$

outer envelope cask body envelope

$$A_{steel} := \frac{1}{8} \cdot \left[\pi \cdot (19.875 - 2.5)^2 - \left(S^2 + 4 \cdot r_3 \cdot S + \pi \cdot r_3^2\right)\right]$$

$$A_{steel} = 28.90027$$

$$\frac{k_{eff}}{k_{steel}} = \frac{A_{steel}}{A_{model}} = 0.61316$$

Heat capacity ρc_p

$$\rho c_{p.eff} = \frac{A_{steel}}{A_{model}} \cdot \rho c_{p.steel} = \frac{A_{steel}}{A_{model}} \cdot (0.286) \cdot (0.13) = 0.0228$$

Btu/in^3-°F

SUMMARY OF CALCULATIONS FOR IMPACT LIMITER SUPPORT STRUCTURE

Radial Conductivity k_r

The total conductance at axial level i for the TAC2D model is (1/8 segment):

$$C_T = \left(\frac{\pi}{4}\right)\frac{k_r H_i}{\ln\left(\frac{r_2}{R}\right)}$$

where $r_2 = 19.625 - 0.4 = 19.225$ in. and $R = 15.798$ in. This gives:

$$k_r = \left(\frac{4}{\pi}\right)\ln\left(\frac{19.225}{15.798}\right)\frac{C_T}{H_i} = \left(\frac{0.250}{H_i}\right)C_T$$

The conductances C_T can be written in general as:

$$C_T = f_1 k_{steel} + f_2 k_{air} + f_3 h_{rad}$$

where f_1, is $A/\Delta r$, f_2 is $Nu(A/\Delta r)$, and f_3 is A computed previously.

Thus

$$k_r = F_1 k_{steel} + F_2 k_{air} + F_3 h_{rad}$$

where $F_j = \left(\frac{0.250}{H_i}\right) f_j$ for i = 2, 3, 5 and j = 1..3

Axial Conductivity k_z

$$k_z = G k_{steel}$$

Table 3.6.5-4 summarizes the calculations performed for the ILSS thermal properties for accident conditions.

TABLE 3.6.5-4
ILSS THERMAL PROPERTIES, TAC2D MODEL, ACCIDENT CONDITIONS

i Level	H_i Height (in.)	Rib Hole Dia. (in.)	Steel conduction $f_1(=A/\Delta r)$ (in.)	Convection $f_2(=NuA/\Delta r)$ (in.)	Radiation $f_3(=A)$ (in.^{2})
1	0.25	Bottom plate			
2	14.1	0.624	6.28	342.6	146.3
3	2.53	0.25	1.97	61.47	26.26
4	0.375	Shear plate			
5	4.5	0.25	4.69	152.1	46.7
6	0.5	Top plate			

i Level	F_1	F_2	F_3 (in.)	G	k_r (@300°F) (Btu/hr-ft-F)	k_z (@300°F) (Btu/hr-ft-F)	ρc_p (Btu/ft^3-F)
1	1.0000	0.0000	0.0000	1.0000	7.64	7.64	64.2
2	0.1113	6.0745	2.5940	0.0720	1.40	0.550	9.71
3	0.1947	6.0741	2.5949	0.2160	2.04	1.65	17.3
4	1.0000	0.0000	0.0000	1.0000	7.64	7.64	64.2
5	0.2606	8.4500	2.5944	0.1670	2.59	1.28	13.3
6	2.0600	0.0000	0.0000	0.6130	15.7	4.69	39.4

k_{steel} = 7.64 Btu/hr-ft-F @300 F
k_{air} = 0.0192 Btu/hr-ft-F @300 F
h_{rad} = 2.01 Btu/hr-ft^2-F @300 F

ILSS PROPERTIES FOR NORMAL CONDITIONS MODEL

Lump the properties from Table 3.6.5-4 at each level into single values of conductivity and heat capacity for the top and bottom structures. Conduction through the liquid neutron shield is conservatively neglected.

Top ILSS

Radial k_r

For conservatism, use only conduction through the steel. Then, equating total conductances gives:

Normal Conditions Model — Accident Conditions Model

$$\left(\frac{\pi}{4}\right)\frac{k_r H}{\ln\left(\frac{r_2}{R}\right)} = \left(\frac{\pi}{4}\right)\sum_i \frac{F_{1,i}\, k_{steel}\, H_i}{\ln\left(\frac{r_2}{R}\right)}$$

or

$$k_r = k_{steel}\left(\frac{1}{H}\right)\sum_i F_{1,i}\, H_i$$

where $H = \sum_i H_i$ is the total height = 22.25 in. Thus:

$$k_r = 0.220\ k_{steel}$$

Axial k_z

Equating resistances:

$$\frac{H}{A k_z} = \sum_i \frac{H_i}{A G_i\ k_{steel}}$$

where $A = \pi(r_2^2 - R^2) = 377.1$ in.^{2}

$$k_z = k_{steel}\frac{H}{\sum_i \frac{H_i}{G_i}} \qquad \text{Thus} \quad k_z = 0.0943\ k_{steel}$$

Heat Capacity

Include the liquid neutron shield capacitance for maximum normal conditions. Equating capacitances:

$$\underbrace{\rho c_p (HA)}_{\text{model}} = \underbrace{\sum_i (\rho c_p)_i H_i A}_{\text{steel}} + \underbrace{(\rho c_p)_\ell V}_{\text{liquid}}$$

where V is the liquid volume = 5800 in.^{3} (maximum normal conditions)

or

$$\rho c_p = \left(\frac{1}{H}\right)\sum_i (\rho c_p)_i H_i + \frac{(\rho c_p)_\ell V}{HA} \qquad \text{Thus}$$

$$\rho c_p = 13.5 + 0.691\,(\rho c_p)_\ell \quad \text{Btu/ft}^3\text{-°F}$$

(TAC2D model uses 0.706 $(\rho c_p)_\ell$, ~2% difference)

Bottom ILSS

All holes are 0.624 in. diameter and there is no shear plate. Thus use level 2 properties for levels 2 – 5. (There is a slightly non-conservative effect in the conductivity of including the steel representing the 12x2 + 7x4 = 42 omitted holes from the top ILSS ribs. This is more than offset by neglecting the neutron shield.)

Radial k_r

$$k_r = k_{steel}\left(\frac{1}{H}\right)\left(F_{1,1}H_1 + \sum_{i=2}^{5} F_{1,2}\,H_i + F_{1,6}H_6\right)$$

$$k_r = 0.165\,k_{steel}$$

Axial k_z

$$k_z = k_{steel}\left(\frac{H}{\frac{H_1}{G_1} + \sum_{i=2}^{5}\frac{H_i}{G_2} + \frac{H_6}{G_6}}\right)$$

$$k_z = 0.0742\,k_{steel}$$

Heat capacity

$$\rho c_p = \left(\frac{1}{H}\right)\left((\rho c_p)_1 H_1 + \sum_{i=2}^{5}(\rho c_p)_2 H_i + (\rho c_p)_6 H_6\right) + \frac{(\rho c_p)_\ell V}{HA}$$

where V = 6274 in.^{3} Thus

$$\rho c_p = 11.0 + 0.748\,(\rho c_p)_\ell \quad \text{Btu/ft}^3\text{-°F}$$

(TAC2D model uses 0.782 $(\rho c_p)_\ell$, ~5% difference)

3.6.5.2.2 Impact Limiters

Inner Portion of Side Impact Limiter

$r_o := 26.25$ in.

$r_i := 20$

$t := 0.006$

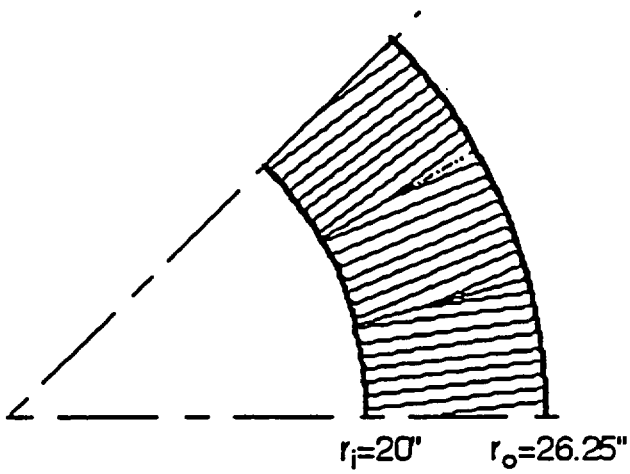

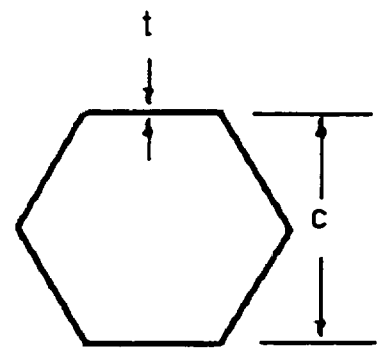

Material is AL 5052 honeycomb, density 10.5 lb/ft^3

$\rho := 10.5$ honeycomb density, lb/ft^3

$k_m := 80$ AL 5052 conductivity, Btu/hr-ft-°F

$\rho_m := 168$ AL 5052 density, lb/ft^3

$c_{p.m} := 0.22$ AL 5052 specific heat, Btu/lb-°F

Radial k_r

$k_r := 2.67 \cdot \left(\frac{t}{c}\right) \cdot k_m$ (Ref: TRUPACT-I SARP, GA-A18695, p. 3.6-19)

density $\rho := 2.67 \cdot \left(\frac{t}{c}\right) \cdot \rho_m$ (p. 3.6-22, above ref.)

Then $k_r := \left(\frac{\rho}{\rho_m}\right) \cdot k_m$ $k_r = 5$ Btu/hr-ft-°F

For accident conditions only, add a radiation term. The heat flux is:

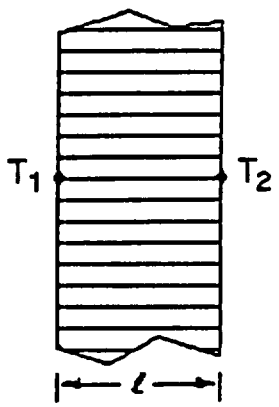

$$q''_{rad} := 0.664 \cdot \sigma \cdot \varepsilon^{1.63 \cdot \left(\frac{\ell}{d} + 1\right)^{-.89}} \cdot \left(\frac{\ell}{d} + 0.3\right)^{-.69} \cdot \left(T_1^4 - T_2^4\right) \square$$

(Ref: *Handbook of Heat Transfer*, 1973, p. 3-127)

$$d = \frac{\text{core circumference}}{\pi}$$

$\varepsilon := 0.8$ = emissivity (conservative)

$\ell := r_o - r_i$

Core circumference = 6 c tan30°

$$c := 2.67 \cdot t \cdot \left(\frac{\rho_m}{\rho}\right) \qquad c = 0.25632$$

$$d := \frac{6 \cdot c \cdot \tan\left(\frac{\pi}{6}\right)}{\pi} \qquad d = 0.28263 \quad \text{in.}$$

$$q''_{rad} := \frac{k_{rad}}{\ell} \cdot \left(T_1 - T_2\right) \square \qquad \sigma := 0.1714 \cdot 10^{-8} \quad \text{Btu/hr-ft}^2\text{-°R}^4$$

$$k_{rad} := \frac{\ell}{12} \cdot 0.664 \cdot \sigma \cdot \varepsilon^{1.63 \cdot \left(\frac{\ell}{d} + 1\right)^{-.89}} \cdot \left(\frac{\ell}{d} + 0.3\right)^{-.69} \cdot \left(\frac{T_1^4 - T_2^4}{T_1 - T_2}\right) \square \qquad \text{Btu/hr-ft-°F}$$

$$= K \cdot \sigma \cdot \left(T_1^2 + T_2^2\right) \cdot \left(T_1 + T_2\right)$$

where

$$K := \frac{\ell}{12} \cdot 0.664 \cdot \varepsilon^{1.63 \cdot \left(\frac{\ell}{d} + 1\right)^{-.89}} \cdot \left(\frac{\ell}{d} + 0.3\right)^{-.69} \qquad K = 0.03957 \quad \text{ft.}$$

Axial k_z

$$k_z := 0.8 \cdot \left(\frac{t}{c}\right) \cdot k_m$$ (Ref: GA-A18695, p. 3.6-20)

$$= 0.8 \cdot \left(\frac{1}{2.67}\right) \cdot \left(\frac{\rho}{\rho_m}\right) \cdot k_m = 1.49813$$ Btu/hr-ft-°F

Heat Capacity

$$\rho \cdot c_{p.m} = 2.31$$ Btu/ft^3-°F

Outer Portion of Side Impact Limiter

$\rho := 7.9$ lb/ft^3 $r_o := 45$ $r_i := 26.25$

$$c := 2.67 \cdot t \cdot \left(\frac{\rho_m}{\rho}\right)$$ $c = 0.34068$ in.

Radial k_r

$$k_r := \frac{\rho}{\rho_m} \cdot k_m$$ $k_r = 3.7619$ Btu/hr-ft-°F

Radiation portion (accident only). Using the previous method,

$$\ell := r_o - r_i$$ $$d := \frac{6 \cdot c \cdot \tan\left(\frac{\pi}{6}\right)}{\pi}$$ $d = 0.37565$ in.

$$K := \frac{\ell}{12} \cdot 0.664 \cdot \varepsilon^{1.63 \cdot \left(\frac{\ell}{d} + 1\right)^{-.89}} \cdot \left(\frac{\ell}{d} + 0.3\right)^{-.69}$$ $K = 0.06881$ ft.

Axial k_z

$$k_z := 0.8 \cdot \left(\frac{1}{2.67} \cdot \frac{\rho}{\rho_m}\right) \cdot k_m \qquad k_z = 1.12716 \quad \text{Btu/hr-ft-°F}$$

Heat capacity

$$\rho \cdot c_{p.m} = 1.738 \quad \text{Btu/ft}^3\text{-°F}$$

Corner Impact Limiter - Normal Conditions

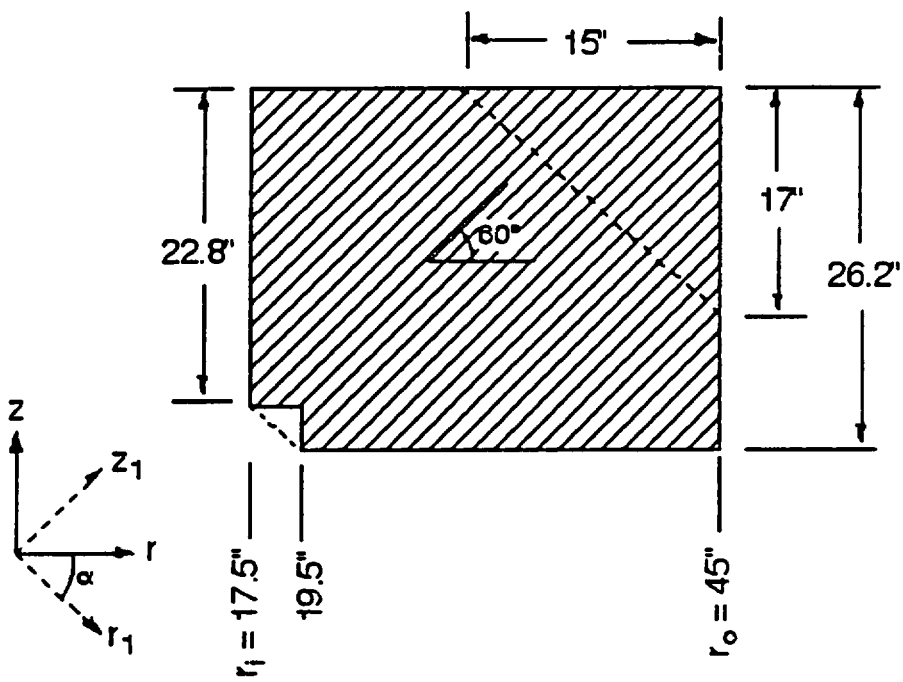

$\rho := 4.2 \quad \text{lb/ft}^3$

$\alpha := 30 \cdot \frac{\pi}{180}$

Shaded area is model, dashed line indicates actual boundaries

Conductivity (k_r and k_z)

$$k_r := k_{r1} \cdot \cos(\alpha)^2 + k_{z1} \cdot \sin(\alpha)^2$$

(Rohsenow and Choi, *Heat and Mass Transfer*)

$$k_z := k_{r1} \cdot \sin(\alpha)^2 + k_{z1} \cdot \cos(\alpha)^2$$

$$k_{rz} = k_{zr} := (k_{z1} - k_{r1}) \cdot \sin(\alpha) \cdot \cos(\alpha)$$

Omit the cross terms k_{rz} and k_{zr} since it is conservative and the code cannot handle them.

$$k_{r1} := 0.8\cdot\left(\frac{1}{2.67}\cdot\frac{\rho}{\rho_m}\right)\cdot k_m \qquad k_{z1} := \frac{\rho}{\rho_m}\cdot k_m$$

$$k_r := k_{r1}\cdot\cos(\alpha)^2 + k_{z1}\cdot\sin(\alpha)^2 \qquad k_r = 0.94944 \quad \text{Btu/hr-ft-°F}$$

$$k_z := k_{r1}\cdot\sin(\alpha)^2 + k_{z1}\cdot\cos(\alpha)^2 \qquad k_z = 1.64981 \quad \text{Btu/hr-ft-°F}$$

<u>Heat capacity</u>

$$\rho V c_{p.model} = \rho V c_{p.actual} \qquad \rho c_{p.model} = \rho c_{p.actual}\cdot\left(\frac{V_{actual}}{V_{model}}\right)$$

$V_{actual} = (V_1 - V_2) + (V_3 - V_4)$ where

$V_1 := \pi\cdot\frac{17}{3}\cdot(45^2 + 45\cdot 30 + 30^2)$ Top frustrum

$V_2 := \pi\cdot 17\cdot 17.5^2$ Top inner cylinder

mid annulus bottom cylinder

$V_3 := \pi\cdot\left[(22.8 - 17)\cdot(45^2 - 17.5^2) + (26.2 - 22.8)\cdot 45^2\right]$

$V_4 := \pi\cdot\left(\frac{26.2 - 22.8}{3}\right)\cdot(17.5^2 + 17.5\cdot 19.5 + 19.5^2)$ Bottom frustrum

$$V_{actual} := (V_1 - V_2) + (V_3 - V_4) \qquad V_{actual} = 1.09038\cdot 10^5 \quad \text{in}^3$$

$$V_{model} := \pi\cdot\left[22.8\cdot(45^2 - 17.5^2) + (26.2 - 22.8)\cdot(45^2 - 19.5^2)\right]$$

$$V_{model} = 1.40679\cdot 10^5 \quad \text{in}^3$$

$$\rho c_{p.model} := \rho\cdot c_{p.m}\cdot\frac{V_{actual}}{V_{model}} \qquad \rho c_{p.model} = 0.71617 \quad \text{Btu/ft}^3\text{-°F}$$

Corner Impact Limiter - Accident Conditions

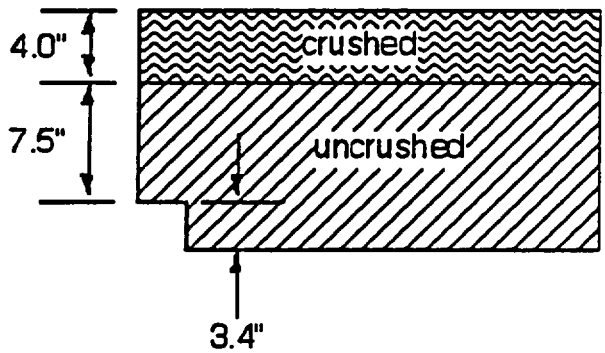

The thermal resistance of the crushed portion is conservatively neglected. Only the uncrsuhed part is accounted for in the effective thermal conductiviy.

Radial k_r - (uncrushed)

$k_r = 0.94944$ Btu/hr-ft-°F

Radiation portion. Use $0.05 \cdot \sigma \cdot \left(T_1^2 + T_2^2\right) \cdot \left(T_1 + T_2\right)$ as an estimate. Add to both radial and axial conductivities

Radial k_r - uncrushed - initial conditions

Model geometry for initial conditions is same as accident conditions (crushed), but impact limiter is initially uncrushed. Use a conductivity that gives the same thermal conductance as that of uncrushed geometry.

$k_{ui} := \left(\frac{26.2}{7.5 + 3.4}\right) \cdot k_r$ $k_{ui} = 2.28214$ Btu/hr-ft-°F

Axial k_z - (uncrushed)

$k_z = 1.64981$ Btu/hr-ft-°F

Axial k_z - uncrushed - initial conditions

Using the same method as above,

$$k_{ui} := \left(\frac{7.5 + 3.4}{26.2}\right) \cdot k_z \qquad k_{ui} = 0.68637 \quad \text{Btu/hr-ft-°F}$$

Heat capacity

Volume in model:

$$V_{model} := \pi \cdot \left[7.5 \cdot \left(45^2 - 17.5^2\right) + 3.4 \cdot \left(45^2 - 19.5^2\right) \right] \ \text{in}^3$$

$$V_{model} = 5.80654 \cdot 10^4$$

$$\rho c_{p.model} := \rho \cdot c_{p.m} \cdot \frac{V_{actual}}{V_{model}} \qquad \rho c_{p.model} = 1.73513 \quad \text{Btu/ft}^3\text{-°F}$$

$$\rho_{model} := \rho \cdot \left(\frac{V_{actual}}{V_{model}}\right) \qquad \rho_{model} = 7.88693 \quad \text{lb/ft}^3$$

End Impact Limiter - Normal Conditions

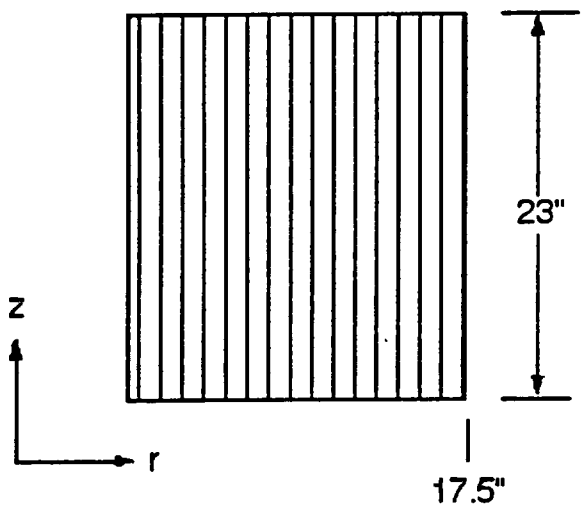

$\rho := 10.5$ lb/ft^3

$c := 2.67 \cdot t \cdot \left(\frac{\rho_m}{\rho}\right)$

$c = 0.25632$ in.

Radial k_r

$k_r := 0.8 \cdot \left(\frac{1}{2.67} \cdot \frac{\rho}{\rho_m}\right) \cdot k_m$ $k_r = 1.49813$ Btu/hr-ft-°F

Axial k_z

$k_z := \frac{\rho}{\rho_m} \cdot k_m$ $k_z = 5$ Btu/hr-ft-°F

Heat capacity

$\rho \cdot c_{p.m} = 2.31$ Btu/ft^3-°F

End Impact Limiter - Accident Conditions

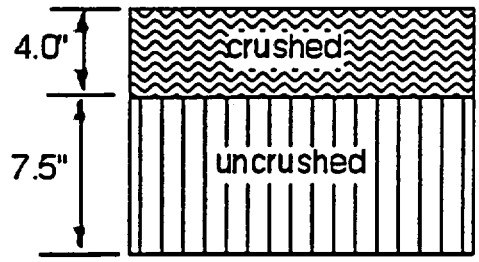

The thermal resistance of the crushed portion is conservatively neglected. Only the uncrsuhed part is accounted for in the effective thermal conductiviy.

Radial k_r - (uncrushed)

$k_r = 1.49813$ Btu/hr-ft-°F

Radial k_r - uncrushed - initial conditions

Model geometry for initial conditions is same as accident conditions (crushed), but impact limiter is initially uncrushed. Use a conductivity that gives the same thermal conductance as that of uncrushed geometry.

$k_{ui} := \left(\frac{23}{7.5}\right) \cdot k_r$ $\quad k_{ui} = 4.59426$ Btu/hr-ft-°F

Axial k_z - (uncrushed)

$k_z = 5$ Btu/hr-ft-°F

Radiation portion (accident only). Using the previous method,

$\ell := 7.5$ in. $\quad d := \frac{6 \cdot c \cdot \tan\left(\frac{\pi}{6}\right)}{\pi}$ $\quad d = 0.28263$ in.

$$K := \frac{\ell}{12} \cdot 0.664 \cdot \varepsilon^{1.63 \cdot \left(\frac{\ell}{d} + 1\right)^{-.89}} \cdot \left(\frac{\ell}{d} + 0.3\right)^{-.69} \qquad K = 0.04207 \text{ ft.}$$

<u>Axial k_z</u> - uncrushed - initial conditions

Using the same method as above,

$k_{ui} := \left(\frac{7.5}{23}\right) \cdot k_z$ $\quad k_{ui} = 1.63043$ Btu/hr-ft-°F

<u>Heat capacity</u>

$\rho c_{p.model} := \rho \cdot c_{p.m} \cdot \left(\frac{23}{7.5}\right)$ $\quad \rho c_{p.model} = 7.084$ Btu/ft^3-°F

$\rho_{model} := \rho \cdot \left(\frac{23}{7.5}\right)$ $\quad \rho_{model} = 32.2$ lb/ft^3

THIS PAGE LEFT BLANK INTENTIONALLY

3.6.6 Radial Dimensions of TAC2D Model

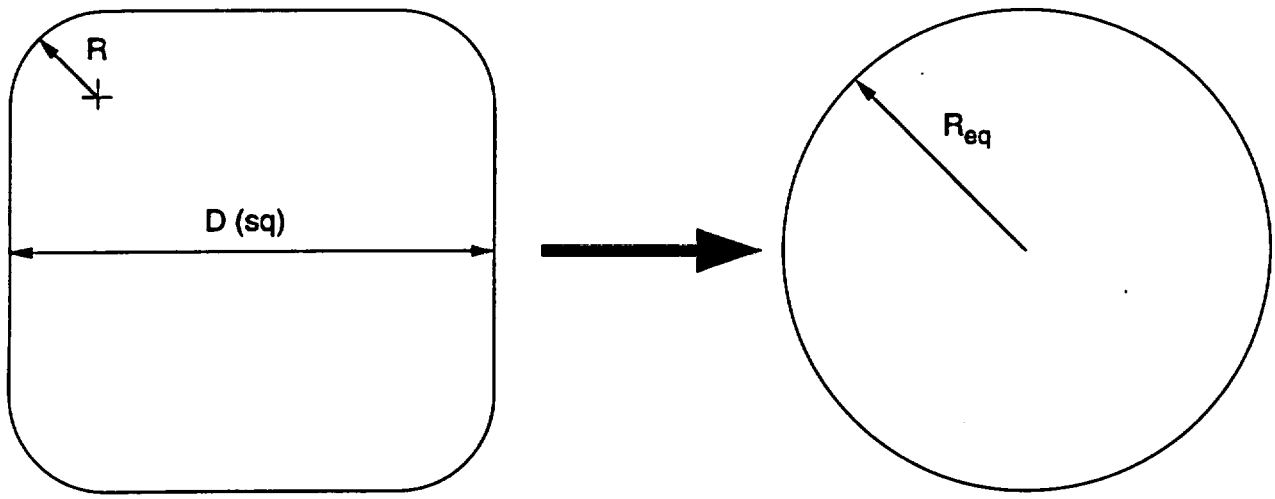

Typical cross section

Calculate the equivalent radii R_{eq} using equal perimeters:

$$P = 4(D - 2R) + 2\pi R = 2\pi R_{eq}$$

$$R_{eq} = \frac{2}{\pi}(D - 2R) + R$$

Thermal properties k_z, ρc_p, and heat generation are adjusted to account for small discrepancies in the cross-sectional area. Table 3.6.6-1 gives values for R_{eq}.

TABLE 3.6.6-1
RADIAL BOUNDARIES OF TAC2D MODEL

Location	Thickness at flats (in.)	D (in.)	R (in.)	P (in.)	R_{eq} (in.)
Cavity liner - inner	0.375	18.16	0.12	72.434	11.528
Cavity liner - outer		18.91	0.500	74.782	11.902
Gap	0.036				
DU - inner	2.65	18.982	0.480	75.104	11.953
DU - outer		24.282	4.470	89.454	14.237
Gap	0.02				
Cask body - inner	1.5	24.322	4.340	89.837	14.298
Cask body - outer		27.322	5.840	99.262	15.798

3.6.7 Effective Radial Gaps for TAC2D Model

Fuel assembly/cavity gap

The fuel cavity size is 8.78 in. The calculations for spent fuel effective conductivity (Sec. 3.6.5.1) were based on an assembly envelope size of 8.432 in. (e.g., WE 15 x 15 or 17 x 17). The gap for the model is thus:

$$0.5 \cdot (8.78 - 8.432) = 0.174 \quad \text{in.}$$

Liner/DU gap at center DU rings

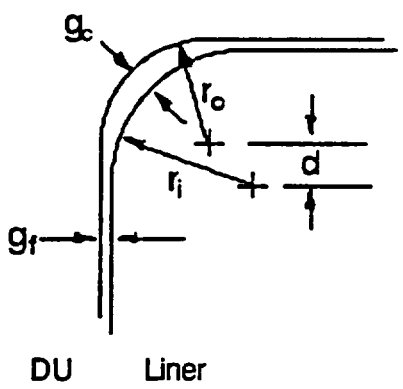

$g_f := 0.036$ in. nominal

$g_c := 0.059$

$r_o := 0.480$ DU

$r_i := 0.500$ cavity liner

$$d := r_i + g_f - r_o \qquad d = 0.056$$

Define the average gap as:

$$g_{avg} := \frac{0.5 \cdot (g_f + g_c) \cdot L_c + g_f \cdot L_f}{L_c + L_f}$$

where L_c and L_f are the lengths associated with the corner and flat sections. Using the DU as a basis and taking a 1/8 section,

$$L_c := \frac{\pi}{4} \cdot r_o + d \qquad L_c = 0.43299$$

$$L_f := \frac{18.982}{2} - (r_o + d) \qquad L_f = 8.955$$

where 18.982 is the distance across flats for theDU inner boundary. Then

$$g_{avg} := \frac{0.5 \cdot (g_f + g_c) \cdot L_c + g_f \cdot L_f}{L_c + L_f} \qquad g_{avg} = 0.03653 \text{ in.}$$

The corner has essentially no effect. Since the model dimensions constrain the gap to be

$11.953 - 11.902 = 0.051$ (see Table 3.6.6-1), the gap conductivity is ratioed by

$\frac{0.051}{0.036} = 1.41667$ to achieve the correct thermal resistance.

Liner/DU gap at end DU rings

Based on the previous results, use the gap at the flats for the average gap.

$$g_{avg} = g_f = 0.051 \text{ in.}$$

No ratioing of conductivity needed since the model gap = actual gap.

DU/Cask body gap

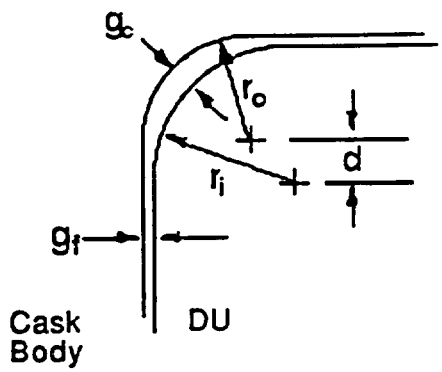

$g_f := 0.020$ in. nominal

$g_c := 0.082$

$r_o := 4.34$ cask body

$r_i := 4.47$ DU

$d := r_i + g_f - r_o$ $\quad d = 0.15$

Use the same method as before

$L_c := \frac{\pi}{4} \cdot r_o + d$ $\quad L_c = 3.55863$

$L_f := \frac{24.322}{2} - (r_o + d)$ $\quad L_f = 7.671$

where 24.322 is the distance across flats for the cask body inner boundary. Then

$$g_{avg} := \frac{0.5 \cdot (g_f + g_c) \cdot L_c + g_f \cdot L_f}{L_c + L_f} \qquad g_{avg} = 0.02982 \text{ in.}$$

Model gap = 14.298 − 14.237 = 0.061 Apply ratio of $\frac{0.061}{0.030} = 2.03333$ to the conductivity.

THIS PAGE LEFT BLANK INTENTIONALLY

3.6.8 Decay Heat Input for TAC2D Model

Decay heat function curve fit (see Fig. 3.4-2):

$$q(x) := 1.356 + 0.2643 \cdot x - 6.716 \cdot 10^{-3} \cdot x^2 + 8.346 \cdot 10^{-5} \cdot x^3 - 5.628 \cdot 10^{-7} \cdot x^4 \ldots + 2.042 \cdot 10^{-9} \cdot x^5 - 3.668 \cdot 10^{-12} \cdot x^6$$

x = in.
q = Watts/in

$Q(x) := 1.0037 \cdot q(x)$ (Adjust to give 617 W total when integrated)

TAC2D model grid spacings are at 16 regular intervals of 9 in.:

ORIGIN := 1

$$X := \begin{bmatrix} 0 \\ 9 \\ 18 \\ 27 \\ 36 \\ 45 \\ 54 \\ 63 \\ 72 \\ 81 \\ 90 \\ 99 \\ 108 \\ 117 \\ 126 \\ 135 \\ 144 \end{bmatrix} \text{ in.}$$

Integrate to obtain heat in TAC2D intervals

$i := 1 .. 16$

$$h_i := \int_{X_i}^{X_{i+1}} Q(x)\, dx$$

Axial Power Profile

$$\sum_i h_i = 617.001 \quad \text{Watts total}$$

$$APP_i := \frac{\left(\frac{h_i}{9}\right)}{\left(\frac{617}{144}\right)}$$

$$h = \begin{bmatrix} 21.486 \\ 34.88 \\ 42.484 \\ 46.259 \\ 47.646 \\ 47.665 \\ 46.991 \\ 46.024 \\ 44.943 \\ 43.747 \\ 42.284 \\ 40.269 \\ 37.288 \\ 32.789 \\ 26.058 \\ 16.188 \end{bmatrix} \text{Watts} \qquad APP = \begin{bmatrix} 0.557 \\ 0.904 \\ 1.102 \\ 1.2 \\ 1.236 \\ 1.236 \\ 1.219 \\ 1.193 \\ 1.165 \\ 1.134 \\ 1.096 \\ 1.044 \\ 0.967 \\ 0.85 \\ 0.676 \\ 0.42 \end{bmatrix}$$

Avg. volumetric heat generation in TAC2D model =

$$q'_{avg} := \frac{Q'_{tot}}{V_{model}} \qquad Q'_{tot} := (4)\cdot 3.413\cdot\left(\sum_i h_i\right) \qquad Q'_{tot} = 8.423\cdot 10^3 \ \text{Btu/hr}$$

$$V_{model} := \frac{\pi\cdot(\overset{\text{gap}}{11.528 - 0.174})^2\cdot 144}{1728} \qquad V_{model} = 33.749 \ ft^3$$

$$q'_{avg} := \frac{Q'_{tot}}{V_{model}} \qquad q'_{avg} = 249.583 \ \text{Btu/hr-ft}^3 \qquad \text{Then} \quad q'_{TAC} := q'_{avg}\cdot APP_i$$

3.6.9 2-D Cross-section Analysis

We constructed a local TAC2D model to obtain the temperature distribution in the x-y plane (i.e., through an axial slice) of the cask at the mid-section. This model provides a detailed temperature distribution in the spent fuel assembly (SFA) and fuel support structure (FSS), whereas these components were "smeared" in the r-z model of Section 3.4. Results of the x-y model are used for two purposes:

- confirm the radial conductivity of the SFA/FSS combined material used in the r-z model (i.e., material no. 4 in Section 3.6.1).
- select the appropriate nodal coordinates from the r-z model that represent maximum and average temperatures at a given cross-section.

Figure 3.6.9-1 shows the model, which assumes symmetry and treats a 1/4-section. Rectangular (x-y) geometry is used, with the gridlines determined by the square outline of the components. The small effect of the rounded corners is neglected. For the round outer skin, the model perimeter is equal to the actual perimeter to preserve the correct heat transfer area.

Properties are given in Section 3.6.1 and use only materials numbered 1–3 and 6–10. We modeled the neutron shield as before with natural convection in a horizontal annulus using the correlation for material 9. The neutron shield is considered a perfectly-mixed coolant at a given cross-section, and therefore is treated with a uniform temperature in this x-y model. To facilitate modeling of the coolant, the effective thermal conductivity calculated by the correlation is converted to an equivalent heat transfer coefficient to be applied to the cask body and outer skin:

$$h = 20.2\, k_e \left(\frac{1}{P_b} + \frac{1}{P_s} \right),$$

where

h = heat transfer coefficient,

20.2 = conduction shape factor (see Section 3.6.2.1),

k_e = effective conductivity (see Section 3.6.2.1),

P_b = perimeter of cask body (TAC2D model),

P_s = perimeter of outer skin (TAC2D model).

Boundary conditions and solar radiation are the same as for the model of Section 3.4. The decay heat is 617 W per assembly with the peaking factor of 1.24 applied.

Figure 3.6.9-2 gives the temperature distribution in the x-y model. These temperatures will be higher than those predicted by the r-z model of Section 3.4 since axial conduction is not accounted for here. However, if the r-z model of Section 3.4 is run with the axial conductivity zeroed out at the mid-section (the section with decay heat peaking factor of 1.24),

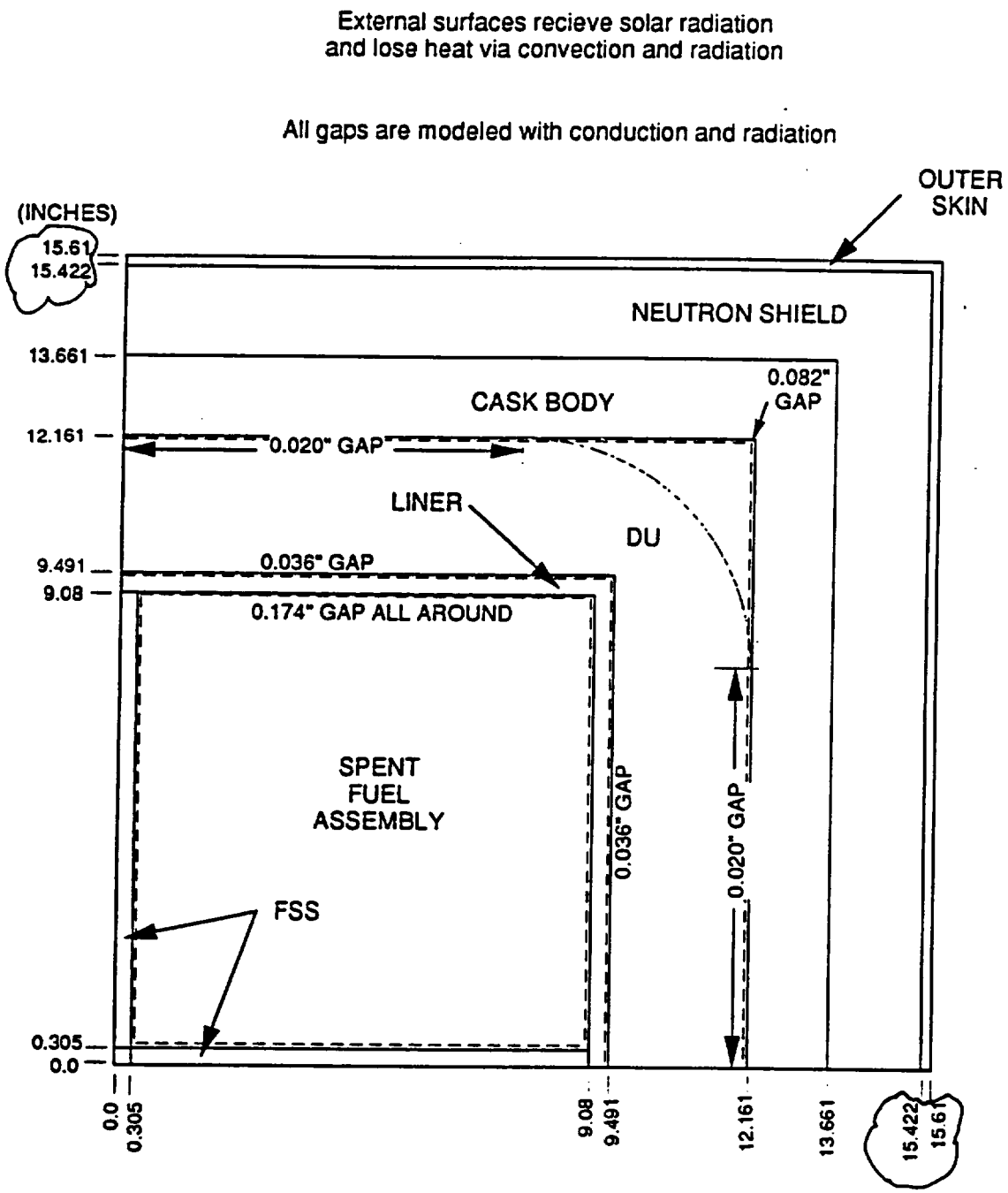

Fig. 3.6.9-1. Cross-section TAC2D model

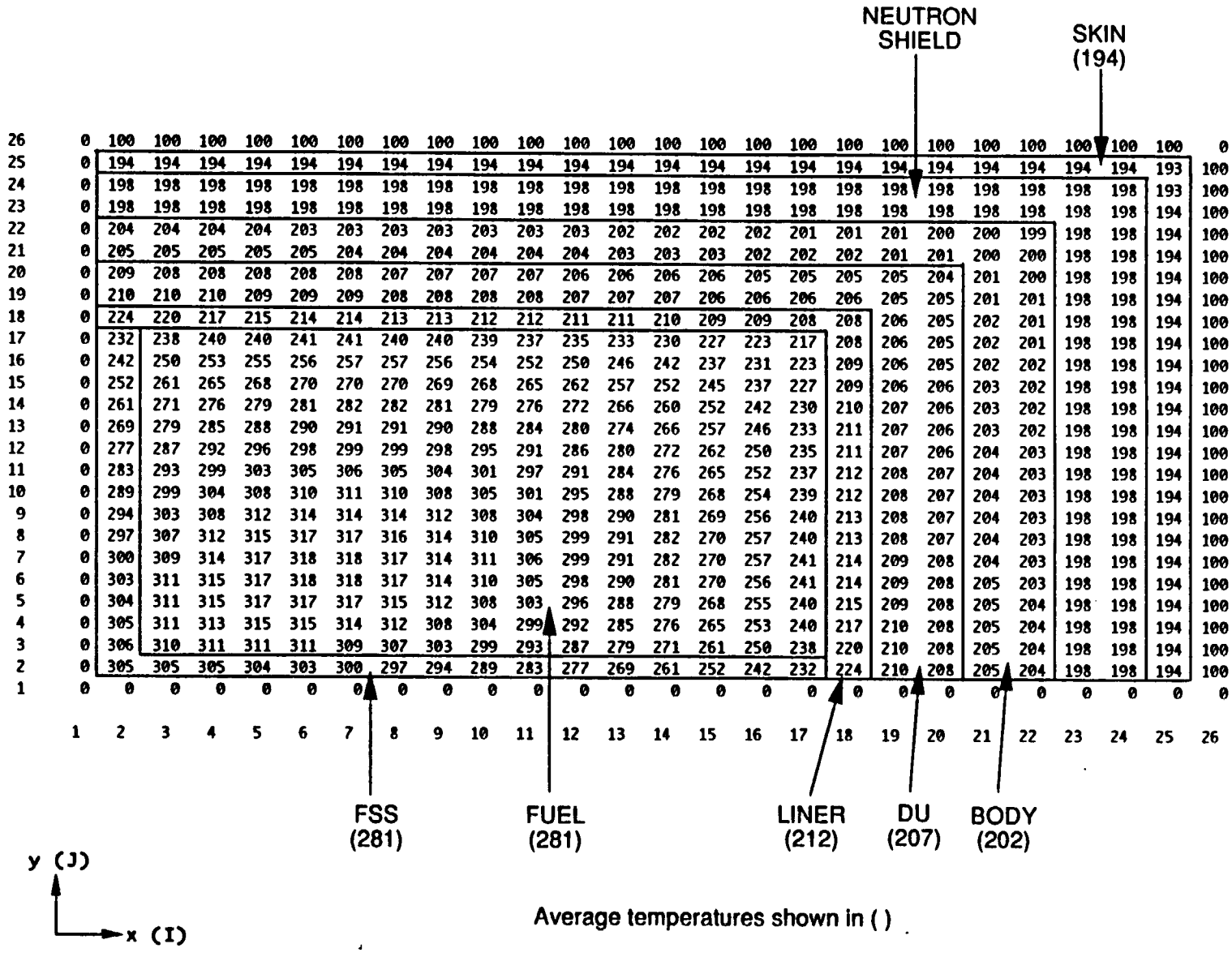

	1	2	3	4	5	6	7	8	9	10	11	12	13	14	15	16	17	18	19	20	21	22	23	24	25	26
26	0	100	100	100	100	100	100	100	100	100	100	100	100	100	100	100	100	100	100	100	100	100	100	100	100	0
25	0	194	194	194	194	194	194	194	194	194	194	194	194	194	194	194	194	194	194	194	194	194	194	194	193	100
24	0	198	198	198	198	198	198	198	198	198	198	198	198	198	198	198	198	198	198	198	198	198	198	198	193	100
23	0	198	198	198	198	198	198	198	198	198	198	198	198	198	198	198	198	198	198	198	198	198	198	198	194	100
22	0	204	204	204	204	203	203	203	203	203	203	203	202	202	202	202	201	201	201	200	200	199	198	198	194	100
21	0	205	205	205	205	205	204	204	204	204	204	204	203	203	203	202	202	202	201	201	200	200	198	198	194	100
20	0	209	208	208	208	208	208	207	207	207	207	206	206	206	206	205	205	205	205	204	201	200	198	198	194	100
19	0	210	210	210	209	209	209	208	208	208	208	207	207	207	206	206	206	206	205	205	201	201	198	198	194	100
18	0	224	220	217	215	214	214	213	213	212	212	211	211	210	209	209	208	208	206	205	202	201	198	198	194	100
17	0	232	238	240	240	241	241	240	240	239	237	235	233	230	227	223	217	208	206	205	202	201	198	198	194	100
16	0	242	250	253	255	256	257	257	256	254	252	250	246	242	237	231	223	209	206	205	202	202	198	198	194	100
15	0	252	261	265	268	270	270	270	269	268	265	262	257	252	245	237	227	209	206	206	203	202	198	198	194	100
14	0	261	271	276	279	281	282	282	281	279	276	272	266	260	252	242	230	210	207	206	203	202	198	198	194	100
13	0	269	279	285	288	290	291	291	290	288	284	280	274	266	257	246	233	211	207	206	203	202	198	198	194	100
12	0	277	287	292	296	298	299	299	298	295	291	286	280	272	262	250	235	211	207	206	204	203	198	198	194	100
11	0	283	293	299	303	305	306	305	304	301	297	291	284	276	265	252	237	212	208	207	204	203	198	198	194	100
10	0	289	299	304	308	310	311	310	308	305	301	295	288	279	268	254	239	212	208	207	204	203	198	198	194	100
9	0	294	303	308	312	314	314	314	312	308	304	298	290	281	269	256	240	213	208	207	204	203	198	198	194	100
8	0	297	307	312	315	317	317	316	314	310	305	299	291	282	270	257	240	213	208	207	204	203	198	198	194	100
7	0	300	309	314	317	318	318	317	314	311	306	299	291	282	270	257	241	214	209	208	204	203	198	198	194	100
6	0	303	311	315	317	318	318	317	314	310	305	298	290	281	270	256	241	214	209	208	205	203	198	198	194	100
5	0	304	311	315	317	317	317	315	312	308	303	296	288	279	268	255	240	215	209	208	205	204	198	198	194	100
4	0	305	311	313	315	315	314	312	308	304	299	292	285	276	265	253	240	217	210	208	205	204	198	198	194	100
3	0	306	310	311	311	311	309	307	303	299	293	287	279	271	261	250	238	220	210	208	205	204	198	198	194	100
2	0	305	305	305	304	303	300	297	294	289	283	277	269	261	252	242	232	224	210	208	205	204	198	198	194	100
1	0	0	0	0	0	0	0	0	0	0	0	0	0	0	0	0	0	0	0	0	0	0	0	0	0	0

Fig. 3.6.9-2. Temperatures (°F) for cross-section model

we can compare the two models directly since both will have no axial conduction. Fig. 3.6.9-3 shows the r-z model with this change. The location at J = 20 has the axial conductivity set to zero and therefore represents the same axial slice and boundary conditions as the x-y model.

The following table shows the two models compare well for the average temperatures of those components explicitly represented:

	x-y model	r-z model no axial conduction
Liner	212°F	213°F
DU	207	207
Cask body	202	203
Neutron shield	197	197
Outer skin	194	194

In addition, the volume-averaged cavity temperature calculated from the x-y model (explicitly representing the SFA and FSS) is 281°F and matches that predicted by the 1-D slice of the r-z model (combined SFA/FSS). This results from a trial-and-error selection for a correction factor on the radial conductivity of the SFA/FSS material in the 1-D model. This factor was established at 1.46 and is therefore used in the complete r-z model, as indicated in Section 3.6.5.1.4.

Further comparisons between the two results establishes the coordinates from the r-z model to use in determining temperatures at various cross-section locations. For example, from Fig. 3.6.9-2, the maximum FSS temperature is 305°F (center). Referring to Fig. 3.6.9-3, this temperature is bracketed by T(3,20) and T(4,20), and can be written as the following normalized linear combination of the two:

$$T(\text{FSS center}) = 305 = 0.696*T(3,20) + 0.304*T(4,20)$$

Similar reasoning is used to obtain the FSS average cross-section temperature, which is 281°F from volume-averaging the x-y model results. In terms of the r-z model:

$$T(\text{FSS avg.}) = 281 = 0.771*T(4,20) + 0.229*T(5,20)$$

The temperature of the FSS radial end (at the interface with the liner) predicted by the x-y model is 232°F and is the same as the interface temperature between the SFA/FSS and the liner calculated by the r-z model.

Table 3.6.9-1 extends this method to all cross-section components. After establishing the equations at the mid-section (J = 20), these are generalized to any axial position by replacing the index 20 with J, i.e.,

$$T(x,y,z) = a_1\ T(I_1,J) + a_2\ T(I_2,J)$$

These equations are the basis for the plot of Fig. 3.4-4.

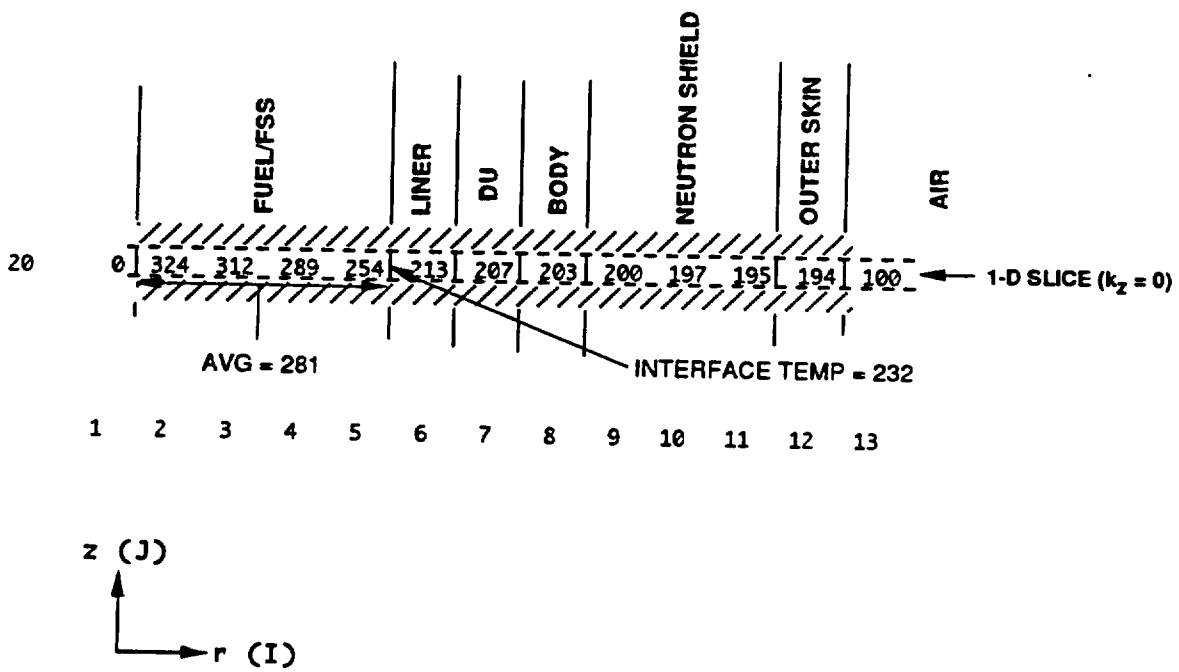

Fig. 3.6.9-3. R-Z TAC2D model results (°F) with zero axial conductivity at midsection

TABLE 3.6.9-1
CORRELATION BETWEEN X-Y AND R-Z MODELS

Location	x-y model	r-z model at J=20			
	Temp. (°F)	I indices of bounding temps		Coefficients	
		I_1	I_2	a_1	a_2
FSS center (max.)	305	3*	4*	0.696	0.304
FSS radial average	281	4	5	0.771	0.229
FSS end	232	Interface temperature (IT) between SFA/FSS and liner			
Liner @ flat (max.)	224	IT	6	0.579	0.421
Liner @ corner	208	6	7	0.167	0.833
Liner avg.	212	6	--	1	--
DU @ flat (max.)	210	6	7	0.5	0.5
DU avg.	207	7	--	1	--
Cask body @ flat	205	7	8	0.5	0.5
Cask body avg.	202	8	--	1	--
Neutron shield	198	Volume avg. of T(9,20)...T(11,20)			
Skin	194	12	--	1	--

*For the accident model, these indices are 4 and 6, respectively, for the same radial locations.

3.6.10 References for Sections 3.2 through 3.6

3.2-1 Glasstone, S., and A. Sesonske, *Nuclear Reactor Engineering*, D. Van Nostrand, 1963, p. 814.

3.2-2 *Thermophysical Properties of Matter*, Thermophysical Properties Research Center, Purdue University, IFI/Plenum, 1970, Vol. 1, pp. 887-889.

3.2-3 Kreith, F., *Principles of Heat Transfer*, 2nd ed., International Textbook, 1968, pp. 215, 593-595.

3.2-4 ASME Code, 1986 Edition, Section III, Division 1, Appendix I, Table I-4.0.

3.2-5 Armco, Inc., Bulletin No. S-45e, p. 9.

3.2-6 "Final Design for Fort St. Vrain Fuel Shipping Cask," GADR-55, General Atomics, Addendum I, 1978.

3.2-7 *Thermophysical Properties of High Temperature Solid Materials*, Thermophysical Properties Research Center, Purdue University, Macmillan, 1967, Vol. 6, pp. 1078-1081; Vol. 5, p. 35.

3.2-8 Deem, H. W., and C. F. Lucks, "Thermal Conductivity of Boron Carbide from 100°C to 800°C," BMI-713, Battelle Memorial Institute, December 10, 1951.

3.2-9 "Materials Selector," *Materials Engineering*, December 1990, pp. 70, 72, 82.

3.2-10 Goodman et al., "The Thermodynamic and Transport Properties of Helium," GA-A13400, General Atomic Company, October 1975.

3.2-11 "Heat Transfer in a Dry, Horizontal LWR Spent Fuel Assembly," PATRAM-83, Vol. II, pp. 1087-1094.

3.2-12 "MODREX Application Study to Support the Sequoyah Nuclear Power Plant," GA-A16673, General Atomics, March 1982, pp. 5-36.

3.2-13 "The CASTOR-V/21 PWR Spent Fuel Storage Cask: Testing and Analysis," EPRI NP-4887, November 1986, pp. 5-6.

3.2-14 "The TN-24P PWR Spent Fuel Storage Cask: Testing and Analysis," EPRI NP-5128, April 1987, pp. 5-17.

3.2-15 "Comparison of HYDRA-II Predictions to Temperature Data from Consolidated and Unconsolidated Model Spent Fuel Predictions," PNL-6630, September 1988.

3.2-16 Curme, G. O., (ed.), *Glycols*, Reinhold Publishing, 1952.

3.2-17 "A Guide to Glycols," Dow Chemical Company, 1992.

3.2-18 Gubareff, G. G., J. E. Janssen, and R. H. Torborg, *Thermal Radiation Properties Survey*, Honeywell Research Center, 1960, Table 403.

3.3-1 *Parker O-Ring Handbook*, Parker Seal Company, 1991, pp. A3-4, A3-36.

3.4-1 "Validation Document for TAC2D_0002," Document 910513, General Atomics, May 1992.

3.4-2 "Topical Report on Actinide-only Burnup Credit for PWR Spent Fuel Nuclear Fuel Packages," DOE/RW-0472, May 1995, Fig. 4-4.

3.5-1 "ANSYS Verification Manual for Revision 5.2," Swanson Analysis Systems, September 1995.

3.5-2 "PATRAN Plus User's Manual," Release 2.4, PDA Engineering, September 1989.

3.5-3 "PAT/ANSYS Interface Guide," Release 2.2, PDA Engineering, September 1989.

3.6.2-1 Holman, J. P., *Heat Transfer*, 5th ed., McGraw-Hill, 1981, pp. 275, 281.

3.6.2-2 Bucholz, J.A., "Scoping Design Analyses for Optimized Shipping Casks Containing 1-, 2-, 3-, 5-; 7-, or 10-year old PWR Spent Fuel," Oak Ridge National Laboratory, ORNL/CSD/TM-149, January 1983.

3.6.2-3 Lewis, G. K., "Shape Factors in Conduction Heat Flow for Circular Bars and Slabs with Various Internal Geometries," *Int. J. Heat and Mass Transfer*, Vol. 11, 1968, pp. 985-992.

3.6.2-4 Kreith, F., *Principles of Heat Transfer*, 2nd ed., International Textbook, 1968, p. 411.

3.6.3-1 "Characteristics of Spent Fuel, High-Level Waste, and Other Radioactive Wastes Which May Require Long-Term Isolation," DOE/RW-0184, U. S. Department of Energy, Vol. 3, Appendix 2A ("Physical Descriptions of LWR Fuel Assemblies"), December 1987.

3.6.3-2 "Characteristics of Potential Repository Wastes," DOE/RW-0184-R1, U. S. Department of Energy, Vol. 1, July 1992.

3.6.4-1 *Marks' Standard Handbook for Mechanical Engineers*, McGraw-Hill, 8th ed., 1978, p. 4-12.

3.6.4-2 "The CASTOR-V/21 PWR Spent Fuel Storage Cask: Testing and Analysis," EPRI NP-4887, November 1986.

3.6.4-3 Arpaci, V. S., *Conduction Heat Transfer*, Addison-Wesley, 1966, p. 465.

3.6.4-4 Kreith, F., *Principles of Heat Transfer*, 2nd ed., International Textbook, 1968, Fig. 7-1.

3.6.4-5 Idel'chik, I. E., *Handbook of Hydraulic Resistance*, AEC-tr-6630, USAEC, 1966, Diagram 8-2.

3.6.5-1 Cox, R. L., "Radiative Heat Transfer in Arrays of Parallel Cylinders," ORNL-5239, Oak Ridge National Laboratory, 1977.

3.6.5-2 "Validation of the TUBERAD Code," Document 910067, General Atomics, February 1990.

3.6.5-3 *Heat Transfer and Fluid Flow Data Book*, General Electric Company, 1970, Sec. G502.2, p.2.

CHAPTER 4
TABLE OF CONTENTS

FIGURES

THIS PAGE LEFT BLANK INTENTIONALLY

4. CONTAINMENT

4.1 Containment Boundary

The containment boundary consists of the cask body (cask body wall, flange and bottom plate), cask closure, gas sample port, drain valve and the primary O-ring seals. One O-ring, located in the inner dovetail groove in the cask closure, seals the interface between the cask body and the cask closure. A second O-ring is located on the gas sample port in the closure, and a third on the drain valve in the bottom head of the cask. Figures 4.1-1 through 4.1-3 show the structural components and the O-ring seals that form the containment boundary.

4.1.1 Containment Vessel

The cask body and closure for the GA-4 cask are fabricated from SA-240, Type XM-19 stainless steel. The cask body wall is 1.5 in. thick. The bottom plate is 9.5 in. thick. The closure is 11.0 in. thick.

4.1.2 Containment Penetrations

A gas sample port in the closure and a drain valve in the bottom plate are the only two penetrations into the containment vessel (see Fig. 4.1-1). All ports are made from SA-240, Type XM-19 stainless steel. We designed all components of the ports to maintain the required leaktight (1×10^{-7} std-cm^3/s) containment during both normal conditions of transport and hypothetical accident conditions.

4.1.3 Seals and Welds

4.1.3.1 Containment Boundary O-ring Seals. The O-ring seals must function properly between –40°F and 143°F during normal conditions of transport. During the hypothetical accident condition thermal event, the O-ring seals must function properly at a temperature of 300°F. The closure primary O-ring is 0.375 in. in diameter and is compressed 25%, nominal. This amount of squeeze, 0.093 in., allows the O-ring seal to function properly during the maximum expected displacement of the cask closure and cask body interface; see Section 4.3. Close-tolerance O-ring seals and special dovetail groove dimensions are used in order to obtain the specified squeeze. The closure seals are Parker E-0740-75 ethylene propylene elastomer.

4.1.3.2 Containment Boundary Welds. We have designed and will qualify, fabricate, inspect, and accept all containment boundary welds in accordance with the requirements of Section III, Subsection NB, of the ASME Code (Ref. 4.1-1); NUREG/CR-3019, "Recommended Welding Criteria for Use in the Fabrication of Shipping Containers for Radioactive Materials"; and NUREG/CR-3854, "Fabrication Criteria for Shipping Containers." Section 1.3.1 describes the Quality Assurance Program.

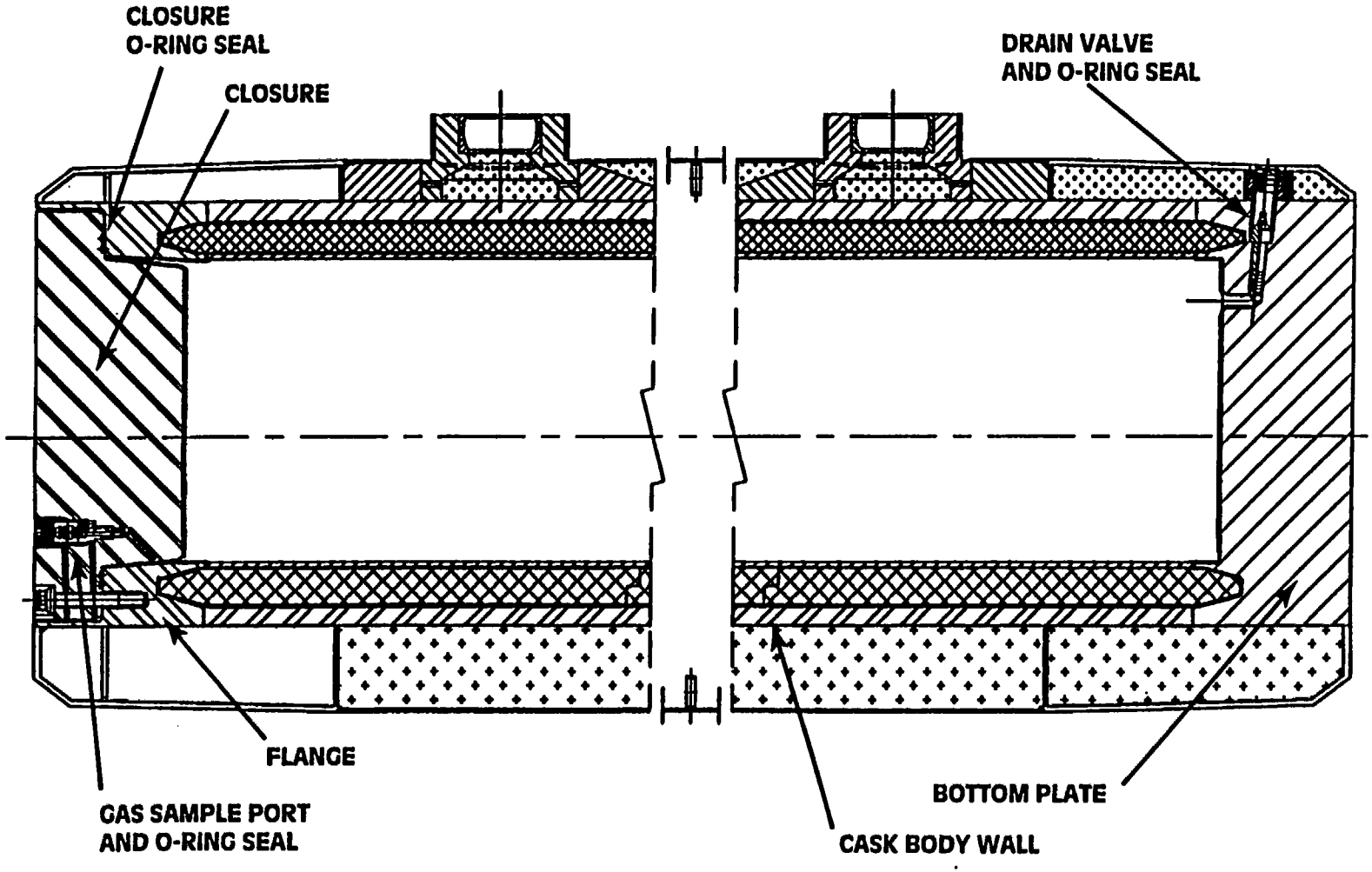

Fig. 4.1-1. Containment boundary

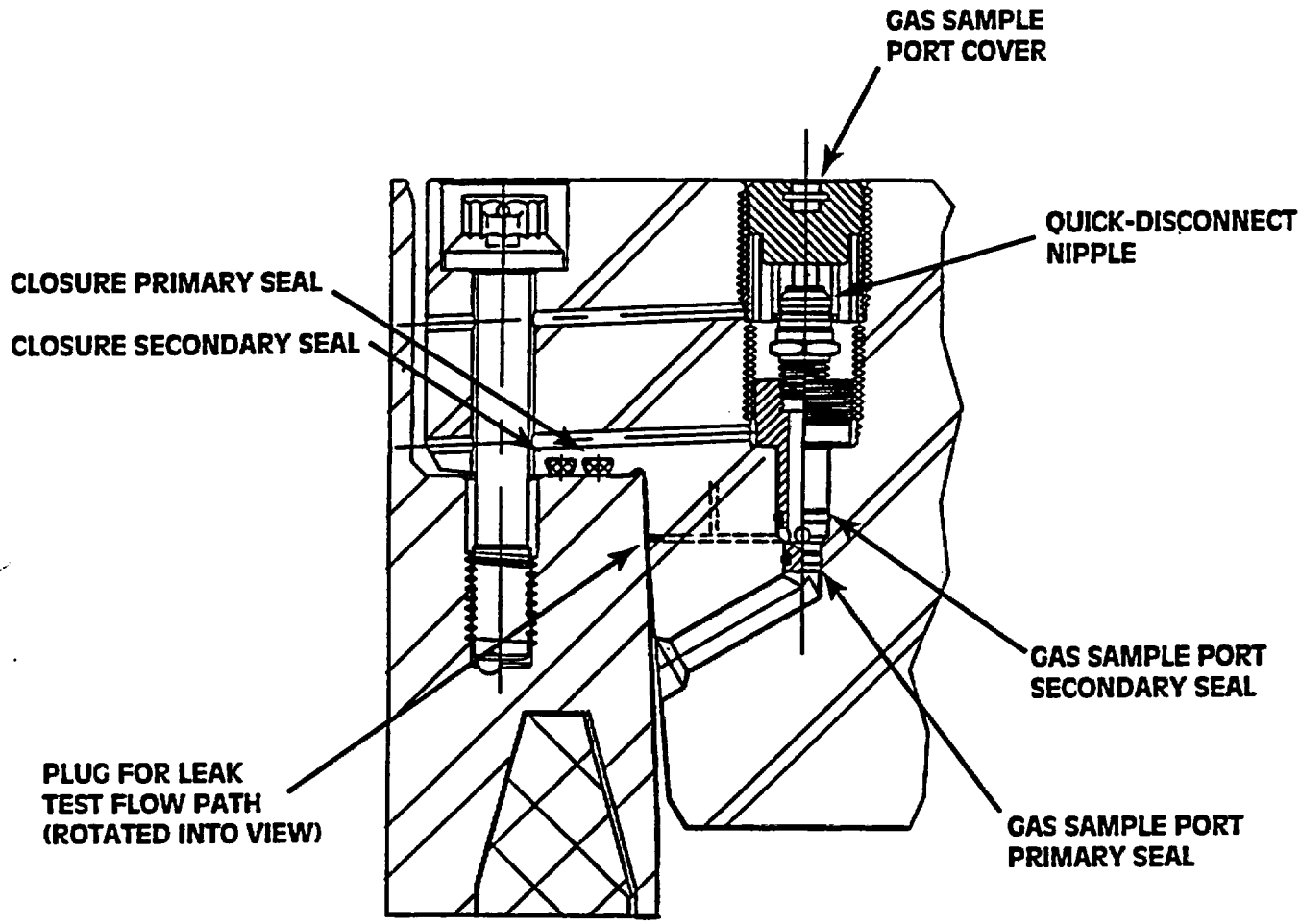

L-717(2)
6-7-96

Fig. 4.1-2. Detail of containment boundary at closure

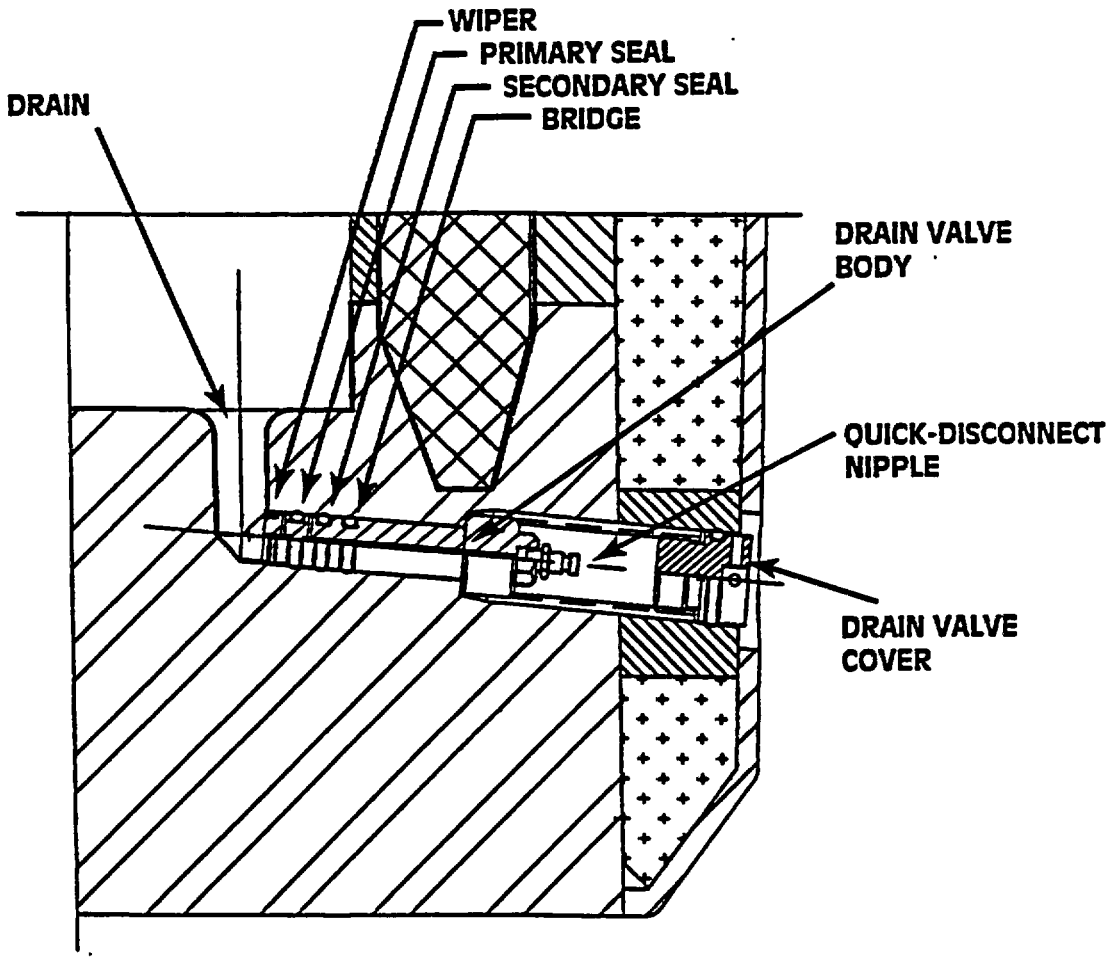

L-717(3)
6-7-96

Fig. 4.1-3. Detail of containment boundary at drain

4.1.4 Closure

The cask closure consists of a Type XM-19 stainless steel plate which is attached to the cask body with 12 1-in. bolts having threaded inserts. The material specification for the bolts is ASME SB-637, Alloy N07718. Each bolt is torqued to 235 ± 15 ft-lb.

THIS PAGE LEFT BLANK INTENTIONALLY

4.2 Requirements for Normal Conditions of Transport

We designed all components of the containment boundary in accordance with established criteria and then performed tests and analysis to verify compliance with the criteria. Analysis shows that, during all normal conditions, the containment vessel meets the structural criteria in Section 2.1 and the O-ring seals remain below allowable temperatures and maintain sufficient compression. We have verified the seal design by performing a test on a full-scale closure and seal configuration (Section 4.5.1).

4.2.1 Containment of Radioactive Material

The cask design permits no release of radioactive material, demonstrated to a sensitivity of $A_2 \times 10^{-6}$ Ci/hr. This criterion is met by maintaining a leaktight containment boundary as defined in ANSI N14.5-1987 (Ref. 4.2-1).

4.2.2 Pressurization of Containment Vessel

We calculated the maximum normal operating pressure (MNOP) in Section 3.4.4. We included this pressure in the loading combinations that were defined in Section 2.1 and evaluated in Section 2.6. The results show that the structural allowable stresses are met.

4.2.3 Containment Criterion

The verifiable containment criterion for a leaktight containment is a leakage test that shows leakage to be less than 1×10^{-7} std-cm^3/s (air) or 1.96×10^{-7} cm^3/s (helium). The cask is designed to a leaktight capability as defined in ANSI N14.5. Section 4.5.1 discusses full-scale closure seal tests, which demonstrate that the primary seal is leaktight for normal conditions of transport. The test procedure for the containment system assembly verification and for periodic leakage tests will be described in the Operation and Maintenance Manual. Results from half-scale model testing will also be used to confirm leaktightness.

For the containment system assembly verification pre-shipment test, ANSI N14.5-1987 requires a leakage test with a sensitivity of 1×10^{-3} std-cm^3/s. A pressure rise test is adequate for this purpose. For the containment system fabrication and periodic verification tests, ANSI N14.5-1987 requires that the leakage test procedure have a sensitivity of 5×10^{-8} std-cm^3/s to demonstrate that the package is leaktight. Section 8.1.3.2 contains a description of the procedure for the containment system fabrication and periodic verification tests.

THIS PAGE LEFT BLANK INTENTIONALLY

4.3 Requirements of the Hypothetical Accident Conditions

We designed all components of the containment boundary in accordance with established criteria and then performed tests and analysis to verify that the criteria were met. Conservative analysis shows (1) that during all hypothetical accident conditions, the containment boundary meets the structural criteria in Section 2.1 and, (2) that the O-ring seals remain below allowable temperatures and maintain sufficient compression. According to the manufacturer's data (Section 3.3), the maximum O-ring temperature of 300°F during the hypothetical accident condition thermal event allows the seal to function for 1000 hr. The maximum O-ring transient local decompression due to bending of the closure caused by a thermal gradient during the thermal event is equal to 0.024 in. (see Sec. 2.7.3) out of an initial minimum nominal compression of 0.093 in. We have verified the seal design by performing a test on a full-scale closure and seal configuration (Section 4.5.1).

4.3.1 Fission Gas Products

Since the containment criterion is a leaktight cask, the quantity of gas fission products is not necessary for containment analysis.

4.3.2 Containment of Radioactive Materials

The GA-4 cask design allows no release of krypton-85 exceeding $10A_2$ in one week and no escape of radioactive material exceeding a total amount A_2 in one week. We meet this criterion by maintaining a leaktight containment boundary as defined in ANSI N14.5-1987 (Ref. 4.2-1).

4.3.3 Containment Criterion

The verifiable containment criterion for a leaktight containment is a leakage test that shows leakage to be less than 1×10^{-7} std-cm^3/s (air) or 1.96×10^{-7} cm^3/s (helium). The cask is designed to a leaktight capability as defined in ANSI N14.5. Section 4.5.1 discusses full-scale closure seal tests and demonstrates that the primary seal is leaktight for hypothetical accident conditions of transport. The test procedure for the containment system assembly verification and for periodic verification leakage tests will be described in the Operation and Maintenance Manual. Results from half-scale model testing will be used to confirm leaktightness.

For the containment system assembly verification pre-shipment test, ANSI N14.5-1987 requires a leakage test with a sensitivity of 1×10^{-3} std-cm^3/s. A pressure rise test is adequate for this purpose. For the containment system fabrication and periodic verification tests, ANSI N14.5-1987 requires that the leakage test procedure have a sensitivity of 5×10^{-8} std-cm^3/s to demonstrate that the package is leaktight. Section 8.1.3.2 contains a description of the procedure for the containment system fabrication and periodic verification tests.

THIS PAGE LEFT BLANK INTENTIONALLY

4.4 Special Requirements

Four PWR fuel elements contain more than 20 curies of plutonium. However, reactor fuel elements are exempt from the requirements of 10 CFR Part 71.63(b); therefore, we have not included a separate inner container.

THIS PAGE LEFT BLANK INTENTIONALLY

4.5 Appendix

4.5.1 Full-scale Closure Seal Tests

4.5.1.1 Summary. The primary O-ring seal of the cask was tested for leakage using a full-scale mockup of the cask closure and flange. The seal material was E-0740-75, an ethylene propylene compound supplied by Parker Seal Group, Parker Hannifin Corporation. The tests were performed at temperatures of ambient, –42°, 250°, and 380°F. Shim plates between the fixture lid and flange, ranging from 0 to 0.038 in., simulated gaps resulting from thermal-induced distortion. The leakage testing was carried out by means of a helium mass spectrometer leak detector (MSLD), following ANSI N14.5-1987 (Ref. 4.2-1). All tests were performed at Wyle Laboratories, Norco, California.

Results showed that the primary seal maintained leaktightness for all test conditions. After pressurization of the test fixture, permeation of the helium gas through the seal was observed to begin in about 20 minutes for the ambient test and in 1–2 minutes for the tests at elevated temperatures. To verify that the MSLD readings were due to permeation and not real leakage, a response check was conducted in which a calibrated leak source of approximately 1×10^{-7} std cm^3/s was inserted in the detector line near the seal. When the leak source was activated, the detector responded within seconds.

4.5.1.2 Test Set-up. A typical test set-up is shown in Fig. 4.5-1 and illustrated schematically in Fig. 4.5-2. The test fixture consists of a lid and flange and is a full-scale representation of the cross section of the cask closure end. Two dovetail grooves in the lid hold the primary and secondary O-ring seals. The grooves and O-ring seals precisely model the full-scale cask. All fixture materials are fabricated from 304 stainless steel. The fixture lid weighs approximately 170 lb and the flange 180 lb. The fixture lid attaches to the flange with 20 1-in. bolts that thread into nuts tack-welded to the bottom of the flange. The bolts are torqued to 100 ft-lb. Shim plates extending all around the fixture's perimeter maintain uniform specified gaps between the lid and flange.

From operational and handling considerations it was not feasible to fabricate the test lid to the actual closure thickness of 11 in. Since the test was a verification of the seal performance under the actual temperatures and amounts of compression experienced in the package, seal and groove dimensions were identical to those in the package. The number of bolts was increased from 12 to 20 in the test only to minimize local deflection between bolts of the relatively thin 1-in. lid. This local deflection is absent in the actual package due to the considerably thicker and stiffer lid. The bolt torque in the test was less than actual (100 versus 235 ft-lb) but the seals are fully compressed in both the test and package configurations. Once the seals are fully compressed in their grooves and metal-to-metal contact is established, additional bolt torque produces no further compression of the seals. For the reduced compression predicted by the accident analysis, shims of a known thickness were inserted between the lid and its base to duplicate this effect.

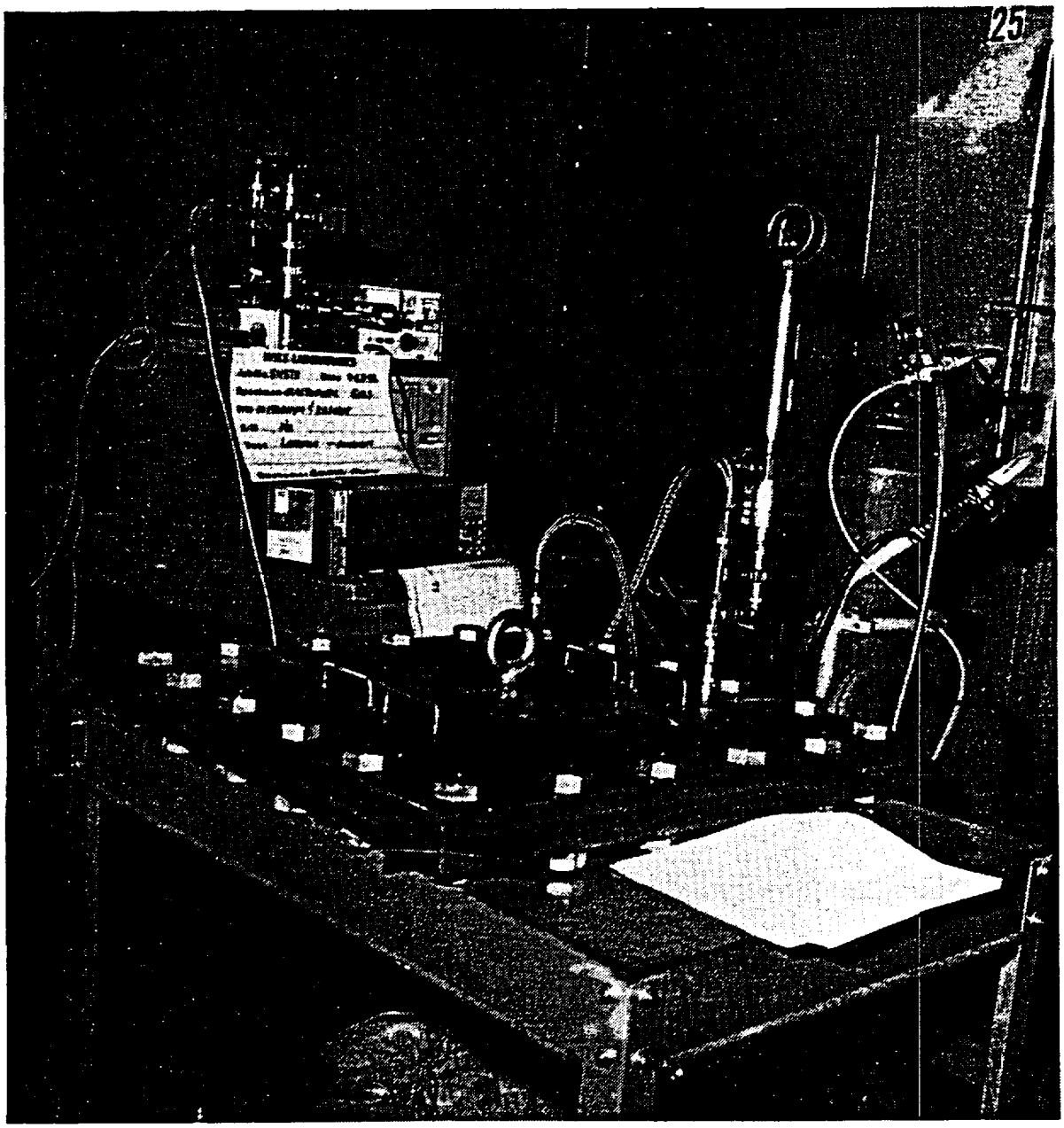

K-885(17)
5-26-93

Fig. 4-5.1. Test set-up for ambient conditions

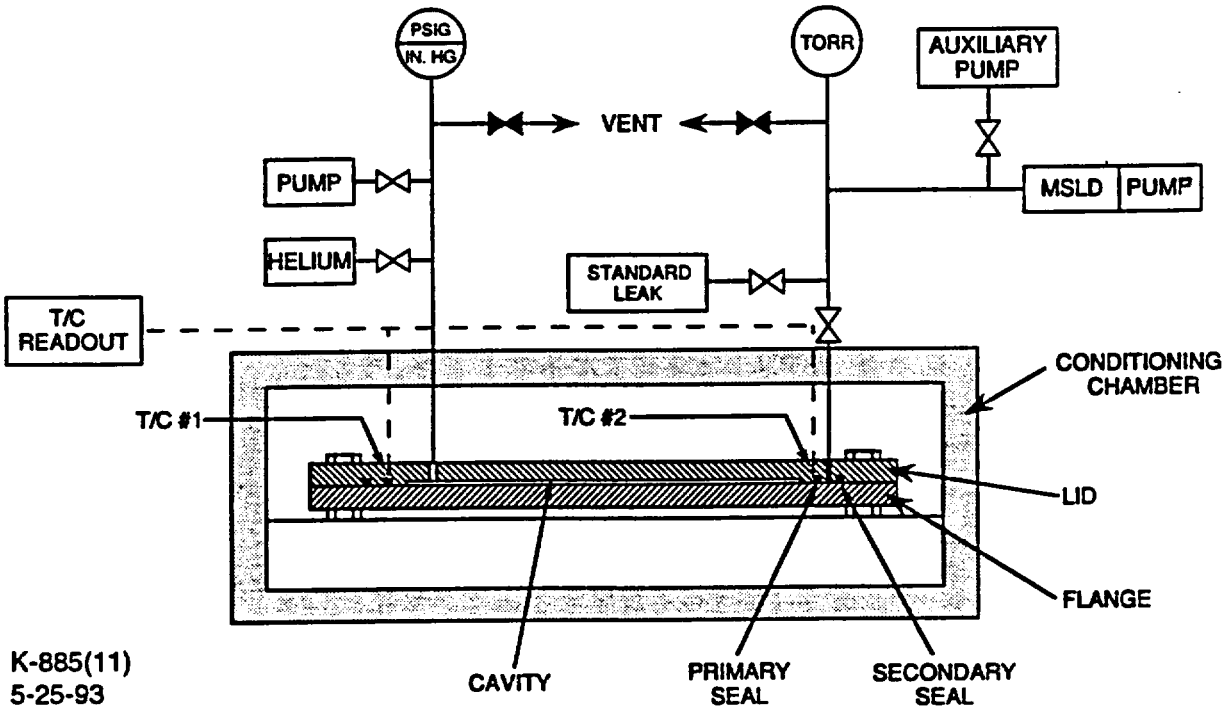

Fig. 4.5-2. Schematic of test arrangement

Prior to testing, the small volume between the flange and lid is initially evacuated. When the test begins, this volume is filled with helium to atmospheric pressure. A second port located between the O-rings is continuously evacuated by the MSLD, and the detector measures the helium leakage past the primary (inner) O-ring. The detector output is recorded by a conventional strip chart recorder.

For the tests carried out in the conditioning chamber, the fixture temperatures near the inner seal are measured by two thermocouples (Type T) and recorded.

4.5.1.3 Test Results. Four tests were carried out with E-0740-75 seals and the results are shown in the following table. One set of seals was used for the test at –40°F, and another set was used for the other three tests. The first two tests simulated normal conditions of transport, while the last two represented hypothetical accident conditions. For the latter conditions, the thermal and thermal stress analyses (Sections 3.5 and 2.7.3) predict a maximum lid/flange gap of 0.024 in., corresponding to a seal temperature of 240°F, while 300°F is the maximum seal temperature, corresponding to a zero gap. The conditions used in the test are therefore conservative.

Gap (in.)	Temp. (°F)	Background[a] (atm cm^3/s)	Leakage[b] (atm cm^3/s)	Permeation time (min)[c]
0	–42	9.3×10^{-9}	7.1×10^{-10}	> 5
0.010	Ambient (~75)	3.0×10^{-8}	$< 1 \times 10^{-7}$	23
0.038	15 hr @ 250	4.8×10^{-8}	"	2
0	380 1 hr above 365 1.5 hr above 350	3.0×10^{-10}	2×10^{-10}	1

[a]Detector reading before introduction of helium.
[b]Increase above background after introduction of helium but before onset of permeation.
[c]After achieving 1 atm cavity pressure.

Test data are summarized above. Results are given in terms of test conditions, i.e., helium leakage at the test temperature with an upstream pressure of 1 atm in the fixture cavity and a downstream pressure of less than 0.01 atm (typically 2–5 millitorr) in the detector line or seal interspace. The definition of leaktight in ANSI N14.5-1987 (Ref. 4.2-1) assumes air at a standard temperature of 77°F (298 K) as the leakage gas. No conversion of test results to air standard conditions was made. Such a conversion would give leakage rates less than the helium rate, and the helium rate is therefore conservative.

The test at –42°F was allowed to proceed for 5 minutes, while the remaining tests were carried out for longer times to investigate the effect of permeation. Figures 4.5-3 through 4.5-5 show the leakage plotted against time for the tests at ambient, 250°, and 380°F. Time 0 corresponds to 1 atm helium pressure in the fixture cavity. (Typically, less than 30 seconds were required to achieve this from the time the valve was first opened.) In Fig. 4.5-3 permeation is clearly evident from the slow rise in detector output following some 20 minutes of no indicated leakage. Figures 4.5-4 and 4.5-5 show permeation beginning much more rapidly, as expected with higher temperatures, with the leakage showing no change for 1–2 minutes after pressurization.

Following the last test, a response check was carried out to verify that an actual leak would be observed within a time much less than 1 minute. The calibrated standard leak of 1.7×10^{-7} was connected to the detector line where it entered the test fixture. With the leak standard valve open, an arbitrary reference point of time 0 was marked and the valve was closed one minute later. The detector responded virtually instantaneously. After another minute the valve was opened again, producing another immediate response. The entire sequence was then repeated, with the same results.

4.5.1.4 Conclusions. The tests carried out confirmed the leaktightness of the E-0740-75 inner (primary) seal under normal and hypothetical accident conditions of transport for the GA-4 cask. The leaktightness is inferred by observing that for ambient conditions the MSLD reading did not increase by more than 1×10^{-7} during a 20-minute period following pressurization of the fixture cavity to 1 atm helium. For elevated temperatures the indicated leakage increased after holding at background for at least one minute. Since a response check showed that an actual leak would be observed within seconds, the indicated "leakage" is actually permeation.

4.5.2 References for Sections 4.1 through 4.2

4.1-1 American Society of Mechanical Engineers (ASME), *Boiler and Pressure Vessel Code.*

4.2-1 American National Standards Institute, "American National Standard for Leakage Tests on Packages for Shipment of Radioactive Material," ANSI N14.5-1987.

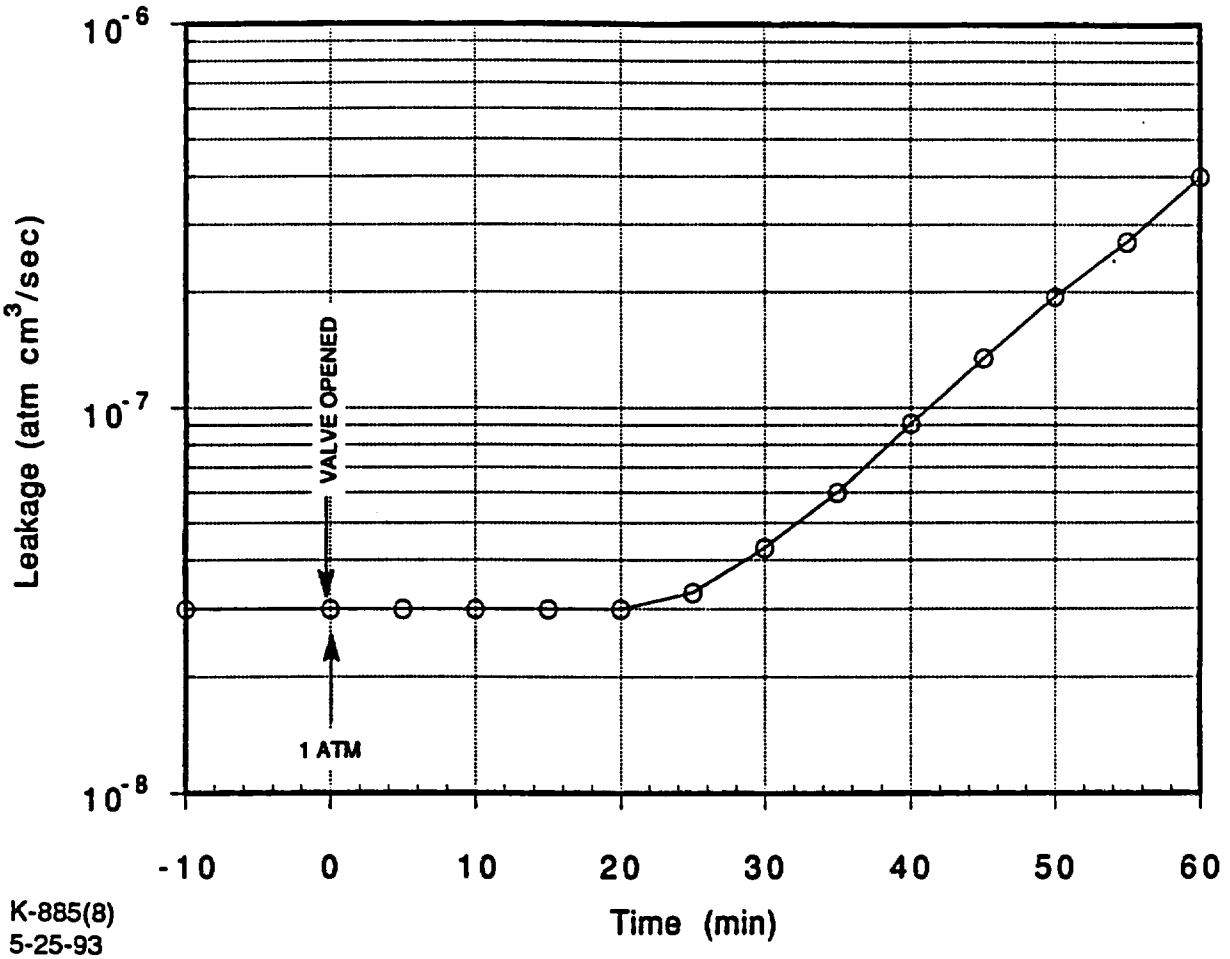

Fig. 4.5-3. Test results, 0.010-in. gap, ambient temperature

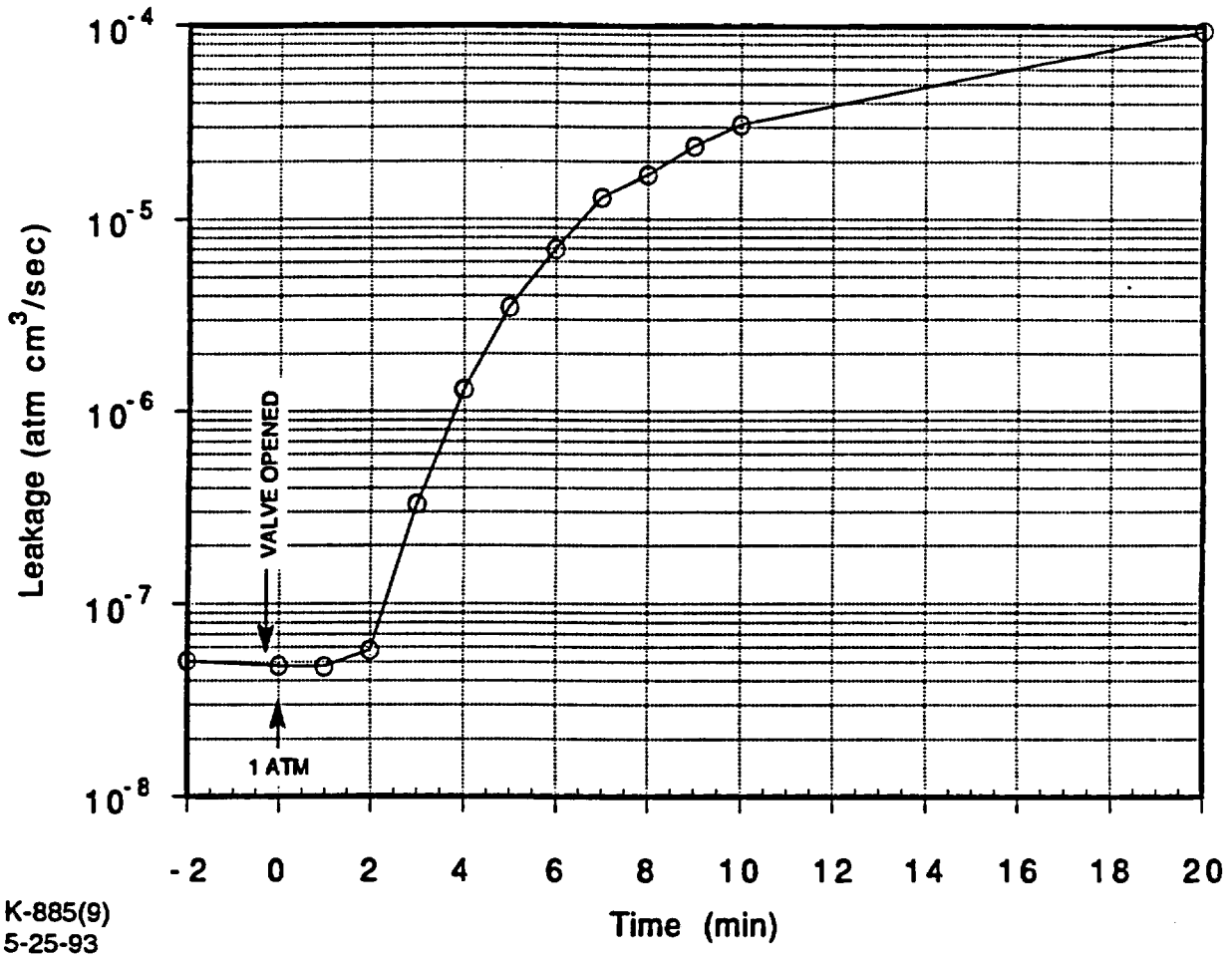

K-885(9)
5-25-93

Fig. 4.5-4. Test results, 0.038-in. gap, 250°F

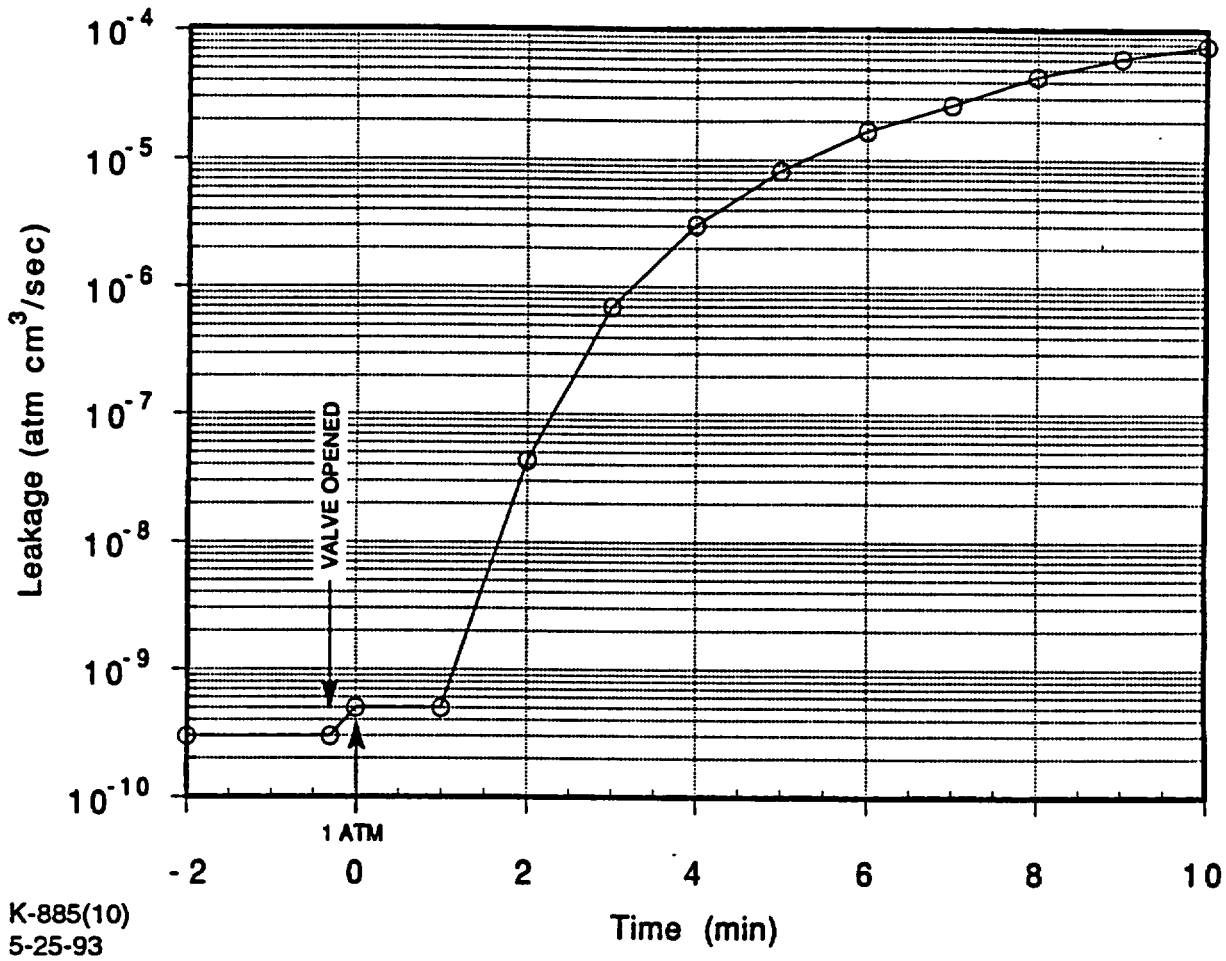

Fig. 4.5-5. Test results, zero-gap, 380°F

CHAPTER 5
TABLE OF CONTENTS

FIGURES

TABLES

5. SHIELDING EVALUATION

The GA-4 legal weight truck cask utilizes a combination of depleted uranium (DU) and stainless steel, primarily for gamma shielding,[ ]
Proprietary Information
.]Optimum amounts and thicknesses of neutron and gamma shielding, with the densest material placed toward the inside of the cask, are provided to achieve the most efficient cask geometry. For simplicity in design and ease of fabrication, the top and bottom ends of the cask use a solid stainless steel structure that provides sufficient shielding for both neutrons and gammas.

5.1 Discussion and Results

The GA-4 cask provides radiation shielding engineered to meet the regulatory requirements of 10 CFR Part 71 for both normal conditions of transport and hypothetical accident conditions. Our approach to shielding design is to optimize the cask shielding configuration for minimum weights and maximum payloads. The optimization method involves use of the most effective shielding materials, square cross-section geometry with rounded corners for gamma shielding, and tapered shielding sections in the non-fuel regions. In addition, the trade-off between the thicknesses of the neutron and gamma shields enables us to select an optimum design in which the cask weight is at a minimum.

The shielding analysis is based on four pressurized-water reactor (PWR) assemblies with fuel burnups of 35 GWd/MTU and a cooling time of 10 years and 45 GWd/MTU and a cooling time of 15 years. We generated the neutron and gamma source data with the SAS2 module of SCALE-4.1, using a representative burnup profile for the active fuel region. The gamma source terms for the non-fuel regions were obtained by using activation ratios related to the active fuel region.

The shielding analyses considered both normal and hypothetical accident conditions to comply with 10 CFR Part 71. The shielding models for these two conditions differ only in the assumption that the neutron shield and outer skin remain intact during normal transport but completely disappear following a hypothetical accident event. This is conservative since, as shown in Section 2.10.11, the neutron shield outer skin will survive the accident conditions.

The results of the analyses (including the high-burnup fuel analyses) are shown in Table 5.1-1. These results show that radiation levels outside the cask are all within the regulatory dose rate limits for transportation. In these tables the package surface is defined as the surface of the top and bottom impact limiters and the cylindrical surface of the outer skin. The dose rate for the side of the package is the peak dose rate that occurs on the outer skin. The "top" and "bottom" package surface dose rates are the peak dose rates found anywhere on the top and bottom impact limiters respectively. The "2 m from vehicle, side" dose rate is the peak dose rate found anywhere on a vertical plane 2 m from the trailer's side edge. The rear dose rate refers to a point 2 m behind the back end of the trailer along the axis of the cask. The "back of cab" dose rate is that found on the back of the tractor cab along the central axis of the cask. The tables intentionally omit the dose rate 2 m in front of the trailer (when the tractor is not attached), since the 2-mR/h dose rate limit at the rear of the tractor cab is more restrictive.

Table 5.1-1 presents the dose rate results with two and three significant digits to be consistent with the results shown on the dose rate maps in Section 5.4. The results are based on three-dimensional (3-D) Monte Carlo calculations. There is a statistical uncertainty of about 4% (one sigma) for the 2-m dose rates. Other calculational uncertainties due to physical modeling and cross sections are relatively small, as demonstrated by validation of the shielding analysis calculational methods.

TABLE 5.1-1
SUMMARY OF MAXIMUM REGULATORY DOSE RATES FOR GA-4 CASK
(mR/h)

Burnup (GWd/MTU)	35			45			
Cooling time (years)	10			15			
Number of assemblies	4			4			
Normal Conditions							
Package Surface	γ	n	**Total**	γ	n	**Total**	**Reg.**
Side	105.5	57.7	163.2	81.6	116.2	197.8	200
Top	8.4	6.0	14.4	8.4	12.0	20.4	200
Bottom	48.1	6.0	54.1	33.8	12.0	45.8	200
2 m from vehicle	γ	n	**Total**	γ	n	**Total**	**Reg.**
Side	6.59	1.68	8.27	3.72	5.05	8.77	10
Rear	1.54	0.15	1.69	1.07	0.29	1.36	10
Back of cab	0.278	0.042	0.32	0.19	0.10	0.29	2
Hypothetical Accident Conditions							
1 m from damaged cask	γ	n	**Total**	γ	n	**Total**	**Reg.**
Side (peak)	103	194	297	75	398	473	1000

5.2 Source Specification

GA used the SAS2 module of SCALE-4.1 (Ref. 5.2-1) to generate the neutron and gamma source terms for PWR fuels. The SAS2 module uses ORIGEN-S, to generate the necessary source term data for shielding and thermal evaluations of spent fuel shipping casks. Table 5.2-1 presents the basis for the source terms used in the shielding analysis for the GA-4 cask. The source specification for the shielding design assumes an axial distribution in the active fuel region; this was obtained from Ref. 5.2-2. This section presents the details of the source term generation, including the SAS2 models and the resulting neutron and gamma source terms for representative PWR spent fuel.

TABLE 5.2-1
BASIS FOR SOURCE SPECIFICATION

Description	GA-4 (PWR)
Initial enrichment (wt % U-235)	3.00
Fuel burnup (MWd/MTU)	35,000/45,000
Cooling time (years)	10/15
Fuel loading (MTU per assembly)	0.469
Assembly type	W 15 x 15

SAS2 Models

We generated the source term data by using the SAS2 control module in SCALE-4.1. The SAS2 control module computes gamma and neutron source terms for fuel assemblies of a given reactor history and cooling time. Time-dependent cross sections for a given set of reactor characteristics are computed from two-dimensional simulations, with one dimensional transport neutronics models that account for resonance self-shielding. The functional modules of SCALE-4 called by SAS2 are BONAMI-S, NITAWL-S, XSDRNPM-S, COUPLE, ORIGEN-S, and XSDOSE.

The PWR model represents a standard Westinghouse 15 X 15 PWR fuel assembly with an axial burnup distribution (Ref. 5.2-3). The fueled region is broken up into eleven axial regions to model the axial burnup distribution as shown in Fig. 5.2-1. Table 5.2-2 gives the axial length of each burnup zone. Six separate SAS2 calculations were performed, one for each burnup level used to approximate the axial distribution. For each case an initial enrichment of 3.0 wt % U-235 was used.

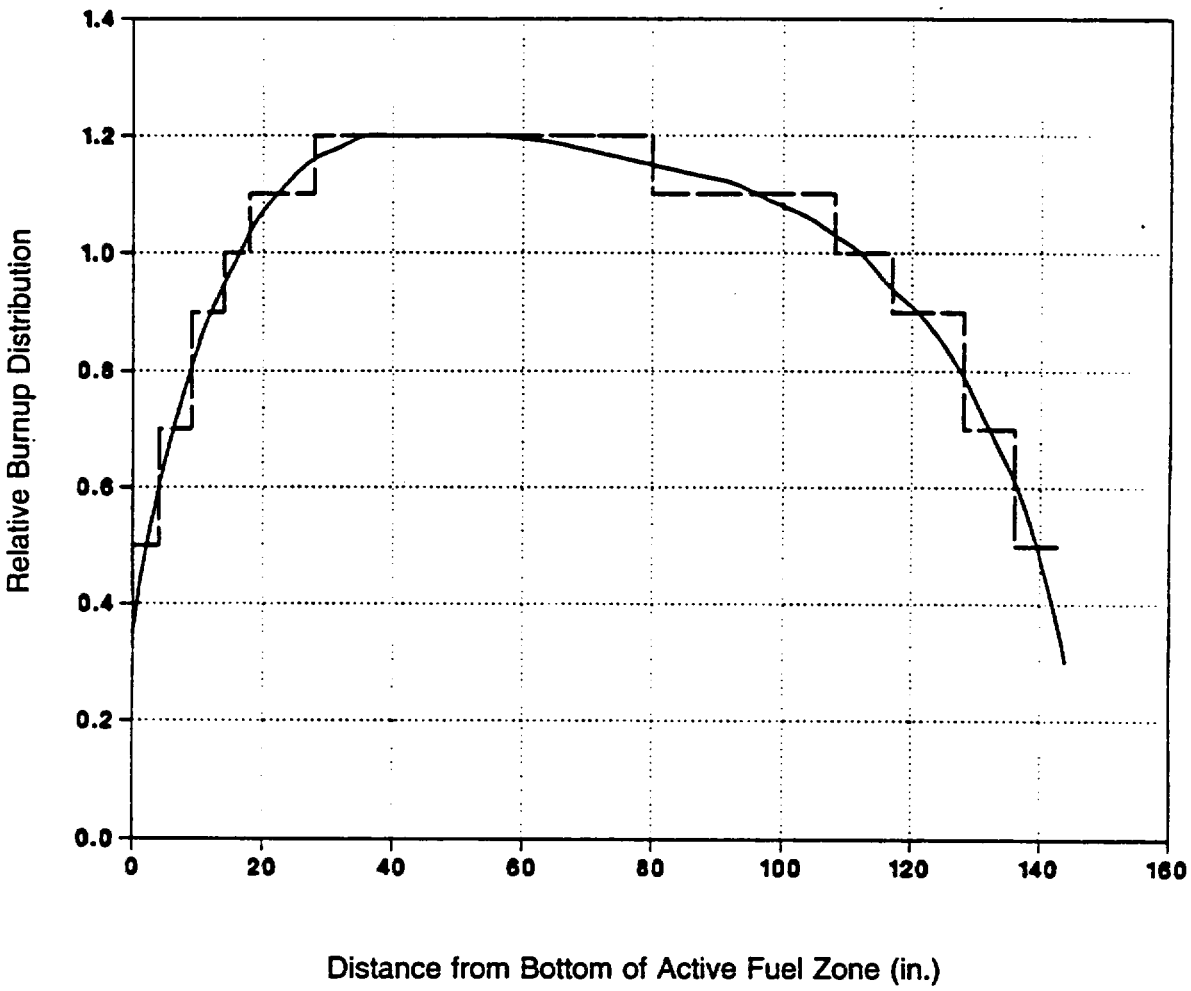

Fig. 5.2-1. Representative PWR axial burnup distribution

For a given burnup, this enrichment produces a conservative source as compared to higher initial enrichments. The fuel is burned for three cycles, with cooling between the cycles and 10 years or 15 years cooling after the last cycle. The SAS2 models include soluble boron to control excess reactivity. Table 5.2-3 lists the input parameters for the SAS2 models.

The radiation sources in a spent fuel assembly come from four basic regions: the active fuel (including such components as fuel, cladding, spacer grids, and instrument or guide tubes); the bottom tie plate and skirt; the plenum (including spring); and the top tie plate. The active fuel region includes both gamma and neutron sources while the other three non-fuel regions only include gamma sources. Only the Co-60 source, from activation of the Co-59 in the non-fueled regions, contributes to the dose rates outside the cask; it is therefore the only activation product considered in these regions.

5.2.1 Gamma Source

The gamma source for the fuel region includes primary gammas, X rays, conversion photons, (α,n) photons, prompt and fission-product gammas from spontaneous fission, and bremsstrahlung radiation. The non-fuel region source terms were obtained by using activation ratios related to the fuel region (given in Ref. 5.2-3, developed by Croff). Tables 5.2-4a, 5.2-4b and 5.2-5 provide the gamma source terms for the fuel and non-fuel regions, respectively. Only gamma groups 10-13 contribute significantly to gamma dose rates outside the cask, so only these gamma groups are treated in the shielding analyses.

TABLE 5.2-2
PWR AXIAL BURNUP DISTRIBUTION

Axial Region	Height Starting from Bottom (cm)	Relative Power
1	10.16	0.5
2	12.70	0.7
3	12.70	0.9
4	10.16	1.0
5	25.4	1.1
6	132.08	1.2
7	71.12	1.1
8	22.86	1.0
9	27.94	0.9
10	20.32	0.7
11	20.32	0.5

TABLE 5.2-3
PWR FUEL ASSEMBLY AND EXPOSURE DATA FOR SAS2 MODULE IN SCALE

Average burnup, MWd/MTU	35	45
Assembly type	W15x15	W15x15
Initial heavy metal loading, MTU	0.469	0.469
Initial U-235 enrichment, weight percent	3.0	3.0
Number of fuel rods per assembly	204	204
Fuel temperature during operation, K	1000	1000
Clad temperature during operation, K	605	605
Moderator temperature during operation, K	581	581
Number of cycles	3	3
Exposure time per cycle, days	313.5	444.4
Shutdown time between cycles, days	78.4	106
Cooling time after discharge, days	3650	5475
Soluble boron-10 concentration, atoms/b-cm		
Cycle 1	4.388E-6	5.00E-6
Cycle 2	4.169E-6	4.75E-6
Cycle 3	4.037E-6	4.60E-6
Moderator density, g/cm^3	0.7113	0.7113
Fuel rod		
Pellet diameter, in.	0.366	0.366
Gap, in.	0.0037	0.0037
Rod o.d., in.	0.422	0.422
Fuel rod pitch, in.	0.563	0.563
Clad material	Zr-4	Zr-4
Active fuel length, in.	144	144
Burnup, GWd/MTU		
Relative power = 0.5	17.5	22.5
Relative power = 0.7	24.5	31.5
Relative power = 0.9	31.5	40.5
Relative power = 1.0	35.0	45.0
Relative power = 1.1	38.5	49.5
Relative power = 1.2	42.0	54.0
Light elements, kg per assembly		
Active fuel		
O	62.6	62.6
Fe	4.6	4.6
Co	0.033	0.033
Ni	4.4	4.4
Zr	102	102
Nb	0.33	0.33
B	0.036	0.036
Top Tie Plate		
Co	0.01275	0.01275
Plenum		
Co	0.0061	0.0061
Bottom Tie Plate		
Co	0.03491	0.03491

TABLE 5.2-4a
PWR FUEL GAMMA SOURCE DATA FOR 35 GWd/MTU AND 10-YEAR COOLED

		Gamma Source Strength (MeV/s per assembly)						
Group No.	Energy Range (MeV)	RP=0.5	RP=0.7	RP=0.9	RP=1.0	RP=1.1	RP=1.2	Total
1	0.0-0.02	4.509E+11	5.606E+11	9.292E+11	8.261E+11	2.619E+12	3.857E+12	9.243E+12
2	0.02-0.03	2.315E+11	2.871E+11	4.739E+11	4.202E+11	1.328E+12	1.950E+12	4.691E+12
3	0.03-0.045	4.514E+11	5.819E+11	9.965E+11	8.988E+11	2.886E+12	4.299E+12	1.011E+13
4	0.045-0.07	4.631E+11	5.821E+11	9.670E+11	8.587E+11	2.715E+12	3.985E+12	9.570E+12
5	0.07-0.1	4.468E+11	5.609E+11	9.399E+11	8.398E+11	2.673E+12	3.950E+12	9.411E+12
6	0.1-0.15	6.256E+11	8.463E+11	1.511E+12	1.386E+12	4.518E+12	6.815E+12	1.570E+13
7	0.15-0.3	1.002E+12	1.254E+12	2.088E+12	1.859E+12	5.895E+12	8.681E+12	2.078E+13
8	0.3-0.45	7.526E+11	9.360E+11	1.549E+12	1.376E+12	4.353E+12	6.397E+12	1.536E+13
9	0.45-0.70	4.190E+13	5.509E+13	9.595E+13	8.726E+13	2.825E+14	4.246E+14	9.873E+14
10	0.70-1.0	3.038E+12	5.339E+12	1.140E+13	1.122E+13	3.889E+13	6.194E+13	1.318E+14
11	1.0-1.5	6.925E+12	9.902E+12	1.847E+13	1.727E+13	5.730E+13	8.787E+13	1.977E+14
12	1.5-2.0	9.001E+10	1.557E+11	3.263E+11	3.175E+11	1.085E+12	1.703E+12	3.677E+12
13	2.0-2.5	4.106E+09	5.516E+09	9.776E+09	8.956E+09	2.919E+10	4.413E+10	1.017E+11
14	2.5-3.0	2.136E+08	3.277E+08	6.396E+08	6.094E+08	2.057E+09	3.206E+09	7.053E+09
15	3.0-4.0	3.378E+07	5.246E+07	1.042E+08	1.004E+08	3.431E+08	5.422E+08	1.176E+09
16	4.0-6.0	1.181E+05	5.130E+05	2.139E+06	2.758E+06	1.211E+07	2.378E+07	4.142E+07
17	6.0-8.0	1.898E+04	8.263E+04	3.448E+05	4.447E+05	1.953E+06	3.835E+06	6.679E+06
18	8.0-10.0	2.957E+03	1.289E+04	5.381E+04	6.941E+04	3.048E+05	5.986E+05	1.043E+06
	Total	5.638E+13	7.610E+13	1.356E+14	1.246E+14	4.068E+14	6.161E+14	1.416E+15

NOTE: RP = relative power

TABLE 5.2-4b
PWR FUEL GAMMA SOURCE DATA FOR 45 GWd/MTU AND 15-YEAR-COOLED

		Gamma Source Strength (MeV/s per assembly)					
Group	Energy Range (MeV)	RP=0.5	RP=0.7	RP=0.9	RP=1.0	RP=1.1	RP=1.2
10	0.7 - 1.0	1.812+12	3.078+12	6.315+12	6.083+12	2.060+13	3.206+13
11	1.0 - 1.5	4.805+12	7.056+12	1.327+13	1.241+13	4.102+13	6.260+13
12	1.5 - 2.0	9.342+10	1.580+11	3.202+11	3.057+11	1.025+12	1.578+12
13	2.0 - 2.5	5.543+08	6.901+08	1.147+09	1.022+09	3.248+09	4.787+09

TABLE 5.2-5
PWR NON-FUEL REGION GAMMA SOURCE TERMS
(MeV/s)

Burnup/ Cooling Time	Energy (MeV)	Bottom Tie Plate	Plenum	Top Tie Plate
35/10	1.0	3.450E+11	6.310E+11	9.450E+11
45/15	1.25	2.121E+11	3.875E+11	5.807E+11

5.2.2 Neutron Source

The neutron source terms consist of the contributions from (α,n) and spontaneous fission. Tables 5.2-6a and 5.2-6b list the neutron source spectrum as provided by SAS2 for each fuel region.

TABLE 5.2-6a
PWR FUEL NEUTRON SOURCE DATA FOR 35 GWd/MTU AND 10-YEAR COOLED

		Neutron Source Strength (n/s per assembly)						
Group No.	Energy Range (MeV)	RP=0.5	RP=0.7	RP=0.9	RP=1.0	RP=1.1	RP=1.2	Total
1	6.43 - 20.0	9.732E+03	4.339E+04	1.822E+05	2.354E+05	1.035E+06	2.035E+06	3.541E+06
2	3.00 - 6.43	1.243E+05	5.116E+05	2.096E+06	2.691E+06	1.179E+07	2.310E+07	4.030E+07
3	1.85 - 3.00	1.598E+05	5.954E+05	2.357E+06	3.002E+06	1.308E+07	2.553E+07	4.472E+07
4	1.40 - 1.85	7.897E+04	3.208E+05	1.309E+06	1.680E+06	7.355E+06	1.441E+07	2.515E+07
5	0.90 - 1.40	9.894E+04	4.237E+05	1.759E+06	2.265E+06	9.941E+06	1.951E+07	3.400E+07
6	0.40 - 0.90	1.035E+05	4.563E+05	1.910E+06	2.466E+06	1.084E+07	2.129E+07	3.707E+07
7	0.10 - 0.40	2.020E+04	8.925E+04	3.739E+05	4.827E+05	2.121E+06	4.167E+06	7.255E+06
8	0.0 - 0.1	0.000E+00	0.000E+00	0.000E+00	0.000E+00	0.000E+00	0.000E+00	0.000E+00
	Total	5.954E+05	2.440E+06	9.986E+06	1.282E+07	5.615E+07	1.100E+08	1.920E+08

TABLE 5.2-6b
PWR FUEL NEUTRON SOURCE DATA FOR 45 GWd/MTU AND 15-YEAR-COOLED

		Neutron Source Strength (n/s per assembly)					
Group	Energy Range (MeV)	RP=0.5	RP=0.7	RP=0.9	RP=1.0	RP=1.1	RP=1.2
1	6.43 - 15.0	2.389+04	9.809+04	3.884+05	4.889+05	2.096+06	4.017+06
2	3.00 - 6.43	2.725+05	1.119+06	4.431+06	5.557+06	2.391+07	4.583+07
3	1.85 - 3.00	3.029+05	1.244+06	4.925+06	6.198+06	2.657+07	5.094+07
4	1.40 - 1.85	1.701+05	6.983+05	2.766+06	3.481+06	1.492+07	2.016+07
5	0.90 - 1.40	2.298+05	9.436+05	3.737+06	4.703+06	2.016+07	3.864+07
6	0.40 - 0.90	2.503+05	1.028+06	4.070+06	5.122+06	2.196+07	4.209+07
7	0.10 - 0.40	4.894+04	2.010+05	7.959+05	1.002+06	4.294+06	8.231+06
8	0.0 - 0.1	0.000+00	0.000+00	0.000+00	0.000+00	0.000+00	0.000+00
	Total	1.298+06	5.331+06	2.111+07	2.657+07	1.139+08	2.183+08

THIS PAGE LEFT BLANK INTENTIONALLY

5.3 Model Specification

5.3.1 Description of Radial and Axial Shielding Configuration

Figures 5.3-1 and 5.3-2 show the axial and radial (at midplane) shielding configurations of the GA-4 cask. Table 5.3-1 lists the pertinent shielding thicknesses for the cask. Each layer of structure and shielding is shaped to fit closely around the fuel cavity to minimize weight. The flat and corner portions of the sidewall have different shielding thicknesses for weight optimization.

The cask weight is further optimized by placing the densest materials toward the inside of the cask. The first layer outside the cavity liner is the DU gamma shielding. The next layer is the Type XM-19 austenitic stainless steel containment boundary wall, followed by the [**Proprietary Information**] neutron shield material. Finally, the entire cask is encased in a smooth Type XM-19 stainless steel skin, to ensure ease of decontamination after contact with the fuel pool water.

The closure and bottom plate of the cask use XM-19 stainless steel with sufficient thickness for both neutron and gamma shielding. The shielding effect of the impact limiters, including the impact limiter housing, on both ends of the cask is disregarded for conservatism.

The shielding configurations for normal transport and hypothetical accident conditions are different only with regard to the neutron shielding and outer skin. The neutron shielding remains intact for normal conditions of transport, whereas complete loss of the neutron shield is assumed for hypothetical accident conditions. The outer stainless steel skin, which encases the neutron shielding between the impact limiters, is also disregarded in the accident condition model.

For normal conditions, the dose rate points are placed at the surface of the package, at 2 m from the edge of the transporter, and at the rear of the tractor cab. The dose rate points for hypothetical accident conditions are located at 1 m from the damaged cask surface after loss of the neutron shield and the impact limiters as well. The locations of the dose rate points used for the normal and hypothetical accident conditions are shown in Section 5.4, along with the dose rate maps.

5.3.2 Shield Regional Densities

Standard reference handbooks and material suppliers provided the material property data for shielding analysis. The ORNL SCALE-4.1 code package (Ref. 5.2-1) contains a standard material data library for common elements, compounds, and mixtures. Suppliers provided the data for other materials.

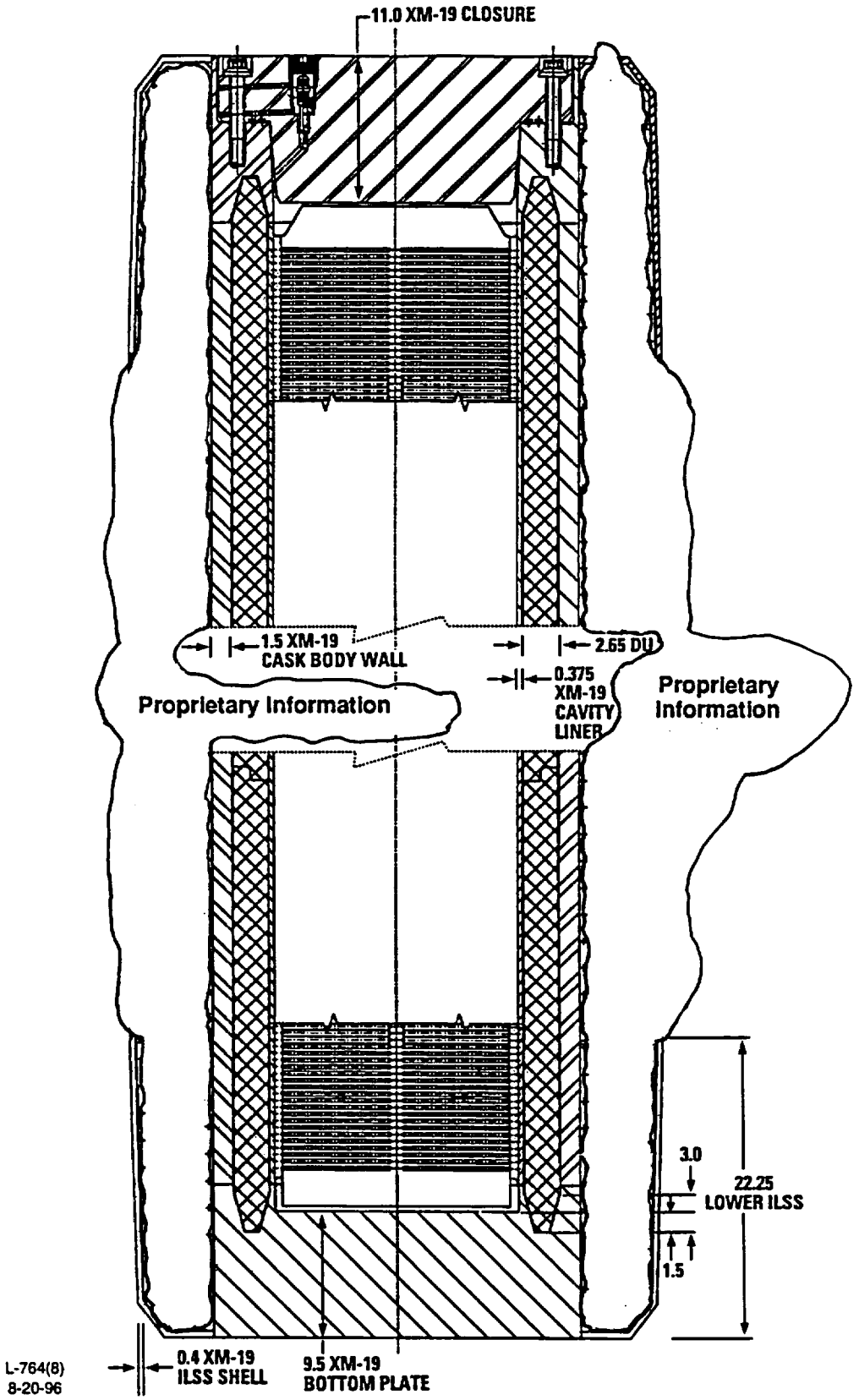

Fig. 5.3-1. Axial shielding configuration on flats

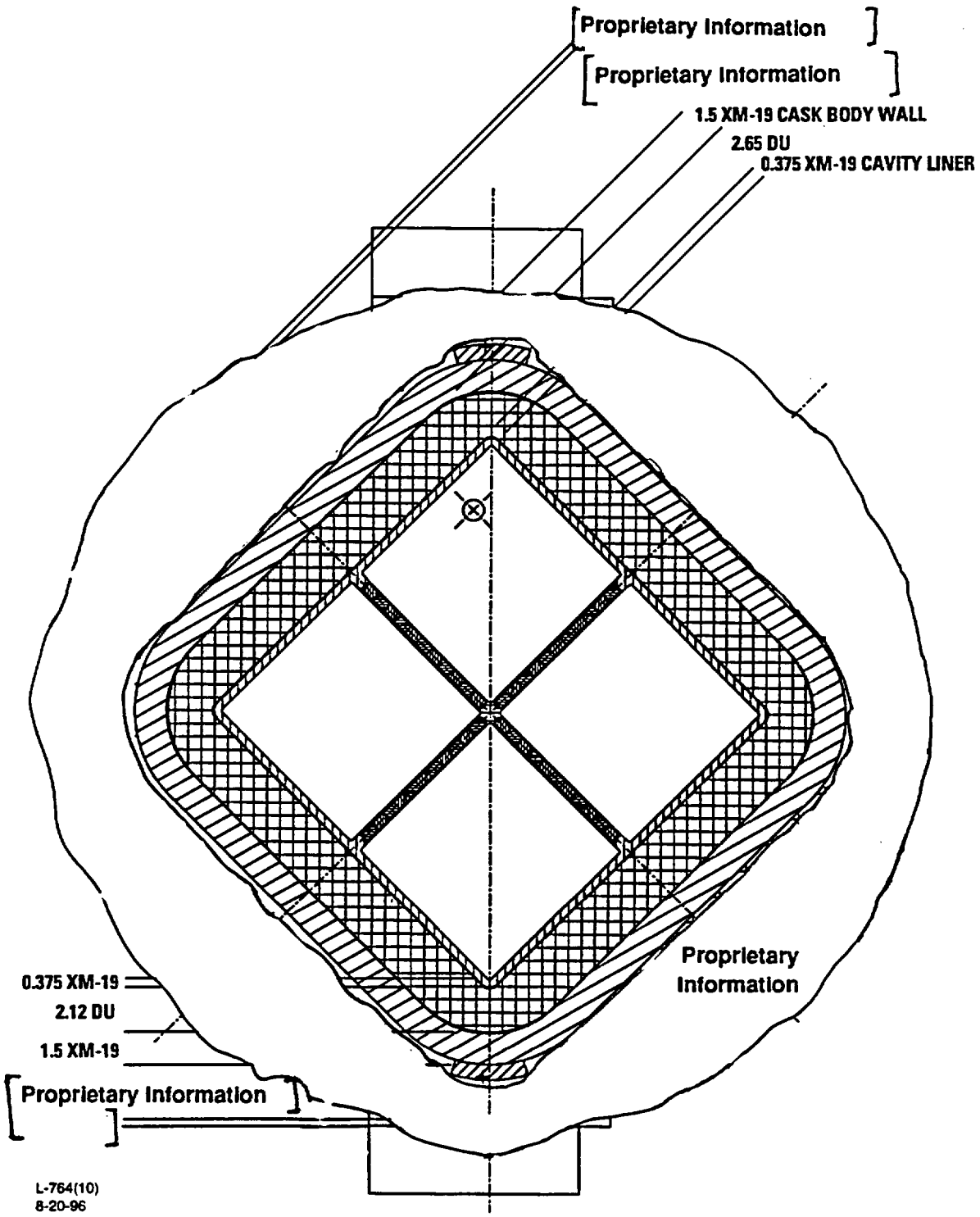

Fig. 5.3-2. Radial shielding configuration at midsection

TABLE 5.3-1
SHIELDING THICKNESS OF GA-4 CASK

Component	Thickness[a] (in.)
Upper section (top 12.5 in. of cask cavity)	
Cavity liner (XM-19)	0.375/0.375
Gamma shield (DU)	2.65/2.12
Cask body wall (XM-19)	1.5/1.5
Neutron shield [Proprietary Information]	[Prop. Info.]
Outer skin (XM-19)	0.4/0.4
Main body (middle 140.75 in. of cask cavity)	
Cavity liner (XM-19)	0.375/0.375
Gamma shield (DU)	2.65/2.12
Cask body wall (XM-19)	1.5/1.5
Neutron shield [Proprietary Information]	[Prop. Info.]
Outer skin (XM-19)	
Lower section (bottom 14 in. of cask cavity)	
Cavity liner (XM-19)	0.375/0.375
Gamma shield (DU)	2.65/2.12
Cask body wall (XM-19)	1.5/1.5
Neutron shield [Proprietary Information]	[Prop. Info.]
Outer skin (XM-19)	0.4/0.4
Cask closure (XM-19)	11.0
Bottom plate (XM-19)	9.5

[a]Flats/corner thicknesses for side wall

Table 5.3-2 provides a compilation of all the relevant materials used for the GA-4 cask. The fuel region of the PWR assemblies is modeled as a homogeneous UO_2 mixture, with the uranium density being equal to the fuel loading (MTU) divided by the volume of the cask cavity fuel region. We conservatively neglected the shielding properties of all other materials in the fuel region. The gas plenum regions were treated as a homogeneous smear of the Zircaloy cladding over the entire plenum region. The top- and bottom-end-fitting regions were modeled as air, thus neglecting all shielding properties of the end-fitting materials. Table 5.3-3 provides the smeared PWR fuel assembly material data used in the analyses.

For shielding analysis we used the same shield regional densities for both normal conditions of transport and hypothetical accident conditions, except for the neutron shield material. The neutron shield region and its associated outer skin is assumed to become a void region after a hypothetical accident thermal event.

TABLE 5.3-2
MATERIAL PROPERTY DATA

Material	Density, g/cm^3 (lb/in.^{3})	Element	Wt %	Atom Density (atoms/barn-cm)
B_4C	2.495 (0.0901)	B-10	14.32	2.150E-2
		B-11	63.94	8.728E-2
		C	21.73	2.720E-2
SS304 or XM-19	7.92 (0.286)	Cr	19.0	1.743E-2
		Mn	2.0	1.736E-3
		Fe	69.5	5.936E-2
		Ni	9.5	7.721E-3
DU	19.00 (0.686)	U-235	0.20	9.613E-5
		U-238	99.8	4.797E-2
[Proprietary Information]				
Air dry, 0°C, 1 atm	0.001293 (0.0000467)	N	75.53	4.199E-5
		O	23.18	1.128E-5
		Ar	0.0129	2.514E-7
Ground soil U.S. average (dry)	1.5 (0.05419)	O	50.2	2.833E-2
		Si	26.5	8.520E-3
		Al	6.7	2.242E-3
		Fe	5.5	8.893E-4
		Mn	0.07	1.151E-5
		Ti	0.45	8.483E-5
		Ca	5.0	1.127E-3
		Mg	1.3	4.830E-4
		K	1.4	3.233E-4
		Na	0.6	2.357E-4
[Proprietary Information]				

TABLE 5.3-3
PWR FUEL ASSEMBLY MATERIAL DATA

Material[a]	Density, g/cm^3 (lb/in.^{3})	Element	Wt %	Atom Density (atoms/barn-cm)
Top nozzle, height = 6.3 in.	0.0	--	--	--
Gas plenum, height = 9.449 in.	0.7044 (0.0254)	Zr	100.0	4.6510E-3
Active fuel, pitch = 0.563 in. height = 144 in. 0.469 MTU	3.169 (0.114)	U-235 U-238 0	2.6 85.5 11.9	2.1217E-4 6.8600E-3 1.4143E-2
Bottom nozzle, height = 3.75 in.	0.0	--	--	--

[a] Sequentially from the top to the bottom of a fuel assembly, with an 8.434-in. by 8.434-in. cross section.

THIS PAGE LEFT BLANK INTENTIONALLY

5.4 Shielding Evaluation

Shielding evaluation, which considered both normal and hypothetical accident conditions, consisted of neutron and gamma shielding analysis to demonstrate shielding adequacy and compliance with 10 CFR Part 71. This section presents the details of the shielding evaluations, including assumptions, cross-section data, flux-to-dose conversion factors, and computer codes used.

5.4.1 Assumptions

We made the following assumptions in the shielding analysis:

1. The radiation sources are uniformly distributed in fourteen separate axial homogenized regions inside the fuel cavity liner. The analysis models the top hardware, gas plenum, eleven active fuel regions, and bottom hardware.

2. No credit is taken for the shielding properties of the end nozzles of PWR fuel assemblies.

3. The model includes shield materials at nominal thickness.

4. An 8-ft-wide semitrailer is used, with 19.6 ft between the top of the impact limiter and the rear of the tractor's cab.

5. The cask is mounted on the trailer with the corner facing downwards.

6. The impact limiters on the top and bottom ends of the cask are treated as void regions, including the 0.25-in. XM-19 impact limiter housing.

7. The fuel assemblies are assumed to be at the ends of the cask cavity in the dose rate calculations for both the top and the bottom of the cask.

5.4.2 Cross-section Data

The computer codes used for shielding analysis include the PATH point-kernel integration code (Ref. 5.4-1), DORT transport code (Ref. 5.4-2), the CSASN module of SCALE-4.3 (Ref. 5.4-3) for cross-section data, and MCNP Monte Carlo Code (Ref. 5.4-4). The cross-section data required for these codes are described below.

The PATH code is a gamma shielding program, based on the common point-kernel integration attenuation coefficients for gamma shielding analysis. No additional cross-section data need be supplied.

For the transport calculations with DORT (gap analysis), the CSASN module of the Oak Ridge SCALE-4.3 package was used to generate the resonance corrected AMPX working library formatted cross sections. The standard SCALE 27 neutron and 18 gamma group structure was chosen in the process, since it is the only coupled set available in SCALE-4.3 with resonance parameters.

The CSASN module processes the two functional modules in a sequence. Those are BONAMI (resonance shielding treatment with Bondarenko data), and NITAWL (resonance shielding treatment with Nordheim method). The resonance corrected library cross sections were fed into ICE module to generate the ANISN library-formatted cross sections.

The sequence CSASN-ICE is identical with the module CSASI in the functional aspect, except that the ANISN library-formatted cross sections were defaulted as binary in the CSASI module. Therefore, the CSASN-ICE sequence was used in this analysis.

Finally, the GIP module was used in the DOS system to generate the group independent library for the DORT calculations.

MCNP is a complete shielding code with built-in cross-section data for neutrons and gammas. The code eliminates the need for external cross-section generation, as required for the transport codes, since MCNP uses a pointwise energy grid for the cross-section data.

5.4.3 Dose Rate Conversion Factors

A standard set of the flux-to-dose conversion factors is provided in ANSI/ANS 6.1.1-1977 (Ref. 5.4-5) for both neutrons and gammas as a function of energy. This set was selected for converting the calculated neutron gamma fluxes from the transport and Monte Carlo codes to the respective dose rates.

Table 5.4-1 gives the conversion factors for the transport calculations with DORT by energy group, corresponding to the 40-group structure used in the calculations. The MCNP Monte Carlo calculations use pointwise energy conversion factors as provided in Table 5.4-2.

5.4.4 Computer Code Selection

Shielding analysis used a variety of validated computer codes, including the two-dimensional (2-D) DORT (Ref. 5.4-2) transport code, the 3-D PATH point-kernel code (Ref. 5.4-1), and the 3-D Monte Carlo MCNP code (Ref. 5.4-4). These codes have been benchmarked and validated in accordance with Quality Assurance Program Requirements for Nuclear Facilities, ASME NQA-1-1989 Edition, Supplementary Requirements for Computer Program Testing Supplement 11S-2.

TABLE 5.4-1
MULTIGROUP FLUX-TO-DOSE CONVERSION FACTORS

Neutron Group	Upper Energy (eV)	Flux-to-Dose Conversion [(mR/h/(γ/cm²-s)]	Gamma Group	Upper Energy (eV)	Flux-to-Dose Conversion [(mR/h/(γ/cm²-s)]
1	2.0000+7	3.264E-1	28	1.0000+7	8.776E-3
2	6.4340+6	2.802E-1	29	8.0000+6	7.477E-3
3	3.0000+6	2.624E-1	30	6.5000+6	6.375E-3
4	1.8500+6	2.583E-1	31	5.0000+6	5.415E-3
5	1.4000+6	2.487E-1	32	4.0000+6	4.617E-3
6	9.0000+5	2.015E-1	33	3.0000+6	3.960E-3
7	4.0000+5	1.050E-1	34	2.5000+6	3.467E-3
8	1.0000+5	2.937E-2	35	2.0000+6	3.019E-3
9	1.7000+4	6.612E-3	36	1.6600+6	2.623E-3
10	3.0000+3	4.651E-3	37	1.3300+6	2.199E-3
11	5.5000+2	4.950E-3	38	1.0000+6	1.830E-3
12	1.0000+2	5.700E-3	39	8.0000+5	1.520E-3
13	3.0000+1	6.456E-3	40	6.0000+5	1.173E-3
14	1.0000+1	7.180E-3	41	4.0000+5	8.750E-4
15	3.0500+0	7.838E-3	42	3.0000+5	6.305E-4
16	1.7700+0	7.974E-3	43	2.0000+5	3.855E-4
17	1.3000+0	8.026E-3	44	1.0000+5	2.719E-4
18	1.1300+0	8.054E-3	45	5.0000+4	1.354E-3
19	1.0000+0	7.992E-3		1.000+4	
20	8.0000-1	7.800E-3			
21	4.0000-1	7.656E-3			
22	3.2500-1	7.600E-3			
23	2.2500-1	7.528E-3			
24	1.0000-1	6.442E-3			
25	5.0000-2	5.760E-3			
26	3.0000-2	5.760E-3			
27	1.0000-2	5.760E-3			
	1.0000-5				

TABLE 5.4-2
POINTWISE ENERGY FLUX-TO-DOSE
CONVERSION FACTORS

Neutron Energy (MeV)	Flux-to-Dose Conversion [(mR/h)/(n/cm^2-s)]	Gamma Energy (MeV)	Flux-to-Dose Conversion [(mR/h)/(γ/cm^2-s)]
2.5E–8	3.67E–3	0.01	3.96E–3
		0.03	5.82E–4
1.0E–8	3.67E–3	0.05	2.90E–4
		0.07	2.58E–4
1.0E–6	4.46E–3	0.15	3.79E–4
		0.2	5.01E–4
1.0E–5	4.54E–3	0.25	6.31E–4
		0.3	7.59E–4
1.0E–4	4.18E–3	0.35	8.78E–4
		0.4	9.85E–4
1.0E–3	3.76E–3	0.45	1.08E–3
		0.5	1.17E–3
1.0E–2	3.56E–3	0.55	1.27E–3
		0.6	1.36E–3
0.1	2.17E–2	0.65	1.44E–3
		0.7	1.52E–3
0.5	9.26E–2	0.8	1.68E–3
		1.0	1.98E–3
1.0	1.32E–1	1.4	2.51E–3
		1.8	2.99E–3
2.5	1.25E–1	2.2	3.42E–3
		2.6	3.82E–3
5.0	1.56E–1	2.8	4.01E–3
		3.25	4.41E–3
7.0	1.47E–1	3.75	4.83E–3
		4.25	5.23E–3
10.0	1.47E–1	4.75	5.90E–3
		5.0	5.80E–3
14.0	2.08E–1	5.25	6.01E–3
		5.75	6.38E–3
20.0	2.27E–1	6.25	6.74E–3
		6.75	7.11E–3
		7.5	7.66E–3
		9.0	8.77E–3
		11.0	1.02E–2
		13.0	1.18E–2
		15.0	1.33E–2

TABLE 5.4-3
EQUIVALENT SHIELDING CODES

Calculation	Code Used	Equivalent Code
2-D Transport	DORT	DOT
3-D Point-kernel	PATH	QAD
3-D Monte Carlo	MCNP	MORSE

5.4.5 Shielding Calculations

We performed shielding calculations to obtain the total dose rate from all contributing source components:

1. Primary neutron source (and subcritical multiplication) from spent fuel.

2. Secondary neutron source from additional fission in fuel and DU.

3. Primary gamma source from fuel and associated hardware.

4. Secondary gamma source from neutron interactions with the fuel assemblies and cask materials.

5. Scattering source from air and ground.

6. Gaps in gamma shield.

The analytical procedures for determination of the various dose rate contributions are described below.

5.4.5.1 Gamma Analysis. We used two codes, MCNP and PATH, to treat the primary gamma source in the active fuel region. The primary gamma source in the associated hardware was analyzed with PATH only.

The MCNP code was first used to calculate the gamma dose rates at the cask midplane. MCNP explicitly models the unconventional cask geometry with its variable shield thicknesses. In the MCNP model, the DU shield and the neutron shield in the cask body were subdivided into several subregions to obtain the radial dependence of the dose rates on the material thicknesses. Dose rates were calculated over several azimuthal regions (1) to determine the azimuthal variation of the dose rates on the cask surface and at 2 m from the edge of the transporter and (2) to ensure adequate shielding. Figures 5.4-1a and 5.4-1b show sketches of axial and radial cross-sections of the MCNP model.

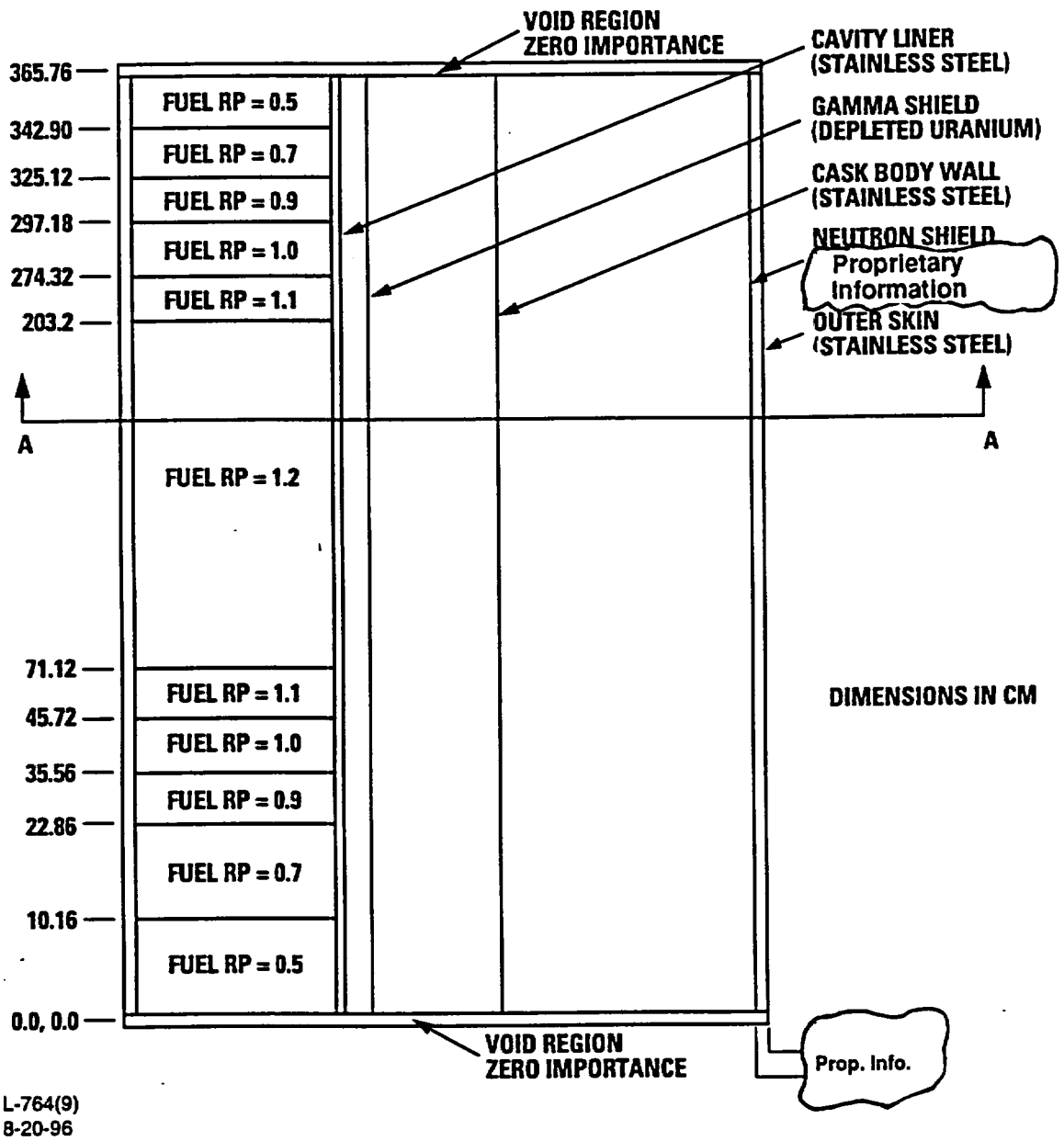

Fig. 5.4-1a. Axial cross-section of MCNP model

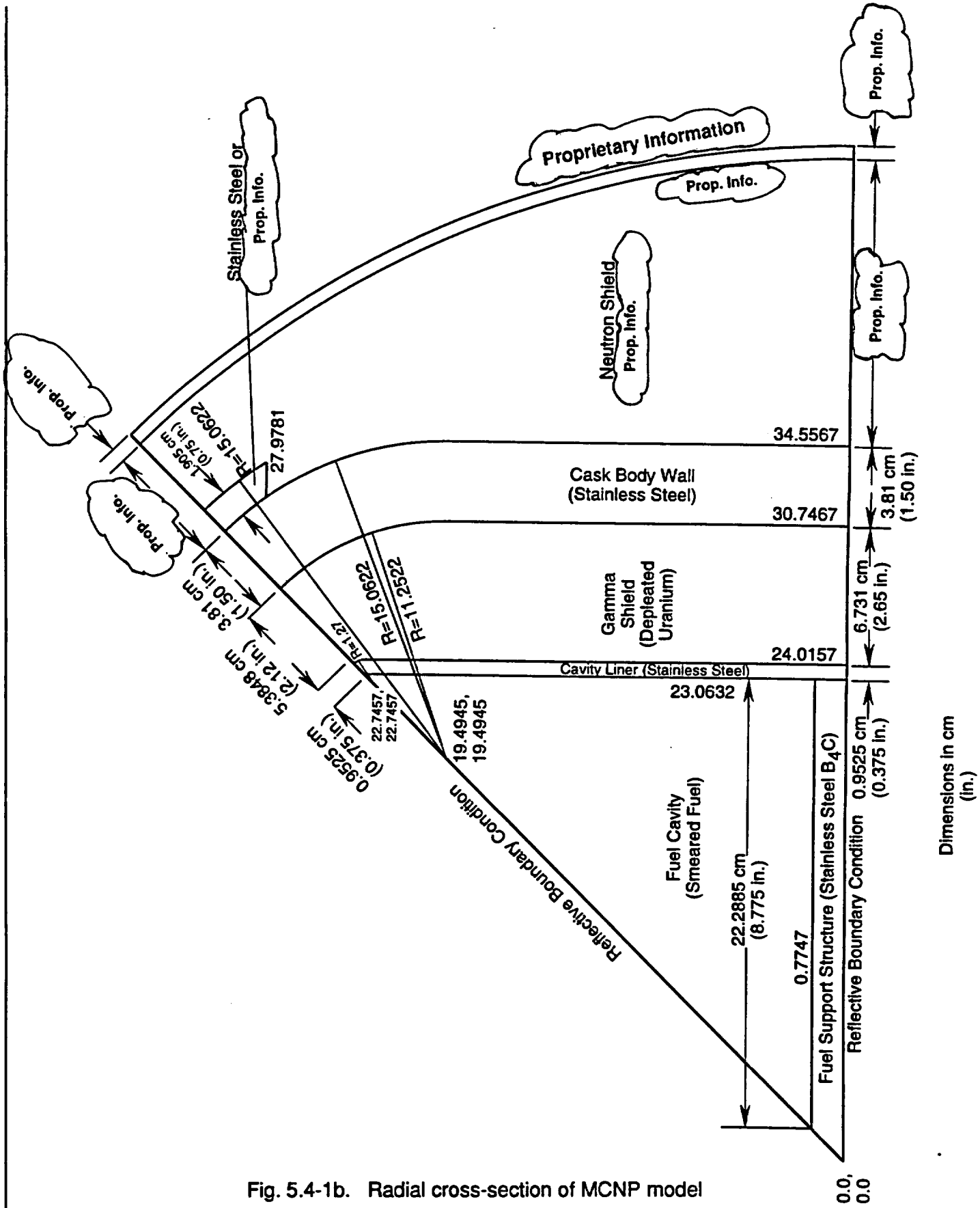

Fig. 5.4-1b. Radial cross-section of MCNP model

The PATH point-kernel gamma shielding code was used to supplement the MCNP code. PATH calculates the exponential attenuation of gamma rays and applies single-medium buildup factors to produce the final results. PATH employs certain approximations as necessitated by the point-kernel integration method and therefore requires corrections to the results. The PATH results were normalized to the MCNP results for a comparable calculation in order to obtain an overall correction factor.

The PATH code enabled us to specify as many dose rate points as desired around the cask. The explicit MCNP 3-D physical model was used to normalize the PATH calculations. The dose rate points were specified at various locations on the package surface, at 2 m from the edge of the transporter, and at the back of the cab. The results at these points encompassed the radial, axial, and azimuthal variations of the dose rates external to the cask.

Corrections to the PATH results were made at the side of the cask to account for the buildup factors through the composite shields, the normalization factor used to correct the PATH results was based on the MCNP results. No corrections were required for the PATH results at the top and bottom of the cask, since stainless steel is the only shielding material used.

The PATH results included the contribution from the primary gamma source in the active fuel and hardware regions. At the midplane of the cask, the dose rate contribution is predominantly from the active fuel. The hardware sources contribute appreciably to the dose rate points at the top and bottom ends of the cask. Figures 5.4-2a and 5.4-2b provide sketches of axial and radial cross sections for the PATH model.

5.4.5.2 Neutron Analysis. MCNP was also used to calculate the neutron dose rates from the primary neutron source in spent fuel, together with (1) the secondary neutron sources from additional fission reactions in the fuel and DU shield, and (2) the secondary gamma dose rates from (n,γ) reactions.

The MCNP model for the neutron analysis at the cask midplane was identical to that for the gamma analysis. The radial model for MCNP represented the exact cask geometry to obtain the azimuthal variation of the dose rates at the cask surface and at 2 m from the edge of the transporter.

An axial MCNP model was also developed to accurately describe the lower end of the cask bottom. The model was used to determine the neutron dose rates on the cask surface under the bottom impact limiters, on the bottom impact limiter surface, and 2 m behind the back of the trailer. The neutron source peaks toward the lower end of the fuel assembly. Also, the cask closure is thicker than the cask bottom plate. This leads to lower neutron dose rates on the top end of the cask. A simple cylindrical MCNP model of the cask was used to determine the dose rate ratio between the top and bottom end surfaces of the cask. Figures 5.4-1a and 5.4-1b provide sketches of the 2-D MCNP model. Neutron dose rates on the top end surface of the cask, on the end of the top impact limiter, and at the tractor cab are found by multiplying this ratio times the dose rates at equivalent locations on the bottom end of the cask. Dose rates on the sides of the top impact limiter and on the sides of the top end of the cask are conservatively set equal to the corresponding dose rates on the cask bottom end.

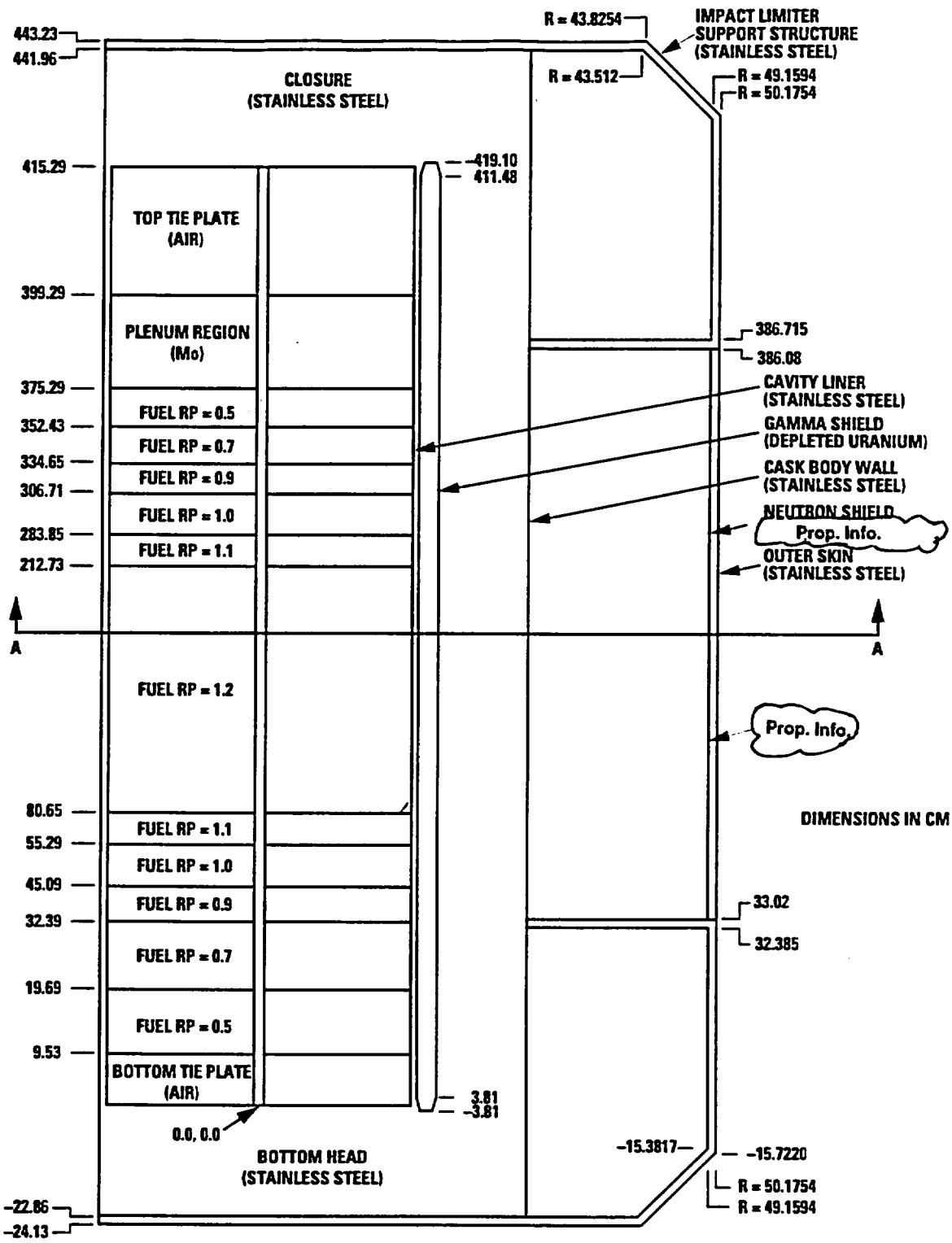

Fig. 5.4-2a. Axial cross-section of PATH model

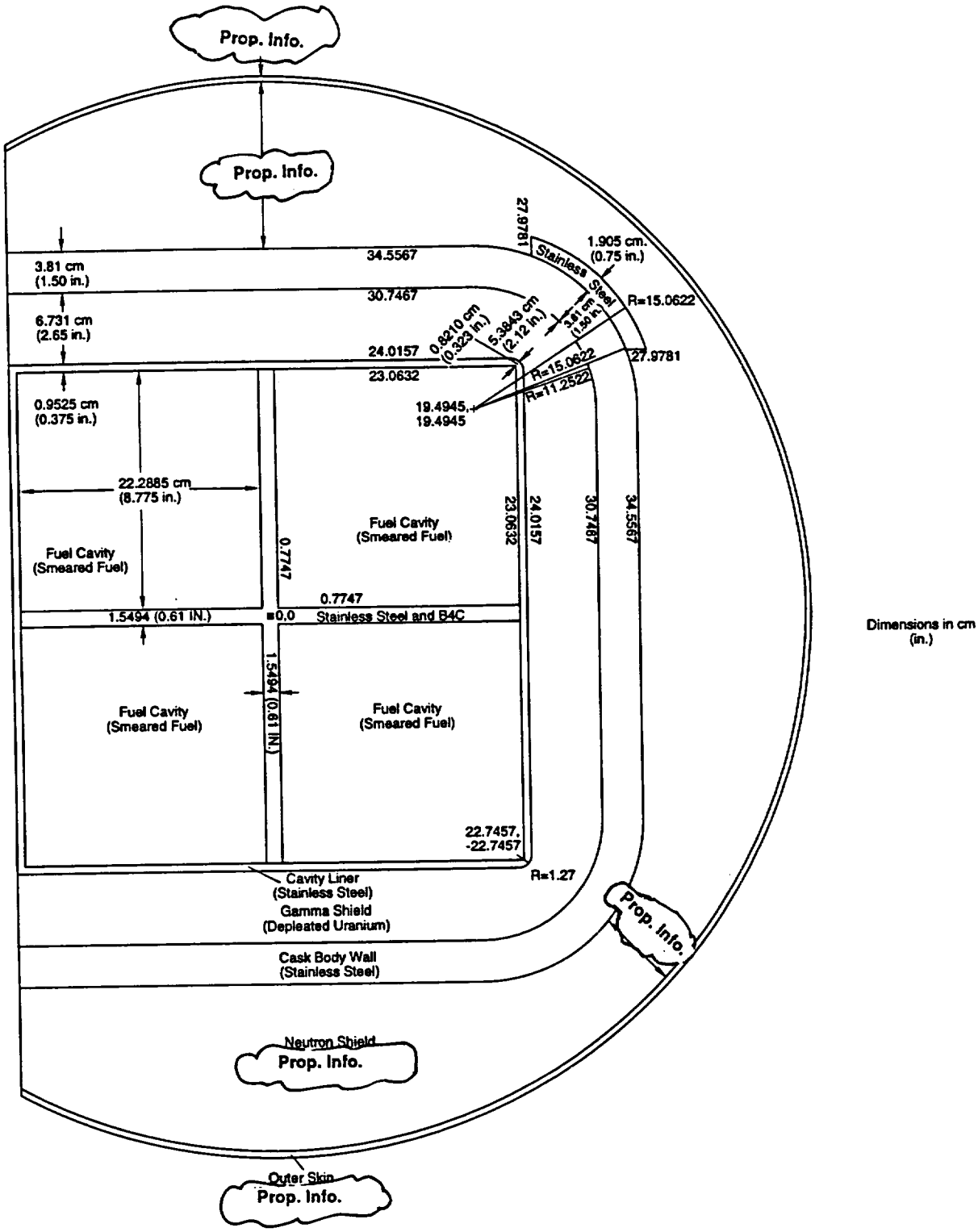

Fig. 5.4-2b. Radial cross-section of PATH model

5.4.5.3 Gap Analysis. The depleted uranium shield is divided (with lap joints) into five pieces. The cavity in the cask body for the DU is fabricated with zero longitudinal gap at room temperature. Under worst conditions the maximum longitudinal gap is 0.041 inches. For conservatism, the gap analysis assumes a gap (crack) straight through the DU of 0.045". Because DORT is a 2-D code we looked at the side and corner of the cask separately and choose the maximum effect to apply to the dose rates.

Figure 5.4-3 shows the 2-D R-Z model used for the flat side DORT calculations. Two separate calculations were performed to get the effects of the crack in DU regions. The same mesh intervals were used for cases with a crack and without a crack. The model covers the region with the peak fuel source. The four square fuel assemblies were cylinderized to conserve the area, and the fuel region radius of 25.32 cm was obtained. The thicknesses of other regions were added to the radius of the fuel region. The only differences between the flat and corner models were the thickness of the DU (Depleted Uranium) and Neutron shield regions. Figure 5.4-4 shows the 2-D R-Z model used for the corner DORT calculations. The material compositions are listed in Table 5.4-4.

This approach yields a conservatively large estimate of the increase in the gamma dose rate due to a gap in the DU. The largest dose rate increase for any point on the cask surface is 8%. The largest dose rate increase for any point at 2-m is 1%. All primary gamma surface dose rates on the side of the cask are increased by 8%, and all primary gamma 2-m dose rates on the side of the cask are increased by 1%.

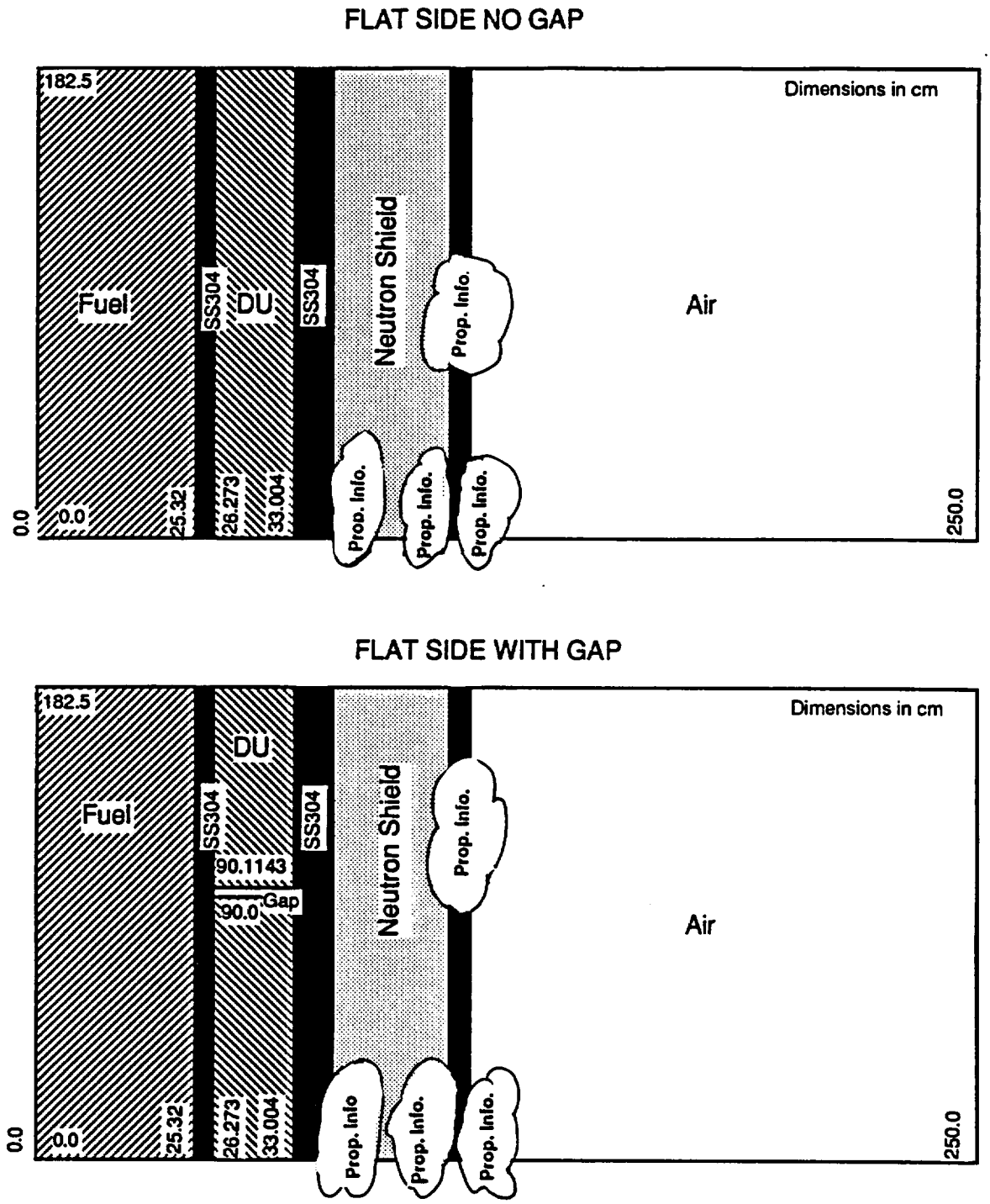

Figure 5.4-3. The flat side 2-D DORT R-Z model

TABLE 5.4-4
MATERIAL COMPOSITION FOR DORT CALCULATIONS

Material	Nuclide	Atom Density (atom/b-cc)
Fuel Region	U-235	1.9331E-4
	U-238	6.2502E-3
	O	1.2887E-2
SS304	Cr	1.7429E-2
	Mn	1.7363E-3
	Fe	5.9358E-2
	Ni	7.7207E-3
Depleted Uranium	U-235	9.6134E-5
	U-238	4.7971E-2
Neutron Shield	Proprietary Information	
Air	N	4.1988E-5
	O	1.1281E-5

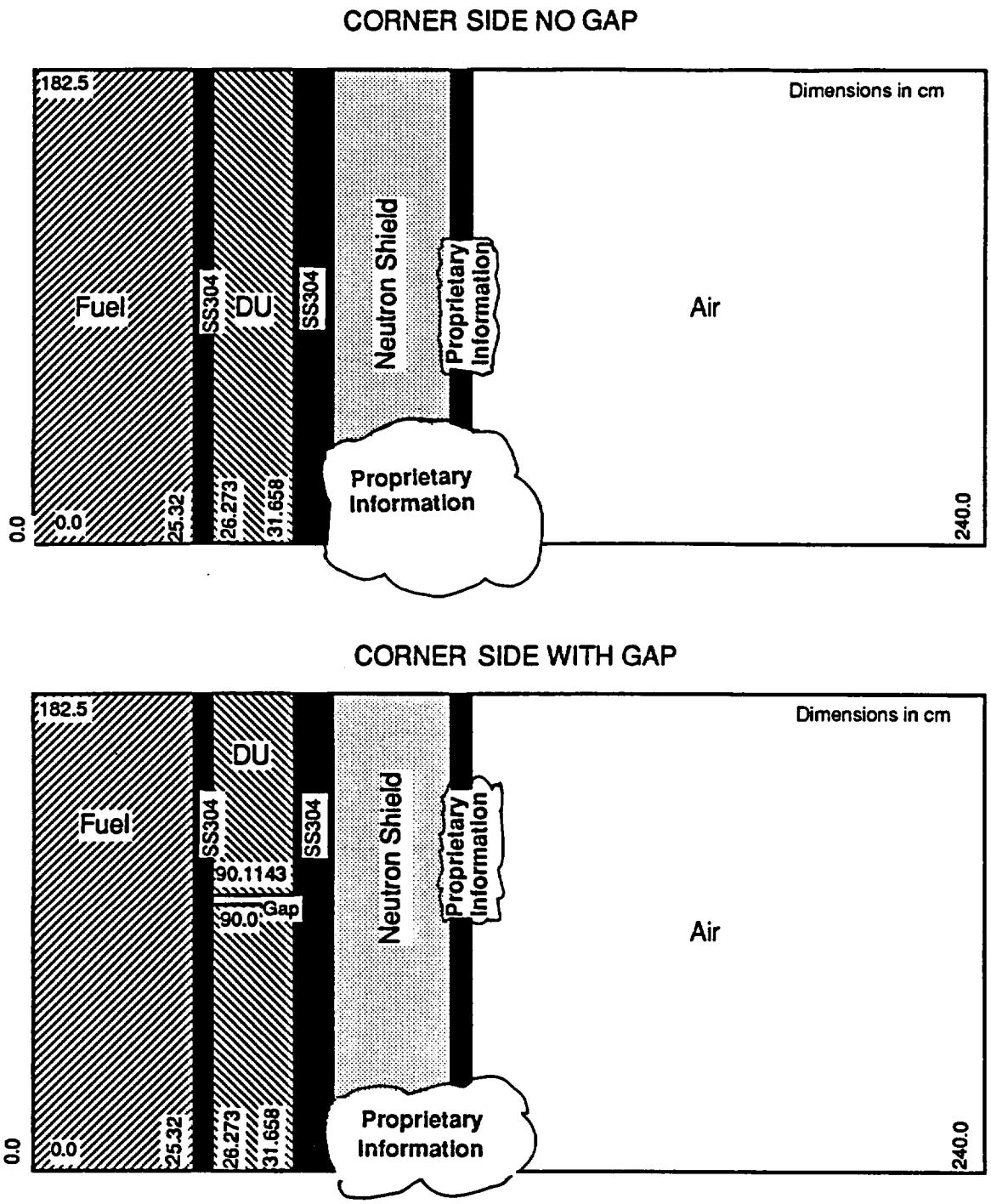

Figure 5.4-4. The corner side 2-D DORT R-Z model

5.4.5.4 Ground Scattering Analysis. Ground scattering is a significant component of the total dose rate external to the cask, especially at 2 m from the transporter. The ground scattering factor is normally greater for neutrons than for gammas because of a higher albedo for neutrons.

Separate ground scattering analyses were performed with MCNP for neutrons and gammas. Since the ground scattering factor is insensitive to the cask geometry, we used an equivalent cylindrical cask model without loss of its generality or applicability.

For each analysis, three MCNP cases were run, (1) without the ground present, (2) with the ground parallel to the cask axis at 3.5 ft below the cask surface to simulate the cask positioned on the semitrailer, and (3) with the ground against the cask sidewall to simulate the cask lying on the ground. The MCNP results with the two ground locations were compared with the corresponding results in the absence of the ground to quantify the increases in the dose rate caused by ground scattering.

The results at the 2-m location were conservatively applied to all dose rate points. The factors were 1.4 for neutrons and 1.1 for gammas.

5.4.6 Shielding Results For Normal Transport Conditions

5.4.6.1 Azimuthal Dose Rate Profile. MCNP results give the azimuthal dose rate profile at the midplane of each cask for normal conditions. Figure 5.4-5 and Table 5.4-5 show the azimuthal dose rate variations at the surfaces of the GA-4 cask for 1/4 segments of the cross section. The statistical uncertainty associated with the MCNP results is between 2 percent and 4 percent (one sigma).

The results in Fig. 5.4-5 and Table 5.4-5 show that the dose rates on the surface of the cask, including all contributions, are below the regulatory limit of 200 mR/h and the dose rates at 2 m are below 10 mR/h.

5.4.6.2 Dose Rate Maps. Figure 5.4-6 depicts the dose rate points for normal conditions of transport as generated with the PATH code, including the effects of gaps, peaking, and ground scatter, with appropriate normalization to the MCNP results. Tables 5.4-6 and 5.4-7 show the neutron and gamma dose rate components for the two burnup and cooling times evaluated. The dose rate at each point includes both neutron and gamma contributions. The calculated total dose rates are all below the 10 CFR Part 71 limits.

5.4.7 Shielding Results for Hypothetical Accident Conditions

The dose rate map for hypothetical accident conditions was obtained in the same manner as for normal transport conditions. Figure 5.4-7 and Table 5.4-8 show the resulting total dose rates. Table 5.4-8 gives the neutron and gamma dose rate breakdown. Note that the impact limiters are not shown in Fig. 5.4-7. Although they are designed to remain attached during a severe accident, the accident case shielding analysis conservatively assumes their absence.

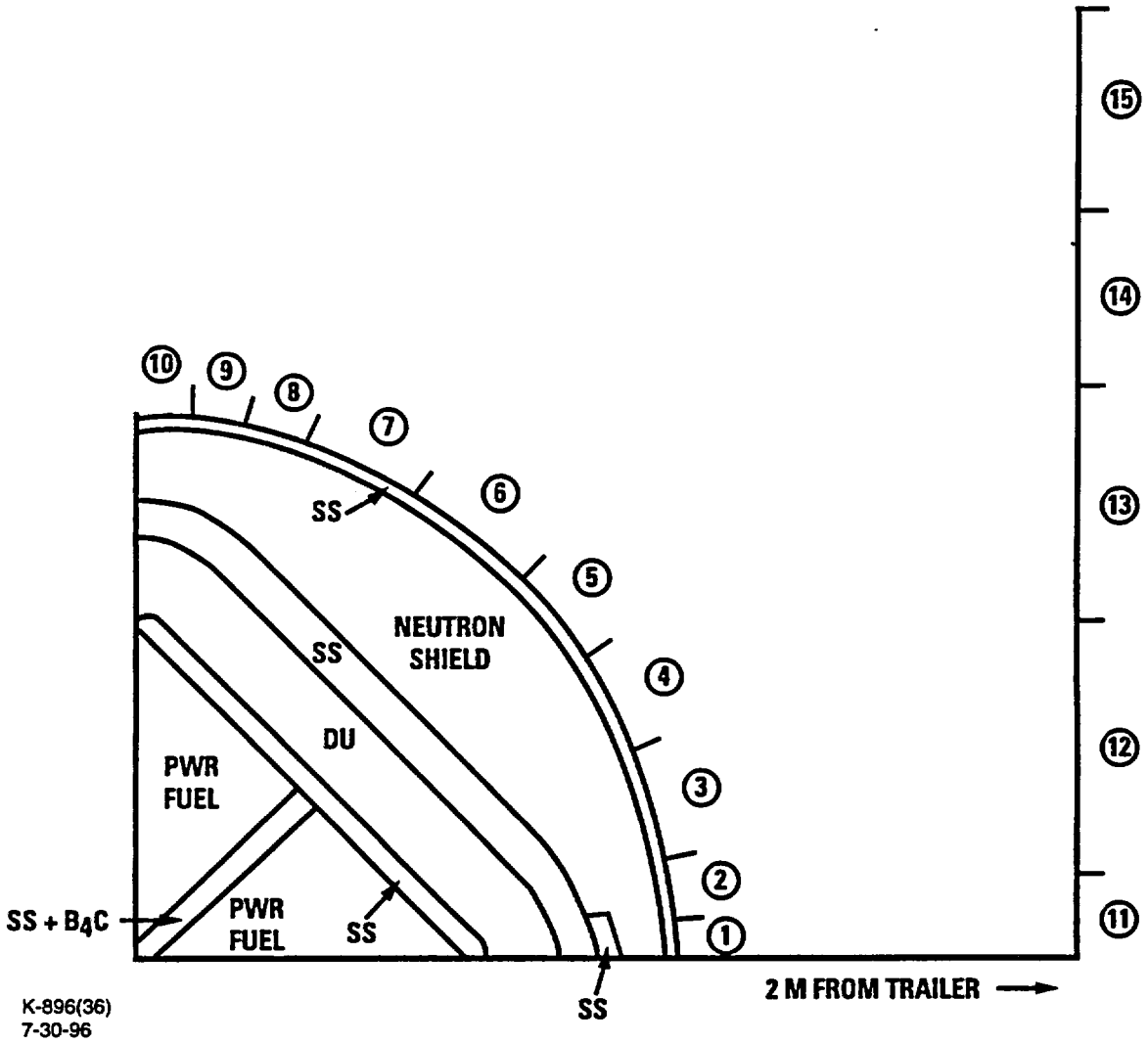

Fig. 5.4-5. Azimuthal midplane dose rate profile for GA-4 cask (mR/h)

TABLE 5.4-5
AZIMUTHAL MIDPLANE DOSE RATE PROFILE FOR GA-4 CASK
TOTAL DOSE RATE (mR/h)
BURNUP/COOLING TIME (GWd/MTU/YRS)

POINT	35/10	45/15
1	139	197
2	142	180
3	121	144
4	107	113
5	100	99
6	100	99
7	107	112
8	124	142
9	152	180
10	163	198
11	7.4	8.8
12	7.6	8.8
13	8.1	8.7
14	8.3	8.3
15	7.2	6.9

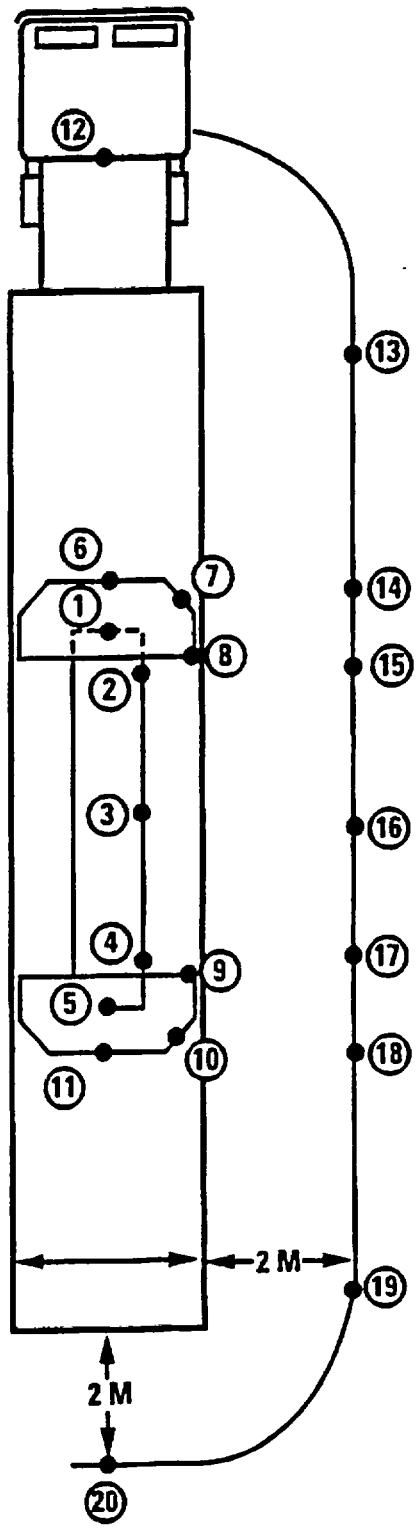

K-213(2)
7-30-96

Fig. 5.4-6. Total dose rate (mR/h) around GA-4 cask for normal conditions

TABLE 5.4-6
GA-4 CASK DOSE RATES (mR/h) FOR NORMAL CONDITIONS
35 GWd/MTU AND 10 YEAR COOLING

POINT	PRIMARY GAMMA	GAP	n, γ	GAMMA GROUND SCATTER	NEUTRON	NEUTRON GROUND SCATTER	TOTAL	10CFR71 LIMIT
1	23.1	0	0.5	2.4	5.0	2.0	33.0	200
2	26.8	2.1	0.9	3.0	8.9	3.6	45.3	200
3	85.0	6.8	4.1	9.6	41.2	16.5	163.2	200
4	41.7	3.3	0.7	4.6	7.4	3.0	60.7	200
5	116.2	0	3.5	12.0	3.5	14.0	180.7	200
6	9.2	0	0.1	0.9	0.7	0.3	11.2	200
7	7.8	0	0.1	0.8	1.4	0.6	10.7	200
8	7.2	0	0.4	0.8	4.3	1.7	14.4	200
9	17.3	0	0.4	1.8	4.3	1.7	25.5	200
10	10.3	0	0.1	1.0	1.4	0.6	13.4	200
11	43.3	0	0.4	4.4	4.3	1.7	54.1	200
12	0.25	0	0.003	0.025	0.03	0.012	0.32	2
13	0.24	0	0.11	0.04	1.10	0.44	1.93	10
14	2.30	0	0.11	0.24	1.10	0.44	4.19	10
15	3.11	0	0.11	0.32	1.10	0.44	5.08	10
16	5.81	0.06	0.12	0.60	1.20	0.48	8.27	10
17	3.80	0	0.12	0.39	1.20	0.48	5.99	10
18	2.83	0	0.12	0.30	1.20	0.48	4.93	10
19	3.15	0	0.12	0.33	1.20	0.48	5.28	10
20	1.38	0	0.01	0.15	0.11	0.04	1.69	10

TABLE 5.4-7
GA-4 CASK DOSE RATES (mR/h) FOR NORMAL CONDITIONS
45 GWd/MTU AND 15 YEAR COOLING

POINT	PRIMARY GAMMA	GAP	n, γ	GAMMA GROUND SCATTER	NEUTRON	NEUTRON GROUND SCATTER	TOTAL	10CFR71 LIMIT
1	14.7	0	1.0	1.6	10.0	4.0	31.3	200
2	26.4	2.1	1.8	3.0	17.9	7.2	58.4	200
3	61.0	4.9	8.3	7.4	83.0	33.2	197.8	200
4	42.1	3.4	1.5	4.7	15.0	6.0	72.7	200
5	80.0	0	7.2	8.7	71.5	28.6	196.0	200
6	5.8	0	0.1	0.6	1.4	0.6	8.5	200
7	4.8	0	0.3	0.5	2.9	1.2	9.7	200
8	6.7	0	0.9	0.8	8.6	3.4	20.4	200
9	17.4	0	0.9	1.8	8.6	3.4	32.1	200
10	6.9	0	0.3	0.7	2.9	1.2	12.0	200
11	29.8	0	0.9	3.1	8.6	3.4	45.8	200
12	0.16	0	0.01	0.02	0.07	0.03	0.29	2
13	0.05	0	0.22	0.03	2.16	0.86	3.32	10
14	0.86	0	0.22	0.11	2.16	0.86	4.21	10
15	1.58	0	0.22	0.18	2.16	0.86	5.00	10
16	2.99	0.03	0.36	0.34	3.61	1.44	8.77	10
17	2.13	0	0.26	0.24	2.59	1.04	6.26	10
18	1.10	0	0.26	0.14	2.59	1.04	5.13	10
19	2.17	0	0.26	0.24	2.59	1.04	6.30	10
20	0.95	0	0.02	0.10	0.21	0.08	1.36	10

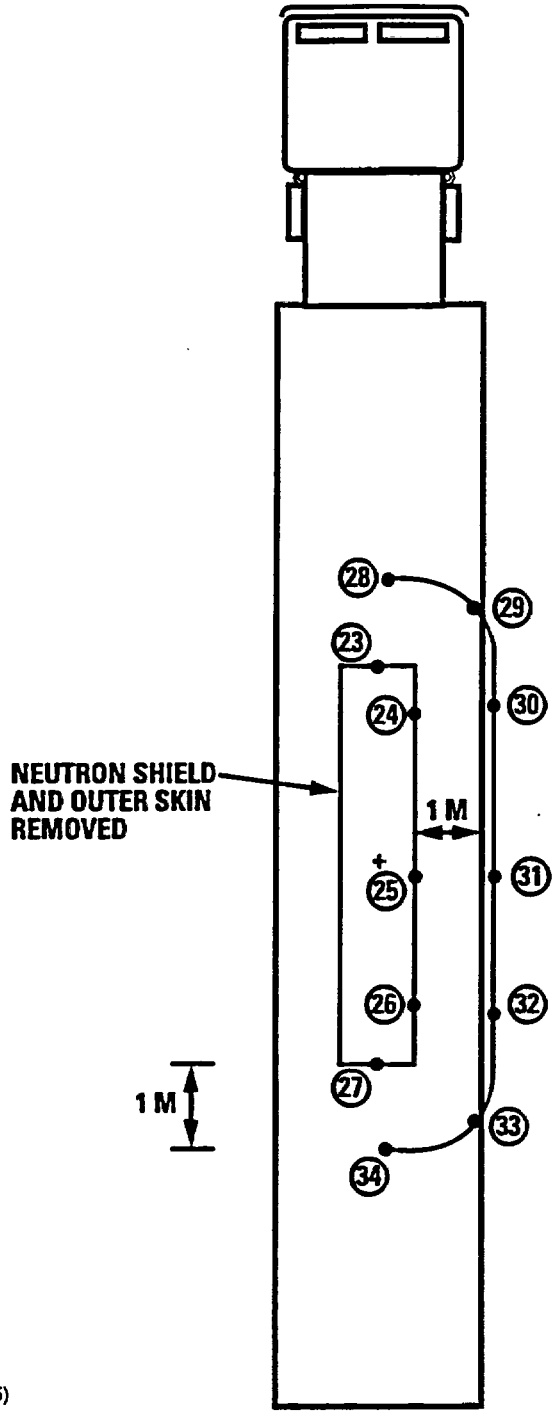

Fig. 5.4-7. Total dose rate (mR/h) around GA-4 cask for hypothetical accident conditions

TABLE 5.4-8
GA-4 CASK DOSE RATES (mR/h)
FOR HYPOTHETICAL ACCIDENT CONDITIONS

Point	Location - 35/10	Gammas	Neutrons	Total	10CFR71 Limit
23	Surface of cask	39	65	104	None
24		187	104	291	None
25		580	1580	2160	None
26		349	537	886	None
27		128	65	193	None
28	1 m from cask[a]	12	60	72	1000
29		10	60	70	1000
30		40	60	100	1000
31		103	194	297	1000
32		60	105	165	1000
33		25	105	130	1000
34		33	105	93	1000

[a]Relative to damaged cask with neutron shield and skin removed.

Point	Location - 45/15	Gammas	Neutrons	Total	10CFR71 Limit
31	1 m from cask[a]	75	398	473	1000

5.4.8 Correlation of Accident Dose Rate to Measured Dose Rate

Since the hypothetical accident conditions cannot be tested before each fuel shipment, the following dose rate condition shall be met for each shipment.

The cask contents shall be so limited that 3.4 times the peak neutron dose rate at any point on the surface of the cask at its midlength plus 1.0 times the gamma dose rate at that location does not exceed 1000 mR/h.

This formula was derived by determining two ratios: the ratio of the calculated peak 1-m accident neutron dose rate to the calculated peak cask surface normal transport neutron dose rate and the ratio of the respective gamma dose rates at the same point. Table 5.4-9 is a compilation of the data used to calculate the ratios. The table also includes references to the tables in this report from which the data were obtained. The maximum neutron dose rate occurs near the midplane of the cask. The maximum ratios for the neutron dose rate (3.4) and gamma dose rate (1.0) were used for conservatism to apply to all configurations.

TABLE 5.4-9
CORRELATION DATA FOR ACCIDENT CONDITIONS

Burnup/Age	Accident Condition			Peak Cask Surface Normal Transport			Ratio (1-meter/surface)	
	1-meter Dose Rate mR/h		Reference	Cask Surface Dose Rate mR/h		Reference		
GWd/MTU/Yrs	Neutron	Gamma	Table/Point	Neutron	Gamma	Table/Point	Neutron	Gamma
35/10	194	103	5.4-8/31	57.7	105.5	5.4-6/3	3.4	0.98
45/15	398	75	5.4-8/31	116.2	81.6	5.4-7/3	3.4	0.92

THIS PAGE LEFT BLANK INTENTIONALLY

5.5 References for Sections 5.1 through 5.4

5.2-1 "SCALE-4.1: A Modular Code System for Performing Standardized Computer Analysis for Licensing Evaluation," CCC-545, Oak Ridge National Laboratory, February 1990.

5.2-2 "Revised Uranium-Plutonium Cycle PWR and BWR Models For the ORIGEN Computer Code," ORNL/TM-6051, September 1978.

5.2-3 "Topical Safety Analysis Report for the Westinghouse MC-10 Cask for an Independent Spent Fuel Storage Installation (Dry Storage)," December 1984.

5.4-1 Su, S., et al., "PATH Gamma Shielding Code User's Manual," GA-A16772 (Rev 1.), General Atomics, May 1987.

5.4-2 "DORT: Two-Dimensional Discrete Ordinates Transport Codes," CCC-484, Oak Ridge National Laboratory, November 1989.

5.4-3 "SCALE-4.3: A Modular Code System for Performing Standardized Computer Analysis for Licensing Evaluation for Workstations and Personal Computers," Vol. 0-3, CCC-545, Oak Ridge National Laboratory, October 1995.

5.4-4 Briesmeister, J. F. (editor), "MCNP — A General Monte Carlo Code for Neutron and Photon Transport," LA-7396-M, Rev. 2, September 1986.

5.4-5 "Neutron and Gamma-Ray Flux-to-Dose Rate Factors," ANSI/ANS 6.1.1-1977 (N666), March 1977.

THIS PAGE LEFT BLANK INTENTIONALLY